

Fall 12-8-2011

# Targeted Molecular MR Imaging of HER2 and EGFR Using De Novo Designed Protein Contrast Agents

Jingjuan Qiao

Follow this and additional works at: [https://scholarworks.gsu.edu/chemistry\\_diss](https://scholarworks.gsu.edu/chemistry_diss)

---

## Recommended Citation

Qiao, Jingjuan, "Targeted Molecular MR Imaging of HER2 and EGFR Using De Novo Designed Protein Contrast Agents." Dissertation, Georgia State University, 2011.  
[https://scholarworks.gsu.edu/chemistry\\_diss/62](https://scholarworks.gsu.edu/chemistry_diss/62)

This Dissertation is brought to you for free and open access by the Department of Chemistry at ScholarWorks @ Georgia State University. It has been accepted for inclusion in Chemistry Dissertations by an authorized administrator of ScholarWorks @ Georgia State University. For more information, please contact [scholarworks@gsu.edu](mailto:scholarworks@gsu.edu).

TARGETED MOLECULAR MR IMAGING OF HER2 AND EGFR USING *DE NOVO* DESIGNED  
PROTEIN CONTRAST AGENTS

by

JINGJUAN QIAO

Under the Direction of Dr. Jenny J. Yang

ABSTRACT

The application of magnetic resonance imaging (MRI) to non-invasively assess disease biomarkers has been hampered by lack of desired contrast agents with high relaxivity, targeting capability, and optimized pharmacokinetics. We developed a novel MRI probe which targets HER2, a biomarker for various cancers and a target for anti-cancer therapies. This multimodal HER2-targeted MRI probe integrates a rationally designed protein contrast agent with a high affinity HER2 affibody and near IR dye. Our probe can differentially monitor tumors with different HER2 levels in both cells and xenograft mice. In addition to its 10-fold higher dose efficiency compared to clinically-approved agent DTPA, our developed agent also exhibits advantages in crossing the endothelial boundary, tissue distribution, and tumor tissue retention as demon-

strated by even distribution of the imaging probe across the entire tumor mass. Additionally, a second series of protein contrast agents that included affibody against EGFR developed with the capability to specifically target EGFR. These contrast agents have been utilized to monitor drug treatments and quantitatively analyze biomarker expression level. Furthermore, we anticipate these agents will provide powerful tools for quantitative assessment of molecular markers, and improved resolution for diagnosis, prognosis and drug discovery.

INDEX WORDS: MRI, Contrast agent, Protein engineering, Gadolinium, Relaxivity, HER2

TARGETED MOLECULAR MR IMAGING OF HER2 AND EGFR USING A *DE NOVO* DESIGNED  
PROTEIN CONTRAST AGENTS

by

JINGJUAN QIAO

A Dissertation Submitted in Partial Fulfillment of the Requirements for the Degree of

Doctor of Philosophy

in the College of Arts and Sciences

Georgia State University

2011

Copyright by  
Jingjuan Qiao  
2011

TARGETED MOLECULAR MR IMAGING OF HER2 AND EGFR USING A *DE NOVO* DESIGNED  
PROTEIN CONTRAST AGENTS

by

JINGJUAN QIAO

Committee Chair: Dr. Jenny J. Yang

Committee: Dr. Aimin Liu

Dr. Zhi-ren Liu

Dr. Lily Yang

Electronic Version Approved:

Office of Graduate Studies

College of Arts and Sciences

Georgia State University

December 2011

## ACKNOWLEDGEMENTS

All the work in this dissertation was carried out under the direction of Dr. Jenny J. Yang; in collaborate with Dr. Zhi-ren Liu. Dr. Yang's knowledge guided my research with valuable suggestions.

I am fortunate indeed to have such knowledgeable committee members who helped to make this a wonderful learning event for me. Throughout my dissertation experience, Dr. Yang provided immeasurably wise and perceptive counsel. I am especially grateful to her for continuously supporting my experiments and ideas, and helping me to express my research goals in writing. My sincere thanks to Dr. Lily Yang, Dr. Hui Mao and Dr. Hans Grossniclaus, each of whom contributed important and unique perspectives throughout the research development and analysis. Their advice and feedback have been more helpful than they may realize.

I want to express many thanks to my friends Dr. Shunyi Li, Dr. Jie Jiang, Shenghui Xue, Fan Pu and other members in Dr. Jenny Yang's lab. I also want to thank Dr. Robert Long, Dr. Liya Wang, and Dr. Hekmatayar for collecting MRI data.

This work is supported by grants from National Institute of Health and National Cancer Institute, as well as a Brain and Behavior Fellowship provided by Georgia State University.

Finally, and most importantly, I would like to thank my parents and my husband, Liangwei Li, for their love, encouragement and quiet patience while supporting my research work.

## TABLE OF CONTENTS

ACKNOWLEDGEMENTS.....	iv
LIST OF FIGURES.....	xiv
LIST OF ABBREVIATIONS .....	xix
Chapter 1. INTRODUCTION .....	1
1.1 Cancer as human diseases .....	1
1.1.1 Biomarkers and its role in diagnosis, prognosis and treatment.....	2
1.1.2 Detection of biomarkers.....	6
1.2 EGFR family function as biomarkers for diagnosis and therapy .....	8
1.2.1 Structure of EGFR family proteins .....	9
1.2.2 Roles of EGFR family in tumor formation and growth .....	11
1.2.3 Distribution of EGFR family members in various cancers and cell lines.....	16
1.3 Targeted reagents for EGFR family .....	18
1.3.1 Intra-cellular inhibitor an extra-cellular ligands of EGFR (HER1).....	19
1.3.2 Engineered antibodies and drugs for HER2.....	21
1.4 Affibody library and screening .....	23
1.4.1 Affibody derived from z-domain of Protein A and screened by phage display.....	23
1.4.2 Z <sub>EGFR:1907</sub> binds to EGFR with highest affinity .....	25



1.5	Clinical imaging techniques and the application.....	26
1.5.1	Magnetic Resonance Imaging and its application .....	27
1.5.2	Near Infra-red imaging and <i>in vivo</i> application .....	28
1.5.3	Other techniques of molecular imaging .....	29
1.6	Molecular imaging.....	30
1.7	Contrast agents for molecular imaging.....	33
1.7.1	MRI contrast agents.....	33
1.7.2	Biomarkers targeted contrast agents .....	36
1.7.3	Criteria of designing ideal contrast agents .....	37
1.8	Objectives of this study, and over view of the dissertation .....	38
Chapter 2.	MATERIAL AND METHODS .....	42
2.1	Molecular cloning of ProCA1-affibody to target HER2 and EGFR.....	42
2.2	Plasmid construction and protein generation .....	42
2.2.1	GST-fusion ProCA1-affibody and purification.....	43
2.2.2	Sub-cloning of tagless ProCA1-affibody and purification .....	43
2.3	PEGylation of ProCA1-affibody .....	45
2.4	Conjugation of near infra red (NIR) dye to ProCA1-affibody .....	45
2.5	Determining the folding condition of ProCA1-affibody .....	46
2.5.1	Mass spectrometry .....	46

2.5.2	Circular dichroism spectroscopy.....	46
2.5.3	Fluorescence spectroscopy.....	47
2.5.4	Nuclear Magnetic Resonance (NMR) spectroscopy .....	47
2.6	Relaxivity measurements and metal binding affinity of ProCA1-affibody.....	47
2.7	Cell culture and mammalian expression.....	48
2.8	Cancer cell targeting.....	49
2.8.1	Enzyme linked immunosorbent assay (ELISA) .....	49
2.8.2	Western blotting.....	50
2.8.3	Radio-active assay on cancer cells.....	51
2.8.4	Immunofluorescent staining in cancer cells .....	52
2.8.5	Flow cytometer assay (FACS).....	53
2.8.6	Magnetic Resonance Imaging (MRI) in cancer cells .....	53
2.9	Animal experiments .....	54
2.9.1	Nude mouse xenograft model.....	54
2.9.2	Nude mouse orthotopic model.....	54
2.9.3	Magnetic Resonance Imaging (MRI) of tumor mouse.....	55
2.9.4	Near infra-red (NIR) imaging of tumor mouse .....	55
2.9.5	Biodistribution and blood circulation measurements.....	56
2.9.6	Biodistribution measurements by ICP-OES .....	56

2.10	Histology analysis .....	57
2.10.1	Preparation of tissue slices .....	57
2.10.2	Immunohistology chemistry (IHC) on paraffin embedded slices .....	58
2.10.3	Immunofluorescent staining on frozen slices.....	58
2.11	Measure immunogenicity of ProCA1-affi.....	59
2.12	Measurement of Acute toxicity.....	59
Chapter 3. DESIGN, PREPARATION AND <i>IN VITRO</i> CHARACTERIZATION OF HER2		
TARGETD PROCA1 USING AFFIBODY .....		
3.1	Introduction.....	61
3.2	Results and Discussion .....	63
3.2.1	Designed HER2 targeted protein based contrast agent with one Gd <sup>3+</sup> binding site.....	63
3.2.2	Generation of targeted ProCA1-affi342 .....	66
3.2.3	Conformational analysis of ProCA1-affibody .....	71
3.2.4	Modified ProCA1-affibody has been increased both in metal binding affinity and relaxivity	73
3.2.5	Other improved properties for modified contrast agents .....	75
3.2.6	Dual label ProCA1-affibody with NIR dye .....	77
Chapter 4. CELLULAR TARGETING CAPABILITY ANALYSIS.....		
		82

4.1	Introduction.....	82
4.2	Results and Discussion .....	83
4.2.1	Selection of cell lines .....	83
4.2.2	Monitoring cell targeting of Affibody variants using western blotting.....	83
4.2.3	Immunofluorescent staining of cancer cells with ProCA1-affi .....	86
4.2.4	Cancer cells treated by different amount of ProCA1-affibody demonstrate the quantitative monitoring capability of designed MRI contrast agents .....	91
4.2.5	Flowcytometry measures the constant binding of ProCA1-affi342 to cancer cells	93
4.2.6	Generation of antibody against ProCA1-CD2-m.....	97
4.2.7	Quantitative analysis of MRI signals in cancer cells .....	100
4.2.8	Cell binding was analyzed by measuring retention of <sup>153</sup> Gd cheleted with ProCA1-affi342.....	100
4.2.9	Summary and future work.....	102
Chapter 5. ESTBLISHING TUMOR MODELS AND MOLECULAR IMAGING OF HER2 IN MOUSE BY MRI AND NIR AND FURTHER ANALYSIS BY HISTOLOGY ASSAYS .....		
5.1	Introduction.....	104
5.2	Results and discussion.....	106
5.2.1	Cell preparation for xenograft tumor model.....	106

5.2.2 MRI on xenograft model indicates the specific targeting of ProCA1-affibody.....	106
5.2.3 NIR imaging shows relative distribution of ProCA1-affibody in various mouse organs.....	110
5.2.4 Immunofluorescent staining of frozen tissue slides can demonstrate the tissue penetration of ProCA1-affibody.....	112
5.2.5 MRI blocking experiment further confirmed the tumor targeting.....	114
5.2.6 Advantages of ProCA1-affibody to antibodies in tumor targeting.....	116
5.3 Conclusion .....	121
Chapter 6. BIODISTRIBUTION AND PHARMOKINETIC STUDY OF DEVELOPED CONTRAST AGENTS	124
6.1 Introduction.....	124
6.2 Results and discussion.....	126
6.2.1 Distribution calculation by NIR signals in different mouse organs.....	126
6.2.2 Bio-distribution and blood retention by $^{153}\text{Gd}$ assay.....	129
6.2.3 Bio-distribution with ICP-OES .....	133
Chapter 7. EFFECTS OF DRUG TREATMENTS DETERMINED BY PROCA1-AFFIBODY ....	136
7.1 Introduction.....	136
7.2 Results and discussion.....	137

7.2.1 Both receptor level and cell survival decrease after been treated by Herceptin.....	137
7.2.2 Monitoring the receptor change after drug treatment using flow cytometry .....	138
7.2.3 ProCA1-affibody can monitor the total receptor change in cancer cells by MRI.....	140
Chapter 8. MONITORING CHANGES IN BIOMARKERS OF DISTRIBUTIONS AND EXPRESSION LEVELS DURING BREAST CANCER PROGRESSION BY TARGETED PROTEIN BASED CONTRAST AGENTS.....	142
8.1 Introduction.....	142
8.2 Results and discussion.....	150
8.2.1 Biomarker changes during the prognosis.....	150
8.2.2 Generation of EGFR targeted contrast agent .....	150
8.2.3 MR imaging of orthotopic tumors .....	154
8.2.4 MRI can monitor distribution of biomarkers.....	157
Chapter 9. OTHER CONTRAST AGENTS WITH MULTIPLE METAL BINDING SITES .....	160
9.1 Designing HER2 targeted contrast agent by using mutated CaM as host protein (ProCA22-affi342).....	160
9.2 Toxicity of protein based contrast agents.....	161
Chapter 10. CONCLUSIONS AND MAJOR DISCOVERIES .....	165

PUBLICATIONS AND MANUSCRIPT IN REVISION .....	170
MANUSCRIPTS IN PREPARATION .....	171
Appendix I .....	172
Establish mammalian expression and purification of HER2-ECD.....	172
Appendix II .....	175
Vaccine and Monkey virus .....	175
REFERENCES .....	184

**LIST OF TABLES**

Table 1 EGFR overexpression rate in different stages of cancers	14
Table 2 HER2 overexpression rate in different stages of cancers	15
Table 3 HER2 inhibitor in clinical use	19
Table 4. Physicochemical characteristics of commercially-available, extracellular, predominantly renally excreted gadolinium-based MR contrast agents.	36
Table 5 Contents of all the variants	41
Table 6 HER2 expression level in various cancer cells	84
Table 7 Biodistribution of Radioactive assay in CD1 mice	132
Table 8 Bio-distribution of ProCA1-affi-m was measured by ICP-OES at various time points	134
Table 9 Bio-distribution of MRI contrast agents was measured by ICP-OES to optimize the modification condition	135
Table 10 Table of different breast cancer types	143
Table 11 Acute Toxicity of ProCA1-affi342	161



**LIST OF FIGURES**

Figure 1.1 Occurrence of different cancers in western countries.	2
Figure 1.2 EGFR family and its targeting molecules	5
Figure 1.3 Algorithm for Herceptin use	7
Figure 1.4 EGF receptor activation.	9
Figure 1.5 Crystal structure of HER2 and HER2-Herceptin complex	11
Figure 1.6 EGFR (A) and HER2(B) are negative prognostic factors in breast cancers	12
Figure 1.7 HER2 expression level of various cancer cells	17
Figure 1.8 Therapeutic effects through antibodies	22
Figure 1.9 Structure and Sequences alignment of affibody	24
Figure 1.10 $Z_{HER2:342}$ is endocytosed into SKBR-3 cancer cells with HER2 over expression	25
Figure 1.11 Spatial resolution and penetration depth of molecular imaging techniques	32
Figure 1.12 Model structure of ProCA1-CD2	35
Figure 2.1 DNA map of PGEX-2T vector	44
Figure 2.2 DNA map of PET-20b vector	44
Figure 3.1 Model Structure of ProCA1-CD2	64
Figure 3.2 Model Structure of ProCA1-affibody.	65
Figure 3.3 Construction of ProCA1-affi342.	66
Figure 3.4 Purification Scheme	67

Figure 3.5 SDS gel of expression and initial purification by GS-4B column	68
Figure 3.6 Purification of PEGylated ProCA1-affi342 with cation exchange column	69
Figure 3.7 SDS gel of purified ProCA1-affi342m from SP column	70
Figure 3.8 Expression of ProCA1-affi342 in PET20b vector	71
Figure 3.9 Tryptophan Fluorescence measurement.	72
Figure 3.10 The secondary structure measured by CD.	73
Figure 3.11 Metal binding affinity measurement.	74
Figure 3.12 Relaxivity of ProCA1-affibody.	75
Figure 3.13 SDS gel to measure the stability of modified contrast agent	76
Figure 3.14 PEGylation substantially reduced the immune responses monitored by poly-antibodies.	77
Figure 3.15 Chemical structure of Cy5.5 dye	77
Figure 3.16 Extinction Coefficient of Cy 5.5 was measured	78
Figure 3.17 Conjugation rate measurement	79
Figure 3.18 MS spectra of free protein and conjugated protein	80
Figure 3.19 NMR spectra of free protein and protein-dye complex	81
Figure 4.1 Western blot of ProCA1-affi been retained in the cancer cells	85
Figure 4.2 ELISA of ProCA1-affi342	86
Figure 4.3 Immunostaining of HER2 on cell membrane.	88
Figure 4.4 Cell staining by ProCA1-affi WT	89
Figure 4.5 Immunostaining for endocytosis studies.	90
Figure 4.6 NIR imaging of living cells.	91

Figure 4.7 Immuno staining of Cancer cells at various time points	92
Figure 4.8 ELISA results to measure the binding to cancer cells	93
Figure 4.9 Binding affinity measurements (A) and Curve fitting of the binding between ProCA1-affi342m and SKOV-3 cancer cells (B)	95
Figure 4.10 Curve fitted by Hill equation	96
Figure 4.11 Competative assay to measure the cell binding	97
Figure 4.12 Western blotting of anti0serum activity	99
Figure 4.13 Purified antibodies from anti-serum	99
Figure 4.14 The HER2 positive cells SKOV-3 can be imaged under MRI after incubated with various concentrations of contrast agents.	100
Figure 4.15 Different concentrations of ProCA1-affi342 been retained in the cancer cells by radioactive assay.	101
Figure 4.16 Radioactive assay to measure the cell binding of ProCA1-affibody.	102
Figure 5.1 NIR imaging on Xenografted mouse.	107
Figure 5.2 MRI of Xenografted mouse with Fast Spin Echo.	108
Figure 5.3 MRI of Xenografted mouse with Gradient Echo.	109
Figure 5.4 NIR imaging of mouse organs.	111
Figure 5.5 IHC staining on mouse tissues for biodistribution studies.	113
Figure 5.6 Magnetic resonance images and image intensities of the mouse tumor pre-blocked by affibody Z <sub>HER2:342</sub> .	115
Figure 5.7 Direct staining with SKOV-3 tumors.	118
Figure 5.8 Compare the tissue penetration with HER2 antibody by IHC.	119

Figure 5.9 The tissue penetration properties of ProCA1 –affi-m were compared with antibody by IHF staining.	120
Figure 6.1 Biodistribution demonstrated by NIR imaging	127
Figure 6.2 Average intensity of each organ by NIR measurement	128
Figure 6.3 Western blotting of quantitative analysis of distribution	128
Figure 6.4 Biodistribution demonstrated by IHC	129
Figure 6.5 Western blotting of blood retention	130
Figure 6.6 Bio-distribution of ProCA1-affi by <sup>153</sup> Gd radioactive assay.	131
Figure 6.7 Blood circulation of ProCA1 series contrast agents	132
Figure 7.1 ELISA assay to monitor the HER2 receptor level changes after being treated with Herceptin in SKOV3 cells.	137
Figure 7.2 Western blotting results indicated that the total receptor number decreased about 35% after five days of treatments with Herceptin	138
Figure 7.3 Drug treatment measured by flow cytometry	139
Figure 7.4 Flow cytometry demonstrated the receptor level change after being treated with Herceptin.	140
Figure 7.5 MR images of SKOV3 cells after various days of treatments by Herceptin	141
Figure 8.1 Histological special breast cancer types	144
Figure 8.2 Progression of DCIS tumors	145
Figure 8.3 EGFR and HER expression levels in a human breast cancer xenograft derived from a basal type of breast cancer cell line (MCF-10DCIS)	149
Figure 8.4 Sequence of ProCA1-affibody-EGFR	150

Figure 8.5 ELISA of cell binding with EGFR high expression	152
Figure 8.6 Immunostaining of cancer cells by ProCA1-affibody-EGFR	153
Figure 8.7 Immuno staining of ProCA1-affi1907 in SKOV-3 cancer cells	154
Figure 8.8 MRI of orthotopic model.	155
Figure 8.9 MRI of orthotopic tumor model with fast spin echo	156
Figure 8.10 MRI of orthotopic tumor model with gradient echo	157
Figure 8.11 MR images can demonstrate the structure difference at the edge and core of the tumor	158
Figure 8.12 Tumor structure can be measured by MRI and IHC	159
Figure 9.1 Measurement of creatinine concentration in mouse blood	162
Figure 9.2 The enzyme in liver of ALT (alanine aminotransferase) and ALP(Alkaline Phosphatase) activity	163
Figure 9.3 Metal concentration in blood has been measured	164

**LIST OF ABBREVIATIONS**

AP	Alkaline Phosphatase
CaM	Calmodulin
CD	Circular dichroism
CD2	Cluster of differentiation 2
CT	X-ray computed tomography
DAPI	4'-6-Diamidino-2-phenylindole
DCIS	Ductal Carcinoma <i>in situ</i>
DMEM	Dulbecco's modified Eagle's medium
ECD	Extracellular domain
EGFR	Epidermal Growth Factor Receptor
ELISA	Enzyme-linked Immunosorbent Assays
FACS	Fluorescence Activated Cell Sorting
FITC	Fluorescein Isothiocyanate
FISH	Fluorescent <i>in situ</i> Hybridization
FRET	Fluorescence resonance energy transfer
GFP	Green fluorescent protein
GRPR	Gastrin Releasing Peptide Receptor
GST	Glutathione-S-transferase
HBSS	Hank's Buffered Salt Solution
HER	Human Epidermal Growth Factor Receptor

HRP	Horseradish Peroxidase
ICP-OES	Inductively Coupled Plasma Optical Emission Spectroscopy
IHC	Immunohistochemistry
IPTG	Isopropyl- $\beta$ -D-thiogalactopyranoside
K <sub>d</sub>	Dissociation constant
MRI	Molecular resonance imaging
NIR	Near infrared
NMR	Nuclear magnetic resonance
OCT	Frozen tissue matrix
OD	Optical density
PBS	Phosphate-buffered saline
PCR	Polymerase chain reaction
PEG	Polyethylene Glycol
PET	Positron-emission tomography
ProCA	Protein Based MRI contrast agents
PSA	Prostate Specific Antigen
SDS-PAGE	Sodium dodecyl sulfate polyacrylamide gel electrophoresis
SNR	Signal to noise ratio
UV	Ultraviolet

## **Chapter 1. INTRODUCTION**

### **1.1 Cancer as human diseases**

Cancer is caused by cells that grow uncontrolled and do not die. Normally, the cells in the human body will follow a rule of growth, division, and death. Programmed cell death is called apoptosis [1]. When this process is broken, cancer will form. Unlike regular cells, cancer cells do not experience programmatic death and instead continue to grow and divide. This leads to a mass of abnormal cells that grows out of control. In addition, cancer progression through different stages causes invasiveness and metastasis [2]

In nowadays, cancer has been one of the most common human diseases, 23% of which will cause death. More than 30% people in the world will receive cancer diagnosis during their life time [3]. As shown in Figure 1.1, breast cancer and prostate cancer have highest occurrence among all the cancers also with relatively high death rate [4]. Cancer diagnosis is mainly achieved by X-ray or biopsy. For example, breast cancer was also been detected by mammo-graphy since 1980s.

Prognosis is a prediction of probable outcome of a disease [5]. Since a lot of factors of individuals will affect the progress of disease, prognosis helps to identify which tumors are more aggressive than others and the possible progression of the tumor [6].



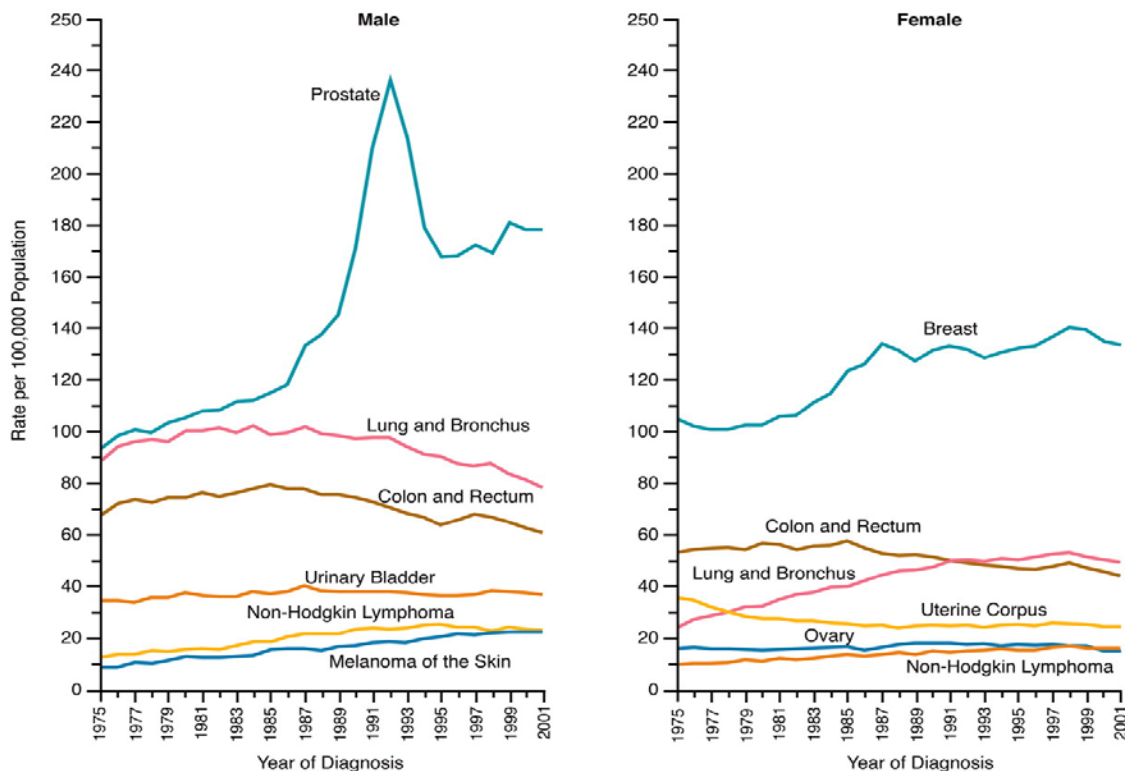


Figure 1.1 Occurrence of different cancers in western countries.

Although the death rate of cancer is decreasing due to the development of diagnosis and therapy, the occurrence of breast and prostate cancers are still increasing. Both of the cancers have highest occurrence in the western countries [7]

### 1.1.1 Biomarkers and its role in diagnosis, prognosis and treatment

Molecular targets, which are called biomarkers were discovered by researchers [8]. Since cancer is one of the common diseases in the world today, cancer biomarkers are of most interests for researchers. An early diagnosis of cancers determines the possibility of curing disease[9] because the tumor will always prognoses into invasive tumor or metastasis into other organs, which makes the therapy even more difficult . Therefore, it is necessary to find a target molecule as a biomarker. In order to diagnose or prognoses the cancers accurately and facilitate early diagnosis that increases the possibility of curing the cancers,

Various diagnosis assays have been developed based on the analysis of biomarkers [10]. For example, From 1970s, cervix cancer diagnosis by cell sample analysis has been offered. PSA (Prostate Specific Antigen) in the urea or blood sample has been used to be widely applied to diagnosing the prostate cancers [11].

The preferred targets for tumors should be present only in tumor cells and easily recognized by targeting reagents during blood circulation. Therefore, cell surface molecules or structures in extracellular matrix are suitable for functioning as biomarkers [12]. For example, PSMA (Prostate Specific Membrane Antigen) and HER2 are cell membrane proteins which express in high level only in specific prostate or breast cancers.

The perfect target structure for use in tumor targeting should be present only in tumor cells, and be easily accessible for targeting agents located in the blood. This makes cell surface structures, or structures located in the extracellular matrix, suitable. It is also important that the target is available during the whole treatment time, so that the cancer cells do not down regulate its expression during treatment. This can be achieved if the target structure is needed for the cancer cell to grow and divide.

Biomarkers have provided valuable information in patient selection. By estimating the highest benefit from the treatment, the treatment population can be enriched by biomarkers identification. Therefore, biomarkers play important roles in two aspects: first, biomarkers will define which patients will benefit from the disease treatment by drugs; second, whether the drugs function properly according to the expected mechanism based on biomarkers [13]. In nowadays, almost half of the new developed molecular entities are involved in biomarker elements.

Although biomarkers have been expected to increase the success rates in cancer diagnosis and treatments, there are still several challenges in clinical application of biomarkers [14]. First, the clearly understanding of biomarkers in the development of cancers is required for the clinical process [15]. Second, reliable testing assay of biomarkers is needed for the reproducible results. Although PSA is widely used for prostate cancer patient screening, it is not accurate, with many false positives that gives wrong information if diagnosis [16]. Third, the detection boundaries have to be defined by the constant testing. Fourth, the possible function of a novel biomarker during a planned therapeutic strategy has to be estimated before been applied [17]. In a summary, all these factors have to be well considered before and during the clinical application of biomarkers.

To be a biomarker, the molecule must possess several properties: it exists in tumor cells rather than normal cells; it can be easily detected by targeting agents either in blood or tissue; the molecule is available during the treatment period. The cell surface molecules or molecules located in extracellular matrix have the highest possibility to be a biomarker.

In nowadays, almost half of the new molecular entries are involved in the development of biomarkers. Targeted prognosis and therapy have increased survival percentage [12]. Designing targeted contrast agents can benefit for the diagnosis and prognosis of diseases. One subject of the biomarkers for cancer is receptor on cell surfaces which are widely studied. The popular receptors like PSA (prostate specific antigen), GRPR (gastrin releasing peptide receptor), EGFR (epidermal growth factor receptor) family have been applied clinically for cancer determination and therapy [18-19]. These receptors always get over expressed in various cancer cells. The expression level is also related with the cancer stage [20-21]. Gastrin releasing pep-

tide (GRP) is a member of bombesin like family of which pre-protein is cleaved into GRP of 27 amino acids or neuromedin C of 10 amino acids [22]. GRP is widely used to conjugate with nanoparticles, quantum dots or other probes to function as a targeted contrast agent against GRPR [19]. Similar as GRP, EGF is the ligand for EGFR, which is the first member of EGFR family (Figure 1.2). There is a high expression level of both EGFR and EGF in various cancer cells, like breast cancers, ovarian cancers and pancreatic cancers [23].

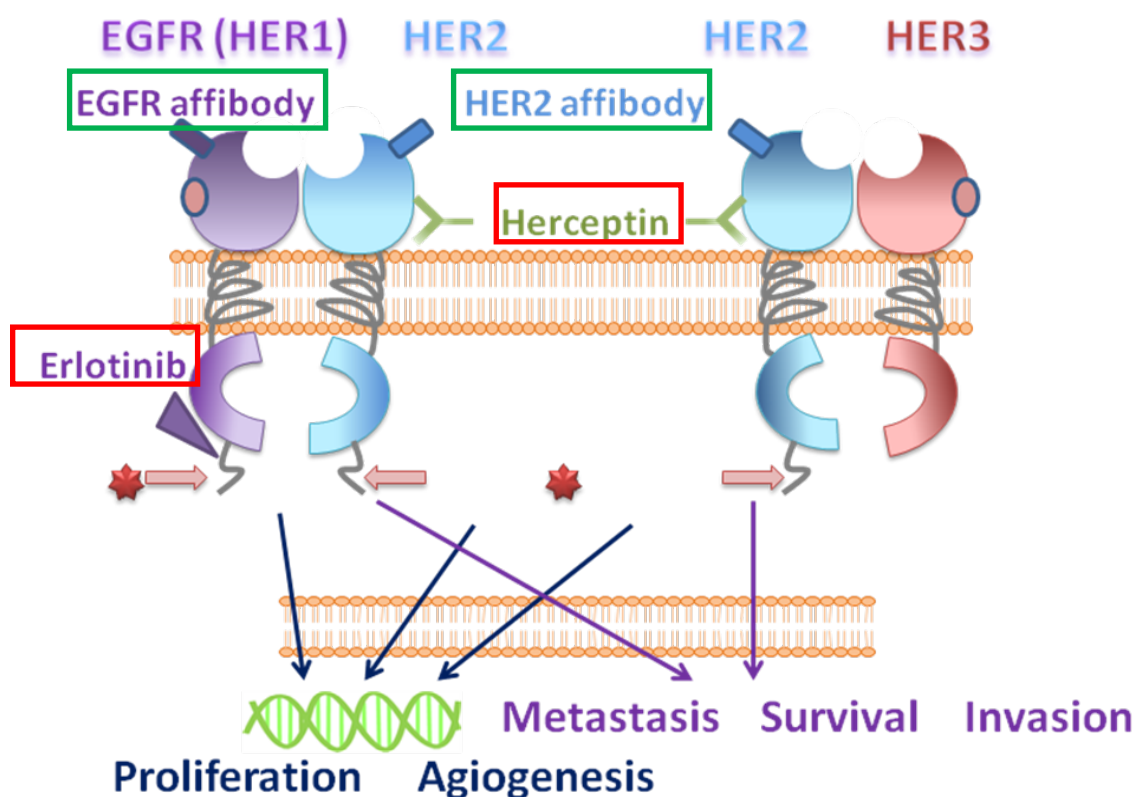


Figure 1.2 EGFR family and its targeting molecules

All the members in EGFR family have an extracellular domain (ECD), a trans-membrane domain and an intra-cellular domain. HER2 is the one that does not have a natural ligand for the ECD which tends to form dimer with other members. HER3 is the one lack of a kinase domain. With some ligand binding in the ECD of either member in the former dimer, the inner kinase pathway may be activated which will promote cell proliferation and agiogenesis.

### 1.1.2 Detection of biomarkers

Many techniques have been developed to measure specific biomarkers at protein, DNA or RNA levels; for example, immunohistochemistry (IHC), enzyme-lined immunosorbent assays (ELISA), fluorescent in situ hybridization (FISH) and real time polymerase chain reaction (RT-PCR), as well as Flowcytometre (Figure 1.3). In order to get reproducible and reliable results from the assays, Validation of the methods is critical to the assay [24].

Take one of the most famous biomarkers for breast cancer, HER2 (human epidermal growth factor receptor 2) as an example (Figure 1.2). Since HER2 is involved in signal pathway by the intracellular kinase domain. The mutation of the kinase gene will result in poor prognosis. Therefore, RT-PCR of the mutated gene can predict the abnormal function of the biomarkers [25]. HER2 gene also encodes a trans-membrane protein with the extracellular domain as a target for antibodies. Several antibodies against HER2 have been developed which makes IHC is widely used to measure the expression level of HER2 protein which is related to the disease stage.

However, most of these established methods are invasive by biopsy or surgery. Unfortunately, the clinical application of targeted therapy is largely limited by current methods for assessment of these cancer biomarkers using invasive methods such as biopsy. One of five HER2/Neu clinical tests, including biopsy and immunostaining (IHC) provides incorrect results, which severely affect the selection of appropriate patients for personalized treatment using HER2/EGFR targeted cancer therapies. Limitations of these methods are mainly because of invasiveness. They cannot monitor the tumor in real time.

As shown in Figure 1.3, current diagnosis of HER2 is first based on IHC results. IHC will predict the expression level of HER2 which is related to the tumor stages. The expression of HER2 is generally divided into 4 levels, and only the highest level is suitable for targeted therapy. The cancers with lower level of HER2 will need further analysis by FISH to determine the HER2 gene. However, IHC needs surgery to get the tissue samples for analysis. FISH also need to use biopsy to get the tissue sample. These invasive techniques may stimulate the tumor growth and metastasis [26].

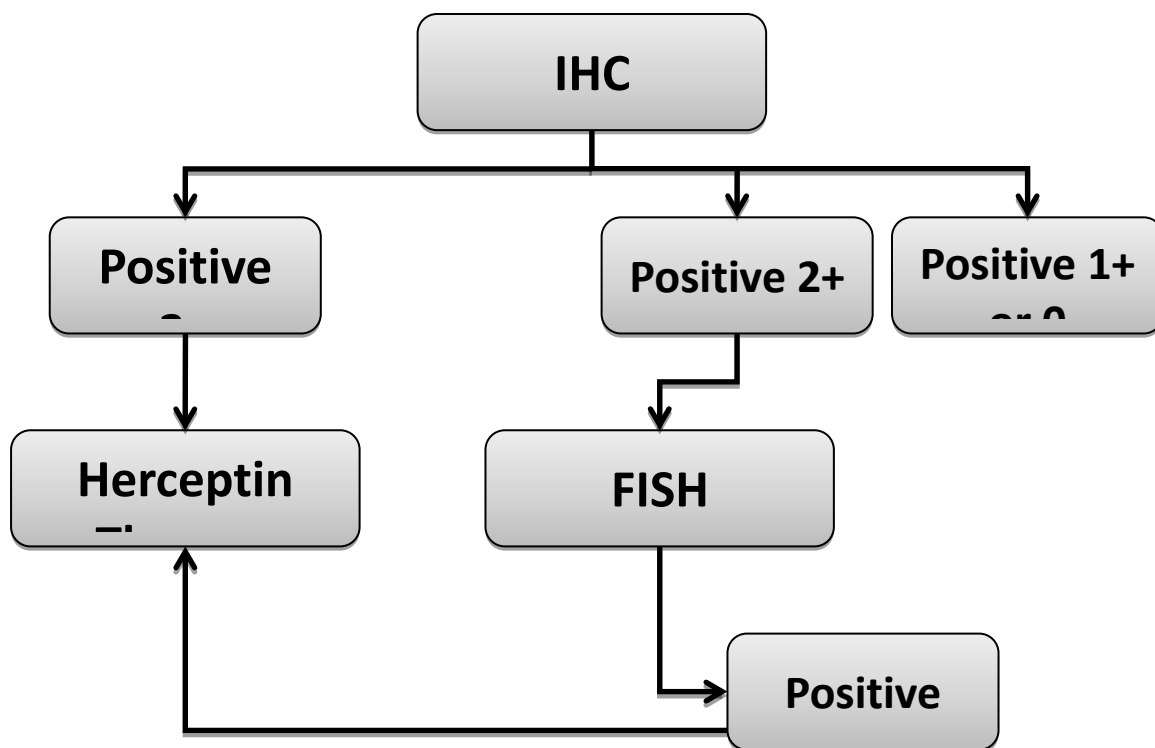


Figure 1.3 Algorithm for Herceptin use

In order to diagnose whether the specific type of breast cancer is suitable for Herceptin therapy, Cancer tissue samples are required for the diagnostic method of IHC. Only the HER2 level detected by IHC is up to stage 3, this type of cancer is illegible for Herceptin treatment. If the expression level is in stage 2, further diagnosis with FISH to amplify the HER2 DNA will be taken to confirm the treatment methods [27].

## 1.2 EGFR family function as biomarkers for diagnosis and therapy

The epidermal growth factors (EGF) induce signal transduction by activating the kinase domain of the epidermal growth factor receptors (EGFR) to promote cellular proliferation and survival (Figure 1.2). EGFRs are comprised of four family members: EGFR/HER1, HER2/Neu, HER3 and HER4, respectively. They share similar structures with an extracellular ligand binding domain, a transmembrane domain, and a functional intracellular tyrosine kinase domain (except for HER3). Different from other three receptor family members, HER2/Neu does not have a natural ligand and its ECD domain is able to adopt an activated state to dimerize with EGFR or HER3 (EGFR/HER2, HER2/HER3). HER2 is the preferred dimerization partner in the EGFR family. HER2/Neu and EGFR are also major prognosis biomarkers over-expressed in various types of cancer cells [28] and tissue samples from cancer patients [20, 29].

Various carcinomas, like glioma, bladder carcinomas and lung cancers, have overexpression of EGFR proteins [30-31]. The EGFR has many ligands, such as EGF and Transforming Growth Factor- $\alpha$ (TGF- $\alpha$ ). As shown in Figure 1.4, ligand binding cause conformational change which exposing the dimerization of domain II. Because of the effects of dimerization, the tyrosine kinase sites located in the intracellular domain get phosphorylated. However, Her2 is not dependent on the ligand activation. HER2 is the preferred dimerization partner for all the other members in the EGFR family. When overexpressed, HER2 homodimers are often formed [32].

### 1.2.1 Structure of EGFR family proteins

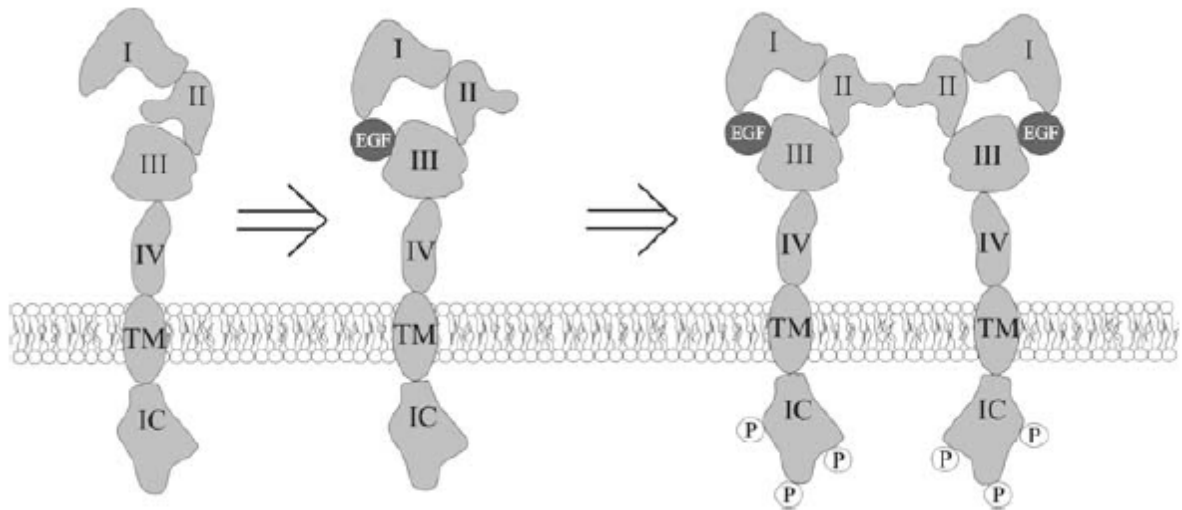


Figure 1.4 EGF receptor activation.

I-IV: domains of the extracellular part of the receptor, TM: transmembrane domain, IC: Intracellular domain. Binding of EGF to the domain one and three of EGFR (HER1) ECD will cause the form change of domain and lead to homo-dimerization.

Figure 1.2 shows that the epidermal growth factors (EGF) induce signal transduction by activating the kinase domain of the epidermal growth factor receptors (EGFR) to promote cellular proliferation and survival. EGFRs are comprised of four family members: EGFR/HER1, HER2/Neu, HER3 and HER4, respectively.

They share similar structures with an extracellular ligand binding domain, a transmembrane domain, and a functional intracellular tyrosine kinase domain (except for HER3). The EGFR has many ligands, such as EGF and Transforming Growth Factor- $\alpha$ (TGF- $\alpha$ ). As shown in Figure 1.4, ligand binding cause conformational change which exposing the dimerization of domain II. Because of the effects of dimerization, the tyrosine kinase sites located in the intracellular domain get [33].



Different from other three receptor family members, HER2/Neu does not have a natural ligand. HER2 is the preferred dimerization partner for all the other members in the EGFR family. When overexpressed, HER2 homodimers are often formed [34-35]. Its ECD domain is able to adopt an activated state to dimerize with EGFR or HER3 (EGFR/HER2, HER2/HER3). Among the EGFR members, HER2 is the one which is lack of natural ligand for the extracellular domain. Therefore, HER2 has to form dimer with other family members to activate the downstream signal pathway [36]. Since HER3 is lack of the tyrosine kinase domain, when HER2 and HER3 form into a heterodimer, binding of the ligand to HER3 will activate the tyrosine kinase function of HER2. Various antibodies or other peptides have been developed to target to HER2 (Figure1.5). To date, there are structures of extracellular domains have been determined mainly by X-ray crystallography [37]. As shown in Figure 1.5, these structures reveal a fixed conformation for HER2 that resembles a ligand-activated state, and show HER2 poised to interact with other ErbB receptors in the absence of direct ligand binding. Herceptin binds to the juxtamembrane region of HER2, identifying this site as a target for anticancer therapies [37]. This binding may facilitate the endocytosis by providing direct interaction of the formed steric barrier to the transmembrane regions [38]. By identify the binding patterns of Herceptin Fab domain and HER2 ECD, a basis of designing new targets for HER2 has been generated for diagnosis and therapeutic effects.

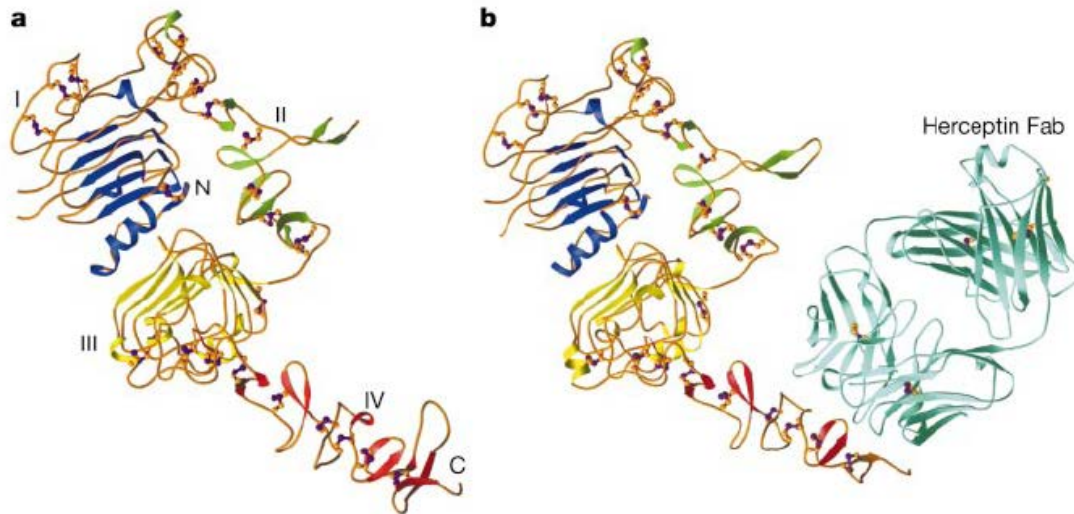


Figure 1.5 Crystal structure of HER2 and HER2-Herceptin complex

The Fab domain of antibody Herceptin targets to the domain 4 of HER2 ECD close to the transmembrane domain. This may facilitate the endocytosis of HER2 after binding with Herceptin. The ADCC (antibody dependent cytotoxicity) will be triggered after binding [37].

### 1.2.2 Roles of EGFR family in tumor formation and growth

As epidermal growth factor receptors, HER family proteins express on the cell membrane. Both of the transmembrane proteins are important in tissue normal growth and development [39]. The expression level of EGFR is relatively low in normal tissues except normal skin epithelial cells. EGFR is also widely expressed in the tumor epithelial cells [40-41]. The expression level of HER2 is about  $10^3$ - $10^4$  per normal cell; however, the expression is up to  $10^6$  per cell in cancer cells especially in breast cancers.

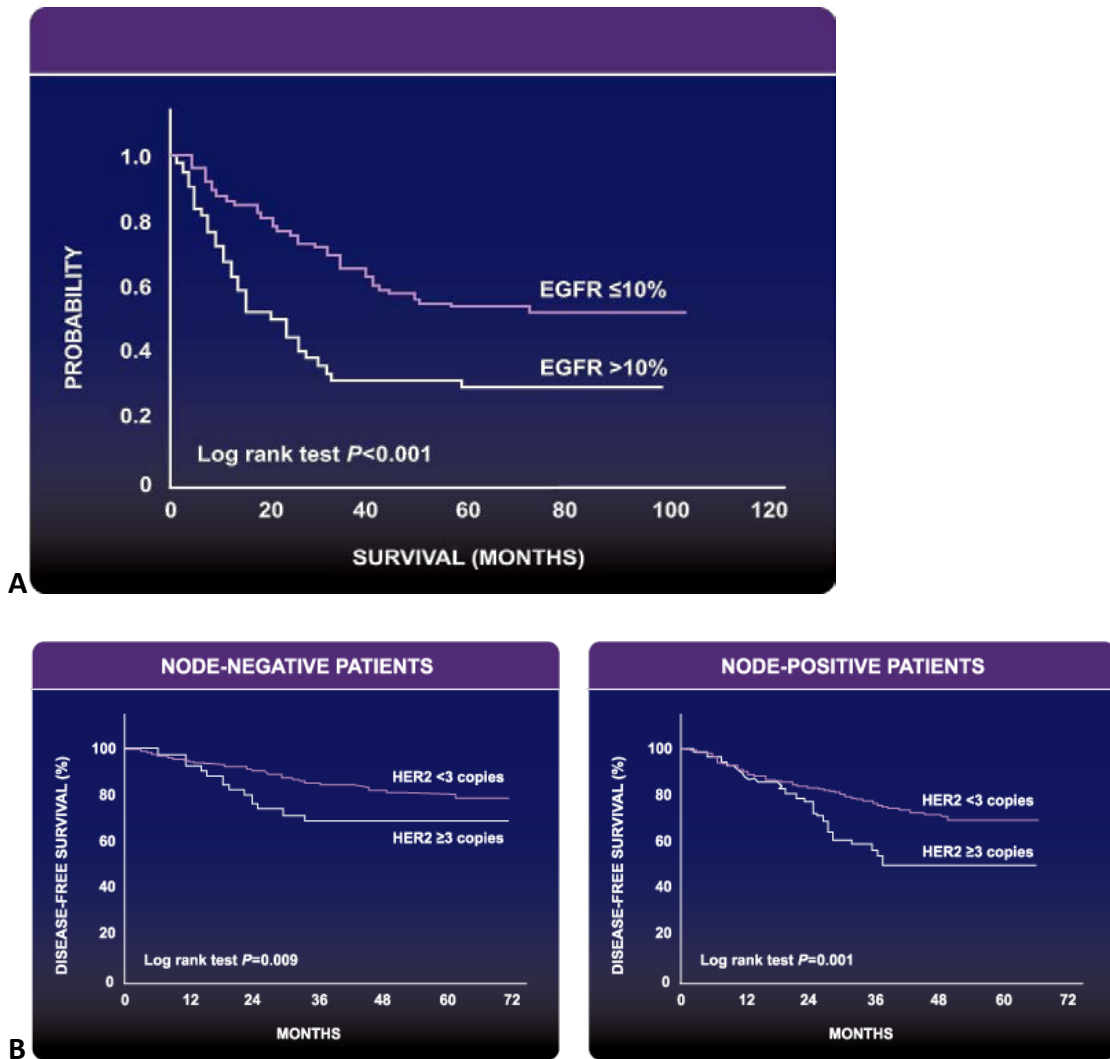


Figure 1.6 EGFR (A) and HER2(B) are negative prognostic factors in breast cancers. Those biomarkers that indicate lower survival rate are called negative prognostic biomarkers. Those cancer cells with higher expression level of EGFR or HER2 will have relatively lower survival rate and shorter survival time [42-43].

EGFR family members play an important role in various tumor etiology including breast cancers, ovarian cancers, pancreatic cancers, prostate cancers and lung cancers (Figure 1.6). The over expression of EGFR proteins as a consequence of amplification of EGFR genes in cancer cells is involved in tumor metastasis and aggressiveness. The reason of the over expression

of EGFR proteins is due to the character of EGFR as they can cause the loss of tumor suppression gene because EGFR is mutationally activated in half of the cancer cells [41].

Among of the members, HER1 and HER2 are two well established biomarkers for diagnosis and treatments. About 30% of the breast cancers have over expression of HER1 or HER2. HER1 over-expresses in many solid tumors. By binding with its ligands, a signaling network will be triggered (Figure 1.2). The tyrosine kinase domain will be activated for the downstream signal path way [1, 44]. Therefore, the cell proliferation and angiogenesis will be promoted and the cell apoptosis will be inhibited [1]. The HER2 positive breast cancer is correlated with high metastasis and low survival rate. HER2/Neu and EGFR are also major prognosis biomarkers over-expressed in various types of cancer cells [28] and tissue samples from cancer patients [20, 29]. Various carcinomas, like glioma, bladder carcinomas and lung cancers, have overexpression of EGFR proteins [30-31]. Table 1 shows that up to 69% percentage of tumors have high expression level of EGFR especially in later stage. Table 2 shows HER2 has high expression level in about 30% tumor cells. However, HER2 expression is also over expressed in the early stages of these cancers, which will benefit for the early diagnosis [45].

Table 1 EGFR overexpression rate in different stages of cancers

Source	N	Definition of HER1/EGFR overexpression/ <i>EGFR</i> amplification	Percentage of tumors overexpressing HER1/EGFR
Onn et al, <i>Clin Cancer Res</i> , 2004	111	2 or 3 staining by IHC	60%
Rusch et al, <i>Cancer Res</i> , 1993	44	Increase detection by Northern analysis	45%
Selvaggi et al, <i>Ann Oncol</i> , 2004	48	2+ or 3+ staining by IHC	37%
Ohtsuka et al, <i>J Thorac Oncol</i> , 2006	48	2+ or + by Western blotting	40%
Dancer et al, <i>Oncol Rep</i> , 2007	32	Two-fold or greater amplification of the <i>EGFR</i> gene by FISH	65%
Bloomston et al, <i>Dig Surg</i> , 2006	71	1+ or higher staining by IHC	69%
Thybusch-Bernhardt et al, <i>Int J Surg Investig</i> , 2001	24	Positive staining by IHC	33%

Table 2 HER2 overexpression rate in different stages of cancers

Source	N	Definition of HER2 overexpression/HER2 amplification	Percentage of tumors with HER2 overexpression/HER2 amplification
Slamon et al, <i>Science</i> , 1987	189	Two-fold or greater amplification of <i>HER2</i> gene by Southern blot	30%
Paik et al, <i>J Natl Cancer Inst</i> , 2000	2034	Definite membrane staining by IHC in any tumor cell	29%
Owens et al, <i>Clin Breast Cancer</i> , 2004	16,092 (FISH)	Two-fold or greater amplification of <i>HER2</i> gene by FISH	23%
	116,736 (IHC)	2+ or higher result by IHC	20%
Seshadri et al, <i>J Clin Oncol</i> , 1993 <sup>4</sup>	1056	Two-fold or greater amplification of <i>HER2</i> gene by slot blot	21%
Andrulis et al, <i>J Clin Oncol</i> , 1998	580	Two-fold or greater amplification of <i>HER2</i> gene by Southern blot, slot blot, and/or RT-PCR	20%

The over expression of EGFR and EGFR2 are associated with poor prognosis (Figure 1.6) [10, 46]. The epidermal growth factors (EGF) induce signal transduction by activating the kinase domain of the epidermal growth factor receptors (EGFR) to promote cellular proliferation and survival (Figure 1.2). HER2/Neu and EGFR are over-expressed in various types of cancer cells [28] and tissue samples from cancer patients. HER2 is a negative prognostic factor [20, 29]. In numerous clinical studies, it is reported to associate with shorter disease-free and overall survival for breast and ovarian cancers as well as increased risk of death. About 30% of all breast cancer cases are associated with expression of HER2/Neu. High expression of HER2/Neu closely correlates with low survival rate [45, 47-48]. The rate of HER2/Neu overexpression was estimated within a wide range of 6-35% in gastric cancer [49], 9-32% in ovarian cancer [50], and in up to 70% of human pancreatic cancer [51]. EGFR also leads to increased cell proliferation and

motility and decreased apoptosis [52]. EGFR is also a negative prognostic factor for multiple tumor types, including non-small cell lung carcinoma (NSCLC) and pancreatic cancer [53].

Co-expression of EGFR and HER2 is found in 10–36% primary human breast carcinomas, and it is generally associated with a poor prognosis compared with expression of a single receptor [34, 54-56]. To date, the roles of EGFR and HER2/Neu in the progression of pre-invasive ductal carcinoma in situ (DCIS) to potentially lethal invasive breast cancer remain under hot debate. HER2/Neu is overexpressed in 60 to 70% of DCIS tissues which is much greater than in invasive breast cancer tissues (~30%). In contrast, overexpression of HER2/neu is not found in normal ductal cells or in hyperplastic ductal cells [57]. In addition, it has been shown that 14 to 91% of human breast carcinomas express a high level of the EGFRs [52]. The majority (70%) of DCIS tissues identified by mammographic microcalcification are of high grade comedo type, which is associated with a high proliferation rate, lack of estrogen receptor, and high expression levels of EGFR and HER2/neu [53]. The importance of EGFR signaling in the growth of DCIS tissues is further supported by study results obtained from examination of the effects of an EGFR inhibitor, iressa, on human DCIS tissues xenografted in nude mice [58-59].

### **1.2.3 Distribution of EGFR family members in various cancers and cell lines**

There are more than 20 cell lines which have high expression level of HER2. They mainly come from breast tumor, ovarian and pancreatic tumors. Among these cell lines, several pairs of positive and negative HER2 cell lines are widely used in research (Table 3) [9].

SKBR-3 is one of the most traditional human breast cancer cell lines. This cell line was derived in 1970 from pleural effusion cells. AU-565 was established from the same patient as

SKBR-3. The AU565 cell line amplifies and overexpresses the HER2 oncogene; it expresses the HER-3, HER-4 and p53 oncogenes. The expression level of HER2 in AU565 is much higher than in SKBR-3. These two cell line are usually used to study the effect of drug or protein to HER2 cell lines. However, their tumorigenicity is very low. As a result of that, they are not proper for a tumor mouse model.

SKOV-3 cell line is a hypodiploid human cell line which originated from ovarain cancer. The Her2 expression level is higher than SKBR-3. It can generate tumor in nude mice with well differentiated adenocarcinoma. Because of its ability to generate well shaped tumors, it is widely used on nude mouse for Her2 tumor model. Compare with SKOV-3, BT474 is another cell line which is also commonly been used for generating tumors. BT-474 was isolated by E. Lasfargues and W.G. Coutinho from a solid, invasive ductal carcinoma of the breast. The expression level of BT474 is similar as AU565. Besides these genital cancers, pancreatic cancer sometime also has a high expression level of Her2, such as MIAPaca-2.

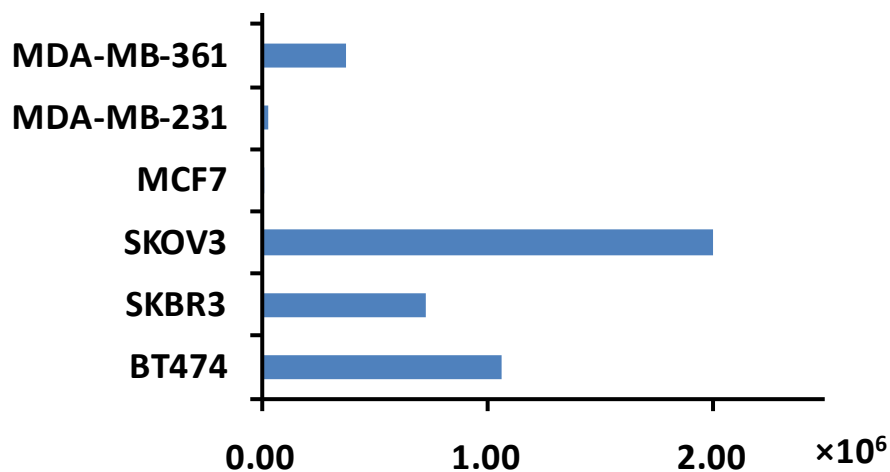


Figure 1.7 HER2 expression level of various cancer cells

The HER2 expression levels have been measured in different cell lines. The cell line SKOV-3, SKBR-3 and BT474 with an expression level up to  $10^6$  per cell are called HER2 positive cell lines. The cell lines with expression level less than  $10^4$  are called HER2 negative cell lines.



Based on the choice of positive cell lines, negative cell lines can be decided as a pair. For example, MCF-7 and MDA-MB-231 come from breast cancer which can be control for SKBR-3 and AU565 (Table 3). By choosing cell lines from similar sources, the species difference can be minimized.

Mouse EGFR-2 is different from HER2 which are from human. However, mouse EGFR-2 is also related to breast cancer of mouse. Both NT5 and EMT-6 are form mouse mammary cancer; EGFR-2 is overexpressed in NT5.

### **1.3 Targeted reagents for EGFR family**

Besides the endogenous ligands for EGFR members, various targeted reagents, like antibodies and peptides, have been developed against EGFR members. Based on the targeted region of the receptor, the targeted reagents can be generally divided into two types. One type of reagents targets to the intracellular domain of EGFR; while another type targets to the extracellular domain of EGFR [2, 60]. The intracellular targeting reagents are inhibitors to the tyrosine kinase domain. The reagents target to the extracellular domain can cause endocytosis, ADCC (antibody dependent cytotoxicity) effects of the cancer cells. The targeted molecules can be antibodies such as, Herceptin, protein domain such as EGF and affibody, peptide, such as Latibnib and small molecules such as Taxol [61]. The traditional cancer treatment like radiation therapy and chemotherapy, will affect all normal cells. To use protein as a drug, it will decrease the toxicity and increase the specificity.

The drugs are summarized in Table 4 [62]. Small molecules like Lapatinib function as the kinase domain inhibitor can inhibit both EGFR and HER2. The HER2 specific antibody like Trastuzumab (Herceptin) only target to the extracellular domain of HER2 which can inhibitor the HER2 expression specifically.

Table 3 HER2 inhibitor in clinical use [63]

<b>Drug</b>	<b>Type</b>	<b>Target</b>	<b>Source</b>	<b>Current clinical status</b>
<u>Monoclonal antibodies</u>				
Pertuzumab	Humanized	HER2	Genentech/Roche	Phase II trials in breast and ovarian cancer with other reagent
Trastuzumab	Humanized	HER2	Genentech/Roche	Lunched for breast cancer in combination with chemotherapy
<u>Tyrosine kinase inhibitors</u>				
Lapatinib	Thioquinazoline	HER1/HER2	GlaxoSmith Kline	Lunched for second-line breast cancer treatment in combination with capecitabine
EKB-569	Cyanoquinoline	HER1/HER2	Wyeth	Phase II trials in colorectal and non-small cell lung cancers
BIBW-2992	Quinazoline	HER1/HER2	Boehringer Ingelheim	Phase II trials in breast, non-small cell lung and head cancers
Neratinib	Cyanoquinoline	Pan-HER	Wyeth	Phase II trials in breast and non-small cell lung cancers
AEE-788	Pyrrrolopyrimidine	HER1/HER2	Novartis	Phase I/II
ARRY-543	Quinazoline	HER1/HER2	Array Bio-pharma	Phase I
BMS-599626	Pyrrrolotriazine	Pan-HER	Bristol-Myers Squibb	Phase I

### 1.3.1 Intra-cellular inhibitor an extra-cellular ligands of EGFR (HER1)

The epidermal growth factor receptors EGFR and HER2/Neu are highly expressed as biomarkers in various cancers and play important roles in cancer progression and survival. They are also the major drug targets. Several targeted drugs such as monoclonal antibodies (Hercep-

tin or Trastuzumab) and small inhibitors (Erlotinib) against HER2 and EGFR have been shown to be effective with patients over-expressing those biomarkers. Unfortunately, the clinical application of targeted therapy is largely limited by current methods for assessment of these cancer biomarkers using invasive methods such as biopsy. One of five HER2/Neu clinical tests, including biopsy and immunostaining (IHC) provides incorrect results, which severely affect the selection of appropriate patients for personalized treatment using HER2/EGFR targeted cancer therapies [34, 64].

The epidermal growth factors (EGF) induce signal transduction by activating the kinase domain of the epidermal growth factor receptors (EGFR) to promote cellular proliferation and survival (Figure 1.3). HER2/Neu and EGFR are over-expressed in various types of cancer cells [28] and tissue samples from cancer patients. HER2 is a negative prognostic factor [20, 29]. In numerous clinical studies, it is reported to associate with shorter disease-free and overall survival for breast and ovarian cancers as well as increased risk of death. About 30% of all breast cancer cases are associated with expression of HER2/Neu. High expression of HER2/Neu closely correlates with low survival rate [45, 47-48]. The rate of HER2/Neu overexpression was estimated within a wide range of 6-35% in gastric cancer [49], 9-32% in ovarian cancer [50], and in up to 70% of human pancreatic cancer [51]. EGFR also leads to increased cell proliferation and motility and decreased apoptosis [52]. EGFR is also a negative prognostic factor for multiple tumor types, including non-small cell lung carcinoma (NSCLC) and pancreatic cancer [53].

### 1.3.2 Engineered antibodies and drugs for HER2

Based on the function as biomarkers of HER2 and EGFR, especially HER2 without a natural ligand, a lot of antibodies have been developed against HER2. Antibodies have therapeutic function by several pathways. Because HER2 mediates cell signaling pathways such as PI3K and MAPK (mitogen activated protein kinase) pathways, antibody targeting to HER2 can cause ADCC effects which make the cancer cells be swallowed by macro cells [65]. At the same time, antibody can inhibit proteolysis of HER2 ECD and inhibition the HER2 DNA repair [35]. Regarding these mechanisms, antibody resistance is also developed by loss of antibody binding, increased downstream signaling and activation of alternative growth factor pathways.

As shown in Figure 1.3 and Table 3, several targeted drugs such as monoclonal antibodies (Herceptin or Trastuzumab) have been developed to against the ECD domain (which region) of the epidermal growth factor receptors EGFR and HER2/Neu expressed at the cell surfaces of various cancers [66-67]. Based on the function as biomarkers of HER2 and EGFR, especially HER2 without a natural ligand, a lot of antibodies have been developed against HER2 (Table 4).

Because HER2 mediates cell signaling pathways such as PI3K and MAPK (mitogen activated protein kinase) pathways, antibody targeting to HER2 can cause ADCC effects which make the cancer cells be swallowed by macro cells [65]. At the same time, antibody can inhibit proteolysis of HER2 ECD and inhibition the HER2 DNA repair [35]. Regarding these mechanisms, antibody resistance is also developed by loss of antibody binding, increased downstream signaling and activation of alternative growth factor pathways.

Due to antibody resistance, other techniques for curing cancer cell through antibodies are shown in Figure 1.8. The Fc domains of antibodies have been conjugated with drugs, toxic proteins, radioisotopes and chemotherapy drugs.

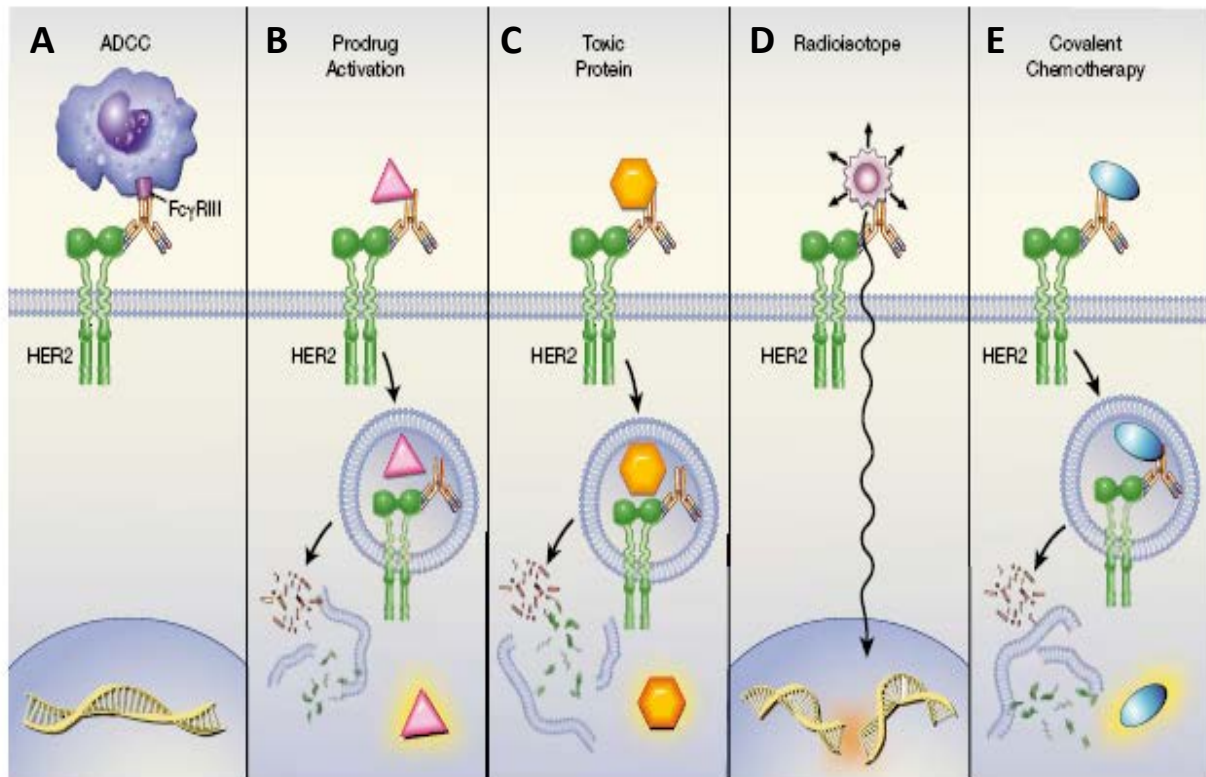


Figure 1.8 Therapeutic effects through antibodies

For antibodies been used as therapeutic reagents, they may kill the cancer cells or get cancer cells apoptosis in different mechanisms [68]. (A) ADCC effects will be triggered by antibody that helps the macro cells to swallow cancer cells. (B) The antibody is conjugated with some prodrugs which function as a drug once gets into cytosol by killing the cancer cells. (C) Some toxic proteins which binds to antibody non-covalently will be released in the cytosol and inhibit the cell growth. (D) For those radioactive labeled antibody, the radioactive reagents will break the DNA replication of cancer cells directly. (E) The antibody can also be conjugated with some clinically available chemotherapy medicine. Antibody will provide the specific targeting and help the chemotherapy medicine to locate in the cancer area which will eliminate the harmful effects to normal cells.

## 1.4 Affibody library and screening

Affibody was selected as our targeted sequence because the suitable size for molecular imaging of moderate circulation time [69]. Affibody is originated from the “z” domain of protein A, which contains 58 amino acids (Figure 2.1). A variant of this affibody called Z<sub>HER342</sub> can specifically target to HER2 with the K<sub>d</sub> of 22 pM. Because of its small molecular weight (7 KDa), there are more advantages than antibodies for the affibody to penetrate deeper tissue and target the HER2 positive sites. Affibody is able to penetrate the blood vessel and well distribution in the tumor mass. Biodistribution in SKOV-3 xenografts indicates that the up-take of reagent in tumor sites by affibody targeting [70-71].

### 1.4.1 Affibody derived from z-domain of Protein A and screened by phage display

Affibody originates from the “z” domain of protein A, which contains 58 amino acids. Affibody molecules with affinity for HER-2 were selected using phage display. The produced affibody molecules were tested for binding to HER-2 ECD immobilized to a Biacore sensorchip. Three generations of affibody for HER2 were developed. Z<sub>HER2-4</sub> is the first generation of affibody with 13 mutations at domain 1 and 2 (Figure 1-9). It has a K<sub>d</sub> for HER2 of 50 nM [72]. A variant of the second generation affibody called Z<sub>HER2:342</sub> has 7 mutations at L9M, Q11N, Q17A, A18L, W24N, T25Q and S26K from previous generation, which has a K<sub>d</sub> for HER2 about 22 pM (Figure 1-9) [73]. EGFR affibody call Z<sub>EGFR:1907</sub> was screened from affibody library by extracellular domain of EGFR which has a K<sub>d</sub> of 43.6 nM for EGFR [74].

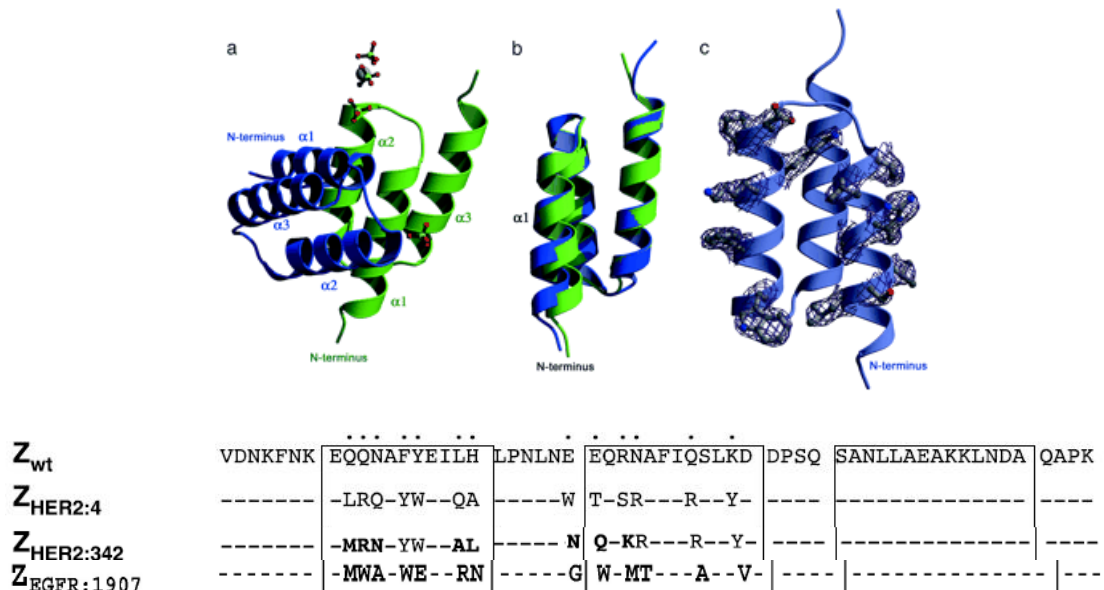


Figure 1.9 Structure and Sequences alignment of affibody

Affibody is a phage display library with 13 amino acids in domain 1 and domain 2 to be random. Different affibody variants are screened by specific antigen like HER2 or EGFR.  $Z_{HER2:4}$  is the first generation of affibody against HER2 and  $Z_{HER2:342}$  is the secondary generation which increase the binding affinity by changing the  $K_d$  from 50 nM to 22 pM.  $Z_{EGFR:1907}$  is a variant specific targets to EGFR.

There are several advantages for the affibody than antibodies as a Her2 targeting moiety. First, it can be quickly diffused in vivo and then target to the biomarkers. Second, the optimized size enables affibody to penetrate cell membrane for endocytosis. The endocytosis allows enough affibody molecules concentrate at the cancer cells, which fulfills the molecular imaging of biomarkers. Third, affibody can also be secreted out of the body in shorter time than antibodies, which will minimize the toxicity. The radioactively labeled affibody was injected into nude mice with SKOV-3 tumor model. Affibody can specifically target to the tumor in 24 hr [75]. Figure 1.10 shows that HER2 affibody  $Z_{HER2:342}$  can bind to cells with high expression level of HER2 and has the endocytosis effects [69]. As a targeting moiety, affibody has several advantages. First, it is relatively stable in vivo compared with peptide fragments. Second, HER2 affi-

body is able to penetrate deeper tissue. Third, Biodistribution in SKOV-3 xenografts indicates the up-take of reagent in tumor sites by affibody targeting.

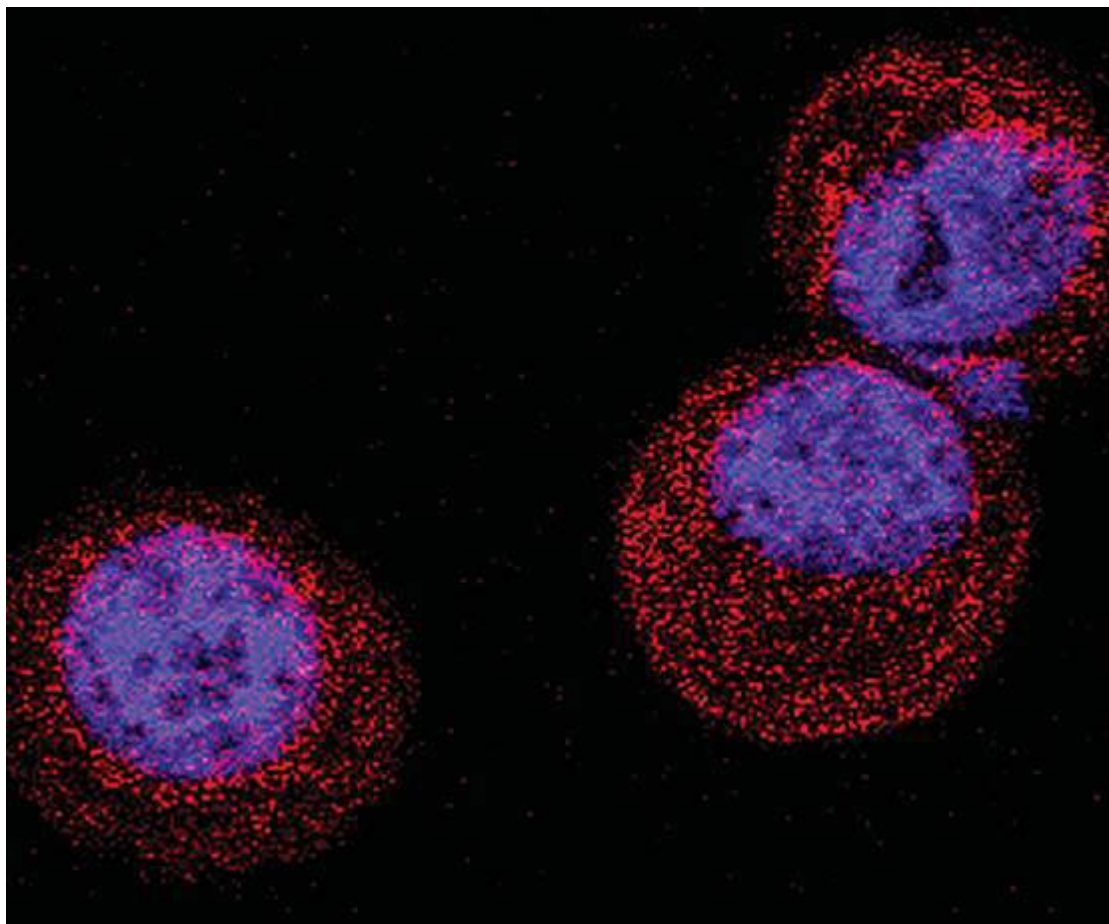


Figure 1.10 Z<sub>HER2:342</sub> is endocytosed into SKBR-3 cancer cells with HER2 over expression. HER2 is a protein on the cell membrane. The cells were stained with fluorescent (Fluo555 with excitation wavelength at 555 nm) conjugated affibody Z<sub>HER2:342</sub>. Staining in the cell plasma indicates that the Z<sub>HER2:342</sub> gets inside of the cancer cells.

#### 1.4.2 Z<sub>EGFR:1907</sub> binds to EGFR with highest affinity

Affibody molecules specific for the epidermal growth factor receptor (EGFR) have also been selected by phage display technology from a combinatorial protein library based on the 58-residue, protein A-derived Z domain. Three selected Affibody variants were shown to selec-



tively bind to the extracellular domain of EGFR (EGFR-ECD). Kinetic biosensor analysis revealed that the three monomeric Affibody molecules bound with similar affinity, ranging from 130 to 185 nM. Head-to-tail dimers of the Affibody molecules were compared for their binding to recombinant EGFR-ECD in biosensor analysis and in human epithelial cancer A431 cells. Although the dimeric Affibody variants were found to bind in a range of 25–50 nM affinities in biosensor analysis, they were found to be low nanomolar binders in the cellular assays. Competition assays using radiolabeled Affibody dimers confirmed specific EGFR-binding and demonstrated that the three Affibody molecules competed for the same epitope. Immunofluorescence microscopy demonstrated that the selected Affibody dimers were initially binding to EGFR at the cell surface of A431, and confocal microscopy analysis showed that the Affibody dimers could thereafter be internalized.

## **1.5 Clinical imaging techniques and the application**

Visualization techniques are widely used to determine the exact location of the tumors before surgery, and also to determine if metastasis is present and to monitor the tumor burden during therapy. The most widely used imaging techniques include: MRI (Magnetic Resonance Image), PET (Positron emission tomography), Ultra sound, GFP (Green Fluorescent Proteins), NIR (Near infra-red) in animals and other radioactive methods.

Based on the function and mechanism, these imaging methods can be classified as two categories [76]. One is an optical image to detect inner but lower imaging, like NIR and fluorescence, has relatively high sensitivity but low resolution. The penetration depth also limits the application of optical images [77]. The other one is spectrum image, like MRI and PET. Most of

the optical image techniques have the limitation in depth. The imaging signal varies due to the depth change in vivo. Spectrum image techniques are able to show much deeper penetration (Figure 1-10). However, the spectrum technique like PET using radio isotopes to create radioactive signals, have disadvantages in harmful components.

### **1.5.1 Magnetic Resonance Imaging and its application**

Magnetic resonance imaging (MRI) is one of the most powerful imaging techniques in preclinical and clinical diagnosis due to its significant advantages in non-invasiveness and no restrictive limitations [78]. MRI measures the water hydrogen properties and interactions in an external magnetic field. MRI is able to detect signals in tissues from 1 mm to 1 m in thickness. The high resolution to distinguish various organs also makes MRI a possible technique in clinical application [79]. Since the MRI signals are from water molecules, the soft tissue such as brain tissue, which contains high amount of water, will demonstrate strong MRI signals called functional MRI (fMRI). Functional MRI is based on the increase in blood flow to the local vasculature that accompanies neural activity in the brain. The hemodynamic response from fMRI is related to neural activities, so fMRI is widely used in neuroimaging [80-81]. For example, the brain tumor is easier to be identified by identifying the change of brain structure using fMRI. For other organs especially tumors, their detections are hindered by the low sensitivity and signal to noise ratio of MRI. Due to the lower proton density, regular tissues demonstrate relatively lower signals in the magnetic field comparing with soft tissues. In order to make MRI suitable for various diseases, contrast agent is required for MRI to image different organs except for the brain tissue. About 1/3 of MRI scanning requires the use of MRI contrast agents [82].

### 1.5.2 Near Infra-red imaging and *in vivo* application

Near Infra-red (NIR) imaging is one type of the optical imaging, which detects the transmission photons, penetrates through the tissue since short wavelength of the red color enables it transparent of tissues [83]. The emission wavelength of NIR is between 700-1000 nm [76]. Like all the other optical imaging, the photon transmission from tissue is largely affected by tissue absorption and scattering. NIR dye can be used for *in vivo* imaging mainly because of three advantages. First, NIR imaging has a high sensitivity even in nano molar level of molecules [84], which benefits a molecular imaging for biomarkers. Second, animal body has relatively low background fluorescence in near infrared region. Third, compared to other fluorescent dyes like green fluorescence, NIR imaging has better penetration capability. This enables non-invasive imaging by NIR dyes.

However, several limitations still hinder the application of NIR imaging in animals. First, most NIR dyes are organic compounds with a molecular weight less than 1.2 KDa [85]. Since these small molecules have relatively short circulation time in animal bodies, they are conjugated to large molecules like nano-particles and proteins for *in vivo* imaging [86-87]. The distribution and pharmacokinetics of NIR dyes have been perturbed by the conjugated molecules. Second, in order to increase the signal to noise ratio (SNR), a filtration wavelength needs to be appropriately selected to minimize the auto-fluorescence [76]. Besides, low toxicity and molecular stability are also required for the NIR dyes. This problem has been solved by molecular modification and conjugation [88].

Although NIR dye has high sensitivity and the intensity is linear to the dye concentration, which is important for the quantitative analysis in the research, the low resolution makes it dif-

difficult to distinguish different organs. In a summary, NIR imaging performs is very efficient in probing the drugs or biomarkers; however, due to low resolution it is not suitable for further studying tissue structure as well as prognosis.

### 1.5.3 Other techniques of molecular imaging

The X-ray technique, a 3 dimensional X-ray imaging tool, is used in mammography for solid organs like bones and CT; however it uses gamma-camera which is radioactive and invasive.

Positron-emission tomography (PET) technology is also commonly used for the clinical diagnosis. PET is an image generated from radionuclides (tracer). This trace can emit pairs of gamma rays which will be detected by the PET system and generated as a three dimensional image [89]. In modern scanners, the PET and CT are combined to demonstrate a comprehensive image of a whole living body. PET can image the soft tissue, while the CT scans the solid organ as bones by X-ray. Both PET and CT have been used for many years in clinical diagnosis because of their high sensitivity and availability [75]. However, the PET imaging is based on the decay of radioisotopes, which is harmful. Those isotopes with shorter half life times were selected, including:  $^{11}\text{C}$ ,  $^{13}\text{N}$ ,  $^{18}\text{F}$ ,  $^{64}\text{Cu}$ ,  $^{68}\text{Ga}$ , and so on [90]. Short half life time requires a sensitive detector in the PET system or high amount of the tracers to generate an image with enough resolution.

A tumor tracing molecule, coupled to a suitable radionuclide (gamma-emitting for use in the gammacamera or positron-emitting for use in PET) is administered, and when the tracer has reached the tumor, images are taken. The most used PET-tracer is FDG - a  $^{18}\text{F}$  labeled glu-

color molecule that visualizes areas with high metabolism, such as tumor and inflammation areas.

Molecular imaging assists the research, diagnosis or therapy of diseases on a molecular level. This requires a series of biomarkers for various diseases and a necessary carrier to facilitate imaging reagents recognizing the biomarkers. Quantum dot is one of the best carriers for the molecular imaging. Quantum dot was first introduced to the fluorescent imaging area; because it solves several problems for the organic fluorophores [88]. The inorganic core and shell will narrow the emission range of the fluorophores within 25-35 nm. The background will dramatically decrease in such a narrow range [88].

## **1.6 Molecular imaging**

Molecular imaging differs from traditional imaging in that probes known as biomarkers are used to help image particular targets or pathways. Molecular imaging is a prospective technique in various areas like life science, physical science and neurology. Most diseases involve a molecular basis; therefore, molecular imaging will facilitate the prognosis and diagnosis. It is also expected to be applied in monitoring drug treatment via imaging biomarkers [56, 76, 91]. The most widely used imaging techniques include: MRI (Magnetic Resonance Image), PET (Positron emission tomography), Ultra sound, GFP (Green Fluorescent Proteins), NIR (Near infra-red) in animals and other radioactive methods. They can be classified as two categories [76]. One is optical image to detect inner but lower imaging, like NIR and fluorescence. Optical image has relatively high sensitivity but low resolution. The penetration depth also limits the application of optical images [77]. The other one is spectrum image, like MRI and PET. Most of the optical

image techniques have the limitation in depth. The imaging signal varies due to the depth change in vivo. Spectrum image techniques are able to show much deeper penetrations (Figure 1.11). However, the spectrum technique like PET using radio isotopes to create radioactive signal, have disadvantages either in harmful components.

Since nowadays, molecular imaging is not only used for studying basic biological process, but also used for understanding the mechanism of disease development in molecular level, it is expected that the molecular imaging will provide better differentiations in prognosis, diagnosis and monitoring therapies by using various biomarkers [92].

Molecular imaging assists the research, diagnosis or therapy of diseases on a molecular level. This requires a series of biomarkers for various diseases and a necessary carrier to facilitate imaging reagents recognizing the biomarkers.

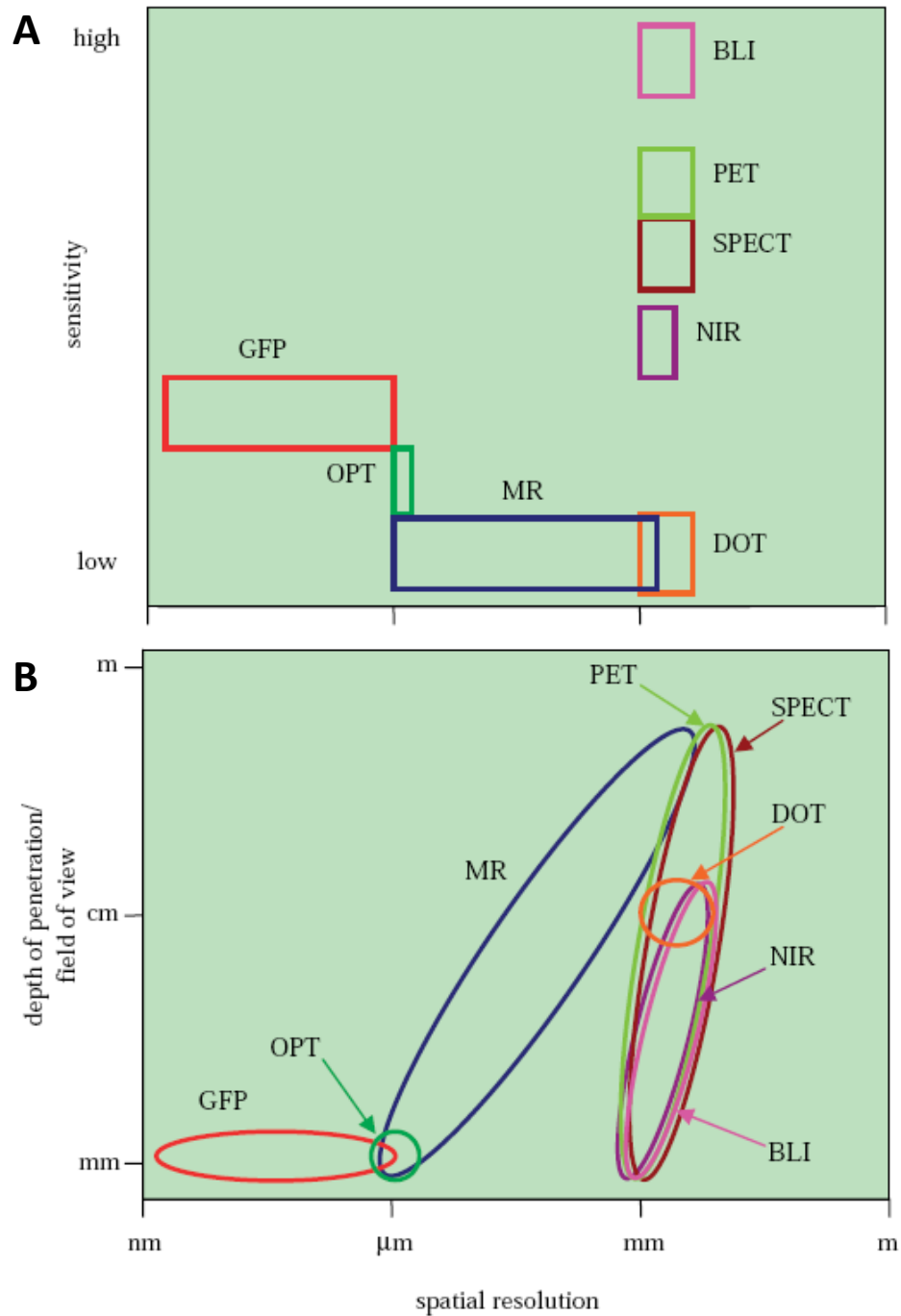


Figure 1.11 Spatial resolution and penetration depth of molecular imaging techniques  
 The x-axis indicates the spatial resolution of different imaging techniques. The y-axis shows the sensitivity in (A) and penetration depth in (B). MRI has the largest spatial resolution comparing with other techniques; however, its sensitivity is very low.

## 1.7 Contrast agents for molecular imaging

Contrast agents in molecular imaging are those reagents which can enhance the signal of imaging or distinguish the disease organs and non-disease organs [93].

In NIR imaging, NIR dye itself function as a contrast agent. Quantum dot is one of the popular carriers for the molecular imaging. Quantum dot was first introduced to the fluorescent imaging area; because it solves several problems for the organic fluorophores [88]. The inorganic core and shell will narrow the emission range of the fluorophores within 25-35 nm. The background will dramatically decrease in such a narrow range [88].

Contrast agents in MRI field are more widely used because MRI has high resolution but low sensitivity. To enhance the sensitivity of imaging, 35% of MRI scans utilize the injection of MRI contrast agents with paramagnetic, ferromagnetic or super paramagnetic metal ions. In this dissertation study, we will focus on developing MRI contrast agents.

### 1.7.1 MRI contrast agents

MRI contrast agents are used to shorten the relaxation time (T1 and T2) of the protons in the tissue area [82]. Based on the mechanisms, MRI contrast agents can be divided into two categories: contrast agents which enhance the same level of longitudinal and transverse relaxation are called T1-weighted contrast agents. Contrast agents with much longer transverse relaxation than longitudinal relaxation is called T2-weighted contrast agents [94]. The most common T1 weighted contrast agents are gadolinium ( $Gd^{3+}$ ) based, since  $Gd^{3+}$  is a lanthanide metal with seven unpaired electrons, high magnetic moment, and long electron spin relaxation time [95]. Most iron based contrast agents are T2 weighted. For Gadolinium based contrast agents,



$Gd^{3+}$  perturbs the surrounded proton relaxivity. In order to increase the exchanged water numbers with  $Gd^{3+}$  and prevent the toxicity of  $Gd^{3+}$ , an encapsulated chelator is required, such as Gd-DTPA and Gd-DOTA [96].

Gadolinium,  $Gd^{3+}$ , a lanthanide metal with seven unpaired electrons, high magnetic moment, and long electron spin relaxation time, is one of the most widely used ions in T1-weighted MRI contrast agents [97]. Since free  $Gd^{3+}$  is highly toxic with  $LD50=0.2$  mmol/kg in mice [96], it must be encapsulated by chelators. Current FDA approved MRI contrast agents are based on small chelators (Table 4). Unfortunately, these clinical contrast agents only have a relaxivity of about  $5 \text{ mM}^{-1} \text{ s}^{-1}$ . For example, Gd-DTPA, has a  $r_1$  relaxivity of  $3.8 \text{ mM}^{-1} \text{ s}^{-1}$  at 20 MHz.[94, 98] In order to detect contrast changes due to the difference of proton relaxation time in organs clinically, a relaxation rate change of  $0.5 \text{ s}^{-1}$  is required [82]. Thus, a local concentration of  $100 \text{ }\mu\text{M}$  of contrast agent is required [82, 99]. In general, about  $0.1\text{-}0.3 \text{ mM/ kg}$  injection dose is needed to obtain high contrast in human and small animal tissues.

The high concentration of contrast agent required for contrast is indicative of low efficiency and results in increased risk for certain disorders. Nephrogenic systemic fibrosis (NSF), a disease found in patients with kidney disease, has been correlated with the use of a gadolinium-based MRI contrast agents and is reported to be related to the release of free  $Gd^{3+}$ [100-103]. Further, small molecular contrast agents have a very short half life time (half-life around  $0.5\text{-}3$  min in the blood vessels of mice and elimination half-life about 1.5 hours in patients [104-105]) that limits the time window for MRI data collection and often requires repeated dose injections. Moreover, such local concentration and detection limits ( $\sim 30 \text{ }\mu\text{M}$  in mouse skeletal muscle for the contrast agent  $[\text{Gd}(\text{HP-DO3A})(\text{H}_2\text{O})]$ [106]) further hinder the number of poten-

tial biological targets for molecular imaging. Therefore, there is an urgent need to develop contrast agents with significantly improved relaxivity, optimal retention time, and potential targeting capabilities.

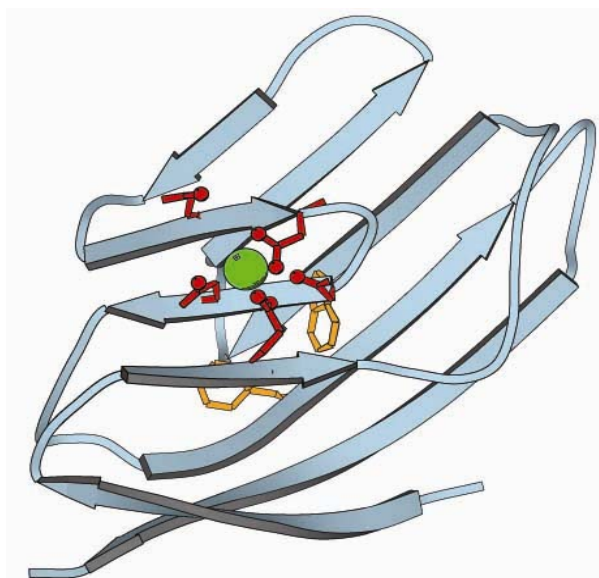
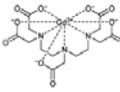
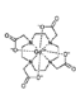
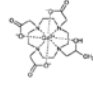
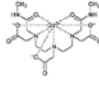
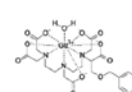
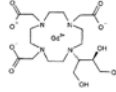
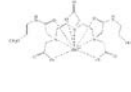
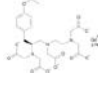



Figure 1.12 Model structure of ProCA1-CD2  
Protein based contrast agents are designed by grafting a metal binding site in the stable protein like CD2. For MRI contrast agents,  $Gd^{3+}$  binding site was designed.

Table 4. Physicochemical characteristics of commercially-available, extracellular, predominantly renally excreted gadolinium-based MR contrast agents.

Brand name	Magnevist	Dotarem	ProHance	Omniscan	MultiHance	Gadovist	OptiMARK	Primovist (Eovist)	Vasovist
Generic name	Gd-DTPA	Gd-DOTA	Gd-HPDO3A	Gd-DTPA-BMA	Gd-BOBTA	Gadobutrol	Gadoversetamide	Gd-EOB-DTPA	gadofosveset trisodium
Chemical structure									
company	Bayer Schering Pharma	Guerbet	Bracco	GE Healthcare	Bracco	Bayer Schering Pharma	Tyco	Bayer Schering Pharma	Bayer Schering Pharma
Year of first approval	1988	1994	1992	1993	2004	2000	1999	2004 in Europe; 2007 in Japan; 2008 in US	
Molecular structure	Linear, ionic	Cyclic, ionic	Cyclic, nonionic	Linear, nonionic	Linear, ionic	Cyclic, nonionic	Linear, nonionic	Linear, ionic	Linear, ionic
Thermodynamic Stability constant (log $K_{eq}$ )	22.1 <sup>1</sup> 22.5 <sup>7</sup>	25.8 <sup>1</sup>	23.8 <sup>1</sup>	16.9 <sup>1</sup>	22.6 <sup>1</sup>	21.8 <sup>1</sup>	16.6 <sup>1</sup>	23.46 <sup>1</sup>	N/A
Conditional stability constant at pH 7.4	18.1 <sup>2</sup> 18.4 <sup>7</sup>	19.0 <sup>2</sup>	17.1 <sup>2</sup>	14.9 <sup>2</sup>	18.4 <sup>2</sup>	N/A <sup>2</sup>	15.0 <sup>2</sup>	N/A <sup>2</sup> 18.7 <sup>7</sup>	N/A <sup>2</sup>
Acid dissociation half life in 0.1N HCl	10 min <sup>2</sup>	> 1 month <sup>2</sup>	3 hours <sup>2</sup>	35 second <sup>2</sup>	N/A <sup>2</sup>	N/A <sup>2</sup>	N/A <sup>2</sup>	N/A <sup>2</sup>	N/A <sup>2</sup>
Osmolality (Osm/kg)	1.96 <sup>1</sup>	1.35 <sup>1</sup>	0.63 <sup>1</sup>	0.65 <sup>1</sup>	1.97 <sup>1</sup>	1.6 <sup>1</sup>	1.11 <sup>1</sup>	0.688 <sup>1</sup>	0.7-0.95 <sup>3</sup>
Viscosity (mPa.s at 37°C)	2.9 <sup>1</sup>	2.0 <sup>1</sup>	1.3 <sup>1</sup>	1.4 <sup>1</sup>	5.3 <sup>1</sup>	4.96 <sup>1</sup>	2.0 <sup>1</sup>		
T1 relaxivity (L/mmol.s <sup>-1</sup> ) 1.5T, plasma	4.1 <sup>4</sup>	3.6 <sup>4</sup>	4.1 <sup>4</sup>	4.3 <sup>4</sup>	8.3 <sup>4</sup>	4.7 <sup>4</sup>	4.7 <sup>4</sup>		
T1 relaxivity (L/mmol.s <sup>-1</sup> ) 3T, plasma	3.7 <sup>4</sup>	3.5 <sup>4</sup>	3.7 <sup>4</sup>	4.0 <sup>4</sup>	6.2 <sup>4</sup>	3.6	4.5 <sup>4</sup>		
Metal chelate (mg/ml)	469 <sup>4</sup>	278.3 <sup>4</sup>	279.3 <sup>4</sup>	287 <sup>4</sup>	334 <sup>4</sup>	605 <sup>4</sup>	330.9 <sup>4</sup>		

### 1.7.2 Biomarkers targeted contrast agents

In order to view by MRI, the local concentration of contrast agents should be up to micro molar level [107]. By concentrating the contrast agents in the tumor area is required for imaging the tumor tissue. As discussed in previous chapters, biomarkers are expressed endogenously and can be detected as an indicator of biological status. Normally, a biomarker will have at least two characteristics: first, the biomarker can be probed by contrast agents for molecular imaging; second, the biomarker is sensitive to drugs or medicine for targeted therapeutics [14]. To generate imaging on biomarkers has benefitted the selection of drug treatments. Therefore, designing contrast agents to target to biomarkers is essential for the clinical diagnosis and therapy.

As discussed in the Chapter 1.1, most of the receptors have their ligands, the ligands themselves can be used as targeted reagents for contrast agents.

### 1.7.3 Criteria of designing ideal contrast agents

In the design of ideal contrast agents, several factors must be considered. First, negligible or low toxicity is a prerequisite. The contrast agents should be thermodynamically and kinetically stable, with high binding affinity and metal selectivity to minimize the release of free  $Gd^{3+}$ . A high metal selectivity for paramagnetic metal ions against physiological metal ions such as  $Zn^{2+}$  and  $Ca^{2+}$  is preferred [108-109]. Second, high relaxivity, especially for T1, is preferred in order to obtain better images with high contrast-to-noise ratio (CNR) and dose efficiency. Third, an ideal contrast agent should have proper vascular retention time allowing for imaging of tissue enhancement, gauging tissue blood perfusion, and evaluating changes in capillary integrity. Different strategies are applied to overcome the drawback of small chelator based MRI contrast agents. For example, the non-covalent binding of small chelators to plasma proteins, such as albumin (MS-325), greatly increases the relaxivity and blood retention time. On the other hand, the applications of this class of contrast agents are limited to the cardiovascular system. Fourth, it should have proper excretion time from the body to allow imaging and reduced toxicity. Molecules that are greater than 70 KDa do not readily pass through the glomeruli (a pore size 60-70 nm in diameter)[105]. For example, the blood retention time for MS-325 in rabbit is increased to over an hour[110]. The slow secretion and perfusion time for macromolecules such as nanoparticles may be a big concern. Finally, targeting specific molecular entities is greatly preferred since it will increase the specificity of MRI as a screening method for cancer

diagnosis with the advantage of nondestructive and spatial resolution. Molecular imaging using MRI contrast agents is also hampered by the low relaxivity, since in most cases these biomarkers have limited number in the disease area. To achieve molecular imaging, developing contrast agents with high dose efficacy, low toxicity, optimal pharmacokinetics, and the capability of targeting and permeability are required.

### **1.8 Objectives of this study, and over view of the dissertation**

The Yang laboratory has first demonstrated MRI contrast agents (ProCA) with strong metal binding affinity, selectivity, and stability, developed by de novo design of  $Gd^{3+}$  binding site(s) into a stable host protein (Figure 1.12). The protein contrast agents exhibit ~20 fold improved MRI relaxivity compared to that of Gd-DTPA at 1.5- 4.7 T field due to controlled correlation time and exchangeable water numbers in the coordination shell [111]. Our study demonstrated a novel strategy to significantly increase the relaxivity of contrast agents by protein design.

There is an urgent need to develop non-invasive and accurate methods for diagnosis and to monitor biomarker levels/distribution and their changes upon treatment by targeted drugs in cancer patients. Based on the advantages of MRI of high resolution and deep tissue penetration and real time, we propose to further develop MRI contrast agents to extend its capability and application in both clinic and preclinical research.

The goals of this research are to develop a novel class of protein-based MRI contrast agents (ProCAs) with improved relaxivity, targeting capability and reduced toxicity to enable

accurate monitoring of the expression level and distribution of the HER2/Neu and EGFR in different types of cancers, and to follow tumor response to treatment using targeted therapeutics.

This dissertation aims to answer several important questions in order to apply this strategy to develop MRI contrast agents for molecular imaging:

Chapter 1 discusses the background and related knowledge of this dissertation.

Chapter 2 describes all the methods and techniques have been used for this dissertation.

Chapter 3 discusses the design of HER2 targeting contrast agents. Methods for expression and purification of designed ProCAs with targeted capability have been optimized. Further modification of ProCAs to increase the solubility, serum stability and reduce the immunogenicity will be achieved by PEGylation. Dural modality of contrast agents for both MRI and NIR have been prepared and characterized. Conformational and metal binding properties have been examined. Furthermore, the relaxation properties have been measured.

Chapter 4 is aimed to evaluate the targeting capability using several methods such as ELISA, western blotting and flowcytometry. The cell targeting capability has been evaluated using different cell lines with both NIR florescence and immunofluorescent staining. The radioactive assay is also used to measure the retention of  $Gd^{3+}$  in cancer cells. In addition, EFGR targeted contrast agents are also determined by the cell assays.

Chapter 5 discusses the design of xenograft animal model with the injection of our designed targeted MRI contrast agents. The optimized condition for imaging has been determined for both MRI and NIR of imaging HER2 under various time points. Further histology analysis for

primary organs shows biodistribution of HER2 and contrast agents. The advantages of ProCA1-affi342 to antibodies are also determined by IHC.

Chapter 6 shows quantitative analysis of the distribution and binding capability of ProCA1-affi342 in cancer cells and animals.

Chapter 7 is aimed to show development of another mouse model by implanting tumor cells in the mammary sites of mice as orthotopic tumor model, which can mimic the real tumor situation. ProCA1-affi342 and ProCA1-affi1907 will be applied to this tumor model to monitor the tumor progression and receptor distribution.

Chapter 8 focuses on drug treatment study by using contrast agents to monitor the tumor changes after treated with specific drugs. Initial results in cell treatments have been achieved by immunology techniques and MRI in cells.

Chapter 9 summarizes other studies related to this dissertation by using designed contrast agents with multiple metal binding sites in developed xenograft models.

Table 5 summarizes all the variants involved in this dissertation.

The contents related with each variant have been listed in the Table 5:

Table 5 Contents of all the variants

<b>Variants</b>	<b>Description</b>	<b>Related Chapters</b>
ProCA1-CD2	Domain 1 of CD2 with a designed $Gd^{3+}$ binding site	1, 3
ProCA1-affi4	First generation of affibody $Z_{HER2:4}$ against HER2 fused to the C-terminal of ProCA1-CD2	3, 4
ProCA1-affi342	Second generation of affibody $Z_{HER2:342}$ against HER2 fused to the C-terminal of ProCA1-CD2	3-8
ProCA1-affi1907	Affibody $Z_{EGFR:1907}$ against EGFR fused to the C-terminal of ProCA1-CD2	8
ProCA1-affi342m	PEGylated ProCA1-affi342	3-8
ProCA1-affi1907m	PEGylated ProCA1-affi1907	8
ProCA22-affi342m	Second generation of affibody $Z_{HER2:342}$ against HER2 fused to the ProCA22 which has four metal binding sites	9
ProCA32-affi342m	Second generation of affibody $Z_{HER2:342}$ against HER2 fused to the ProCA22 which has two metal binding sites	9



## **Chapter 2. MATERIAL AND METHODS**

### **2.1 Molecular cloning of ProCA1-affibody to target HER2 and EGFR**

The affibody sequences  $Z_{\text{HER2-2:4}}$ ,  $Z_{\text{HER2-342}}$  and  $Z_{\text{EGFR-1907}}$  were cloned to the C-terminal of ProCA1-CD2 in the pGEX-2T plasmid. Their sequence alignments have been carried out by on-line software Clustal W2 (Figure 1.9). The affibody peptide consists of 58 amino acids and 13 amino acids of them are involved in the targeting moieties, which are located in the helix 1 and 2. The sequences have been divided into three fragments and inserted into the plasmid. The model structure of ProCA1-CD2 with  $\text{Gd}^{3+}$  binding site was been generated by SWISSMODEL [112-113]. The affibody structure was shown in Figure 1.9 [114]. The model structure of ProCA1-affibody was generated by linking two parts of the structure files with GSGG linker (Figure 3.1).

### **2.2 Plasmid construction and protein generation**

After the fusion of affibody into the ProCA-CD2 plasmid by PCR, the DNA products were prepared by Miniprep (Qiagen). All sequences were verified by automated sequencing on an ABI PRISM-377 DNA sequencer (Applied Biosystems) in the Advanced Biotechnology Core Facilities of Georgia State University. Protein concentration is calculated using extinction coefficient of UV280 nm.

### **2.2.1 GST-fusion ProCA1-affibody and purification**

The designed ProCA1-affibody were expressed as GST-tag fusion proteins in Escherichia coli BL21(DE3) transformed with the plasmid constructs in LB medium with 100 mg/L of ampicillin and were grown at 37 °C overnight. On the second day, 50-60 ml inoculating LB medium with the E coli BL21 (DE3) is transfer to the big flask with 1L LB medium. 1ml ampicillin (1:1000) is added into the LB medium. The optical density (OD) of the cultured medium is measured at 600nm. The big flask is shaking in 37 °C, 220rpm for cell growth. When the OD increases to 0.6-0.8 (usually growth for 2 hours), the 1.5 mM IPTG is added into the LB medium, and the protein will be expressed. The cell pellets are collected when OD grows over 2.0 for further purification. For low temperature expression, the temperature is changed to room temperature (25°C) after induction for 16~18 hours overnight.

### **2.2.2 Sub-cloning of tagless ProCA1-affibody and purification**

The DNA sequence of ProCA1-affibody in PGEX-2T (Figure 2.1) vector was cleaved by BamH1 and EcoR1 restriction enzymes. The BamH1 site locates between GST tag and ProCA1-affi, while EcoR1 site locates at the C-terminal of ProCA1-affibody. Then the DNA sequence of ProCA1-affibody was attached to the cleaved PET-20b vector (Figure 2.2).

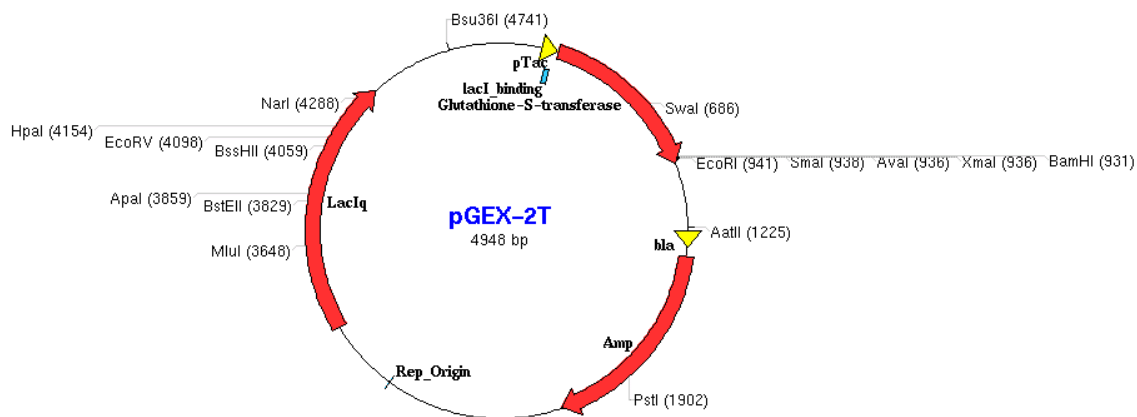


Figure 2.1 DNA map of PGEX-2T vector

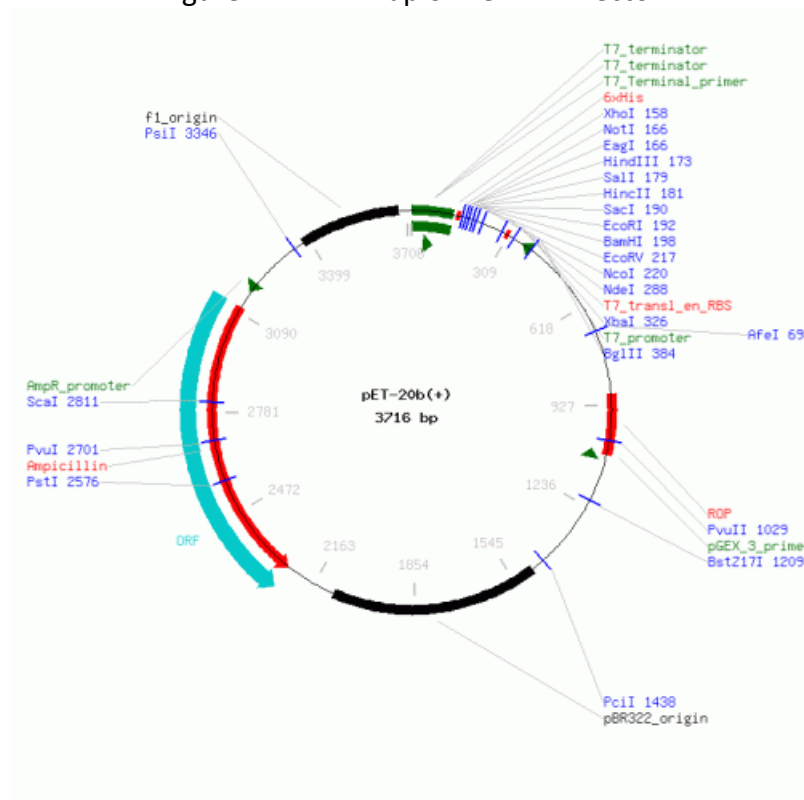


Figure 2.2 DNA map of PET-20b vector

### **2.3 PEGylation of ProCA1-affibody**

Methyl-PEO<sub>n</sub>-NHS esters, the deviant of Polyethylene glycol (PEG) with different molecular weights of 0.3, 0.6, 2.4, 5, 12 and 20 KDa were selected to modify the designed proteins. PEGylation was carried out in phosphate buffered saline buffer with a 1:5 ratio of protein and PEGs. Modified ProCA1-affibodies were further purified by FPLC and confirmed by the MALDI-TOF mass spectrometric analysis.

### **2.4 Conjugation of near infra red (NIR) dye to ProCA1-affibody**

A Cys amino acid has been cloned to the C-terminal of ProCA1-affibody by PCR. The Maleid group in the NIR dye can be linked to the –SH group specifically. The protein has been dissolved in degassed PBS (pH 7.0-7.5) by dialysis at a concentration around 1 mg/ml. Tris-(2-carboxethyl)phosphine (TCEP) was added to reduce the protein in N<sub>2</sub> environment. Half an hour later, the NIR dye Cy5.5 in DMF solvent was added in to the reduced protein solution. The conjugation reaction was kept in N<sub>2</sub> to keep reducing environment. The ratio of protein to Cy5.5 is around 5:1. Shake the mixture and keep the reaction for 2 hr. Then dialysis or cation exchange column will be used to separate the free dye. The absorbance at 650 nm (Cy5.5) and 280 (protein) will be measured to calculate the conjugation yield (Figure 3.16).

## 2.5 Determining the folding condition of ProCA1-affibody

### 2.5.1 Mass spectrometry

The MALDI mass spectrometry analysis was performed on an Applied Biosystems 4800 *plus* MALDI TOF/TOF analyzer mass spectrometer (Framingham, MA). The data were acquired in a linear positive mode with sinapinic acid as matrix. The instrument was equipped with a Diode-pumped Nd:YAG laser at 355-nm. The mass spectra were acquired as an average of 3 shots with a same laser intensity attenuator setting (4002 arbitrary unit) for all samples. Protein samples were prepared as a 200  $\mu$ M solution in 10 mM Tris buffer (pH 7.4). Matrix was prepared as a 10 mg/mL solution of Sinapinic acid in a 1:1 acetonitrile: 0.1% TFA solution. A 10:1 matrix:sample mixture was prepared, applied to the sample plate as 1  $\mu$ L drops, and allowed to air dry. The molecular weight been measured indicates the conjugation of NIR dye to the ProCA1-affibody proteins. The relative peak intensity ratio of the non-conjugated and conjugated ProCA1-affibody was used for the estimation of the conjugation rate. This work was completed by Dr.Siming Wang and Yanyi Chen.

### 2.5.2 Circular dichroism spectroscopy

The CD spectra of samples were recorded in a Jasco-810 spectropolarimeter at 25 °C. The far-UV CD spectrum of 20  $\mu$ M ProCA1-affi342 were measured in a 1-mm pathlength cell in 10 mM Tris-Cl (pH 7.4) and the near-UV CD spectrum of those protein studied with a concentration of 100  $\mu$ M were collected in the same buffer. All spectra were obtained as the average of at least ten scans with a scan rate of 100 nm/min. The ellipticity was measured from 190 to 260

nm (far-UV) and 250 to 340 nm (near-UV) and then converted to mean residue molar ellipticity after subtracting the spectrum of buffer as the blank.

### **2.5.3 Fluorescence spectroscopy**

Fluorescence emission spectra were recorded on a PTI fluorimeter at 25 °C using a 1-cm path length cell. Intrinsic tryptophan fluorescence emission spectra were recorded from 300 to 400 nm with the excitation wavelength at 282 nm. The slit widths were set as 2 and 4 nm for excitation and emission, respectively. Tryptophan spectra from 300-400 nm of the different proteins studied were acquired at a concentration of 2 μM in 10 mM Tris-Cl (pH 7.4).

### **2.5.4 Nuclear Magnetic Resonance (NMR) spectroscopy**

NMR spectra were collected on a 600 MHz NMR spectrometer. 1-D <sup>1</sup>H-NMR at 25 °C was measured to determine the folding of ProCA1-affibody and the conjugation with NIR dye. This part of work was done by Dr. Hing Wong.

## **2.6 Relaxivity measurements and metal binding affinity of ProCA1-affibody**

Relaxation times, T<sub>1</sub> and T<sub>2</sub>, were determined on the 1.41T Minispec Relaxometer (mq60 NMR Analyzer, Bruker) at 37 °C. The ProCA1-affi and ProCA1-affi-m (modified by PEG) were diluted with 10 mM Tris buffer, pH7.0. Proteins prepared with a series of concentrations: 40-120 μM, were applied for the relaxation time measurement. The relaxivities, r<sub>1</sub> and r<sub>2</sub>, were obtained by fitting the relaxation times as a function of the Gd<sup>3+</sup> concentrations. The Gd<sup>3+</sup> -

binding affinities with ProCA1-affi and ProCA1-affi-m were investigated by the competitive assay with the dye Fluo5N (a metal ion indicator, Invitrogen Molecular Probes). The fluorescence spectra were collected on a fluorescence spectrophotometer (Photon Technology International, Inc.) with a 10 mm path length quartz cell at room temperature [111].

## 2.7 Cell culture and mammalian expression

SKOV-3 cells were cultured in 5% CO<sub>2</sub> at 37°C in 75 cm<sup>2</sup> flasks in McCoy-5A medium containing 10% fetal bovine serum (FBS) with 100 µg/ml Penicillin-Streptomycin. The other mammalian cancer cell lines are cultured in the same condition with different medium. The AU565 cells were cultured in 1640 medium. The MDA-MB-231 cells were cultured in DMEM medium with low glucose. The EMT-6 cells were cultured in waymouth medium. All the cells were thawed at 37 °C and transferred into a 25T flask with 8 ml medium. After growing to a confluence over 90%, the cells will be suspended by 2% Trypsin and washed with HBSS buffer by centrifuging. Finally the cells are passaged into several 50T or bigger flasks. The cells were frozen in commercial frozen medium containing 2% EDTA and 10% DMSO. Normally, about 10<sup>6</sup> cells will be frozen in 1 ml frozen medium.

For the mammalian expression, the LEC1 HER2 pSGHV0 cell line with stable transfection of HER2-ECD DNA was obtained from Dr. Leahy's group in Johns Hopkins University. The cells were thawed rapidly at 37 °C. Spin the cells for 5 minutes at 1000rpm and aspirate freezing media. The cells were re-suspend in 1 ml Alpha MEM, 5%Dialized FBS, 100nM Methotrexate, 0.5 mg/ml geneticin. The cells were then transferred to 4 ml of the same in a T25 flask, 5%CO<sub>2</sub>, 37 degrees. Once expanded to have enough cells to seed a roller bottle (3-5 confluent T150's

would do it), they are switched to DMEM / F12, 5%FBS, 100nM MTX. Weekly monitoring of expression medium by ELISA was done to ensure expression has not lost. The DMEM / F12 is HEPES buffered since our roller apparatus is without CO<sub>2</sub>. Once the single roller bottle is confluent, we use that to split into 1L flasks. After 3 days in 5% serum to insure attachment, serum is reduced to 1% for collection of media and further purification. The 1L flasks are generally fed 50 ml /flask, twice a week.

## **2.8 Cancer cell targeting**

### **2.8.1 Enzyme linked immunosorbent assay (ELISA)**

The cell lysate was made for the coating of ELISA. Take one flask of cancer cells and suspend with 2% Trypsin. Wash the cells for three times and count  $1 \times 10^8$  of cells into a centrifuge tube. The 1 ml RAPI buffer and 0.1% protease inhibitor cocktail was added into the cell pellets. The cells were suspended and keep in 4 °C for 1 hr shaking. Centrifuge the cells and get the supernatant as cell lysate. AU565 and EMT-6 cells lysate with various dilutions was coated in a 96-well plate (BD bioscience) at 37 °C degree overnight. On the second day, the medium was changed. Different amounts of ProCA1-affi342 and ProCA1-affi342m were incubated with cells for 1 hr in room temperature. The plate was washed and the CD2 antibody was used as a primary antibody to detect the binding proteins in the cells. HRP conjugated goat anti-mouse IgG conjugated was used as the secondary antibody. Substrate (OPD,o-phenylenediamine dihydrochloride) was added into each well. After incubation, the absorbance was measured at 492nm using a Victor V 1420 multiple counter from PerkinElmer.



In the sandwich ELISA, the CD2 monoclonal antibody was coated on 96-well microplate at a concentration of 100ng/well with carbonate/bicarbonate buffer (pH 7.4) and incubated at 4°C overnight. The second day, coating buffer was removed and the plate was washed with Tris buffer saline (TBS) three times. The remaining protein-binding sites in the coated wells was saturated by adding 200 µl blocking buffer (5% nonfat dry milk/TBS, per well). The plate was covered and incubated for 2 hours at room temperature. Diluted proteins or tissue extracts from mice experiment were added to each well and incubated at 37°C for 2 hours. Each cell treatment was done in triplicate. TBS was used to wash each well three times after incubation. Diluted polyclonal CD2 antibody was added to each well and incubated at room temperature for 2 hours. The plate was washed with TBS four times. HRP conjugated secondary antibody was added to the 96-well plate in blocking buffer and incubated at room temperature for 2 hours. After incubation, the plate was washed four times with TBS. The substrate of HRP was prepared for detection of protein signals. OPD (o-phenylenediamine dihydrochloride) was used as the substrate. After incubation, the absorbance was measured at 492nm using a Victor V 1420 multiple counter from PerkinElmer.

### **2.8.2 Western blotting**

The AU565, originally from human breast cancer, has an expression level of HER2 at about 106 per cell. The EMT6 is a HER2 negative cell line from mouse breast cancer. The ProCA1-affi342 and ProCA1-affi342m were incubated with the two kinds of cells at 4 and 37 °C, respectively, for 1 hr. Then the cells were washed 3 times, 5 min each with Tris buffer. After this, the cells in T25 were lysate with 200 µL RAPI buffer for 3 hr in 4 °C. Then the cell lysate was cen-

trifuged and the supernatant was collected for western blotting. The primary antibody was generated on rabbit by using ProCA1-CD2-m as antigen. The secondary antibody was AP conjugated (Invitrogen). The ProCA1-affi342 or ProCA1-affi342m retained in the cancer cells will be detected by antibody and the signal will be shown on the developed film.

### **2.8.3 Radio-active assay on cancer cells**

Cancer cells AU565 and EMT-6 were collected into 1.7 ml tubes by trypsin and centrifuging. After careful washing 3 times with HBSS buffer, the cells were incubated with radioactive reagent  $^{153}\text{Gd-ProCA1-affi342}$  and  $^{153}\text{Gd-ProCA1-affi342m}$ .  $^{153}\text{GdCl}_3$  (Novagen) was also used as negative control. The incubation time is 1 hr by shaking. Then the cells were spin down by keeping both the pellets and supernatant. Wash the cells with HBSS buffer for 5 times, the washing buffer was also collected. Finally, all the samples including cell pellets and washing buffer were measured by  $\gamma$ -counter. The amount of  $^{153}\text{Gd}$  retained in the cancer cells was calculated based on the standard curve (Figure 2.3).

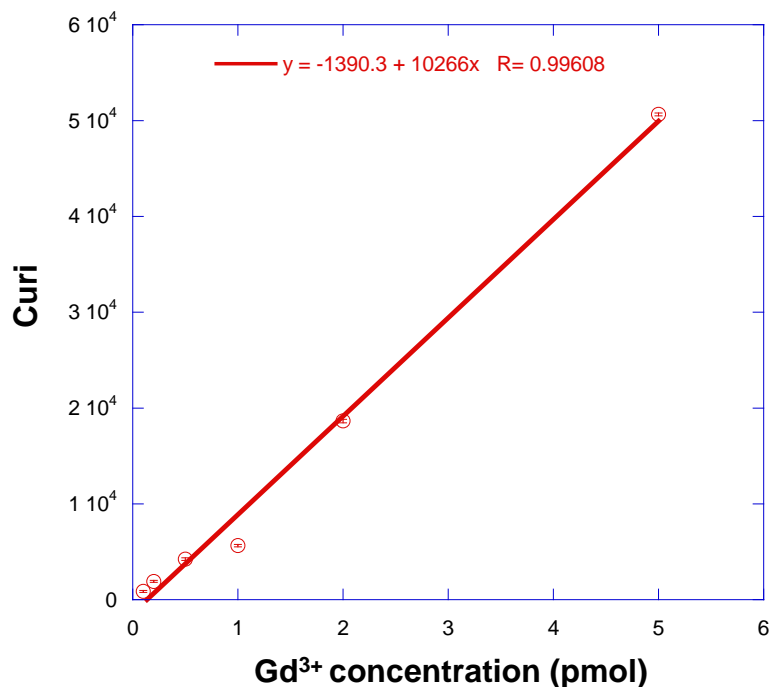


Figure 2.3 Standard curve of radioactive GdCl<sub>3</sub>

#### 2.8.4 Immunofluorescent staining in cancer cells

Three cell lines (AU565, SKOV-3 and MDA-MB-231) were seeded in different chambered microslides (BD Biosciences) and treated with ProCA1-CD2, ProCA1-affibody, and ProCA1-affibody-m at 37°C for one hour. The second day, cells were washed and fixed with 4% paraformaldehyde for 15 minutes at room temperature. Then cells were permeabilized with 0.1% Triton X-100 in 10 mM HEPES pH7.0. ImageiTMMFX signal enhancer (Molecular Probes) and subsequently incubated with the respective antibodies for 1 hour. After extensive wash, cells were incubated with Alexa Fluor 488nm goat anti-mouse IgG (Molecular Probes) at a 1:1000 ratio. Cells were washed three times for 5 minutes with TBST. Finally, microslides were mounted in ProLong Gold antifade reagent with DAPI (Molecular Probes). Slides were scanned in a confocal

microscopy lab with the Confocal Microscope (Zeiss. LSM510) using 40x or 63x objectives. Two lasers were used here, 488nm for FITC and blue for UV. The final images were acquired by adjusting detector gain and amplifier offset to get the best images.

### **2.8.5 Flow cytometer assay (FACS)**

The cancer cells SKOV-3 and MDA-MB-231 were cultured for the flow cytometer study. The cells were lysated and suspended to transfer into a 5 ml FACS tube. The cells were washed for 5 times by HBSS buffer. Then the PAb-ProCA1-CD2 (Appendix I) was added into the cells with 1:500 dilutions. After 1 hr incubation in room temperature, the cells were washed with HBSS buffer for 3 times. Secondary antibody goat anti rabbit with FITC conjugation was added and incubate for 40 min. After extensive washing, the cells were counted by the FACS machine with the number of 2,000. The accumulated fluorescent intensity was measured.

### **2.8.6 Magnetic Resonance Imaging (MRI) in cancer cells**

SKOV-3 and MDA-MB-231 cells were collected and washed with 10 mM HEPES buffer (pH7.0) three times. Up to  $10^7$  cells were incubated with Gd-ProCA1, Gd-ProCA1-affibody and Gd-ProCA1-affibody-m at 37°C for 1 hour. After incubation, cells were washed with TBS three times, 5 minutes each time. Cell pellets were collected in eppendorff tubes and measured by MR imaging. T1 weighted MR images were acquired using an inversion recovery sequence (TR = 4000ms, TE = 12ms, IR=500ms) on a 7T MRI scanner. After cell MR imaging, cells were washed twice with ice-cold PBS. PBS was removed and cell pellets were lysed with 1×RIPA lysis buffer

supplemented with 1mM NaF, 1mM PMSF and 1:1000 dilution of protease inhibitor cocktail. Whole cell lysates were rotated at 4°C for 60 minutes. To remove cell debris, cell lysates were centrifuged (15,000×g, 10min at 4°C). Cell lysate supernatant was collected and stored at -80°C until use. 2× loading dye was added to the supernatant and boiled at 100°C for 5 minutes. Western blotting was applied to check the contrast agent in cells by using the CD2 antibody against the contrast agents.

## **2.9 Animal experiments**

### **2.9.1 Nude mouse xenograft model**

The nude mice are two weeks old. In 3-5 days after purchase, the mice are ready for use. The tumor cells are scratched from flask and washed with HBSS buffer for three times. The cells are counted and then suspended with saline to get a suspension of  $5 \times 10^6$  cells per 100  $\mu$ l saline. The suspension is mixed with gel matrix in same volume. This procedure is completed on ice. Every mouse is subcutaneous injected with 100  $\mu$ l mixture on each spot. Every mouse has two or three spots on its back. After two to three weeks, the mice will generate tumor of 0.5-1 cm.

### **2.9.2 Nude mouse orthotopic model**

The human breast cancer cell line MCF-10DCIS was used to generate the orthotopic model in nude mice. The tumor cells are scratched from flask and washed with HBSS buffer for three times. The cells are counted and then suspended with saline to get a suspension of  $5 \times 10^4$

cells per 50  $\mu$ l saline. Inject the cells into the mammary spot of the mouse. After about one week, the tumor between 0.5 to 1 cm will be generated.

### **2.9.3 Magnetic Resonance Imaging (MRI) of tumor mouse**

The tumor mouse will be anesthetized with constant isoflurane and located in the MRI machine for a pre-injection scanning. The tumor mouse will be injected by tail vein injection with our contrast agents in 10 mM HEPES buffer, pH7.0. The concentrations of our contrast agents are between 3 to 5 mM. About 100  $\mu$ L of the contrast agents will be injected into each mouse. The mouse will be scanned on a 4.7 MRI scanner at various time points after injection: 10 min, 30 min, 2 hr, 24 hr, 48 hr and 72 hr. For every time point, three pulse sequences are used: Fast spin echo (TR=2 s, TE=0.022 s or 0.066 s) Gradient echo (TR=0.116 s, TE=2.9 s ) Gradient echo DCE (TR=0.050 s, TE=2.9 s ) 3D image of Gradient echo was also scanned.

### **2.9.4 Near infra-red (NIR) imaging of tumor mouse**

Engineered protein contrast agents were PEGylated and labeled with Cy5.5 (ProCA1-affibody-Cy5.5). The protein was stored in 10mM HEPES buffer at concentration of roughly 5mM. 100  $\mu$ L of Cy5.5 PEGylated protein was injected into the mouse tail vein. Fluorescence imaging was taken at different time points using an IVIS imaging system (Xenogen Corporation). The mouse was maintained under isoflurane anesthesia during imaging. Images were processed using the living imaging 3.1 from Xenogen Corporation. The excitation filter wavelength of 650

nm was used to scan the mouse NIR imaging. Another excitation wavelength of 604 nm was also used to scan the background. The emission wavelength is 740 nm.

### **2.9.5 Biodistribution and blood circulation measurements**

The biodistribution of ProCA1-affi342m has been measured in the regular CD1 mouse and nude mouse with tumors. The mice will be kept in the metabolism cages for 2 days before experiments. Then mice were injected with 100  $\mu\text{M}$   $^{153}\text{Gd}$ -ProCA1-affi342m in 10 mM HEPES buffer (pH7.0) of 100  $\mu\text{L}$  by tail vein injection. The mice are all kept in the metabolism cages individually under monitoring. The total monitoring time is 8 hours. All the urea and feces will be collected. The blood will also be collected from thigh vein every 1 hr. At the end of 8<sup>th</sup> hour, all the mice will be sacrificed and dissected. All the primary organs, like liver, kidneys, lung, heart, spleen, tumor and muscle were collected for measurements, as well as the carcass. The radioactivity of all the collected organs and blood samples will be measured by  $\gamma$ -counter. From the standard curve of Figure 2.3, the amounts of  $^{153}\text{Gd}$  in each organ or blood were calculated. Then the amount of  $^{153}\text{Gd}$  will be divided by the total injection amount and bodyweight to get a normalized percentage of each sample in each organ per kg of body weight.

### **2.9.6 Biodistribution measurements by ICP-OES**

Besides using radioactive assay for the biodistribution study, we also used ICP-OES to measure the retention of Gd inside the mouse body. After MRI experiments, we collected all the primary organs, like liver, kidneys, lung, spleen, heart, tumor and muscle. All the organs

were dissolved in 30% optimal nitric acid in the containers. The containers were heated at 80-100 °C overnight until all the organs were dissolved. Based on the previous radioactive distribution results, the dissolved organ solution will be diluted by 2% optimal nitric acid to the measurement range of ICP-OES (50-5000 nM). By measuring the intensity of two excitation wavelengths at 368.4 nm and 342.2 nm [115], the concentration will be obtained based on the commercial GdCl<sub>3</sub> samples. The original Gd<sup>3+</sup> concentration in all the samples was calculated by multiplying the measured concentration with dilution times.

## **2.10 Histology analysis**

### **2.10.1 Preparation of tissue slices**

After MRI experiments, all the organs will be frozen in liquid Nitrogen with OCT embedded. Then the frozen tissue will be kept in -80 °C. Before section the tissues, the frozen samples have to be removed from freezer and equilibrate at -20°C for approximately 15 minutes. This may prevent cracking of the block when sectioning. Section tissue at a range of 6-8 µm and place on positively charged slides. Allow sections to air dry on bench for a few minutes before fixing (this helps sections adhere to slides).

After sections have dried on the slide, they will be fixed in optimal fixative (10% Neutral buffered formalin) for 10 minutes at room temperature. The staining procedure will be proceeding immediately.



### **2.10.2 Immunohistology chemistry (IHC) on paraffin embedded slices**

The paraffin on the section needs to be removed before staining by Xylen and the staining procedure will be proceeding immediately. First, wash sections in water three times for 5 minutes each. Incubate sections in 3% hydrogen peroxide for 10 minutes. Wash sections in water twice for 5 minutes each. Wash section in HEPES buffer for 5 minutes. Block each section with 100-400  $\mu$ l blocking solution for 1 hour at room temperature. Remove blocking solution and add 100-400  $\mu$ l primary antibody diluted in recommended antibody diluent to each section. Incubate overnight at 4°C. Remove antibody solution and wash sections in wash buffer three times for 5 minutes each. Add 100-400  $\mu$ l HRP conjugated secondary antibodies, diluted in HEPES buffer with 1% Triton, to each section. Incubate 30 minutes at room temperature. If using ABC avidin/biotin method, prepare ABC reagent according to the manufacturer's instructions and incubate solution for 30 minutes at room temperature.

Remove secondary antibody solution and wash sections three times with wash buffer for 5 minutes each. Add 100-400  $\mu$ l DAB or suitable substrate to each section and monitor staining closely. As soon as the sections develop, immerse slides in water. If desired, counterstain sections in hematoxylin. Wash sections in dH<sub>2</sub>O two times for 5 minutes each.

### **2.10.3 Immunofluorescent staining on frozen slices**

Wash sections in wash buffer twice for 5 minutes. Incubate for 10 minutes at room temperature in 3% H<sub>2</sub>O<sub>2</sub> diluted in methanol. Wash sections in wash buffer twice for 5 minutes. Block each section with blocking solution for one hour at room temperature. Remove blocking solution and add 100-400  $\mu$ L diluted primary antibody to each section. (Dilute antibody in

blocking solution). Incubate overnight at 4°C. Refer to product datasheet to determine the recommended dilution. Remove antibody solution and wash sections three times with wash buffer for 5 minutes each. Add 100-400 µL secondary antibody with fluorescent dyes labeled, diluted in blocking solution to each section. Incubate 30 minutes at room temperature. Remove secondary antibody solution and wash sections three times in wash buffer for 5 minutes each. Add anti-fade reagents with DAPI dye on the section and seal the tissue section with nail polish.

### **2.11 Measure immunogenicity of ProCA1-affi**

PEGylated contrast agents (P40-ProCA1-affi) and non PEGylated ProCA1-affi with or without adjuvant were injected into rabbits for antibody generation. The first injection was mixed with Complete Freund's Adjuvant and the subsequent boosts (every 2 to 3 weeks) were mixed with Incomplete Freund's Adjuvant. Rabbit blood was collected at different time points (every two to three weeks). Each time, 10ml blood was collected and centrifuged. The serum was collected in clean tubes and stored in -80°C. The immunogenicity of P40-ProCA1 was analyzed by western blotting and ELISA.

### **2.12 Measurement of Acute toxicity**

The 2 mM of ProCA1-affi-m in 100 µL saline was injected into the two regular CD1 mice in each group for toxicity analysis. The control group was injected with 100 µL saline only. After 2 days, the mice were sacrificed and blood was collected to get the blood serum. The enzymes

of creatinine and ALT, ALP in the blood serum were measured to analyze the toxicity in kidneys and liver (Research Animal Diagnostic Laboratory, University of Missouri).

### Chapter 3. DESIGN, PREPARATION AND *IN VITRO* CHARACTERIZATION OF HER2 TARGETD PROCA1 USING AFFIBODY

#### 3.1 Introduction

As one of the most advanced imaging techniques, MRI plays an important role in clinical diagnosis and treatment [116]. Therefore, in recent decades, the development of MRI contrast agents has been the hottest topic in radiology because of the unique characteristics of MR images [117-118]. However, there are limitations for MRI application in the clinic due to its low sensitivity and specificity. As discussed in Chapter 1.6, molecular imaging of MRI requires contrast agents for significantly improved relaxivity since relaxivity determines the sensitivity of the MRI contrast agents [119]. The relaxivity of about  $5\text{mM}^{-1}\text{s}^{-1}$  of current approved MRI contrast agents such as DTPA could not detect biomarkers with expressed numbers of up to  $10^6$  on the cell surface (Figure 1.7) [18]. Therefore, there is a strong need to develop MRI contrast agents with a high relaxivity and targeting capability for molecular imaging of disease biomarkers [120].

Previously developed protein-based MRI contrast agent (ProCA1-CD2) in the Yang laboratory showed high relaxivity with 10-20 folds increased compared with DTPA (Figure 3.11)[111]. The designed contrast agents were created by designing a metal binding site in domain 1 of CD2. By developing protein based MRI contrast agents, there are several advantages: first, larger water number enables higher relaxivity than small chelators; second, protein is convenient to covalently link with other ligands for targeting to biomarkers; third, humane proteins can eliminate side effects.

In order to produce MRI contrast agents with high relaxivity for clinical application, there are several challenges. First, we need develop a method to express and purify proteins with high yield and low cost. Current injection dose for mice for DTPA is 50 mmol/kg [121]. Second, we need increase solubility of the protein MRI contrast agent. If our contrast agent has a 10 fold increase in relaxivity, protein concentration of 1 mM is required. However, the solubility of ProCA1 is less than 0.7 mM. Although conjugated small chelator molecule such as DTPA to soluble macro molecules may produce large surface exposure to water and some increase the relaxivity [107, 122], large molecules always have the problem in solubility and tissue penetration. Third,  $Gd^{3+}$  is the most common used metal for MRI contrast agents since this molecule has seven free electrons [123]. In order to prevent the competitive binding of physiological metals such as  $Ca^{2+}$ ,  $Mg^{2+}$  and  $Cu^{2+}$  binding to the contrast agent chelators, strong metal selectivity should be achieved in designing the MRI contrast agents. In addition, stability of protein-Gd complex is important to prevent the release of free  $Gd^{3+}$  that is linked to NSF (nephrogenic systemic fibrosis). It is important to maintain relaxivity and serum stability under different conditions. Finally, the targeted protein contrast agent against biomarker will provide us with molecular specificity to against the tumor and further reduce the adverse effect.

In this chapter, we will first discuss our rationale in designing a new protein-based MRI contrast agent called ProCA1-affi342 with the addition of an affibody, which is capable of producing a molecular image of breast cancer by targeting to biomarker HER2. We have developed a novel multimodal molecular imaging probe to target cancer marker HER2/neu using magnetic resonance and near infrared imaging (NIR) (Figure 3.3). We employed a protein-based MRI contrast moiety (ProCA1) that was developed by de novo designing the  $Gd^{3+}$  binding site(s) into a

stable host protein, the domain 1 of rat CD2 (10 KDa). Due to the unique features of the designed metal binding properties, the protein contrast agent exhibited a significant improved T1 relaxivity for MRI contrast enhancement compared to that of commonly used Gd-DTPA (Diethylenetriamine Pentaacetic Acid) at 1.4- 4.7T field strength [111]. A high affinity HER2 affibody [37, 72] was engineered into the C terminal of the designed Gd<sup>3+</sup>-binding protein by a flexible linker. The small molecular size (16 KDa) provides good tissue penetration. We also introduced an optical imaging capability by conjugating a near-IR dye Cy5.5 to a Cys residue at C-terminal of the protein to facilitate imaging analyses (Figure 3.3). To increase protein solubility, blood circulation time, and reduction of immunogenicity, the designed HER2 targeting protein contrast agent was PEGylated using PEG-40, a molecule with tri-branches of 12 units PEG (denoted as ProCA1-affi343-m) (Figure 3.1) The protein generation method was optimized to obtain a high production yield. The biophysical characterization of conformational properties, the metal binding affinity and selectivity, and relaxivity were performed using various spectroscopic methods.

## 3.2 Results and Discussion

### 3.2.1 Designed HER2 targeted protein based contrast agent with one Gd<sup>3+</sup> binding site

Figure 3.1a [111] shows the model structure of the designed protein-based MRI contrast agent (ProCA1-CD2). It was designed with following considerations: First, ProCA1 a designing a metal binding site in domain1 of CD2 was used. Second, a targeting peptide called affibody Z<sub>HER2:342</sub> was cloned to the C terminal of ProCA1-CD2 (Figure 3.2). As discussed in Chapter 1

(1.4), affibody Z<sub>HER2:342</sub> with 58 amino acid has a strong binding affinity to HER2 that is comparable to antibody of 22 pM. The small size of affibody will provide a better tissue and tumor penetration. Third, a flexible five residues GGSGG linker is added between affibody and ProCA1 to avoid the interference between them. Thus the contrast capability of ProCA1-CD2 and Targeting capability of affibody to the biomarkers, like HER2 and EGFR are expected to be not altered much.

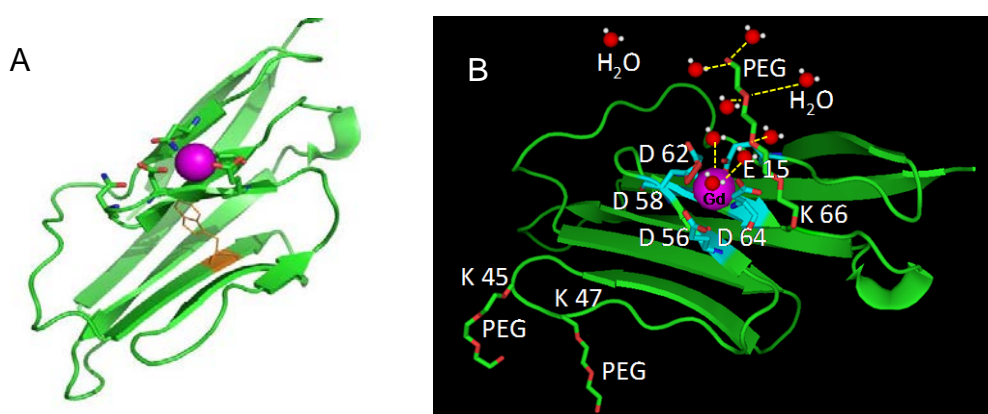


Figure 3.1 Model Structure of ProCA1-CD2 and PEGylated ProCA1-CD2

(A) The model structure indicates the metal binding pocket with four Aspartates (D) and one Glutamate (E). The PEG chain can be conjugated to the Lysine (K) to produce hydrophilic surface and increase the exchangeable water number. (B) The PEGylation sites locate in the lysine which has free amine residue.

In order to make the ProCA1-affi342 suitable for *in vivo* imaging with high solubility, low immunogenicity and proper blood retention time, we further improved the protein based contrast agents ProCA1-affi342 for *in vivo* imaging by protein modification with various sizes of polyethylene glycol (PEG) chain ('PEGylation'). Figure 3.1 shows the modeled structure of the designed contrast agent ProCA1-CD2 with Gd<sup>3+</sup> binding site and the cartoon structure of the secondary and outer sphere water molecules associated with PEG chain.

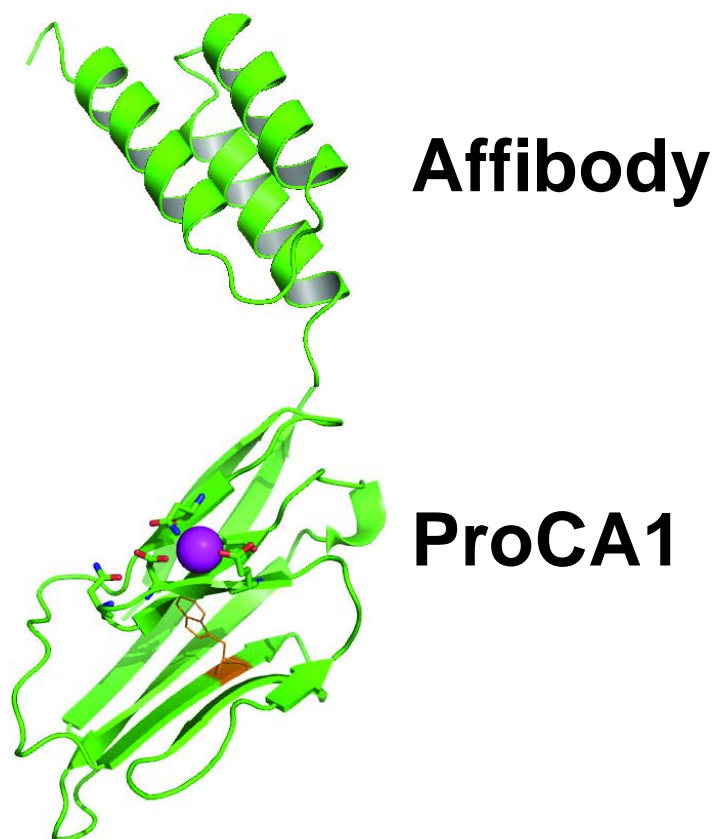


Figure 3.2 Model Structure of ProCA1-affibody.

The affibody was linked to ProCA1-CD2 by a flexible linker. Both ProCA1-CD2 and affibody keep their original folded structure. The ProCA1-CD2 functions as contrast agent domain, which will have MRI signal in magnetic field. The affibody provides the targeting domain to bind the disease biomarkers.

Since MRI technique has relatively low sensitivity, we also created a dual modality for the ProCA1-affi342 (Figure 3.3) by addition of fluorescence probe with high sensitivity. A Cysteine was added by gene cloning to the C-terminal of ProCA1-affi342. The NIR (Near infra-red) dye Cy5.5 with maleimide group was conjugated to the Cysteine residue. The NIR image with high sensitivity can help to probe our MRI contrast agents in achieving molecular imaging.



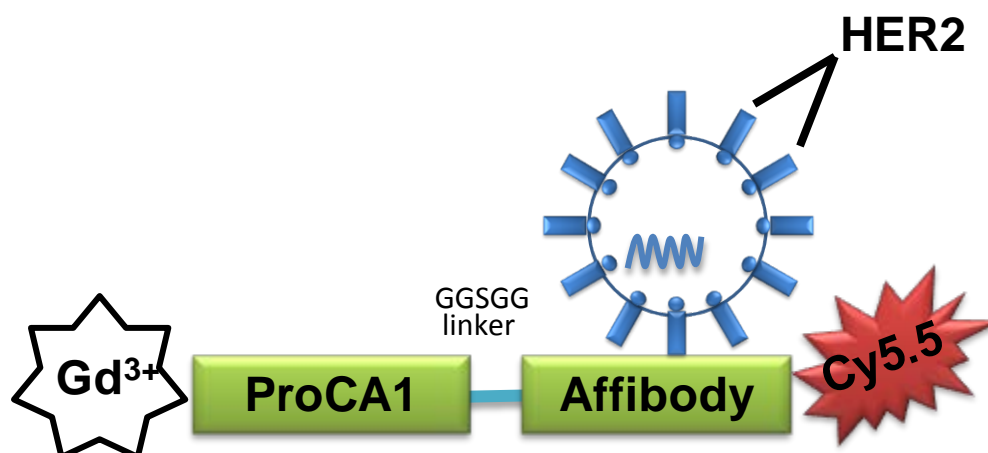


Figure 3.3 Construction of ProCA1-affi342.

The model structure of multimodal HER2 targeted MR imaging probe created by connecting a high affinity HER2 affibody  $Z_{\text{HER2-342}}$  at the C-terminal of a *de novo* designed protein contrast agent ProCA1.CD2 with a designed  $\text{Gd}^{3+}$  binding site. A near IR fluorescence dye Cy5.5 was then conjugated to the added Cys at the C-terminal of the fusion protein. The designed probe was further modified by a tri-branched polyethylene glycol (PEG) with 40 PEG subunits (ProCA1-affi342-m).

To compare the specificity of targeting, we have also created a series of ProCA1-affibodies, such as ProCA1-affi-WT, ProCA1-affi2-4 and ProCA1-affi342 (Figure 1.9). It is reported that affibody342 has highest binding affinity ( $K_d=22 \text{ pM}$ ) with HER2-ECD [72]. Our cell binding data also indicates that ProCA1-affi342 has strongest binding with HER2 overexpressed cells. Therefore, affibody342 was selected as our targeting sequence.

### 3.2.2 Generation of targeted ProCA1-affi342

In order to get high yield of ProCA1-affi342, two methods for expression and purification such as GST-fusion and Tagless methods have been studied.

Figure 3.5 shows the expression of GST fusion of ProCA1-affi342 using PGEX-2T vector with ampicillin antibiotic property. The protein was expressed in LB medium at 37 °C for 6 hours. Then the ProCA1-affi342 was purified by GS-4B column with GST fusion at the N-terminal. After the purified protein (Figure 3.4) was eluted by PBS (Phosphate buffer saline), the protein was PEGylated with PEG-40 directly in PBS, pH 7.4. The reaction needs 1-2 hr in room temperature, and then the PEGylation was stopped by free amino acids like glycine. The protein was further purified by cation exchange SP column (Figure 3.6). SDS-gel had been stained by coomassie blue for protein and Iodine for PEG (Figure 3.7). From the first step, 40-80 mg/L of LB medium proteins can be obtained. The yield of further purification is 80-90%.

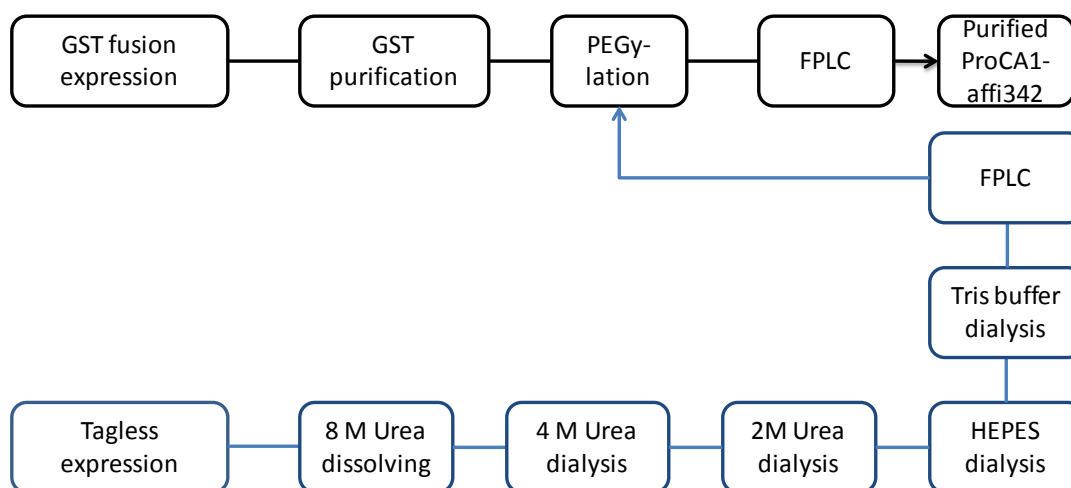


Figure 3.4 Purification Scheme

The procedure of GST scheme (black line) needs three days of the whole procedure, while refolding assay takes one week to get a purified protein.

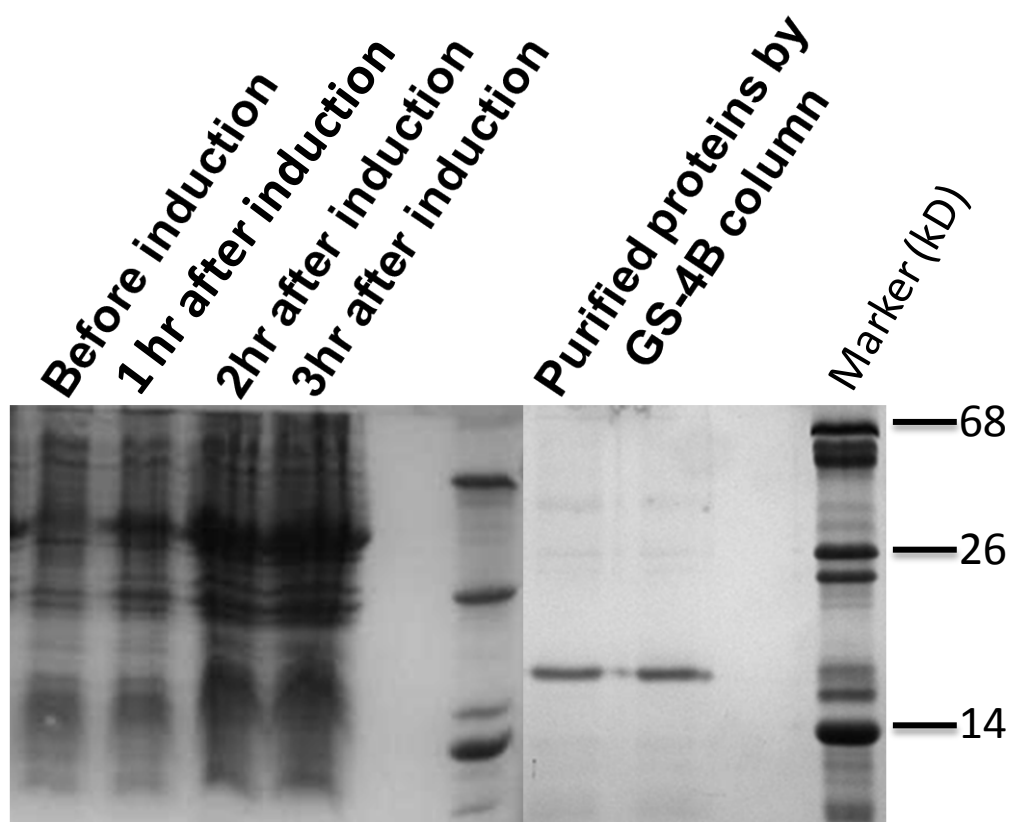


Figure 3.5 SDS gel of expression and initial purification by GS-4B column  
The highest expression level of ProCA1-affi342 reached 3 hours after induction with IPTG. After cleaved from GST tag by Thrombin, the pure protein was eluted from the GS-4B column.

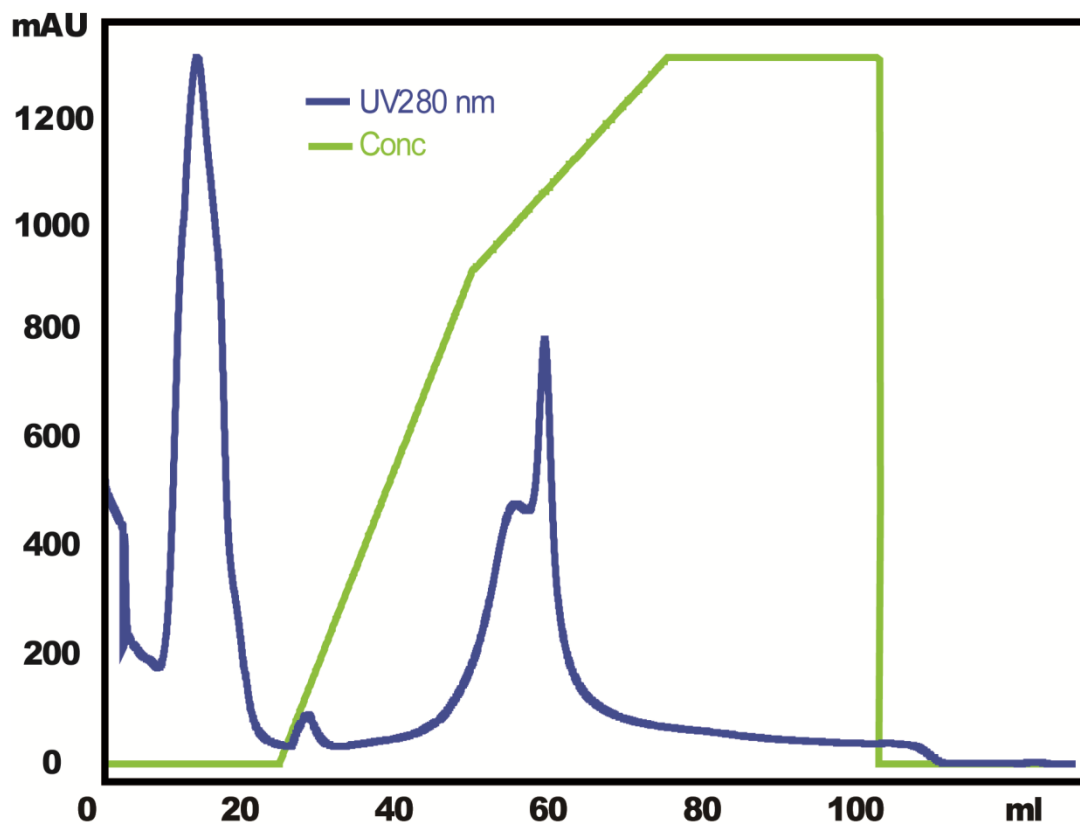


Figure 3.6 Purification of PEGylated ProCA1-affi342 with cation exchange column  
The ProCA1-affi342m was purified by pH gradient. The protein was eluted out between pH7.2-7.4. The elution peak is not asymmetry because the PEGylated ProCA1-affi342 is a mixture with different PEGylation number.

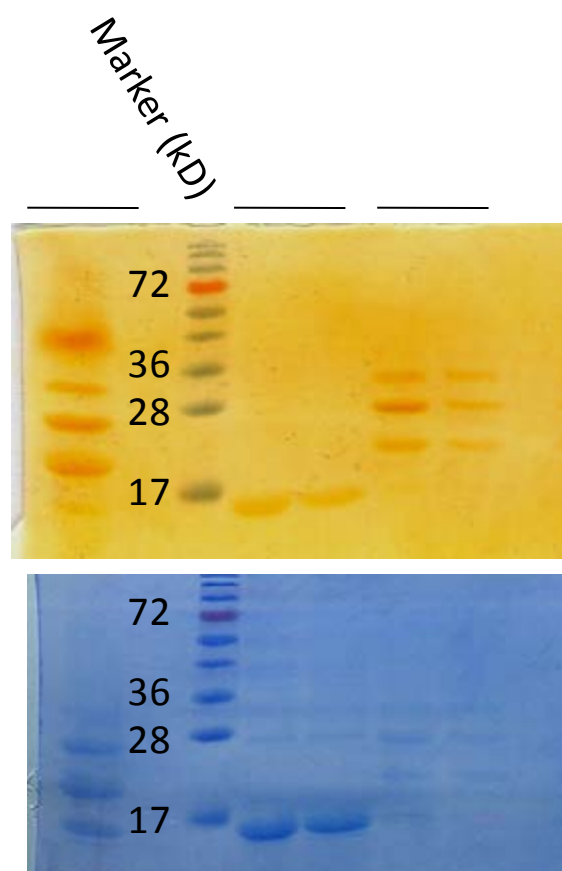


Figure 3.7 SDS gel of purified ProCA1-affi342m from SP column

After purification, the free PEG reagent has been removed. The SDS-PAGE gel has been stained with iodine and coomassie blue in consequence. The coomassie blue stains for proteins and the iodine stains for PEG residues.

For the tagless method, the DNA of ProCA1-affi342 was sub-cloned to PET20b vector. The protein expressed was tagless and insoluble in the inclusion body (Figure 3.8). After refolding with Urea, the protein was purified by cation exchange SP column to obtain a pure protein

The refolded protein obtained from inclusion body cause lower stability and the refolding procedure is time consuming (Figure 3.4). Since the purified protein from GST fusion methods are more soluble and folded, we decide to use GST fusion method to purify targeted protein contrast agent.

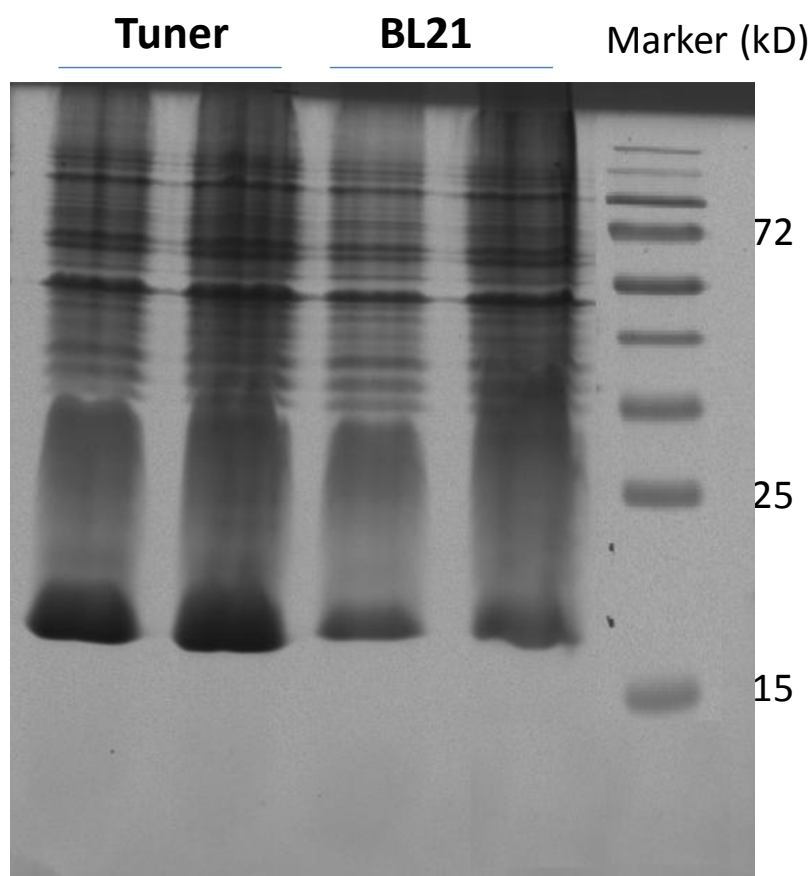


Figure 3.8 Expression of ProCA1-affi342 in PET20b vector

The expression of ProCA1-affi342 in different *E. coli* shows that the expression level in tuner strain is much high than that in BL21(DE3).

### 3.2.3 Conformational analysis of ProCA1-affibody

The tryptophan fluorescent spectrum (Figure 3.8) and far UV CD (Figure 3.9) were used to exam the secondary structure of ProCA1-affi342. The excitation wavelength for the fluorescent scan is 280 nm; the emission range is 260-420 nm. The far UV CD spectrum at the range of 190-260 nm was scanned to compare the secondary structure of ProCA1-affi with its original protein ProCA1-CD2.

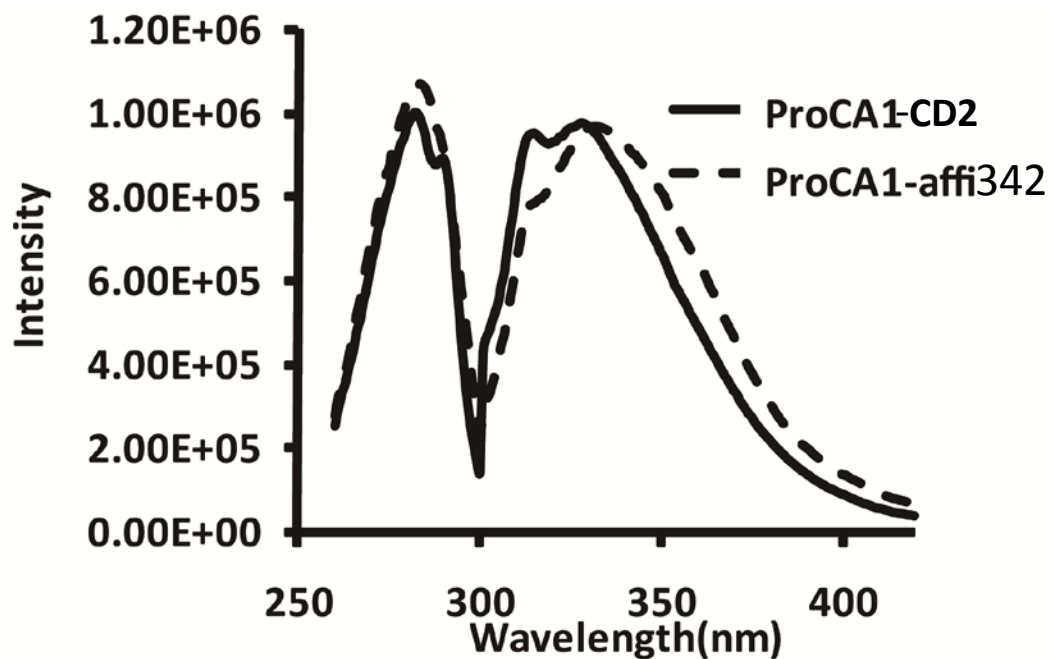


Figure 3.9 Tryptophan Fluorescence measurement.

The ProCA1-CD2 or ProCA1-affi342 of 5  $\mu$ M concentration in HEPES buffer (10 mM, pH7.2) was measured in 10 mm cuvette. The excitation wavelength for the fluorescent scan is 280 nm; the emission range is 260-420 nm. Compare with the host protein ProCA1-CD2, the emission peak of ProCA1-affi342 is red shifted due to the fusion with affibody.

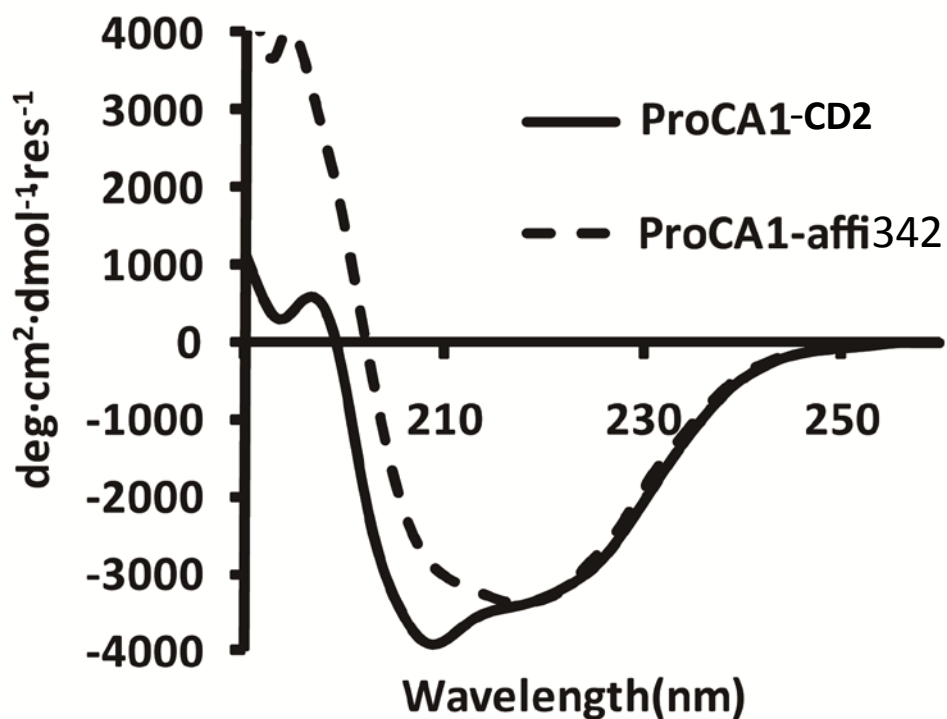


Figure 3.10 The secondary structure measured by CD.

The ProCA1-CD2 or ProCA1-affi342 of 20  $\mu\text{M}$  concentration in HEPES buffer (10 mM, pH7.2) was measured in 1 mm cuvette. The far UV CD spectrum at the range of 190-260 nm was scanned to compare the secondary structure of ProCA1-affi with its original protein ProCA1-CD2.

#### 3.2.4 Modified ProCA1-affibody has been increased both in metal binding affinity and relax- ivity

The designed MRI contrast agent was expressed in *E. coli* and subsequently purified (Figure 4.2). The binding affinity was measured by competitive assay using dye Fluo5N. The eq-



uation 1 was used to calculate the  $K_d$ . Similar to the parental protein ProCA1-CD2, the designed protein (ProCA1-affi) had a strong metal binding affinity with  $K_d$  for  $Gd^{3+}$  at  $1.86 \times 10^{-12}$  M [111] (Figure 3.10). ProCA1-affi also exhibited R1 and R2 relaxivities of 21 and 30  $mM^{-1}s^{-1}$  at 1.41 T, respectively (Figure 3.11). PEGylation resulted in about 15% increases in the relaxivity for both R1 and R2 [124]. The developed protein with conjugated NIR dye exhibited fluorescence excitation and emission maxima at 640 and 695 nm, respectively, and excitation coefficient constant of  $0.21 \mu M^{-1}cm^{-1}$  (Figure 4-3).

$$f = \frac{([P]_T + [M]_T + K_d) - \sqrt{([P]_T + [M]_T + K_d)^2 - 4[P]_T[M]_T}}{2[P]_T} \quad (\text{Equation 1})$$

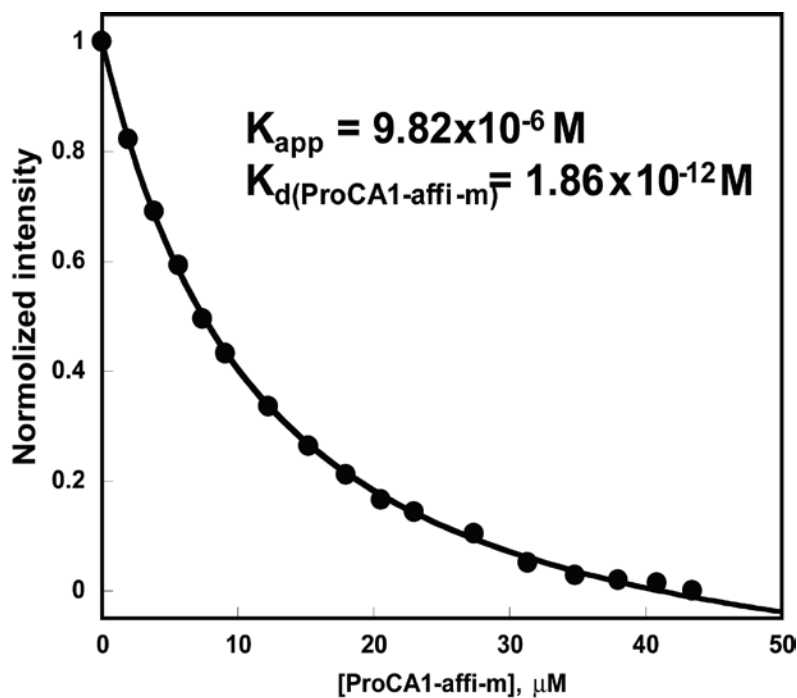


Figure 3.11 Metal binding affinity measurement.

The metal binding of ProCA1-affi342m with  $Gd^{3+}$  was measured by competitive method using Fluo5N [111]. The binding affinity of  $K_d$  is  $1.86 \times 10^{-12}$  M.

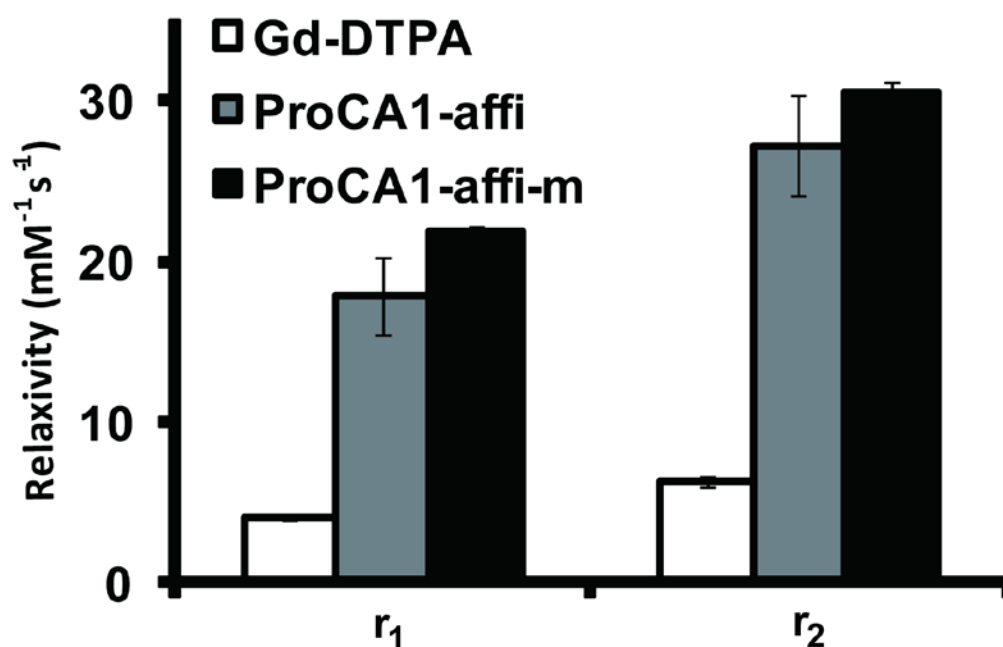


Figure 3.12 Relaxivity of ProCA1-affibody.

The relaxivity of ProCA1-affi342 with (gray) and without PEGylation (ProCA1-affi342m, black) and clinically used Gd-DTPA (white) were measured under the magnetic field of 1.41 T at 37 °C. The developed contrast agent exhibited 5-6 fold greater relaxivity in both  $r_1$  and  $r_2$ .

### 3.2.5 Other improved properties for modified contrast agents

Modifying the proteins with PEG may have advantages in increasing solubility, which enables the ProCA1-affi342 to be concentrated to 5 mM for animal experiments. The stability of ProCA1-affi342 and ProCA1-affi342m was compared by keeping the protein in 37 °C overnight. Figure 3.12 shows that the PEGylated ProCA1-affi342m is much more stable than the original ProCA1-affi342. PEGylation well protects the protein from degradation and cleaving by protease. The immunogenicity was further studied by western blotting. Antibody generativity against the protein contrast agent (both PEGylated and native protein) in the rabbits was examined by western blotting. The experiments were carried out by SDS-PAGE of ProCA1-

PEG2.4k, ProCA1-PEG0.6k and ProCA1 and detected by anti-serum collected from immunoinoculated rabbits. The results showed that addition of adjuvant induced stronger immune responses. PEGylation modifications of the protein dramatically reduced immune responses in the rabbits. Figure 3.13 suggests that the immunogenicity of the protein contrast agent may not be very strong, especially without addition of adjuvant.

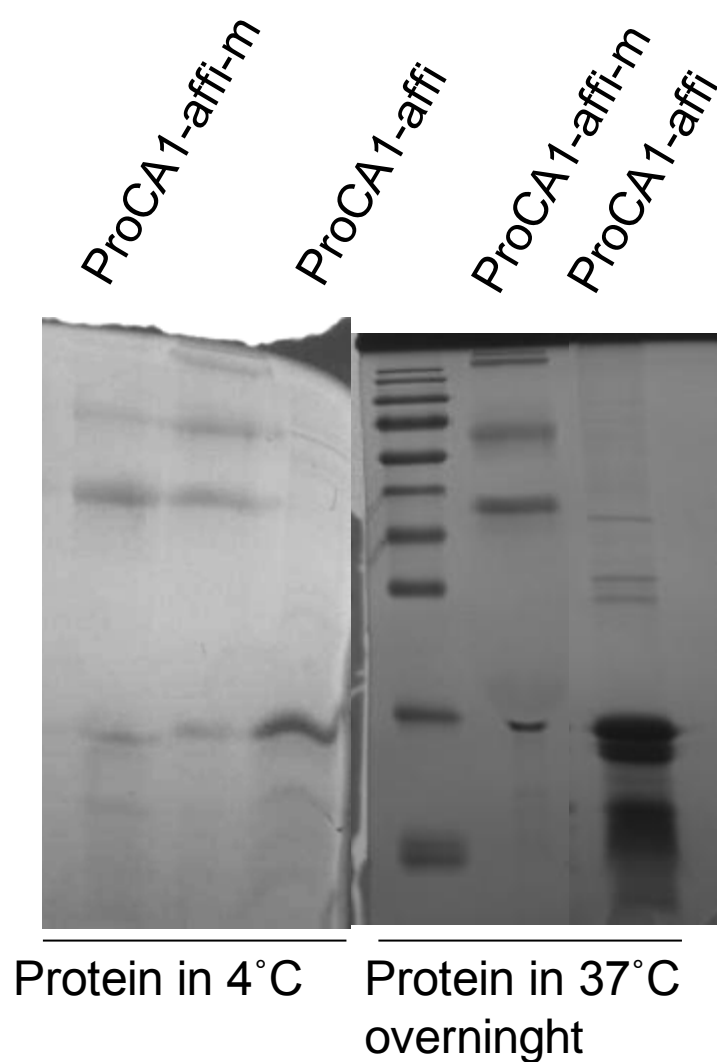


Figure 3.13 SDS gel to measure the stability of modified contrast agent  
The Gel shows that after staying in 37 °C for overnight, the original protein without PEGylation had some degradation, however, the PEGylated protein did not have much change.

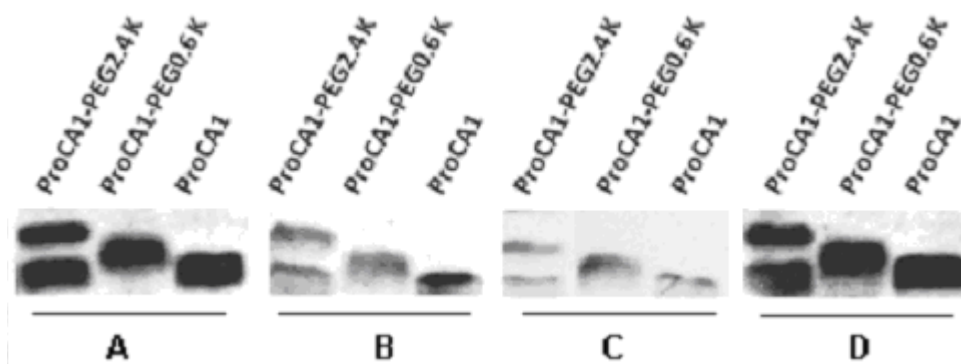


Figure 3.14 PEGylation substantially reduced the immune responses monitored by poly-antibodies.

The commercial CD2 polyclonal antibody PAb-ProCA1 was used as positive control (D). The other antiserum was prepared from the blood collected after two times of injection of native protein ProCA1 mixed with adjuvant (A). ProCA1 in the absence of adjuvant (B). ProCA1 - PEG2.4k mixed in absence of adjuvant (C).

### 3.2.6 Dual label ProCA1-affibody with NIR dye

In order to create a dual moiety for contrast agent for both MRI and optical imaging, a NIR dye Cy5.5 (Figure 3.15) was conjugated to the ProCA1-affibody. Before conjugation, extinction coefficient of the dye in PBS buffer was measured (Figure 3.15). The conjugation efficiency can be calculated from the UV-VIS absorbance (Figure 3.16) and extinction coefficient of protein (Obtained from Protein Calculator) and dye.

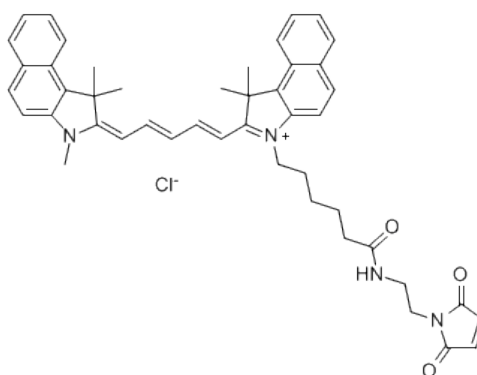


Figure 3.15 Chemical structure of Cy5.5 dye (GE Health care)

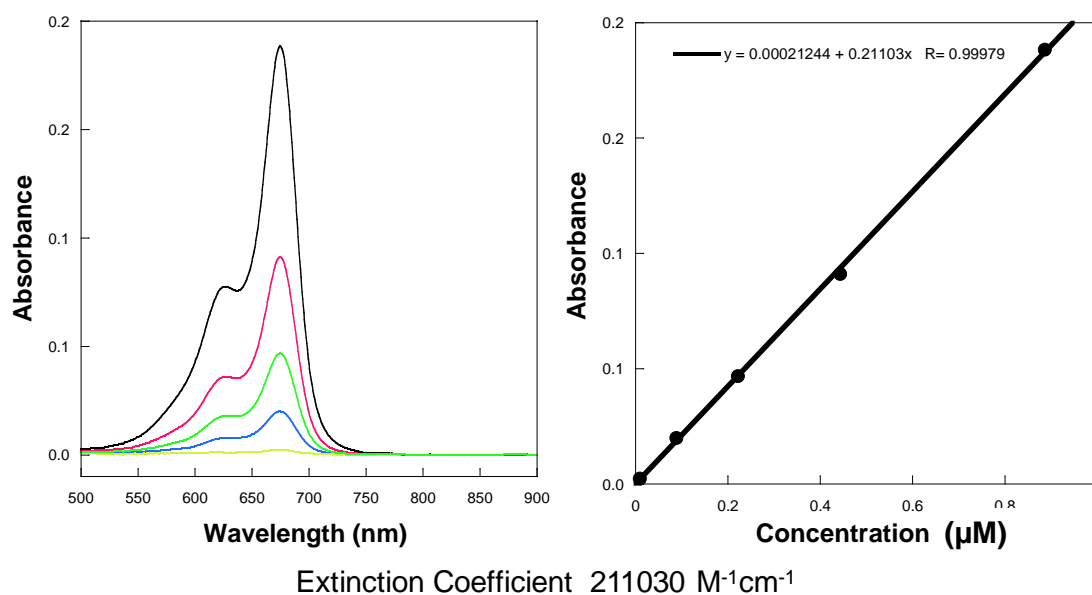


Figure 3.16 Extinction Coefficient of Cy 5.5 was measured

The dye Cy5.5 was dissolved in HEPES buffer at four different concentrations: 10 μM, 25 μM, 45 μM and 90 μM. The absorbance spectra in the vis-NIR range (500-900 nm) were scanned. The linear curve was fitted by the absorbance at peak of 680 nm and concentration.

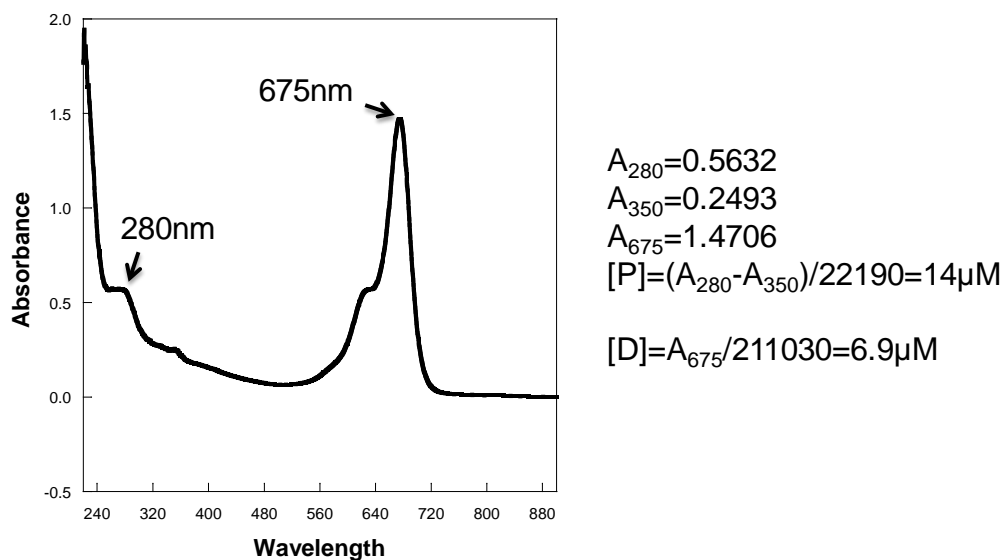


Figure 3.17 Conjugation rate measurement

The conjugation efficiency was calculated by scanning the ProCA1-affi342m-cy5.5 in HEPES buffer (10 mM, pH7.0) of a whole spectrum between 220-900nm. The protein concentration was calculated by the  $Abs_{280}$ . The dye concentration was calculated by  $Abs_{675}$ .

MS spectra and NMR were also used to verify the conjugation of NIR dye to the ProCA1-affibody (Figure 3.17). Since Cy5.5 is a very sensitive dye and MRI is a relatively low sensitive technique which requires high amount of contrast agent, we label a small portion of ProCA1-affi342 with Cy5.5 to produce non-saturated NIR imaging. 1D-NMR also confirmed that the dye was successfully conjugated to the ProCA1-affi342 by viewing the peak shifting (Figure 3.18).

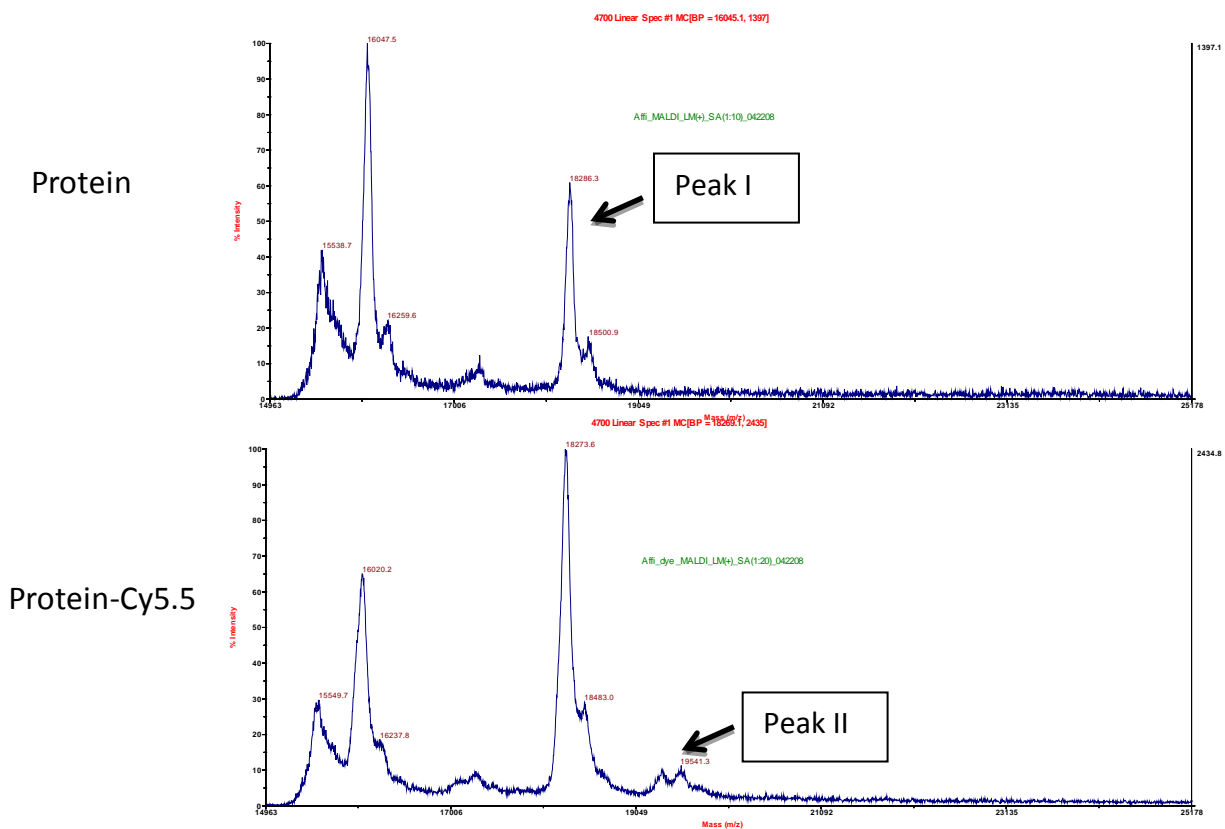


Figure 3.18 MS spectra of free protein and conjugated protein

MALDI-TOF mass spectrometry analyses the mixture after PEGylation with PEG40 (2.4KDa) and fraction purified by ion-exchange FPLC. There were two major peaks in the PEGylation mixture. Peak I was native ProCA1 with measured molecular weight of 11,192 KDa, peak II was ProCA1-affibody-Cy5.5 with measured molecular weight of 13,527 KDa.

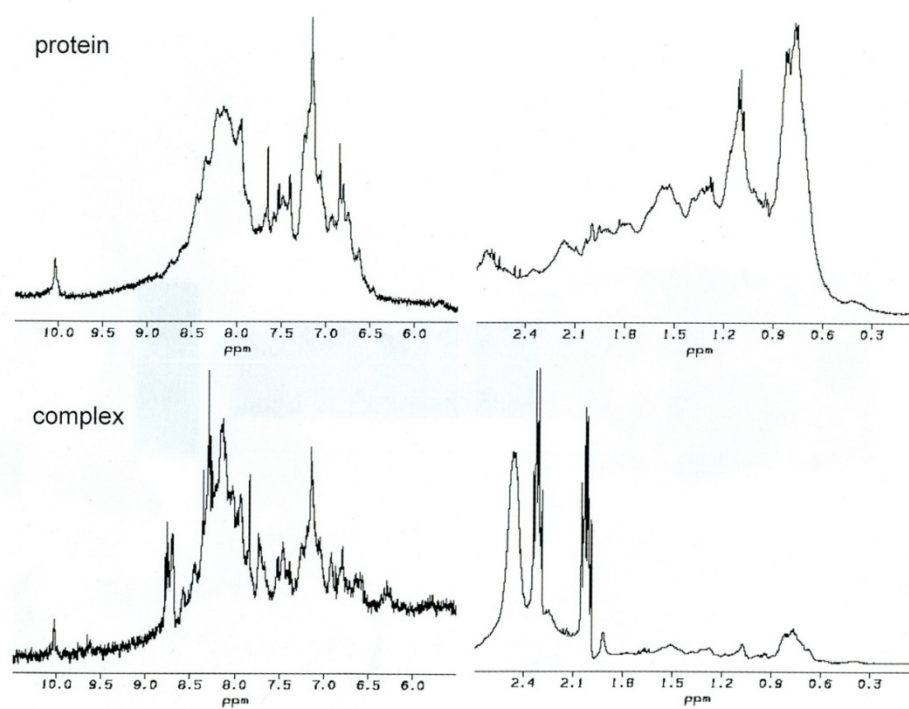


Figure 3.19 NMR spectra of free protein and protein-dye complex  
About 100  $\mu\text{M}$  of ProCA1-affi342 and ProCA1-affi342-cy5.5 complex were dissolved in 10 mM Tris buffer (pH7.0). The NMR spectra at 600 MHz were obtained.



## Chapter 4. CELLULAR TARGETING CAPABILITY ANALYSIS

### 4.1 Introduction

As the discussion in Chapter 1.7, in order to achieve molecular imaging, contrast agent should have very strong affinity to its biomarker. In addition, a strong selectivity over other receptors or non-cancer cells is also very important. Further, quantitative measurement of the biomarker level by the contrast agents is also important for the diagnosis and prognosis of the disease states. Moreover, to achieve molecular imaging of biomarkers by MRI, we also need to have enriched biomarkers. Since endocytosis especially receptor-mediated endocytosis was reported to facilitate the enrichment of MRI contrast agents in the cancer cells [125].

In this dissertation, we selected the suitable protein of peptide for tumor targeting. The cancer cell lines were also well considered for the *ex vivo* and *in vivo* research model. As mentioned in Chapter 1.4, affibody is a Phage display library, several generations of affibody proteins were screen out by targeting to the extracellular domain of biomarker HER2 (Figure 4.1). Two of them with high binding affinity to HER2 were selected in our research. The two affibody sequences, Z<sub>HER2:4</sub> and Z<sub>HER2:342</sub> together with wild type affibody were fused to ProCA1-CD2. These sequences were selected because Z<sub>HER2:4</sub> is the commercial available affibody product. Z<sub>HER2:342</sub> is the reported affibody which has highest binding affinity to HER2 [126]. Wild type affibody was also added to be a non-specific control. At the same time, cancer cell selection is also very important for the research.

In Chapter 3, we reported our design, preparation, and characterization of the conformation, biophysical properties like relaxivity and metal binding affinity of ProCA1-affi342 against HER2 biomarker. In this chapter, we will focus on evaluate the cell targeting capability

of the designed contrast using various methods such as western blotting, immunofluorescent staining and ELISA. Tumor cell lines with different HER2 expression levels were selected. The endocytosis capabilities of ProCA1-affi342 to accumulate in cancer cells were also investigated. These results comparisons between ProCA1-affi342 and other affibody series or PEGylated ProCA1-affi342m confirm the designing strategy and modification advantages.

## **4.2 Results and Discussion**

### **4.2.1 Selection of cell lines**

We used three human cancer cell lines, AU565, SKOV-3 and MDA-MB-231. AU565 is a human breast cancer cell line, with HER2 expression level  $1 \times 10^6$  HER2/cell. SKOV-3 is an ovarian cancer cell line with estimated  $3 \times 10^6$  HER2/cell [127]. MBD-MDA-231 is a breast cancer cell line with modest HER2 levels ( $\sim 3 \times 10^4$  HER2/cell) [128]. EMT-6 is a HER2 negative mouse breast cancer cell line.

### **4.2.2 Monitoring cell targeting of Affibody variants using western blotting**

In order to select a proper affibody variant for HER2 targeting, three variants were compared by using the western blotting. All the three variants: ProCA1-affi342, ProCA1-affi4 and ProCA1-affi WT were added into AU565 and EMT-6 cells respectively.

Table 6 HER2 expression level in various cancer cells

Positive Cell Lines		Negative Cell Lines		Source
Names	HER2 Number	Names	HER2 Number	
AU565	$1.0 \times 10^6$	MCF-7	$2.0 \times 10^4$	Human Breast Tumor
SKBR-3	$7.3 \times 10^5$	MDA-MB-231	$1.8 \times 10^4$	
BT474	$1.06 \times 10^6$			
SKOV-3	$3.0 \times 10^6$			Human Ovarian Tumor
MIAPaca-2	$1.0 \times 10^6$	Panc-1	Under $2.0 \times 10^3$	Pancreatic Tumor
NT5	$1.0 \times 10^6$	EMT-6	Under $2.0 \times 10^3$	Mouse Mammary Tumor

Two different concentrations 3  $\mu\text{M}$  and 10  $\mu\text{M}$  were used. After being treated with the proteins for 2 hr in 37  $^\circ\text{C}$ , the cells were lysed and the cell lysis was used for western blotting. The antibody against ProCA1-CD2 was used to detect the contrast agents. Figure 4.2 shows that in HER2 positive cell line AU565, the ProCA1-affi342 was retained most in the lysis, which means this variant binds most to the HER2 positive cell line. The second generation variant ProCA1-affi4 and wild type also shows some non-specific binding. The cells without treatment were used as negative control. In the HER2 negative cell line EMT-6, all the three variants show some binding which may due to the non-specific attachment to the cell membrane. ProCA1-CD2 without targeting sequences was also added to the cells for a negative control (Figure 4.1c).

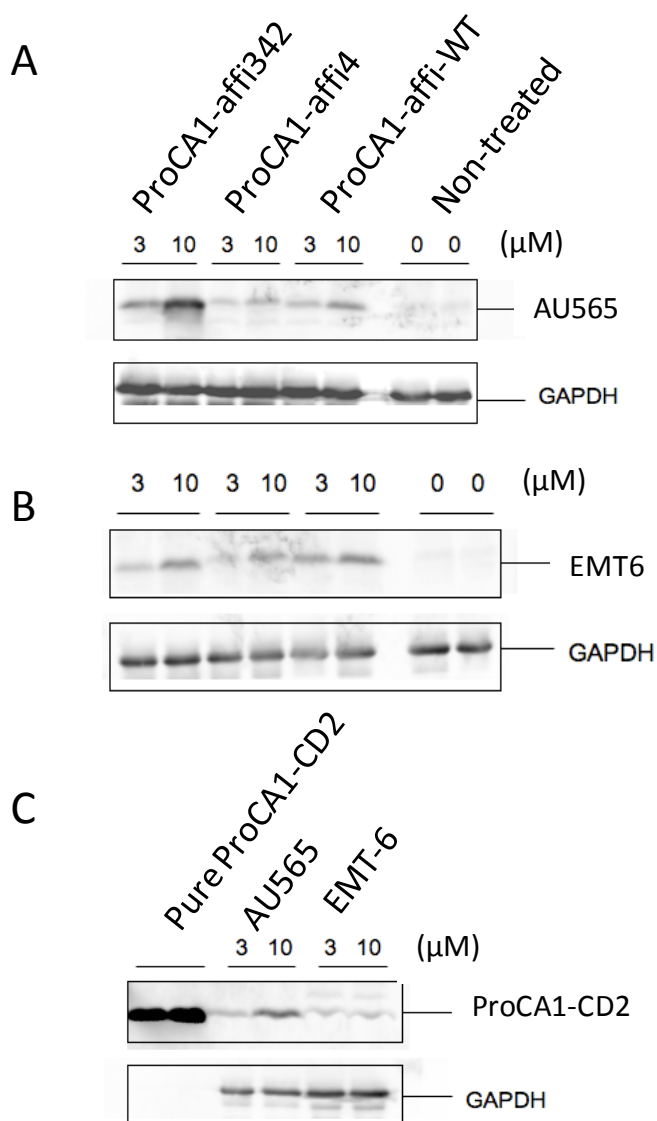


Figure 4.1 Western blot of ProCA1-affi been retained in the cancer cells

The cells were treated with different generations of ProCA1-affibody and the retention of the protein in the cell lysis was measured to calculate the binding capability. The AU565 cell with HER2 overexpression shows obvious binding to ProCA1-affi342. ProCA1-affi2-4 and ProCA1-affi-WT also have some non-specific binding (A). In the HER2 negative cells EMT6. Only ProCA1-affi342 shows weaker binding (B). ProCA1-CD2 was used as negative control which also has some non-specific binding in both cell lines (C).

ELISA was further used to confirm the specific binding of ProCA1-affi342 to the HER2 positive cell lines (Figure 4.3). ELISA is a method with more accurate quantitative analysis of protein and protein interactions. Equal number of SKOV-3 and MDA-MB-231 cells were cultured and treated with ProCA1-affi342 and ProCA1-342m respectively for 2 hr in 37 °C. After carefully washing with HBSS buffer, the cells were lysed and the lysis was used to coat the ELISA plates. Then the ProCA1-affi342 or ProCA1-affi342m retained in the will be detected by PAb-ProCA1-CD2. The final absorbance read from ELISA was substrate from the absorbance of SKOV-3 cells with the one of MDA-MB-231 cells. The results show that the contrast agents can target to the HER2 positive cells lines. The PEGylated ProCA1-affi342 keeps the tumor binding capability.

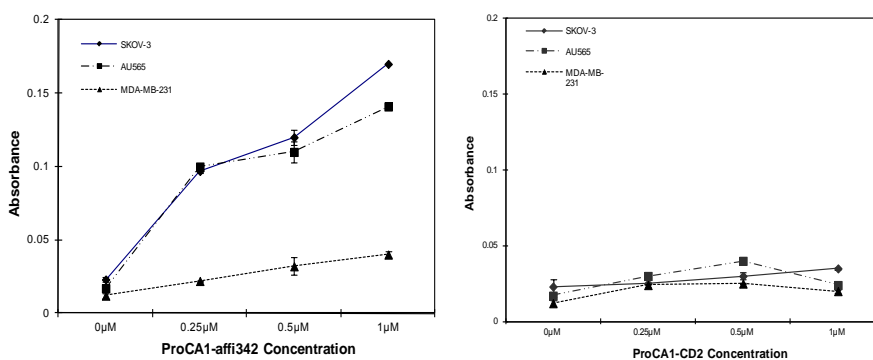


Figure 4.2 ELISA of ProCA1-affi342

Indirect ELISA was used to measure the ProCA1-affi342 and ProCA1-affi342m binding to the cancer cells. Cell lysis of AU565 (HER2 positive) and EMT-6 (HER2 negative) was used to coat the ELISA plate. Then the ProCA1-affi342 and ProCA1-342m was added and detected by primary antibody and secondary antibody with HRP conjugation. Finally, OPD was added to react with HRP and the Abs450 was read. The x axis is protein concentration. The y axis is the absorbance of AU565 substrates with EMT6.

#### 4.2.3 Immunofluorescent staining of cancer cells with ProCA1-affi

We next examined whether the designed ProCA1-affi can target to cancer cells by cell binding analyses. Binding of the Gd-ProCA1-affi to the selected cells was first analyzed by im-

munofluorescence staining using the polyclonal antibody against PEGylated parental protein ProCA1 (PAb-ProCA1). A substantial staining intensity of ProCA1-affi bound to AU565 cells was observed and increased as incubation times increased. In contrast, the EMT-6 cells demonstrated very weak staining (Figure 4.4). It was evident that the Gd3+ ProCA1-affi bound to the cell surface HER2 with a clear membrane staining pattern in AU565 cells at 4 °C (Figure 4.4). The wild type affibody variant, ProCA1-affi WT was also used to stain the cancer cells, Figure 4-5 shows that the wild type variant can only non-specifically attach to the cell membrane. However, binding of the Gd3+ proteins to the cells triggered receptor mediated internalization at 37 °C as demonstrated by the staining of the intracellular ProCA1-affi. The majority of the contrast agents entered the cells after 120 minutes incubation (Figure 4.6). The Gd3+ ProCA1-affi was stable after internalization at 120 minutes, indicating that the designed Gd3+ ProCA1-affi withstood protein degradation during and after endocytosis. The immunostaining results were consistent with NIR fluorescence imaging results (Figure 4.7).

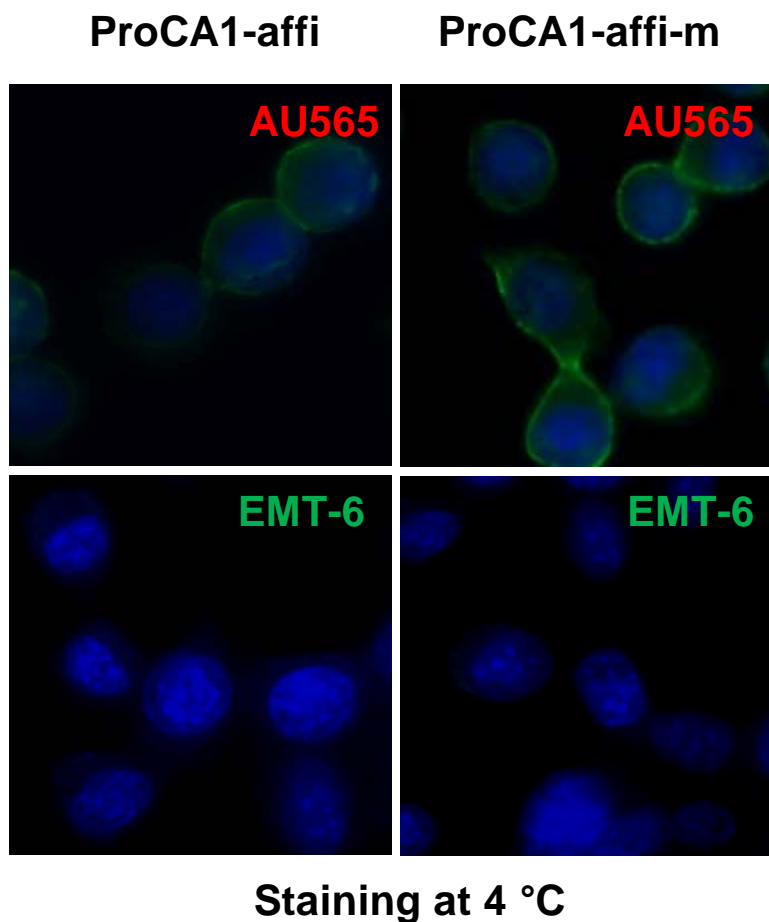


Figure 4.3 Immunostaining of HER2 on cell membrane.

At 4 °C, the HER2 positive (AU565) and negative (EMT-6) cancer cells were treated with ProCA1- affi and ProCA1 -affi-m respectively for 2 hours. The HER2 expressed on the cell membrane of AU565 was revealed by the green color from the goat-anti-rabbit secondary antibody (Invitrogen) for self-generated rabbit antibody against ProCA1-affi-m. The blue color shows the nuclear staining. The imaging was taken under 40x objective in Zessis microscope.

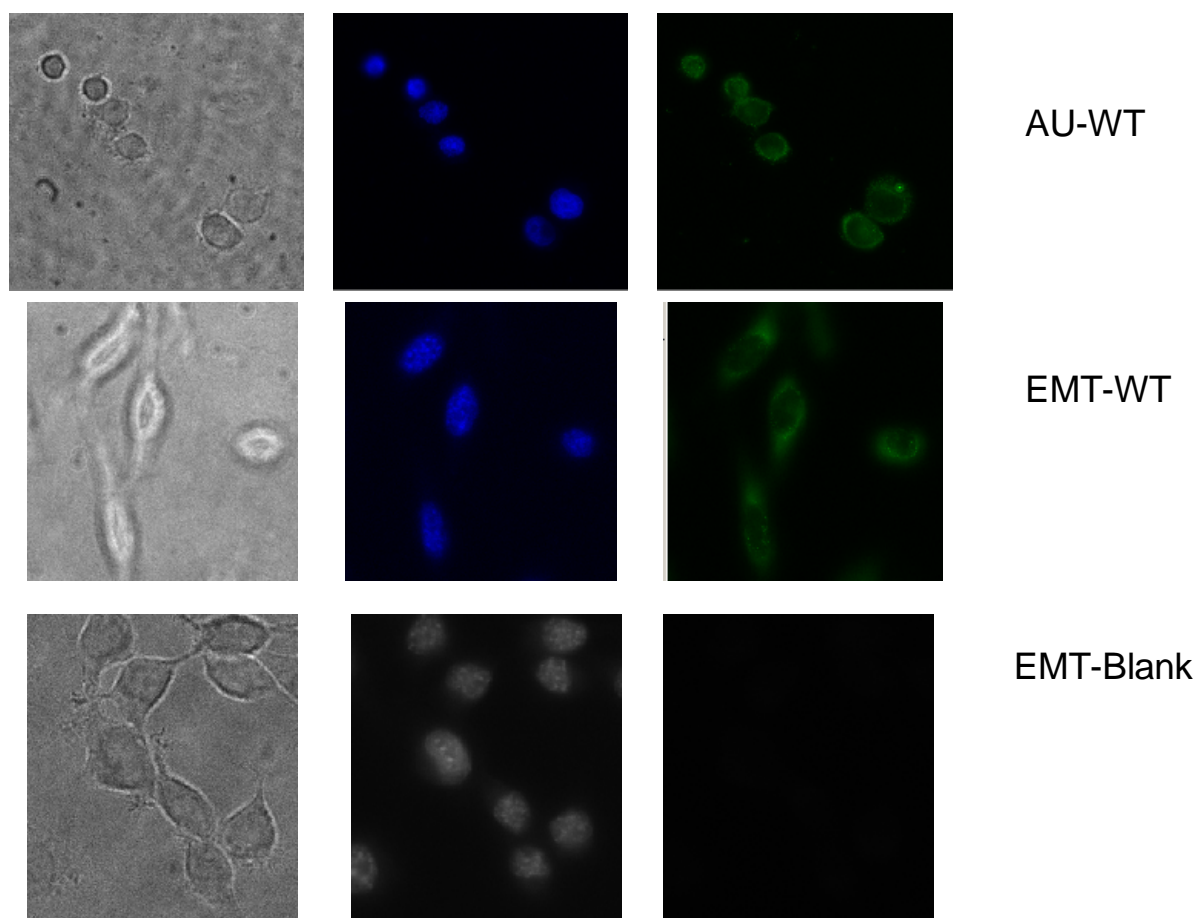


Figure 4.4 Cell staining by ProCA1-affi WT

When the tumor cells were stained by ProCA1-affi WT, both the AU565 with high HER2 expression level and the HER2 negative EMT-6 got staining on the cell membrane. This indicated that the wild type affibody only non-specifically binds to the cell membrane. The EMT-6 cell without adding affibody was used as negative control. The imaging was taken under 40x objective in Zeiss microscope.



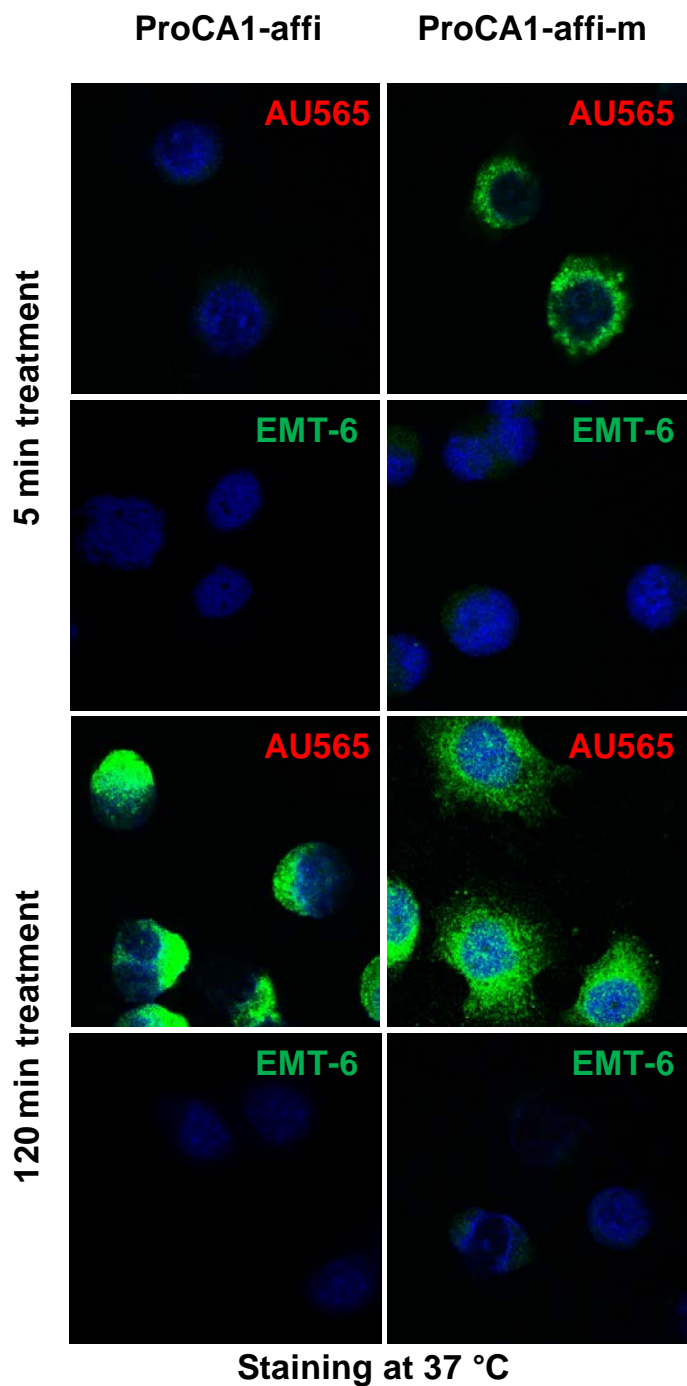


Figure 4.5 Immunostaining for endocytosis studies.

At 37 °C, the cancer cells with HER2 positive (AU565) and negative (EMT-6) were treated with ProCA1 -affi and ProCA1 -affi-m respectively for 5 min and 2 hours. The immunofluorescence staining studies revealed that ProCA1- affi and ProCA1- affi-m bind to HER2 positive cell extensively and were largely relocated into the cytosol via endocytosis after 2 hours (green color). The blue color shows the nuclear staining. At both 4 and 37 °C, negative staining was obtained in EMT-6 cells that lack HER2 expression. The imaging was taken under 40x objective in Zeiss microscope.

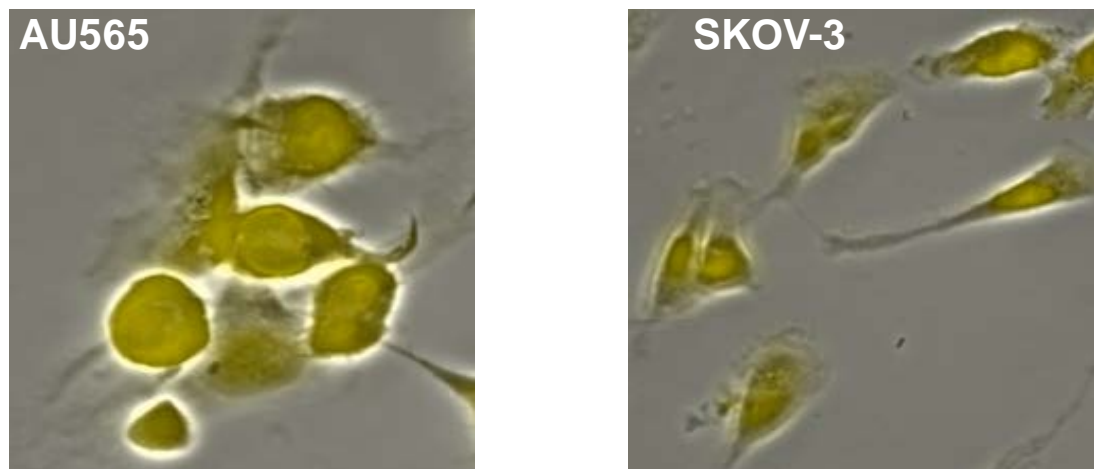


Figure 4.6 NIR imaging of living cells.

The living cells AU565 and SKOV-3 with overexpression of HER2 can be directly detected by ProCA1-affi342mCy5.5 which will generate NIR signals.

#### **4.2.4 Cancer cells treated by different amount of ProCA1-affibody demonstrate the quantitative monitoring capability of designed MRI contrast agents**

In order to get quantitative results from in vivo data, ProCA1-affi342 has to be constantly retained by cancer cells and get endocytosis. Figure 4.7 shows that in HER2 positive cell line AU565, ProCA1-affi342 can penetrate the cell membrane which makes the cell plasma been stained with FITC conjugated antibodies. On the other hand, the modified protein ProCA1-affi342m can get endocytosis faster than the original ProCA1-affi342, which means the PEG residues facilitate the binding of proteins to cell membrane. The HER2 negative cell line EMT 6 was stained for negative control. According to Table 3, cancer cell express different levels of HER2, in this dissertation, four cell lines have been measured by ELISA of the binding with Pro-

CA1-affi342. The ELISA results (Figure 4.8) show that the retained ProCA1-affi342 will be increased as the incubation concentration increasing. The absorbance is highest in SKOV-3 indicates that SKOV-3 has highest HER2 expression level, while EMT-6 is negative.

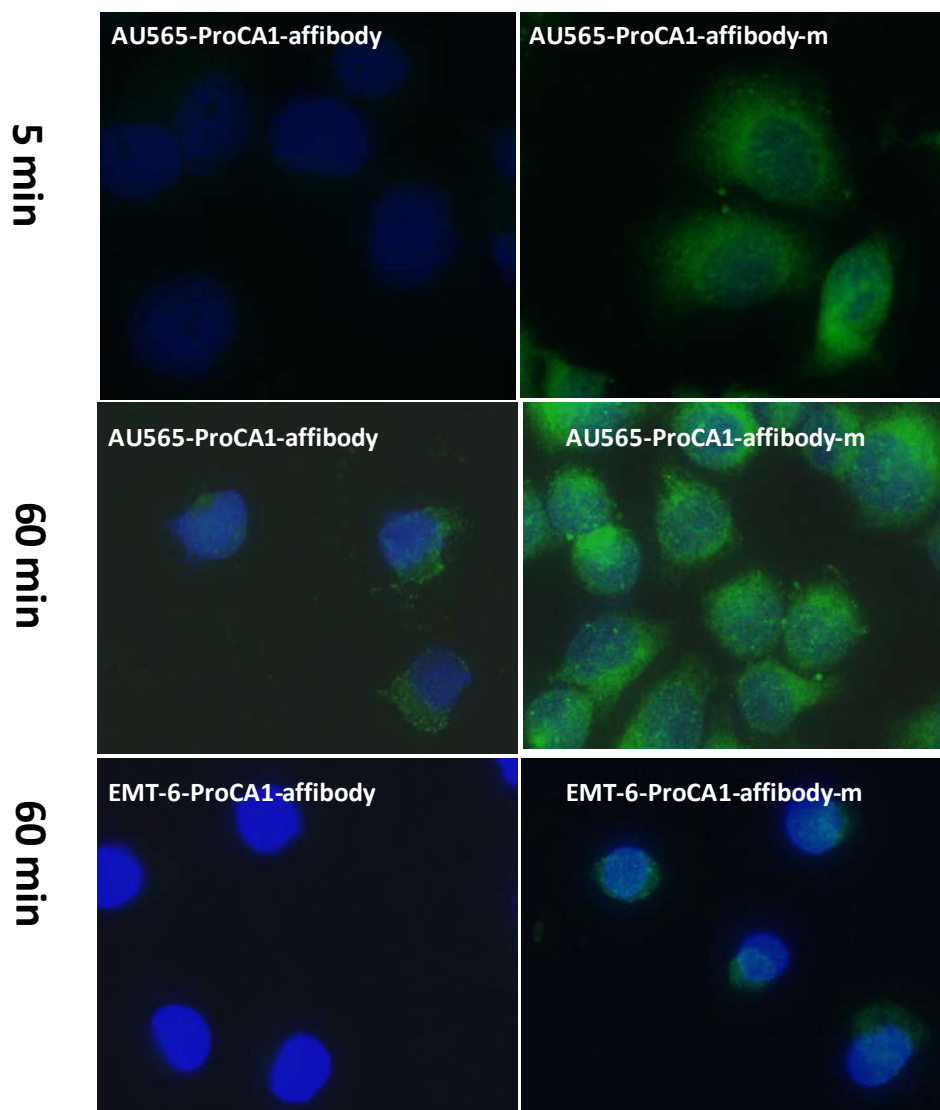


Figure 4.7 Immuno staining of Cancer cells at various time points

The cells were treated with ProCA1-affi342 and ProCA1-affi342m with different time length. In shorter time (5 min), the binding of ProCA1-affi342m to the HER2 positive cells AU565 had been observed. At longer incubation time (60 min), both ProCA1-affi342 and ProCA1-affi342m can target to the AU565. Therefore, the modified ProCA1-affi342 with PEGylation can target to the cancer cells with HER2 overexpression in shorter time. However, the EMT-6 negative cells also had some staining with ProCA1-affi342m treatment, which means ProCA1-affi342m has more non-specificity also.

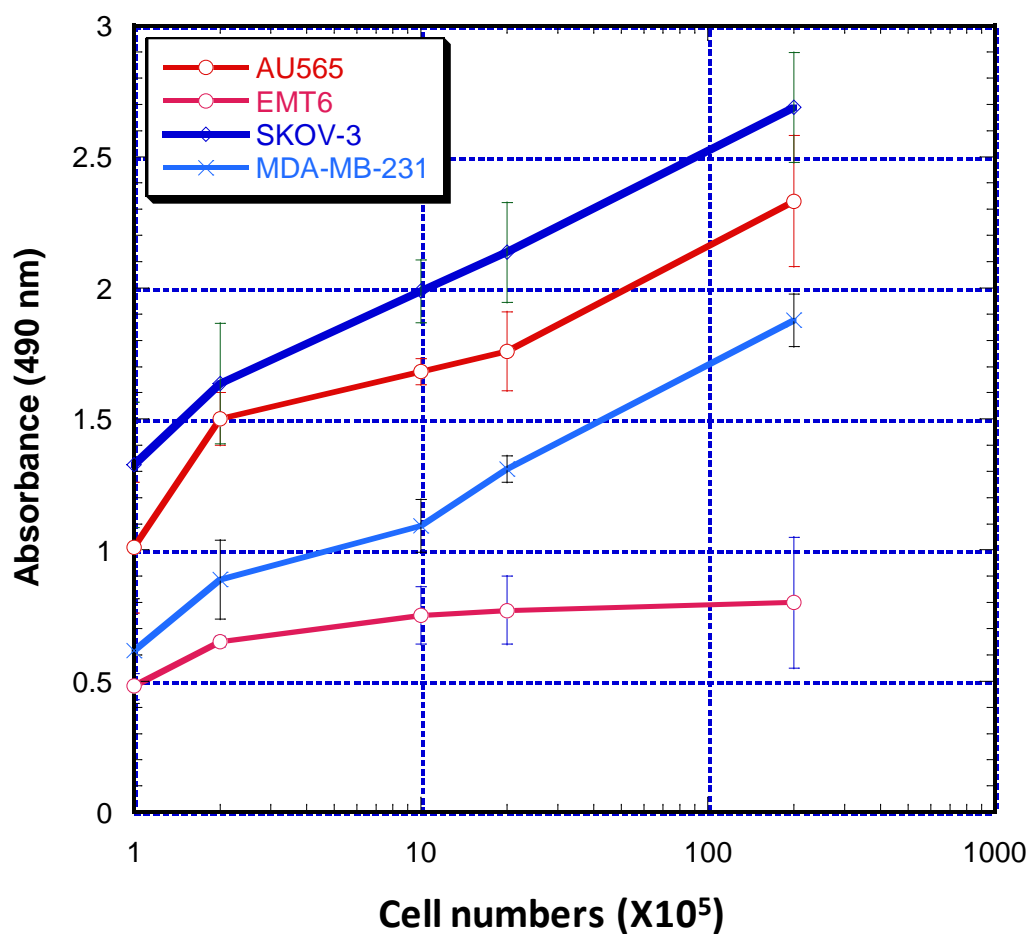


Figure 4.8 ELISA results to measure the binding to cancer cells

In order to detect the expression level of HER2 in different cancer cells, all the cells were lysate for the ELISA. The cell lysis was diluted into four different concentrations and detected by ProCA1-affi342. SKOV-3 has highest expression level. EMT-6 is a HER2 negative cell line.

#### 4.2.5 Flowcytometry measures the constant binding of ProCA1-affi342 to cancer cells

Flowcytometry is also another common way to quantitatively analyze the cell binding capability (Figure 4.9). The binding constant can be fitted by this assay. In this assay, the cells were incubated with ProCA1-affi342m for 2 hr to enable enough endocytosis. Then the cells were washed by HBSS buffer and stained by fluorescent conjugated antibody. After that,  $2.0 \times 10^4$  cancer cells were counted by Flowcytometre machine and the fluorescence was

measured. Figure 4.9 shows the binding constant of ProCA1-affi342. However, the binding cannot be well fitted by the Hill equation (Equation 2) either (Figure 4.10). This is probably due to the other molecules in the cell environment affecting the binding. In order to get the binding affinity between ProCA1-affi342 and cancer cells, larger number of cells needs to be measured to get a more statistical result and the measurement needs to be repeated multiple times.

$$\Delta S = \frac{[M]^n}{K_d^n + [M]^n} \quad (\text{Equation 2})$$

Besides the direct measurement of binding constant between ProCA1-affi342m, the binding was also measured by competitive assay. Commercial Affibody Z<sub>HER2:4</sub> with FITC conjugated was incubated with the cells first. After 2 hr, the non-specific binding was washed and a series of concentration of ProCA1-affi342m was added. The fluorescence was measured 2 hr later. Due to the competition of ProCA1-affi342 to Z<sub>HER2:4</sub>, the fluorescence value decreased as the increasing of ProCA1-affi342m concentration.

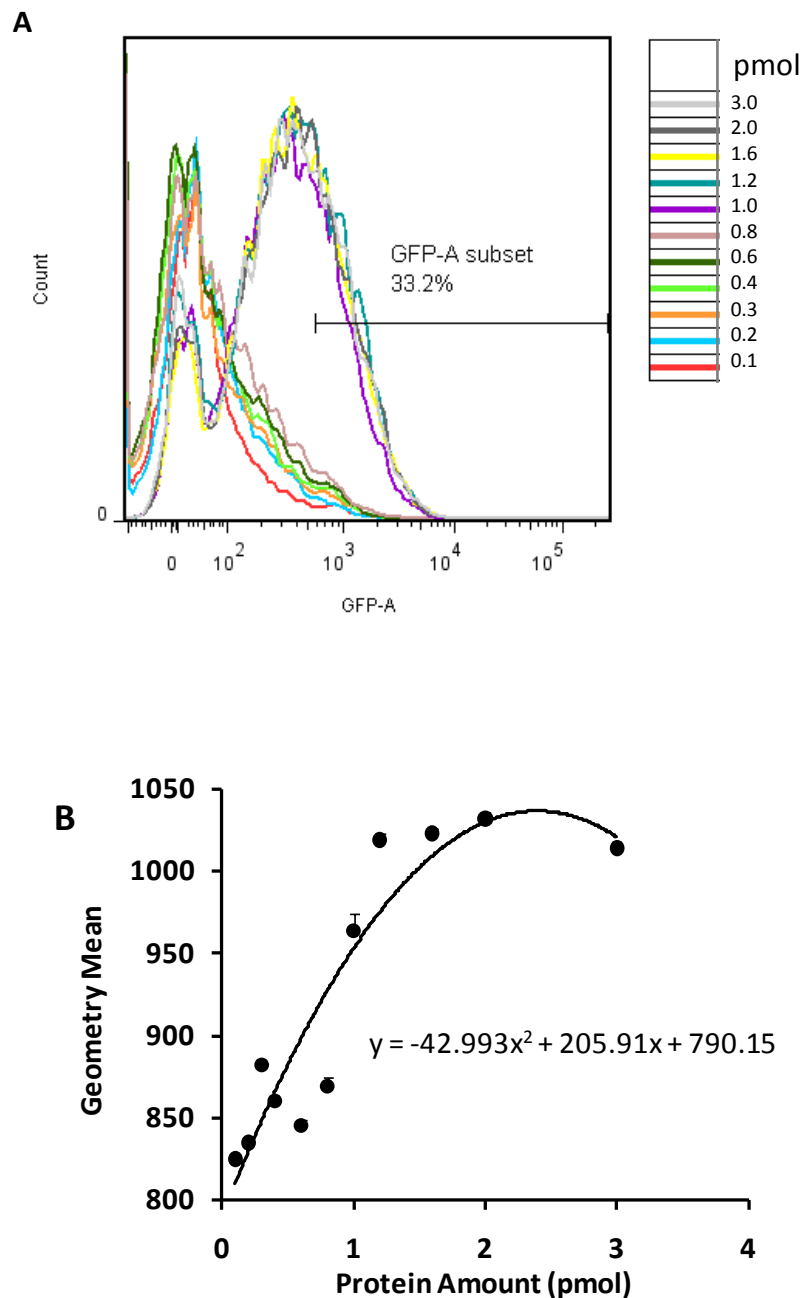


Figure 4.9 Binding affinity measurements (A) and Curve fitting of the binding between ProCA1-affi342m and SKOV-3 cancer cells (B)

The cells were treated by ProCA1-affi342 with different concentrations for 1 hr in 37 °C. Then the cells were washed and detected by FITC conjugated antibodies. (A) Shows the initial flow cytometry curve obtained. X-axis is the fluorescent intensity; y-axis is the counted cell numbers of been stained. (B) With the peak area and protein concentrations, the curve has been fitted. However, a binding affinity has not been derived from this curve which may due to the impurity of cell mixture.

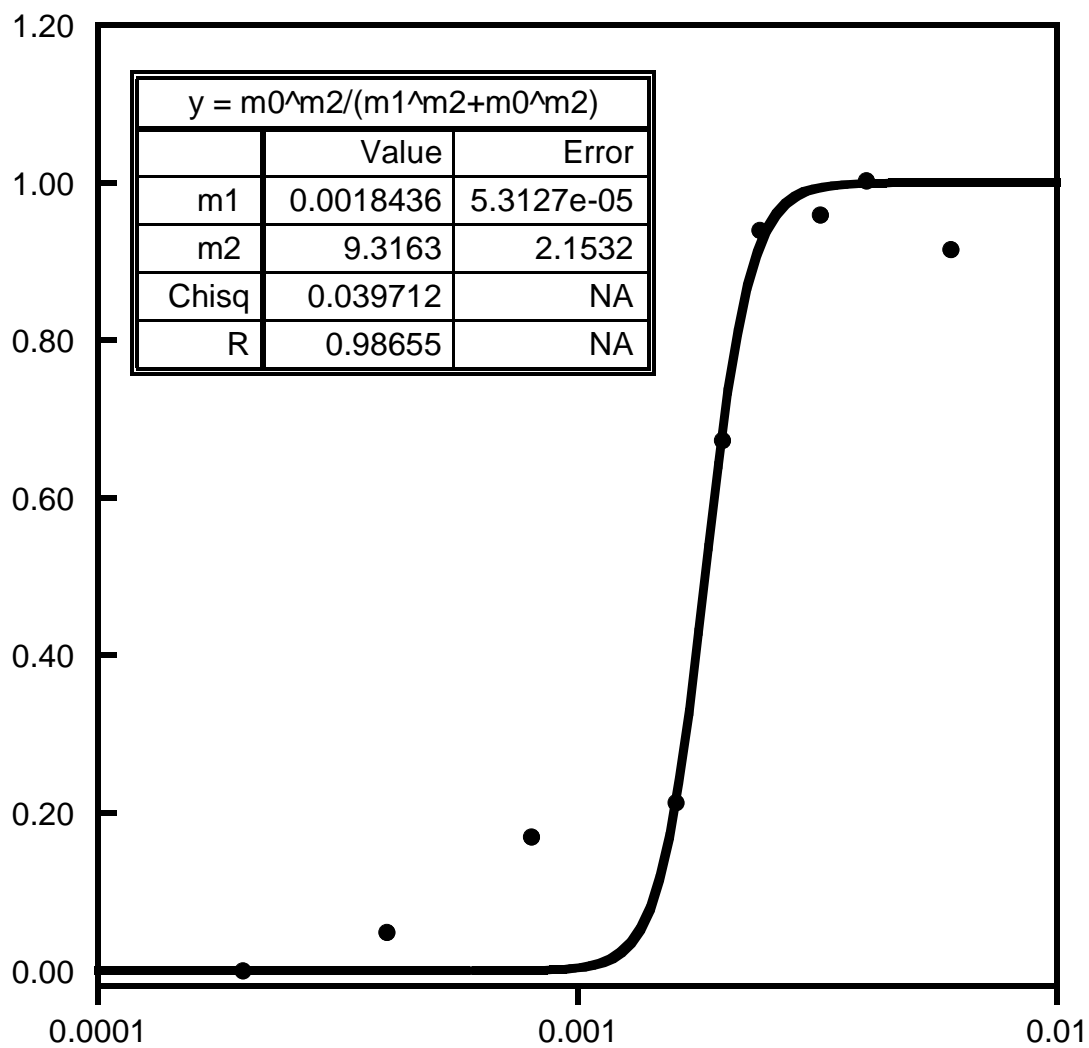


Figure 4.10 Curve fitted by Hill equation

Normalized data were fitted by Hill equation shown in the figure.  $M_0$  is the protein concentration,  $m_1$  is the dissociation constant ( $K_d$ ) and  $m_2$  is the cooperate number.

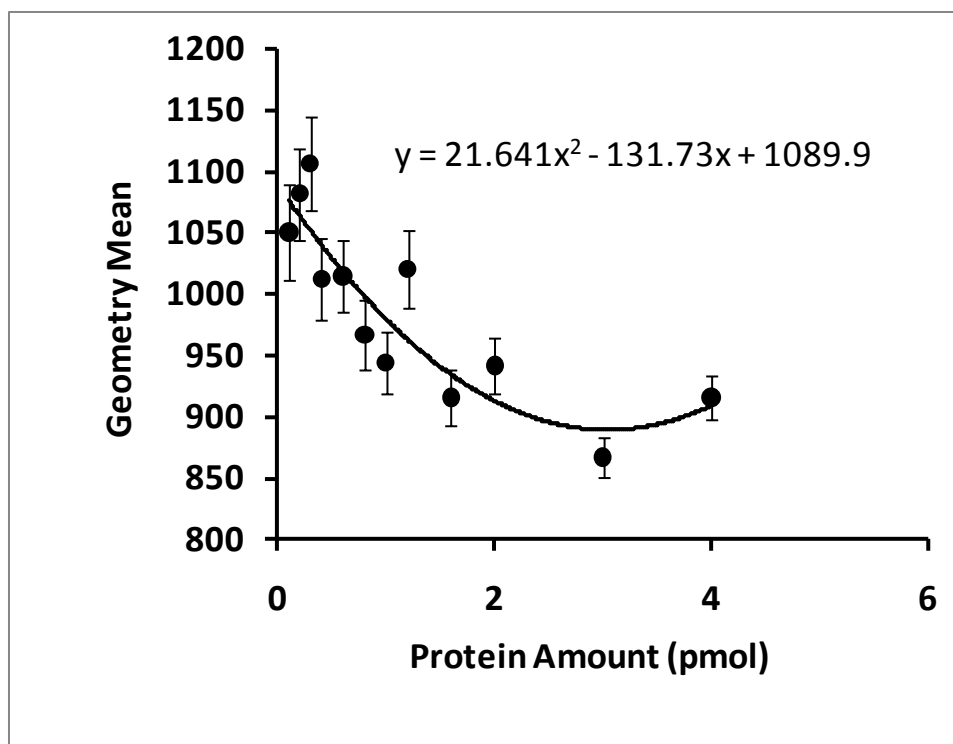


Figure 4.11 Competitive assay to measure the cell binding

The cells were treated by both ProCA1-affi342 and ProCA1-affi4-FITC. The concentration of ProCA1-affi4-FITC is 2 pmol in stable. The concentration of ProCA1-affi342 range is from 0 to 4 pmol.

#### 4.2.6 Generation of antibody against ProCA1-CD2-m

Although there are commercial antibodies against CD2 protein, we mostly use PEGylated contrast agents for our research. The detection sensitivity of commercial available antibodies will be decreased due to the modification covers epitopes of the antibodies. Therefore, the polyclonal antibodies against PEGylated protein have been generated in our group. The purified ProCA1-CD2 with PEGylation was injected to New Zealand white rabbit at the concentration of 5 mg/ml in HEPES buffer once every week for six weeks. The protein was mixed with adjuvants before injection, since adjuvants can stimulate the immune system to generate as much antibody as possible. The first time injection is called inoculation, which uses the complete adju-



vant. Complete adjuvant is harmful to animal body which can only be allowed to use once during the whole procedure (ICUCA protocol 7206). The non-complete adjuvant is used for the following injections, which are also called boosts. Rabbit blood starts to be collected after the third boost. The blood serum containing antibodies will be harvest after centrifuging. The activity of anti-serum was measured by western blotting. The same quantity of PEGylated ProCA1-CD2 was loaded to each lane of SDS-PAGE gel. The anti-serum was diluted 2000 times and 5000 times to be used. Pre-bleeding from the rabbit without injection of antigen was used as negative control. Figure A1 shows that the generated antibody has high specificity by identifying the PEGylated ProCA1-CD2 clearly even by 5000 times dilution.

In order to use the generated anti-serum more sufficiently and keep the generated antibodies for longer time, the antibody was extracted out from the serum and purified. The antibodies were purified by precipitation methods. First, octanoic acid was added slowly with the amount of 28  $\mu\text{L}/\text{mL}$  blood serum [129]. In this step, most of the lipids and other hydrophobic contents will be removed from the serum. Second, saturated ammonium sulfate was used to make the antibodies been precipitated. The precipitated antibody will be pure and can be dissolved in PBS buffer for long time storage (Figure 4.13).

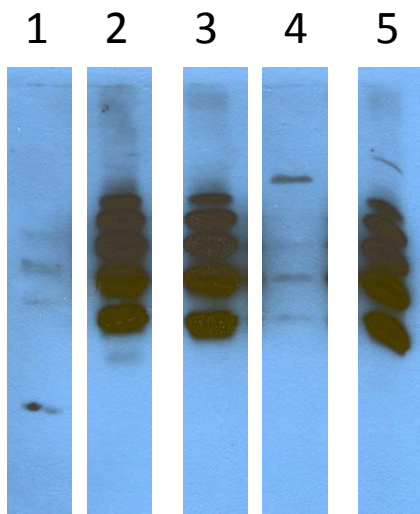


Figure 4.12 Western blotting of anti0serum activity

Lane 1 and 4: detected by pre-bleeding serum Lane2: detected by final bleeding with 5000 times dilution Lane3: detected by final bleeding with 2000 times dilution Lane5: detected by anti-serum of ProCA1-affi342m.

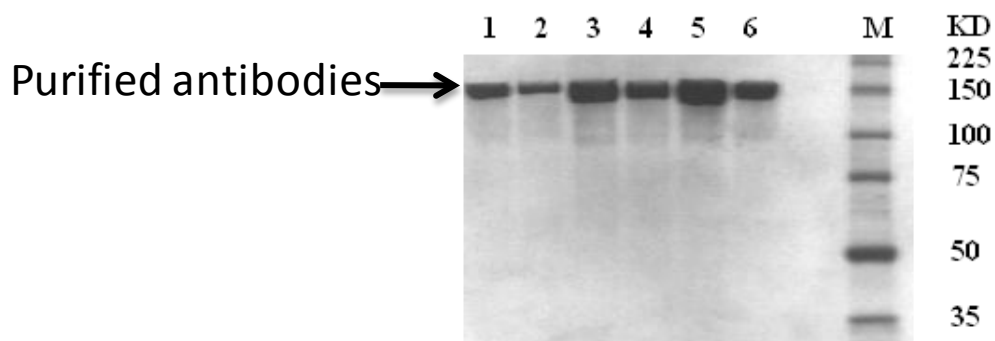


Figure 4.13 Purified antibodies from anti-serum

Lane 1-6: antibodies purified from different anti-serums. The antibodies in non-reduced gel show a molecular weight of 150 KDa.

#### 4.2.7 Quantitative analysis of MRI signals in cancer cells

MRI is a technique with high resolution which makes quantitative analysis possible *in vivo*. Here we measured the retention of Gd-ProCA1-affi342m in cancer cells under 7T MRI machine. The cancer cells were incubated with a series concentration of ProCA1-affi342m. The images were scanned with two pulse sequence. In the gradient echo, we can identify the gradual changes of MRI intensity as the concentration change of ProCAs. In the spin echo, the difference is not visible (Figure 4.14), which indicates than this pulse sequence is not optimized for your contrast agents.

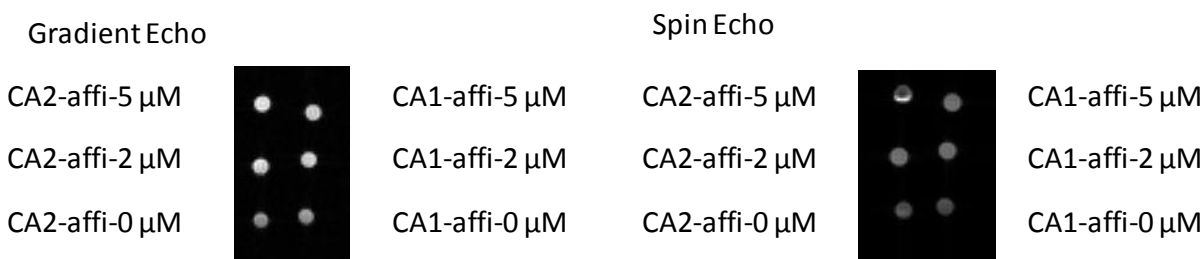


Figure 4.14 The HER2 positive cells SKOV-3 can be imaged under MRI after incubated with various concentrations of contrast agents.

The cells were treated with Gd-ProCA1-affi342 or Gd-ProCA22-affi342 with different concentrations for 1 hr and then washed. The image indicates the specific binding of contrast agents to SKOV-3, the HER2 positive cells.

#### 4.2.8 Cell binding was analyzed by measuring retention of $^{153}\text{Gd}$ cheleted with ProCA1-affi342

Binding of the  $\text{Gd}^{3+}$  ProCA1-affibody to the two testing cell lines was further analyzed by quantification of cell bound  $\text{Gd}^{3+}$  by  $\gamma$ -counting the trace of isotope  $^{153}\text{Gd}^{3+}$  in the  $\text{Gd}^{3+}$  ProCA1-affibody complexes (Fig. 4.15). The results supported our immuno-analyses that  $\text{Gd}^{3+}$  ProCA1-affibody was retained 3-4 folds greater in HER2 positive AU565 cells than HER2 negative EMT-6

cells (Fig. 4.16). Measuring the amount of bound  $Gd^{3+}$  from  $\gamma$ -counting revealed that the  $Gd^{3+}$  ions were bound to cells at  $\sim 0.1$  fmole Gd/cell. Under assumption that  $1 \times 10^7$  cells make a volume of 50 – 100  $\mu$ L, this binding capacity led to the accumulation of  $Gd^{3+}$  at 10 – 20  $\mu$ M in the cell pellets. This local concentration is sufficient to produce strong MRI contrast, especially with the high relaxivity protein contrast agent reported here.

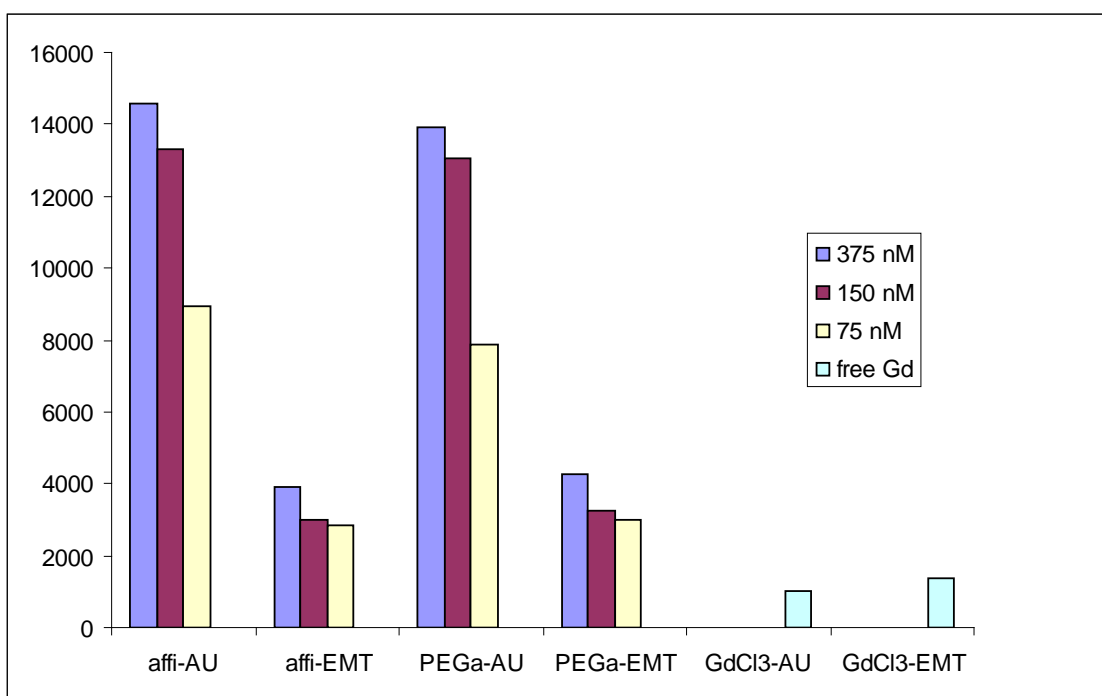


Figure 4.15 Different concentrations of ProCA1-affi342 been retained in the cancer cells by radioactive assay.

By treated the cancer cells with various concentrations of  $^{153}Gd$ -ProCA1-affi342, the HER2 positive cell line AU565 shows constant binding of the proteins to cells, however, in the HER2 negative cell line, the binding shows non-specifically.

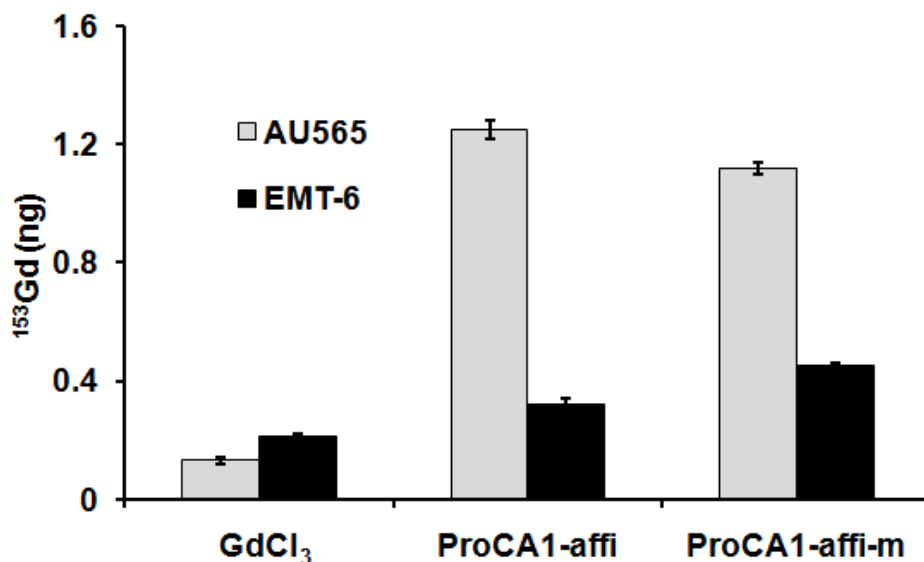


Figure 4.16 Radioactive assay to measure the cell binding of ProCA1-affibody.  $^{153}\text{GdCl}_3$ , and  $^{153}\text{Gd}$  loaded ProCA1 -affi and ProCA1-affi-m were incubated with cultured cancer cells for 2 hours. After careful washing, the radioactive signaling in the cell pellets was measured using  $\gamma$ -counter. The retention of ProCA1-CD2-affi or ProCA1-CD2-affi-m with  $\text{Gd}^{3+}$  in HER2 positive cells (AU565) was  $\sim 3$ -4 folds greater than that in the HER2 negative cells (EMT-6) and non-specific uptake in  $^{153}\text{GdCl}_3$  treated cells.

#### 4.2.9 Summary and future work

In this chapter, various binding assays have been used to measure the binding of  $\text{Gd}^{3+}$  with ProCA1-affi342 and ProCA1-affi342 with cancer cells of high expression HER2. The results show that the fusion of affibody342 does not affect the metal binding site, which indicates a similar metal binding affinity ( $K_d=1.86$  nM) as native protein ProCA1-CD2. Cell binding assays demonstrate that ProCA1-affi342 can specifically target to the cancer cells with high expression of HER2. We also tried initial quantitative analysis of the cell binding assay to obtain the binding affinity of ProCA1-affi342 with HER2 in cancer cells. However, the fitting of the affinity is not reliable (Figure 4.9-10). This may due to the non-homogenous of the cell lysate solution and

non-stable cell status. Further analysis using Biacore, relaxometer or flow cytometer with higher numbers of cells to eliminate or decrease the affecting parameters will be applied.

## **Chapter 5. ESTBLISHING TUMOR MODELS AND MOLECULAR IMAGING OF HER2 IN MOUSE BY MRI AND NIR AND FURTHER ANALYSIS BY HISTOLOGY ASSAYS**

### **5.1 Introduction**

Molecular imaging specifically probes the molecular abnormalities of diseases to allow earlier detection, monitoring of disease progression, and molecular assessment of treatments [130]. Molecular imaging using the modality of magnetic resonance imaging (MRI) has significant advantages in pre-clinical research and clinical diagnosis and prognosis as MRI offers superior spatial resolution without depth limitation, exquisite soft tissue contrast, clinical availability, while avoiding ionizing radiation [131]. However, many applications of MRI rely on the administration of contrast agents to amplify the contrast of the interested regions to obtain both sensitivity and specificity [132]. Developing contrast agents that can be specifically targeted to various biomarkers allowing real-time imaging of biological events at the molecular level will have great clinical importance [133-135]. To achieve molecular imaging by MRI, especially to quantitatively monitor the expression level of the disease biomarkers, it is essential to develop contrast agents with high relaxivity, target capability, optimized pharmacokinetics, tissue penetration and low or no toxicity [136].

As discussed in Chapter 1.2, human epidermal growth factor receptor (EGFR) type 2 (HER2/neu) is a cell surface receptor of the EGF family that is overexpressed in breast, ovarian, urinary bladder and many other carcinomas. In the case of breast cancer, HER2 overexpression is typically associated with younger patients and generally poor prognoses with substantially higher probabilities of relapse after treatment [45, 48]. In addition, the HER2 mediated recognition system has been widely employed as a drug target for anti-cancer therapies. Unfortunate-

ly, current diagnosis of HER-2 positive tumor relies mostly on the use of fine needle biopsies with subsequent immunohistochemistry (IHC) analysis and/or fluorescent in situ hybridization (FISH). These methods suffer from several drawbacks including sampling errors, misinterpretation due to lack of quantization, and discordance between primary tumors and metastases. Thus, assessment of HER2/neu levels by non-invasive MR imaging will provide a tremendous tool for cancer diagnosis/prognosis, design of treatment strategies, and monitoring the effectiveness of the treatment.

In order to measure the *in vivo* function of ProCA1-affi342, suitable tumor model was selected. In this chapter, there are mainly two tumor models being discussed. One is subcutaneous model, which the cancer cells were injected under the surface skin [62]. SKOV-3 and MDA-MB-231 cell lines were selected because they have moderate tumorigenicity and well differential shape. The moderate means the tumor growing speed of these cell lines in nude mice is around 4-8 weeks which is easy to control and monitor [137]. Since we inoculate two different cell lines on each flank of the nude mouse, the selected cell lines should have similar tumorigenicity. Therefore, the cell lines of AU565 with rare tumorigenicity and EMT-6 which can generate tumors within one week were not selected for our research. Another tumor model is the orthotopic model which can mimic the real tumor situation by injecting tumor cells in the original sites, for example, the breast cancer cell line MCD-10DCIS will be injected to the mammary sites of the nude mice.



## 5.2 Results and discussion

### 5.2.1 Cell preparation for xenograft tumor model

The SKOV-3 and MDA-MB-231 cells were cultured and passaged in Coy's 5A and DMEM medium respectively. Cells were scraped from the flask and suspended in HEPES (10 mM, pH7.2). Then the cells will be washed with HEPES buffer for three times and counted. Finally the cells will be diluted in to  $5 \times 10^6$  /100  $\mu$ L medium. The injection medium is 50% HEPES buffer with 50% percent matrix gel (BD bioscience). Each spot on the mouse flank will be injected with 100  $\mu$ L of the cells.

### 5.2.2 MRI on xenograft model indicates the specific targeting of ProCA1-affibody

We then tested whether our designed contrast agent would result in MRI contrast enhancement in xenograft models of these two human cancer cell lines. The SKOV-3 tumor with a high HER2 expression was subcutaneously implanted in the right flank, while the MBD-MDA-231 with a low HER2 expression was implanted in the left flank of the same mouse for direct comparison (Figure 5.1). The contrast agent  $Gd^{3+}$  ProCA1-affi-m at concentration of 3 mM (10 fold lower than clinically-approved contrast agent DTPA) was administrated via the tail vein (80  $\mu$ L). Pre- and post-contrast MRI were collected at different time points using T1 and T2 weighted fast spin echo or T1 weighted gradient echo sequences. After 3 hr, HER2 positive tumor exhibited significant contrast enhancement. Strong contrast enhancement was observed in the SKOV-3 tumor 24 hours after injection, while there were no significant changes in contrast in the MBD-MDA-231 tumor (Figure 5.2 and Figure 5.3). Such MRI contrast enhancement

was decreased after 24 hrs post injection. In parallel, the mice were imaged using an optical animal imaging system (Figure 5.1). Consistent with MR imaging, we observed a strong NIR light emission from the SKOV-3 tumor at 24-hour post-administration of the contrast agent, however, the NIR intensities at the MBD-MDA-231 tumor site were much less than that of the SKOV-3 tumor (Figure 5.4).

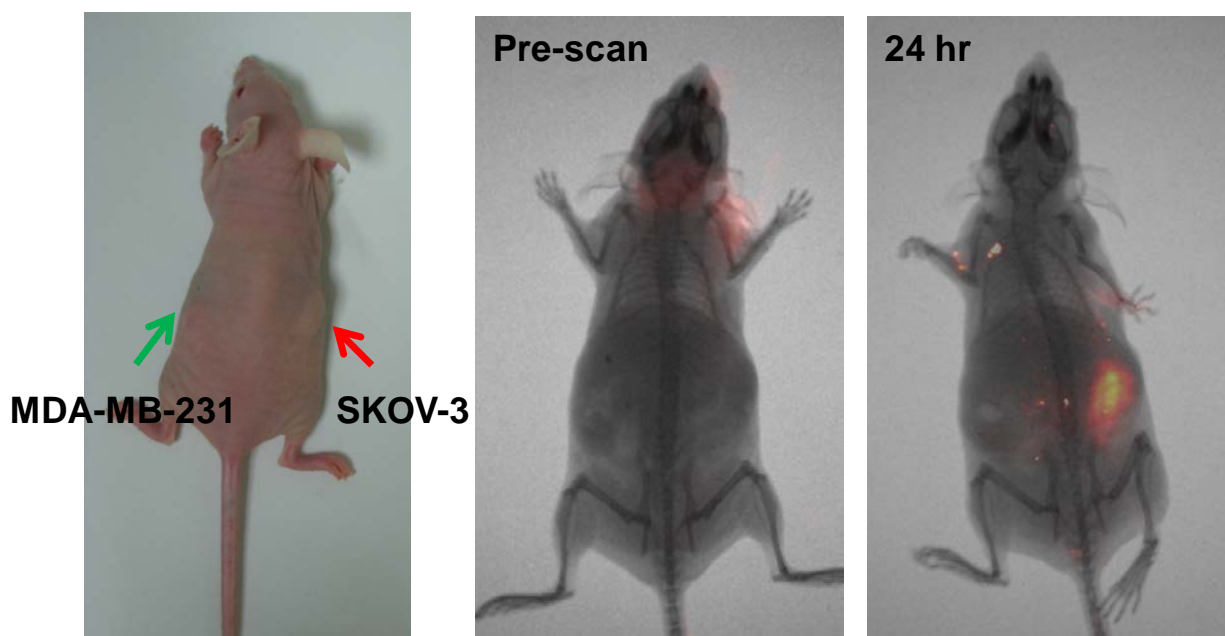


Figure 5.1 NIR imaging on Xenografted mouse.

NIR fluorescence imaging (Kodak 8000) revealed that ProCA1-Affi is able to target to the HER2 positive tumor (SKOV-3, right) 24 hr after injection from tail vein. No significant near IR signal was detected in the HER2 negative tumor (MDA-MB-231, left).

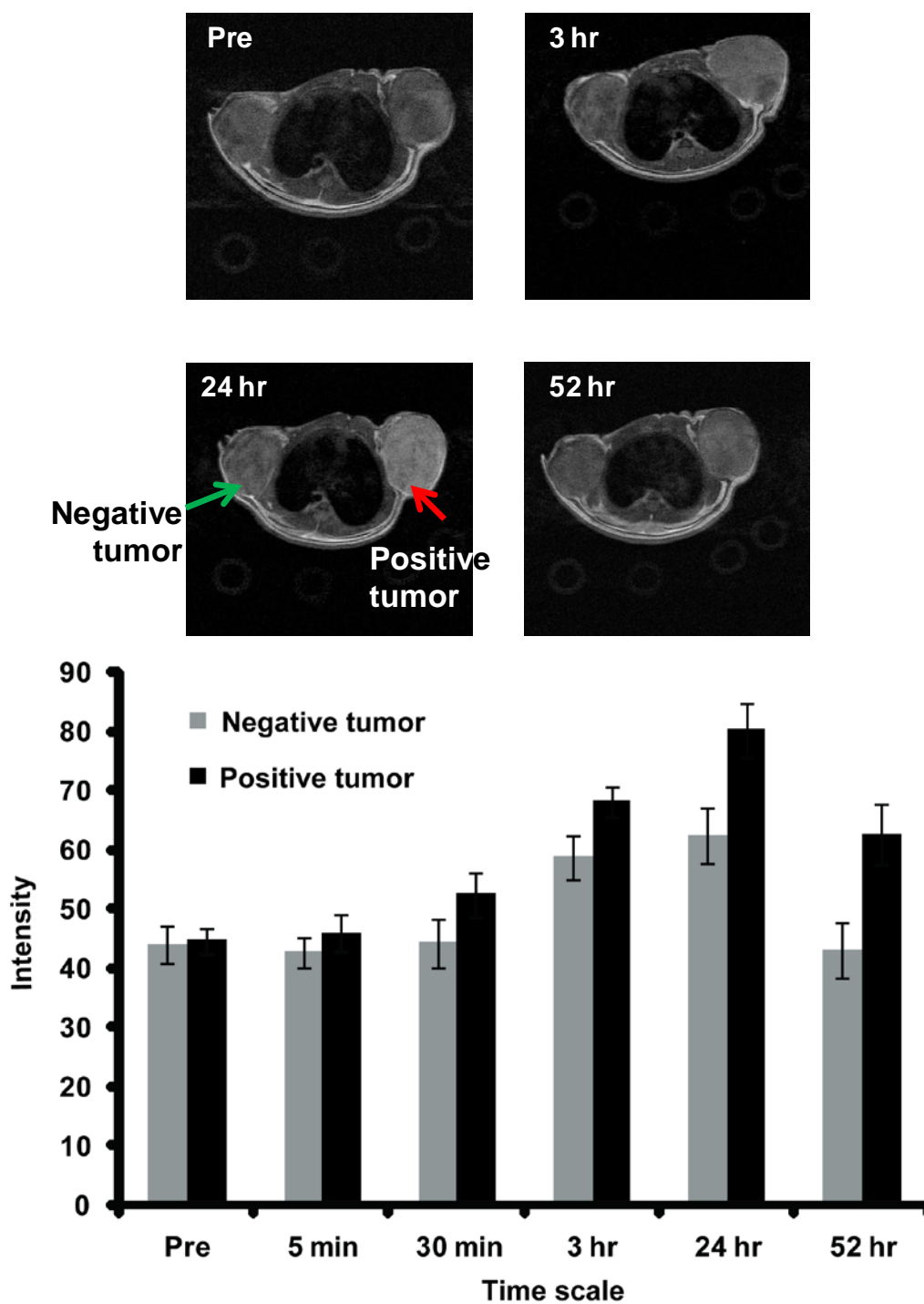


Figure 5.2 MRI of Xenografted mouse with Fast Spin Echo.

Fast spin echo transversal MR images collected prior to injection and at various time points post injection of 3.0 mM of ProCA1-affi-m in HEPES saline via tail vein. The MRI signal on the positive tumor (SKOV-3, right) exhibits significant enhancement at 3 hr post injection and reaches maximum enhancement at 24 hours post injection. The slight differences in MRI signals result from the use of different pulse sequences for imaging.

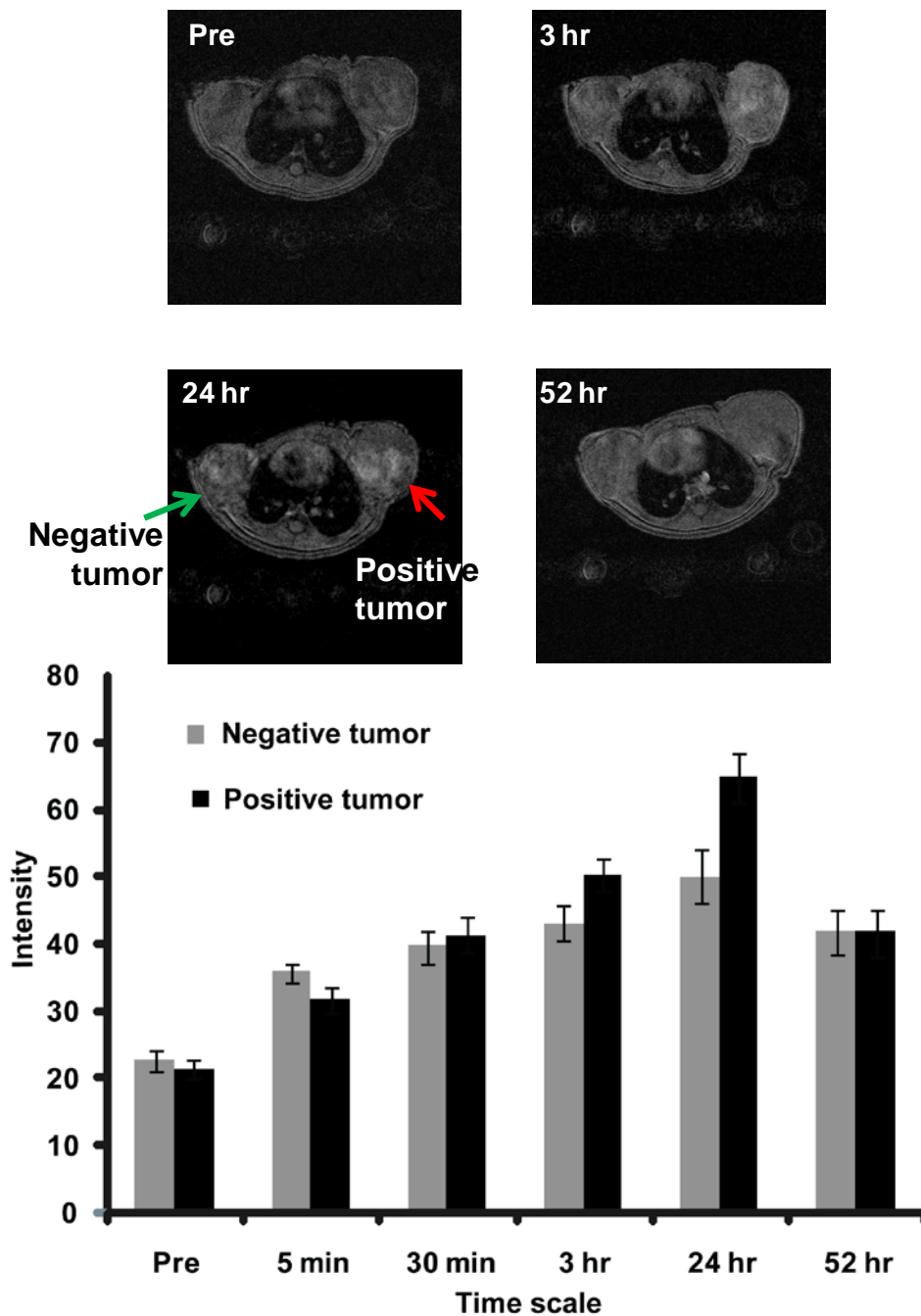


Figure 5.3 MRI of Xenografted mouse with Gradient Echo.

Gradient echo transversal MR images collected prior to injection and at various time points post injection of 3.0 mM of ProCA1-affi-m in HEPES saline via tail vein. The MRI signal on the positive tumor (SKOV-3, right) exhibits significant enhancement at 3 hr post injection and reaches maximum enhancement at 24 hours post injection. The slight differences in MRI signals result from the use of different pulse sequences for imaging.

### **5.2.3 NIR imaging shows relative distribution of ProCA1-affibody in various mouse organs**

To further analyze the HER2 targeting properties of the protein contrast agent, tumors and organs from the imaged mice were collected 48 hours after administration of the agent (Figure 5.4). The organs and tumors were imaged using optical animal imaging. It was clear that there were very high levels of accumulation of Cy5.5 in the liver, kidneys, and the SKOV-3 tumor. There were medium levels of the NIR dye at lung. In comparison, the level of Cy5.5 at the MBD-MDA-231 tumor was quite low (Figure 5.4). The results strongly suggested that our protein contrast agent led to the HER2 specific MR image enhancement.

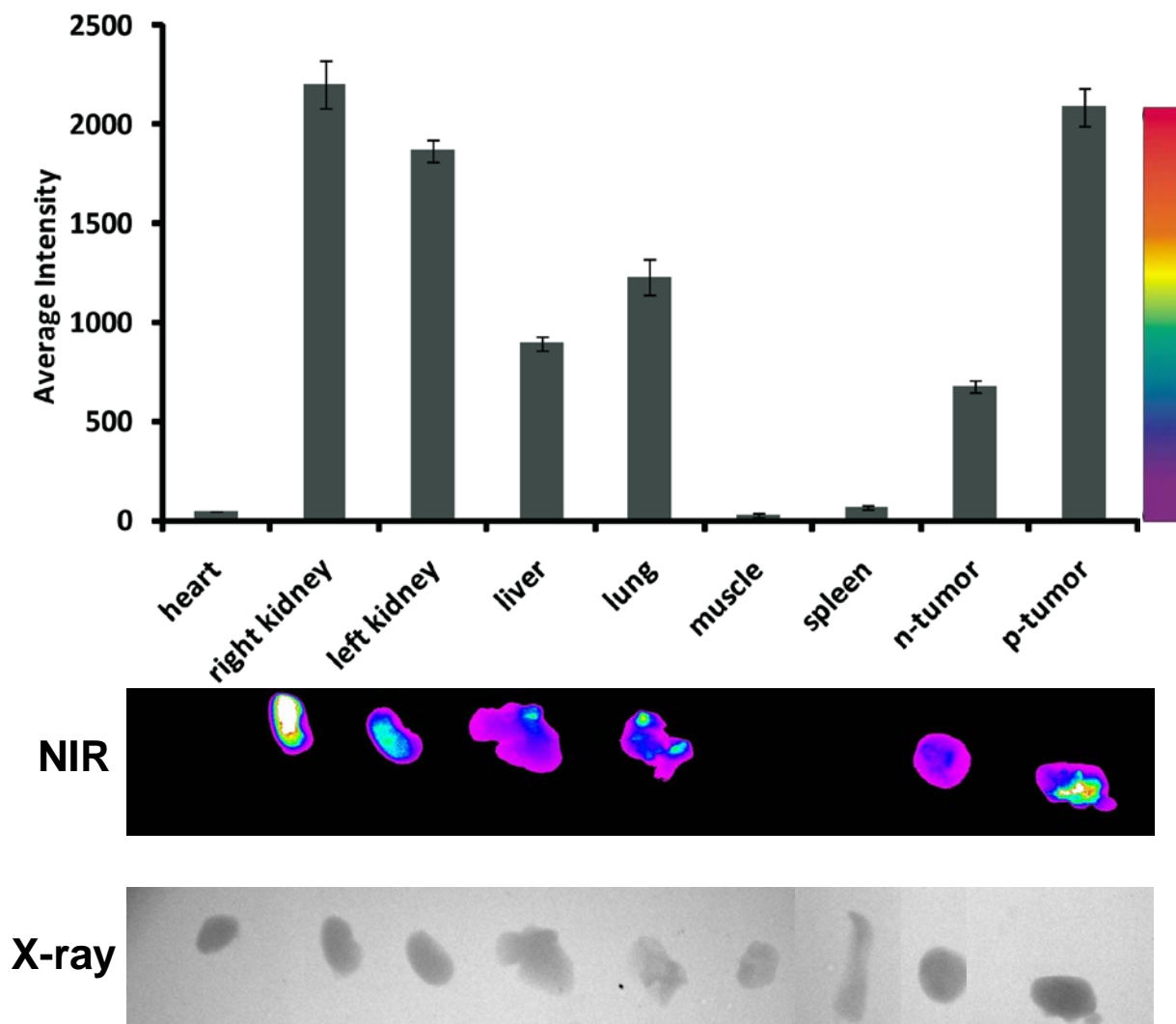


Figure 5.4 NIR imaging of mouse organs.

NIR images of the dissected mouse organs. General bio-distribution was obtained based on the NIR signal and western blot assay. The ProCA1-affi-m mainly distributed in the positive tumor, liver and kidney.

#### **5.2.4 Immunofluorescent staining of frozen tissue slides can demonstrate the tissue penetration of ProCA1-affibody**

To further verify the contrast agent targeted to the HER2 positive tumor, we carried out immunohistochemistry (IHC) staining using the antibody PAbPGCA1 with tissue slides made from the tumor samples collected from the imaged mice as well as selected organs. The strongest staining was observed with liver and the SKOV-3 tumor tissue slides (Figure 5.5). Close examination of the staining patterns of the tumor slides revealed distribution of the designed protein both inside and outside the cancer cells with substantial stronger staining inside the cancer cells, indicating internalization of the protein contrast agent. This staining pattern provided a strong support for the cancer cell targeting by the contrast agent. The kidney slides also gave strong immunostaining consistent with the NIR imaging finding. Interestingly, the areas near proximal tubes showed the strongest staining (Figure 5.5), suggesting that the protein contrast agent may be secreted through the kidney. This is consistent with observations that there were good levels of both  $Gd^{3+}$  (by  $\gamma$ -counting of  $^{153}Gd^{3+}$ ) and the protein (by NIR fluorescence) in the urine of mice that were injected with the contrast agent. Immunostaining of tissue sections from MBD-MDA-231 tumor revealed very weak staining (Figure 5.5).

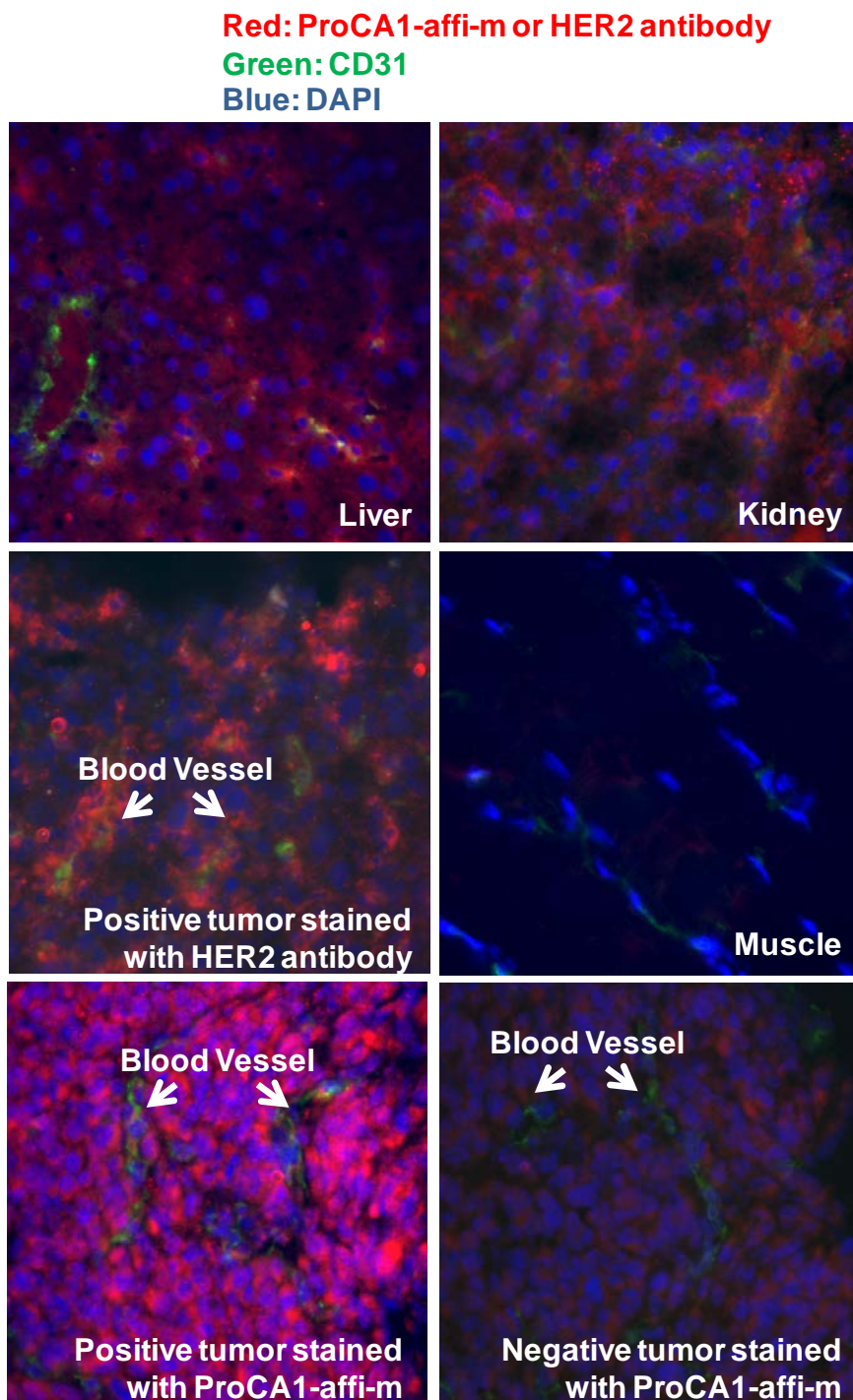


Figure 5.5 IHF staining on mouse tissues for biodistribution studies.

Immune histology fluorescent (IHF) staining was applied to various tissue slides stained by antibody against ProCA1-affi-m (red), Blood vessels biomarker CD31 (green), and nucleus DAPI (blue). The slides stained without primary antibody were used as blank control.



### 5.2.5 MRI blocking experiment further confirmed the tumor targeting

To further verify the HER2 specific MRI contrast enhancement, we carried out a competition assay based on the assumption that if our protein contrast agent targeted HER2 and led to HER2 specific MRI contrast enhancement, affibody alone would be a strong competitor for the binding to the cell surface HER2 and consequently block the binding by our designed protein. Nude mice that carried SKOV-3 tumors were pre-injected with buffer saline or 3 mM of HER2 affibody  $Z_{HER2-342}$  labeled with Cy5.5 twice at 12 hr and 2 hr.  $Gd^{3+}$  ProCA1-affi-m (80  $\mu$ L) at a concentration of 3 mM was subsequently administered to the mice by intravenous injection. The mice were then scanned at a 4.7 T MRI scanner via the same procedures. Our results demonstrated that the MRI contrast enhancements were not observed at the SKOV-3 tumor site in the mice that received HER2 affibody labeled with Cy5.5, while the contrast enhancements in the liver and kidney in the same mouse were not affected by the administration of HER2 affibody (Figure 5.5). NIR imaging did exhibit high intensity in the tumor, which indicates that the affibody binds to the positive tumor and blocks the binding of MRI contrast agents. Conversely, the administration of the saline prior to injection of the designed protein contrast agent did not block the MRI contrast enhancement (Figure 5.6). The results with HER2 affibody blocking strongly support our conclusion that the MRI contrast enhancement from administration of  $Gd^{3+}$  ProCA1-affi-m is HER2 specific.

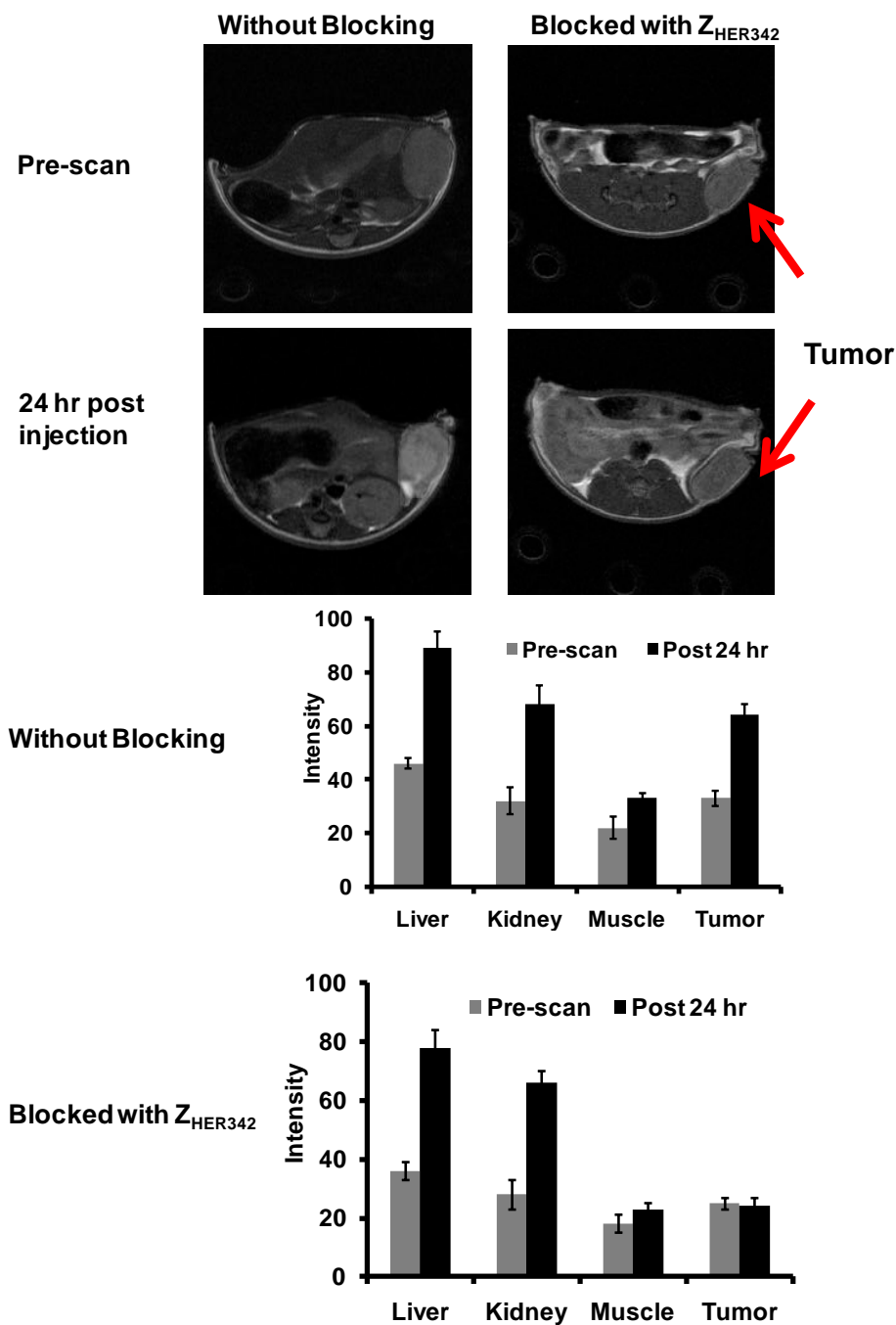


Figure 5.6 Magnetic resonance images and image intensities of the mouse tumor pre-blocked by affibody Z<sub>HER2:342</sub>.

In the blocking experiment, the mice were born with SKOV-3 tumor on the right back. The affibody ZHER342 of 3 mM in HEPES buffer was intravenous injected into the mice for 12 hr and 4 hr before taking MR images [138]. The mice were also scanned at various time points of 4 hr and 24 hr.

### 5.2.6 Advantages of ProCA1-affibody to antibodies in tumor targeting

Since antibodies have been widely used in drug and imaging probe deliveries in molecular marker targeted applications [133, 135] we further compared the immunofluorescence staining patterns of our designed protein agent and a commercially available HER2 antibody. To this end, ProCA1-affi-m (10 mg/kg) or the HER2 antibody (10 mg/kg) was administered in the SKOV-3 tumor bearing nude mice via tail vein. 24 hours post injection, tissue sections were prepared from the tumor tissue, and the sections were analyzed either by immunofluorescence staining using the antibody PAbPGCA1 (for analyses of ProCA1-affi) or direct application of the second antibody against rabbit IgG to detect the bound anti-HER2 antibody. The tissue sections from both cases were also co-stained with the antibody against CD31. At 24 hours post injection, the anti-HER2 antibody was mainly concentrated around endothelial cells as revealed by co-localization with anti-CD31 staining. This is in sharp contrast to the even distribution of ProCA1-affi-m in the entire tumor (Figure 5.5). The distributions of the anti-HER2 antibody to the area distant from endothelial cells were clearly quite reduced as demonstrated by weak immunostaining in the areas where there was no CD31 staining (Figure 5.8). We further examined the distribution of our protein agent and the anti-HER2 antibody at an early time point. Tissue sections from the SKOV-3 tumors were prepared 4 hours after administration of ProCA1-affi-m or the anti-HER2 antibody. Interestingly, while the ProCA1-affi-m was largely concentrated with the CD31 staining in the tumor, the anti-HER2 antibody was not detectable by the immunofluorescence staining analyses. (Figure 5.8). The results strongly suggested that our designed protein agent was able to cross the endothelial and distribute to the deep tumor tissue a few hours after administration while the large size of antibody (~160 kDa) significantly hindered endo-

thelial and tissue penetration. Consistent with the 50% reduction of MRI intensity at the tumor site by affibody blocking shown in Figure 5.6, the fluorescence immunostaining at the same tumor site also exhibited about  $60-90 \pm 20\%$  decrease in intensity (Figure 5.8). Taken together, our developed MRI contrast agent exhibits a potential capability for future quantitative analysis of the biomarker in vivo.

A very crucial requirement for application of an agent for delivery of both drugs and imaging probes to target a disease marker is the capability of the agent to cross the endothelial barrier and to allow for proper tissue penetration and distribution. In particular, even distribution of an imaging probe throughout the entire cancer site is vitally important for quantitative or semi-quantitative assessment of a particular cancer marker. HER2 is evenly expressed across the entire SKOV-3 tumor as revealed by immunostaining using a commercially available antibody (Sigma). Co-staining using an antibody against the endothelial marker CD31 revealed that the distribution of HER2 is not dependent on the distance to the vessels (Figure 5.9).

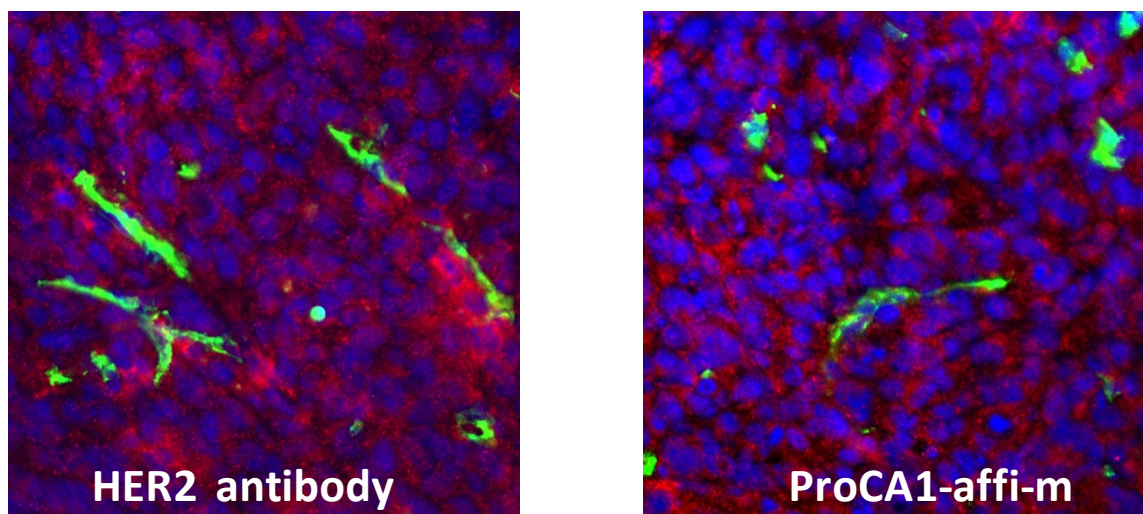


Figure 5.7 Direct staining with SKOV-3 tumors.

Immunofluorescent histology of tumor tissue (Xenograft SKOV-3 model) stained by HER2 antibody and ProCA1-affi324-m

Presumably, the proper size of ProCA1-affi-m provides a great advantage to target the molecular markers. To evaluate the tissue distribution and endothelial penetration of our designed protein contrast agent, we conducted immunofluorescence staining of the designed protein in the tissue sections prepared from various organs after systematic administration of the protein using the antibody PAbPGCA1. The tissue sections were also co-stained with the antibody against CD31. It was clear that high levels of ProCA1-affi-m were targeted to the SKOV-3 tumor at 24 hours post injection, and the protein was distributed in the entire tumor evenly since its intensity is not changed significantly upon increasing the distance from vessel staining CD31 to 40  $\mu\text{m}$  (Figure 5.7). The results from the immunofluorescence staining suggested that the designed protein contrast agent had excellent endothelial and tumor tissue penetration, and was not simply trapped in the blood in the micro-vasculature of the tumor tissue.

**Red: ProCA1-affi-m or HER2 antibody**  
**Green: CD31**  
**Blue: DAPI**

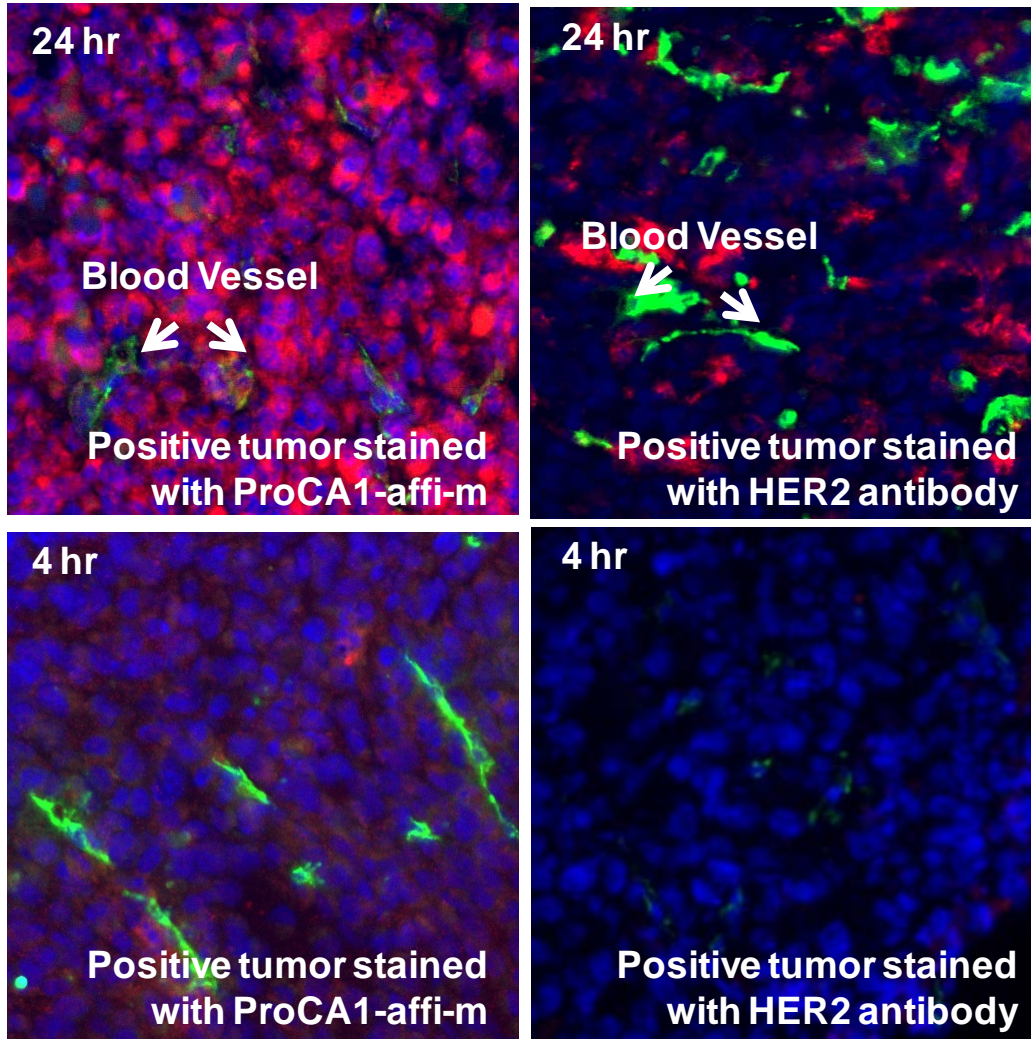


Figure 5.8 Compare the tissue penetration with HER2 antibody by IHC.

Immune histology fluorescent (IHF) staining was applied to various tissue slides stained by antibody against ProCA1-affi-m (red), Blood vessels biomarker CD31 (green), and nucleus DAPI (blue).

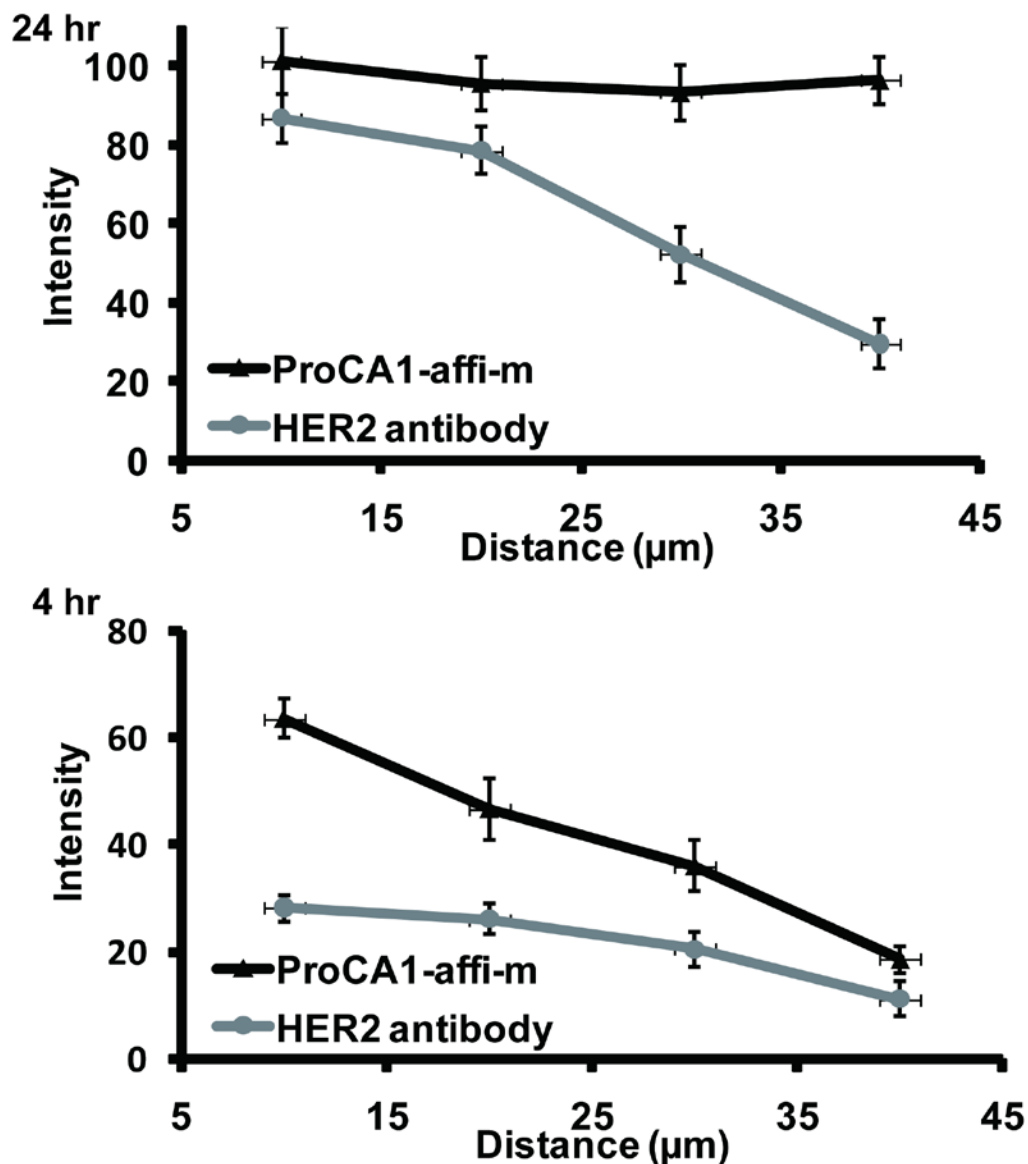


Figure 5.9 The tissue penetration properties of ProCA1 –affi-m were compared with antibody by IHF staining.

The tumor slides are from the mice which were dissected 24 hr and 4 hr after injection with ProCA1-affi-m or antibody. After 4 hr, ProCA1 –affi-m began to distribute around the blood vessel. The antibody had not been detected in the tumor tissue. After 24 hr, ProCA1-CD2-affi was evenly distributed in the tumor tissue and the antibody mainly concentrated around the blood vessel.

HER2 has been validated as a very important prognosis and treatment marker for cancer patients expressing HER2, especially in the case of breast cancer. Development of Herceptin

(trastuzumab) and other HER2 targeting drugs has resulted in significant improvement in patient survival. Unfortunately, current methods for determination of HER2 status rely on invasive biopsy coupled with IHC using a qualitative scoring system [139]. These methods suffer from both high false positive and false negative results, and large discordance in detection of HER2 expression in primary tumors and metastases due to heterogeneity in tissue sampling. These methods also cannot detect HER2 expression levels and patterns in the entire cancer site. According to a recent study by Philips et al., one in five HER2 clinical tests provided incorrect results[140]. Therefore, there is a great need to develop MRI contrast agents with specificity and sensitivity for HER2 imaging [141].

### 5.3 Conclusion

In this present study, we demonstrate the success in molecular imaging of HER2 by developing a novel class of multiple modality contrast agent. To our knowledge, there is no previous report of effective imaging of HER2 expression cancer *in vivo* by noninvasive MRI with desirable tissue penetration and using only a single injection. Our approach in designing protein-based molecular imaging contrast agent differs greatly from previous reported studies in several aspects and represents a significant advance in molecular imaging by MRI. First, high relaxivity value in both T1 and T2 achieved by designing a  $Gd^{3+}$  binding site into a stable scaffold protein [142] allows for increased sensitivity in the detection of disease markers by MRI. Our achievement of MR imaging in animal with 100-fold lower dose usage than clinically used non-targeting agent DTPA is also likely due to improved pharmacokinetic properties such as retention time and biodistribution. Such significant improvements in *in vivo* dosage efficiency will poten-



tially reduce potential  $Gd^{3+}$  toxicity risks, such as NSF (Nephrogenic Systemic Fibrosis). Second, the relatively small molecular size of the designed agent provides a unique opportunity to target the imaging probe to the molecular marker in the entire tumor mass. This property is of vital importance, especially for quantitative assessment of the molecular marker based on the imaging results. Several approaches have been employed to develop targeted MRI contrast agents [134-135, 143-149]. To increase contrast effects, high payload contrast molecules were created by either encapsulating a large number of Gd-DTPA, conjugating multiple contrast agents such as polylysine-Gd-DTPA (PAMAM) [150], or using supermagnetic iron oxide nanoparticles [107, 151]. The antibody approach was widely utilized as the targeting moiety either directly conjugated with high payload contrast agent or elegantly applied in multiple steps to pre-label the tumor as a biotin-labeled antibody[152]. These pioneering studies demonstrated the feasibility of the targeting approach; however, the large size of the antibody-conjugated imaging probes is likely to severely limit the endothelial penetration and even-distribution of the probes in the whole tumor (Figure 5.7). On the other hand, our contrast agent exhibits endothelial penetration capabilities and an excellent distribution in the entire cancer mass as revealed by its adequate distribution near the blood vessel four hour after administration, and the nearly-uniform distribution observed 24 hours post injection. One potential application of our developed MRI contrast agent is for quantitatively or semi-quantitatively assessing the HER2 levels in the entire tumor site using MR imaging, which is impossible with any current methods. Since HER2 is overexpressed in a large percentage of breast, ovarian, gastric, urinary bladder and a number of other carcinomas, the developed contrast agents may be beneficial for imaging of HER2 in several types of cancer. *In vivo* real time monitoring of the changes in

HER2 expression levels and patterns will provide vital information for evaluation of the efficacy of drug treatments and for designing further strategies for cancer treatments.

Based on the results on the animal model studies, we can also have the model for dynamic study. Since the protein in the small animals in dynamic circulation relies on different cell types [153], only the orthotopic tumor model can be applied to fulfill the requirements of dynamic situation [154]. In the future research, we will select the cell lines for orthotopic model with both breast and ovarian cancers.

## Chapter 6. BIODISTRIBUTION AND PHARMOKINETIC STUDY OF DEVELOPED CONTRAST AGENTS

### 6.1 Introduction

Biodistribution is the process of monitoring where a compound or reagent spread in an animal body [155]. It also includes the kinetic changes of reagents in bloods which is called blood retention or circulation [156]. The secretion time is also dependent on biodistribution. For example, the gadolinium distributing to the bone may have long term retention. The biodistribution of a molecule *in vivo* is dependent on several factors. Molecular weight first defines where a molecule will travel to. Small molecules like metals less than 5 kDa tends to distribute to liver [157]. Macro molecules tend to concentrate in spleen. The structure and surface charge will also define the distribution of specific molecules.

Several imaging methods such as NIR fluorescence and PET have been applied in molecular imaging for disease biomarkers for expression level determination. Antibodies are commonly used to target to the biomarkers. While these imaging techniques are highly sensitive, which suffer from two major problems: lack of spatial imaging resolution, and limited tumor penetration due to the large size of the antibodies (~150 kDa). Thus, there is an urgent need for the development of a non-invasive imaging method with the capability to quantitatively determine the expression level and spatial distribution of biomarkers [34].

As discussed in Chapter 1.6 for the criteria of MRI contrast agents, in order to achieve MRI contrast enhancement, as a blood pool contrast agent, it should have long retention time. For achievement of molecular imaging, enough circulation time for targeting is needed. Howev-

er, too long time may cause toxicity by heavy metals [158]. Current small molecules do not have good retention time with a half life time less than 5 minutes [159].

In this chapter, we are going measure the biodistribution and metabolism by radioactive assay and ICP-OES. By comparing with the biodistribution of non-targeted and targeted reagents, pegylation and non pegylation, the modified protein demonstrate long circulation time and better distribution.

Current methods for determination of disease state largely rely on invasive biopsy coupled with a qualitative scoring system such as Immunohistochemistry (IHC) to measure the biomarker expressions such as PSA and HER2 receptors on the cell surface. Fluorescence *in situ* hybridization (FISH) was also used to detect gene amplification by measuring the number of copies of the HER2 gene in the nuclei of tumor cells[139, 160-161]. These methods cannot detect biomarker expression levels and patterns in the entire tumor especially in quantitative level. Therefore, incorrect results on HER2/Neu clinical tests were observed in one of five breast cancer patients [140].

As one of the leading diagnostic techniques in clinical and preclinical settings,[54, 162-163] MRI has the unique advantages of high resolution in capturing the 3-dimensional images with good body depth and without ionized radiation[164-166]. In this dissertation, we developed a targeted contrast agent to HER2 and established a quantitative analysis method in cell level. Biodistribution was also studied to calculate the retention of contrast agent in various organs.

## 6.2 Results and discussion

### 6.2.1 Distribution calculation by NIR signals in different mouse organs

Besides quantitative analysis in cell level, we also calculated the biodistribution of our contrast agents using various methods. Since our dual labeled ProCA1-affi342m is also conjugated with NIR, once the mouse organs were dissected out from mouse body two days after injection, the NIR signal will be less affected by tissue depth. We can draw some quantitative conclusions. From Figure 6.1, we can see out contrast agents mainly stays in positive tumor and kidneys. Liver and negative tumor also had some retention. However, there was not so much contrast agents remaining in the muscle and lung. Figure 6.2 is a scale bar calculated from the integral intensity from Figure 6.1. Western blotting (Figure 6.3) of tissue extract and IHC of frozen tissue slides (Figure 6.4) were also measured to see the biodistribution. These results are consistent with the NIR image data. Based on these results, we can conclude that the ProCA1-affi342m can still be detected in primary organs after two days of injection. Since large molecules tends to filtered by kidneys, and NIR monitors the signal from the Cy5.5 dye which linked to the C-terminal of ProCA-affi342m, kidneys have relatively higher intensity than other organs. Muscle has little blood circulation which makes it completely dark without contrast agents retention and been referred as negative control.

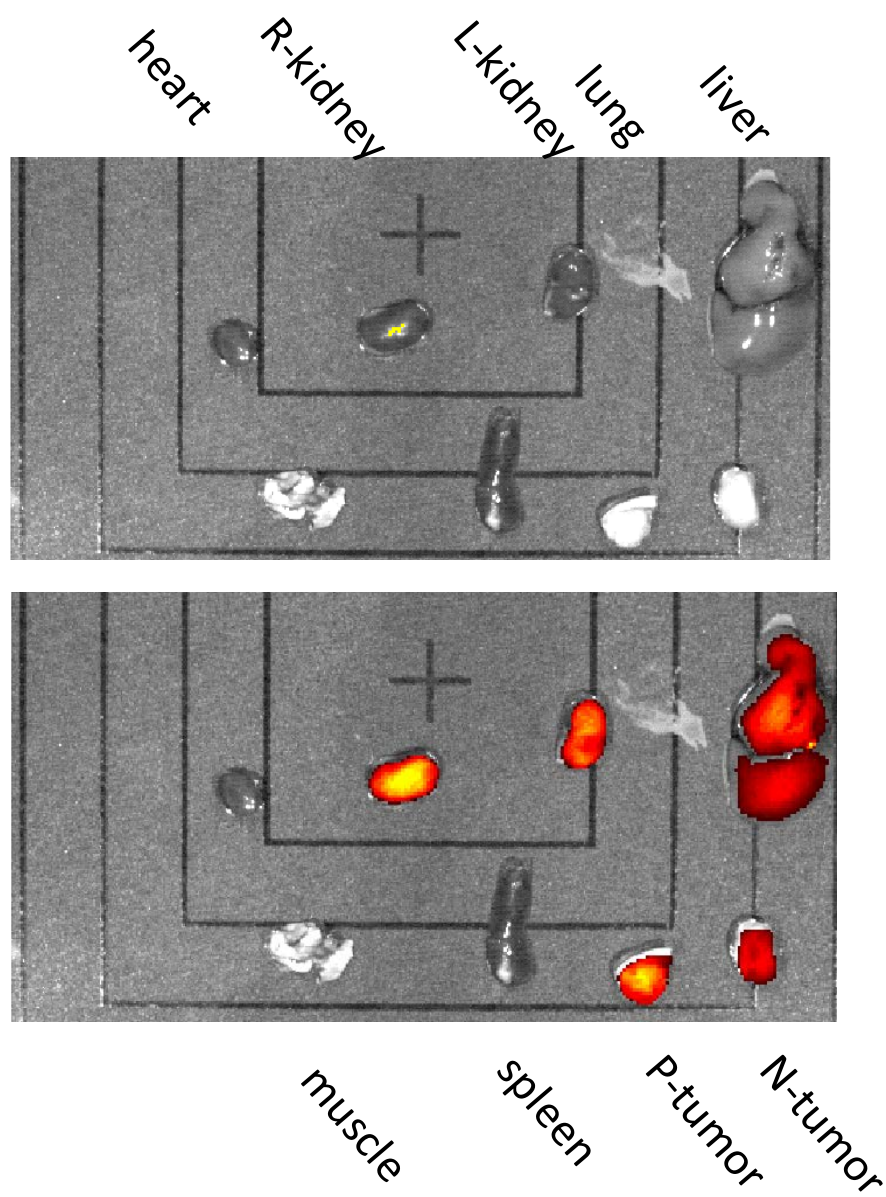


Figure 6.1 Biodistribution demonstrated by NIR imaging

The contrast agent concentrates in the positive site. The liver, kidneys are also the primary organs to accumulate contrast agents.

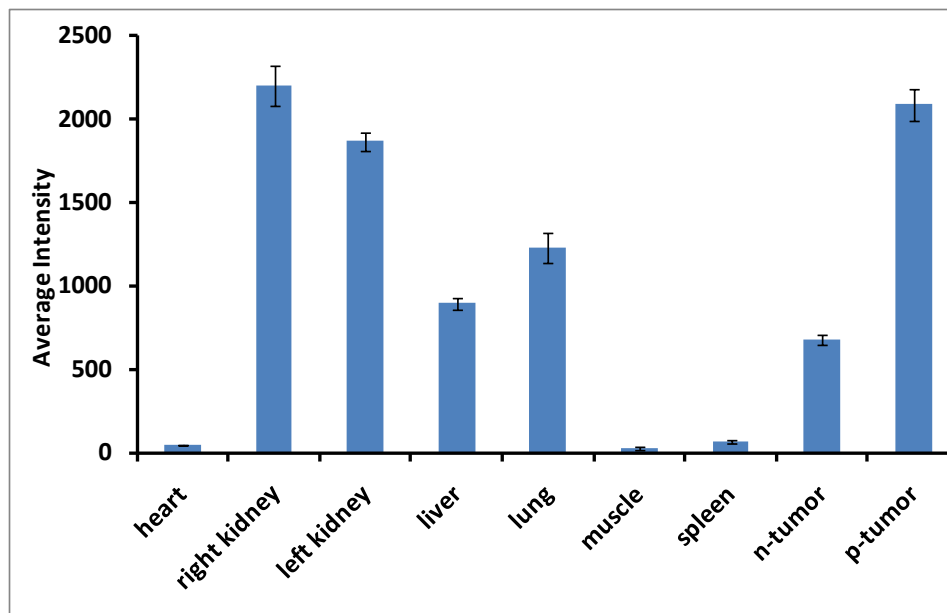


Figure 6.2 Average intensity of each organ by NIR measurement

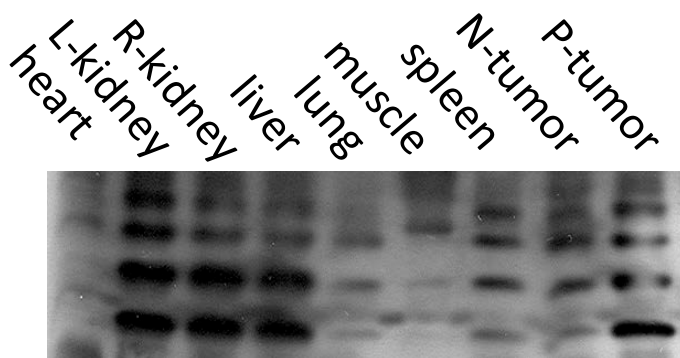


Figure 6.3 Western blotting of quantitative analysis of distribution  
The primary organs after MRI have been dissected and lysate. The lysis was detected by western blotting to estimate how much protein has been retained by each organ.

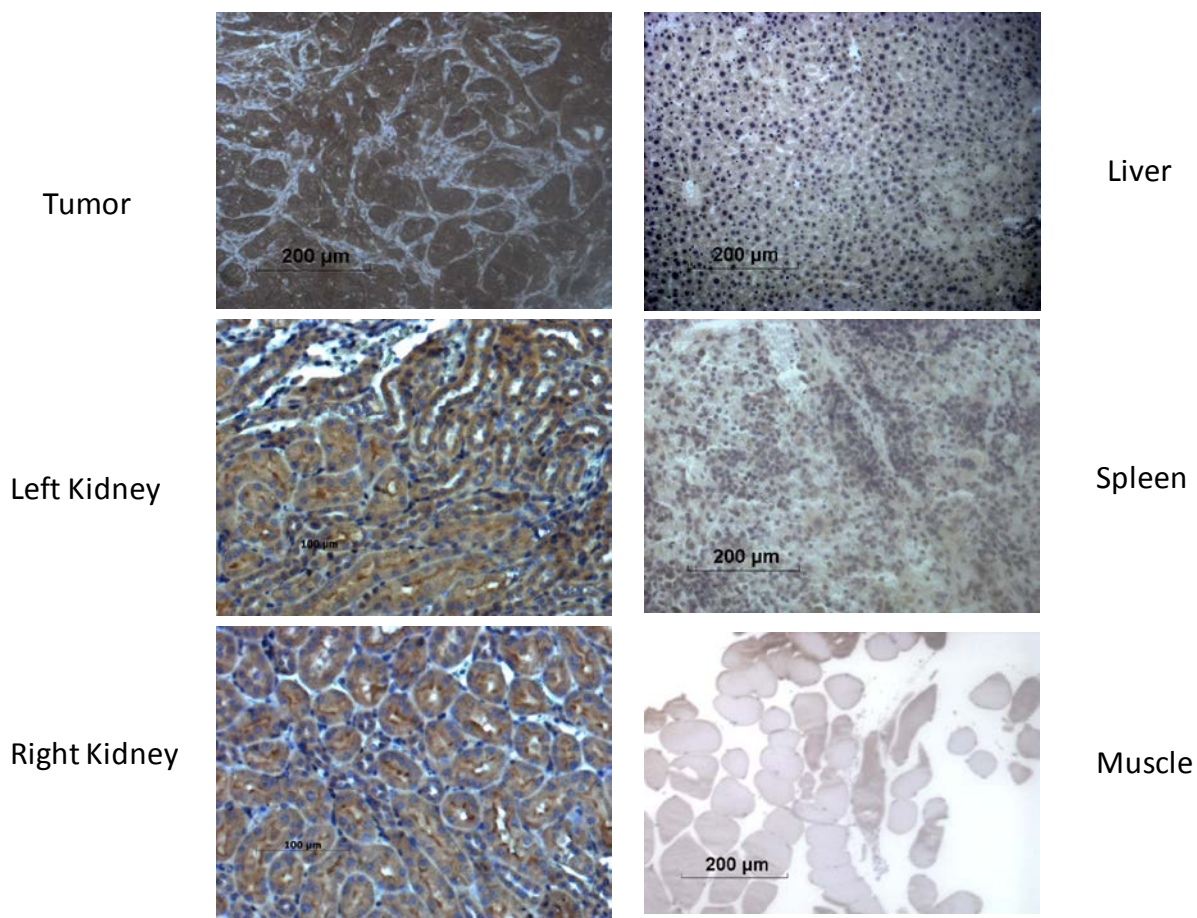


Figure 6.4 Biodistribution demonstrated by IHC

Primary organs were also embedded in paraffin and detected by PAb-ProCA1 for IHC to measure the general distribution of ProCA1-affi342m to each organ.

### 6.2.2 Bio-distribution and blood retention by $^{153}\text{Gd}$ assay

Before measuring the biodistribution with radioactive assay, the general blood retention of ProCA1-CD2 had been measured by western blotting (Figure 6.5). Two different concentrations of ProCA1-CD2 had been injected into the CD1 mice of 100  $\mu\text{L}$  with tail vein injection. After different time points of 5 min to 4 hr, mice blood was taken from tail drop or eye ball bleeding. The blood serum was measure by western blotting of the retention of ProCA1-CD2. Even after 4 hr, ProCA1-CD2 still had some retention in mouse blood without degradation.



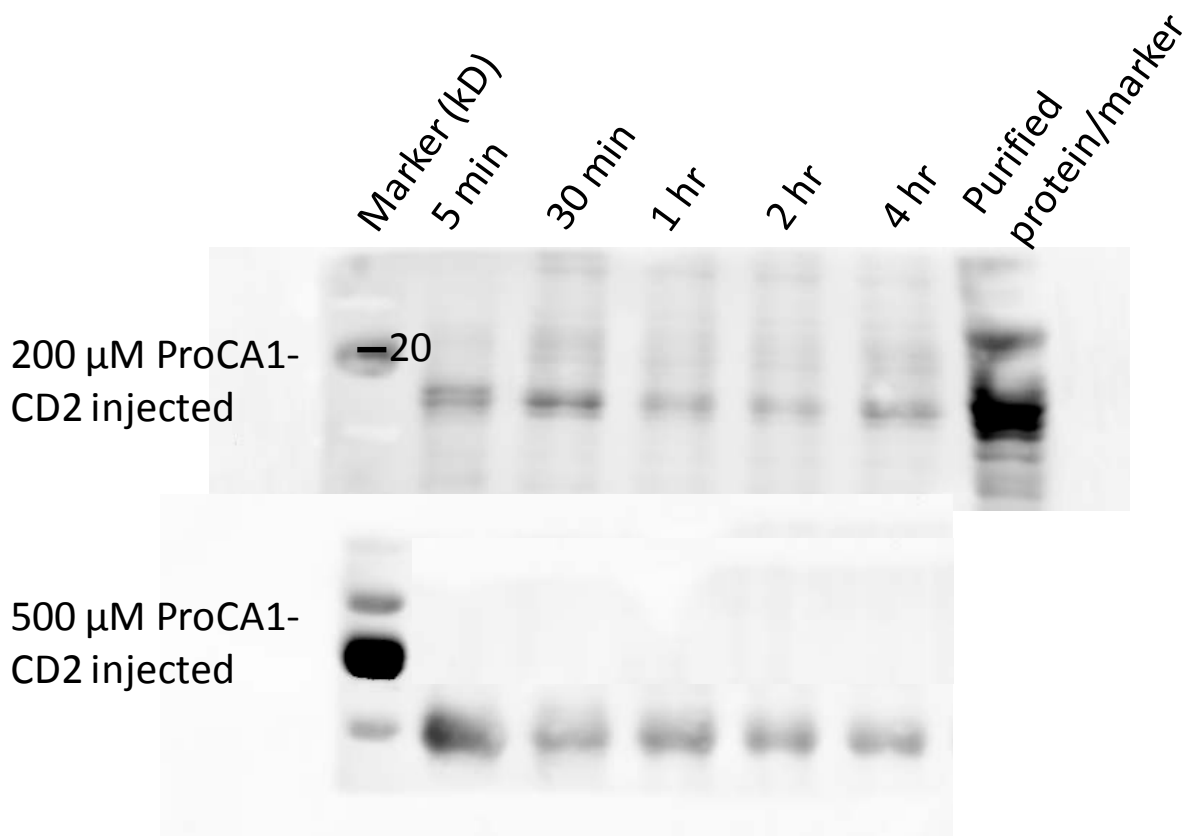


Figure 6.5 Western blotting of blood retention

The mice have been injected with 200 μM (up) and 500 μM (bottom) of ProCA1-CD2 respectively. The concentration of ProCA1-CD2 in blood has decreased from 5 min to 4 hr.

The previous measurements are based on the distribution of ProCA1-affi342m, because the protease cleavage and disassociation always exist in animal blood circulation, the distribution of  $Gd^{3+}$  was also measured by radioactive assay (Figure 6.6) or ICP-OES (Table 8). From Table 7, we can see free Gd circulates mostly to spleen and liver, while Gd-ProCA1-affi342m circulates more to the lung and liver. Figure 6.7 summarizes the distribution of contrast agents with different modification. Most of the  $GdCl_3$  and non-modified proteins stays in the liver. The modified protein stays more in lung and liver. These results indicate that there are some disas-

sociation which led the small molecules circulates to liver. Based on the blood circulation diagram (Figure 6.7), the modification of contrast agents largely increased the blood circulation time.

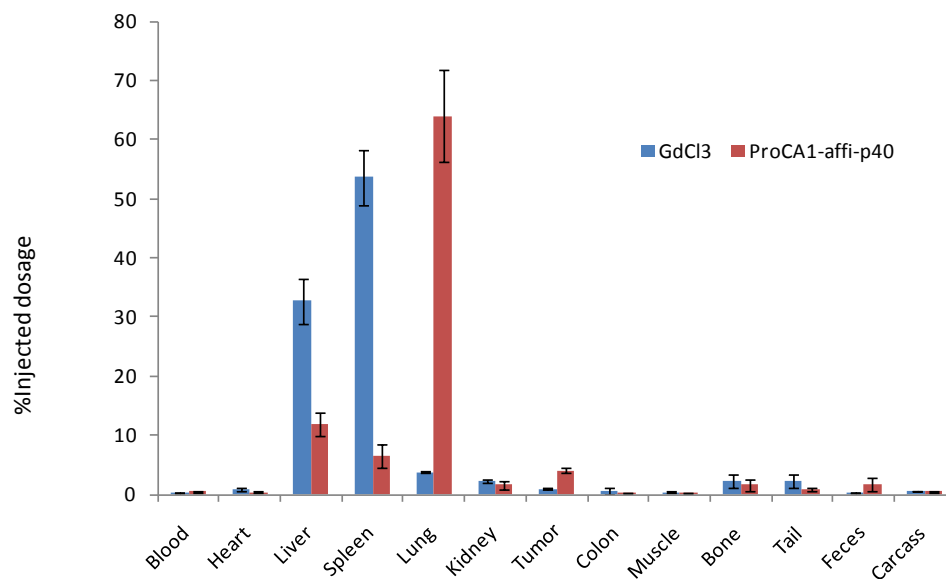


Figure 6.6 Bio-distribution of ProCA1-affi by  $^{153}\text{Gd}$  radioactive assay. Injected  $\text{GdCl}_3$ ,  $100\ \mu\text{M}$ ,  $100\ \mu\text{L}$ , via tail vein. The accumulation of  $^{153}\text{Gd}$  was measured after 12 hr injection

Table 7 Biodistribution of Radioactive assay in CD1 mice

	<i>GdCl3/1</i>	<i>GdCl3/2</i>	<i>CA-1/1</i>	<i>CA-1/2</i>	<i>CA-2/1</i>	<i>CA-2/2</i>	<i>CA1-P40/1</i>	<i>CA1-P40/2</i>
Blood	0.8	0.9	1.5	2.4	2.2	3.0	2.7	2.5
Heart	0.2	0.3	0.1	0.1	0.1	0.1	0.1	0.1
Liver	63.3	64.6	68.4	63.9	75.4	72.2	38.1	27.8
Spleen	8.7	9.4	5.8	7.4	4.1	5.0	2.2	1.3
Lung	1.0	1.1	0.6	2.5	0.6	1.0	26.5	47.0
Kidney	1.6	1.5	1.4	1.8	1.3	1.3	1.9	0.9
Colon	4.6	1.0	3.4	2.0	1.6	1.5	2.0	1.0
Tail	1.6	3.7	1.5	1.7	0.9	1.7	1.6	0.9
Feces	0.9	0.7	0.2	0.2	0.3	0.4	2.3	0.9
Urine	1.5	1.2	0.3	0.3	0.2	0.2	1.6	0.6
Carcass	16.7	15.5	16.7	17.6	13.3	13.5	20.9	11.4

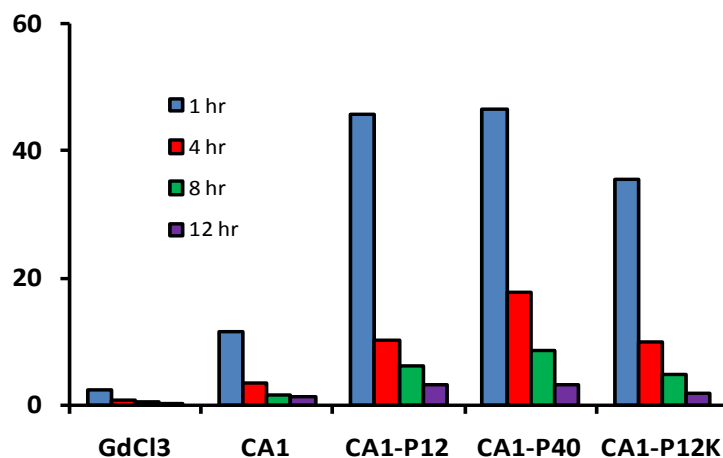


Figure 6.7 Blood circulation of ProCA1 series contrast agents

The mice were injected with  $^{153}\text{Gd}$ -ProCA1 series proteins. The radioactivity of the blood samples collected at different time points were measured. The ProCA1-CD2 with 40 units of PEGylation size has longest circulation time.

### 6.2.3 Bio-distribution with ICP-OES

As described in Chapter 2.0, the radioactive assay is a very sensitive technique to monitor the Gd distribution. ICP-OES which can measure the total metal concentration is another method to measure the Gd distribution. All the mouse organs were dissolved in concentrated Nitric Acid overnight. Small liquid drop will be formed after all the organs being dissolved. The liquid drop was diluted with 2% Nitric Acid based on the original weight of each organ. Then the total  $Gd^{3+}$  concentration will be measured by the ICP-OES. Table 6 listed the percentage of total  $Gd^{3+}$  injection in each organ. Since  $GdCl_3$  circulates fast in animal body, it may be secreted out of the body within 5 min. Therefore, the mouse was sacrificed right after being injected with  $GdCl_3$ . For the protein contrast agents, different time points have been measured. It shows that in shorter time, most of the contrast agents stay in the liver and lung, however, after one day, half of the reagents secreted out of the liver and the tumor accumulate more up to 7.59% of the total injection. After two days, the lung still retains more than 30% of the contrast agents. Correlated with our MRI data, the tumor receives highest signal after one day injection of ProCA1-affi342m. Liver and lung are the two organs accumulate most of the ProCA1-affi342m. Further optimized modification may be needed to make more protein contrast agents target to tumor.

Table 8 Bio-distribution of ProCA1-affi-m was measured by ICP-OES at various time points

Unit: %total injection

	<i>GdCl3</i>	<i>ProCA1-affi-P40 (4 hr)</i>	<i>ProCA1-affi-P40 (24 hr)</i>	<i>ProCA1-affi-P40 (&gt;2 d)</i>
Heart	0.8	0.6	0.4	0.2
Liver	35.5 ± 2.1	36.8 ± 1.7	18.5 ± 2.8	17.9 ± 3.4
Spleen	50.3 ± 4.5	22.9 ± 2.6	5.0 ± 1.9	13.4 ± 3.2
Lung	3.8 ± 0.1	38.7 ± 3.6	39.4 ± 4.5	30.6 ± 5.7
Kidney	2.6 ± 0.1	3.9 ± 1.1	3.1 ± 0.9	4.6 ± 0.7
Muscle	0.2	0.4	0.1	0.6
Tumor	1.1 ± 0.1	2.1 ± 0.1	7.5	3.7 ± 0.8

The distribution of different contrast agents are also compared especially the different distribution between PEGylated and non-PEGylated ProCA1-affi342. Table 9 shows the percentage of total after one day of injection. Without PEGylation, most of the contrast agent goes to spleen instead of lung, similar like free GdCl<sub>3</sub>. We may conclude that PEGylation causes the contrast agents move from spleen to lung.

Table 9 Bio-distribution of MRI contrast agents was measured by ICP-OES to optimize the modification condition

Unit: %total injection

	<i>GdCl3</i>	<i>ProCA1-CD2</i>	<i>ProCA2-P40</i>	<i>ProCA1-affi-P40</i>
Heart	0.8	0.6	0.9	0.4
Liver	35.5 ± 2.1	38.1 ± 3.4	22.6 ± 2.1	18.5 ± 2.8
Spleen	50.3 ± 4.5	45.4 ± 2.6	28.2 ± 3.4	5.0 ± 1.9
Lung	3.8 ± 0.1	7.3 ± 0.8	14.7 ± 1.3	39.4 ± 4.5
Kidney	2.6 ± 0.1	2.5 ± 0.1	2.7 ± 0.1	3.1 ± 0.9
Muscle	0.2	0.3	0.4	0.1
Tumor	1.1 ± 0.1	N/A	N/A	7.5

## Chapter 7. EFFECTS OF DRUG TREATMENTS DETERMINED BY PROCA1-AFFIBODY

### 7.1 Introduction

As described in Chapter 1.2, two common anti-cancer drugs, Herceptin, and Erlotinib which operate via the same HER pathway will be selected [153, 167] (Figure 1-1). Herceptin (trastuzumab) is a humanized antibody that targets the extra-cellular domain of HER2/Neu [168]. Herceptin is a clinically approved antibody against HER2 in breast and ovarian cancers. While the drug is well studied in treating breast cancer clinically, it is important to determine whether treatment of HER2/Neu positive cancer with Herceptin will lead to any changes in HER2 levels and distribution in tumors [83]. Erlotinib is a tyrosine kinase inhibitor of EGFR and can promote tumor regression in various xenograft models [169]; it can also be used to treat the mammary tumor cells which are EGFR positive [170]. In the treated cancer cells, the EGFR level will be down regulated [171]. Since the erlotinib is an inhibitor to the kinase site in the intracellular domain of EGFR family, the trastuzumab is an antibody against the extracellular domain of HER2. The two drugs can be applied together to cancers [172]. The Herceptin and ProCA1-affi342m have different epitope on HER2 extracellular domain [173], which enables the detection of HER2 expression in tumors by ProCA1-affi342m.

In this chapter, drug effects on the HER2 receptor expression levels were examined using cultured cancer cells such as SKOV-3 and MDA-MB-231. The drug of Herceptin was chosen because it is a targeting drug for HER2. The dosage of 5  $\mu\text{M}$  was used based on the estimated tumor cell numbers and reported receptor level (Chapter 1.2.3).

## 7.2 Results and discussion

### 7.2.1 Both receptor level and cell survival decrease after been treated by Herceptin

Before measured by MRI, we confirmed the effects of drug treatment in the cell level by ELISA, western blotting and flowcytometry. For ELISA and western blotting, the cells were treated with Herceptin for 3 and 5 days. Then the cells were lysed and the cell lysis was detected by antibody against ProCA1-CD2m. Both results (Figure 7.1 and 7.2) indicate that the total receptor decreased up to 35%. The receptor change may due to two factors: first Herceptin may cause cell death so that the total number of cancer cells will decrease; second the expression level of HER2 will also decrease on treatment.

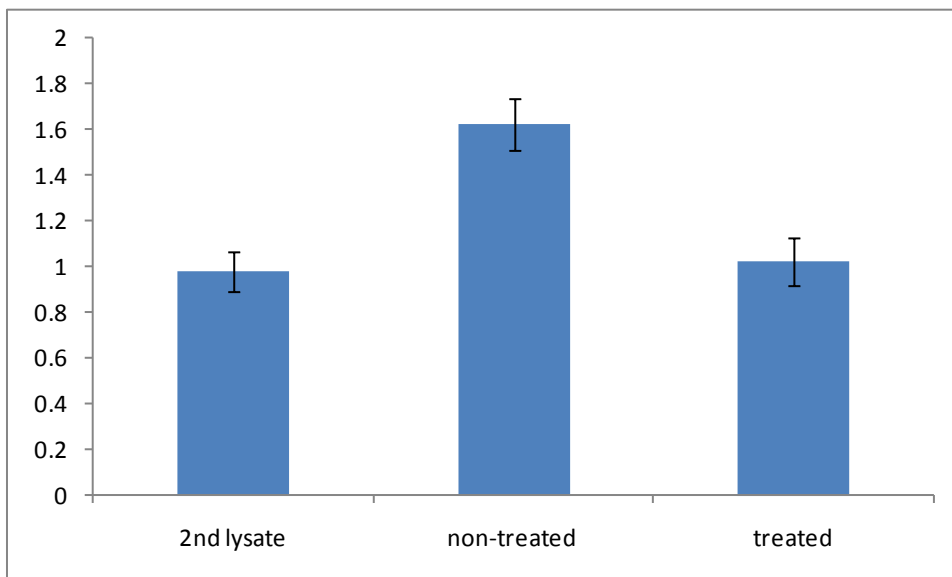


Figure 7.1 ELISA assay to monitor the HER2 receptor level changes after being treated with Herceptin in SKOV3 cells.

1 day: seed cells to 6 well plates (5000) 2 day: add 4 pmol Herceptin (3 times receptor)  
4-6 day: change medium and add another 4 pmol Herceptin Cell lysate was collected at day 4 and day 6.



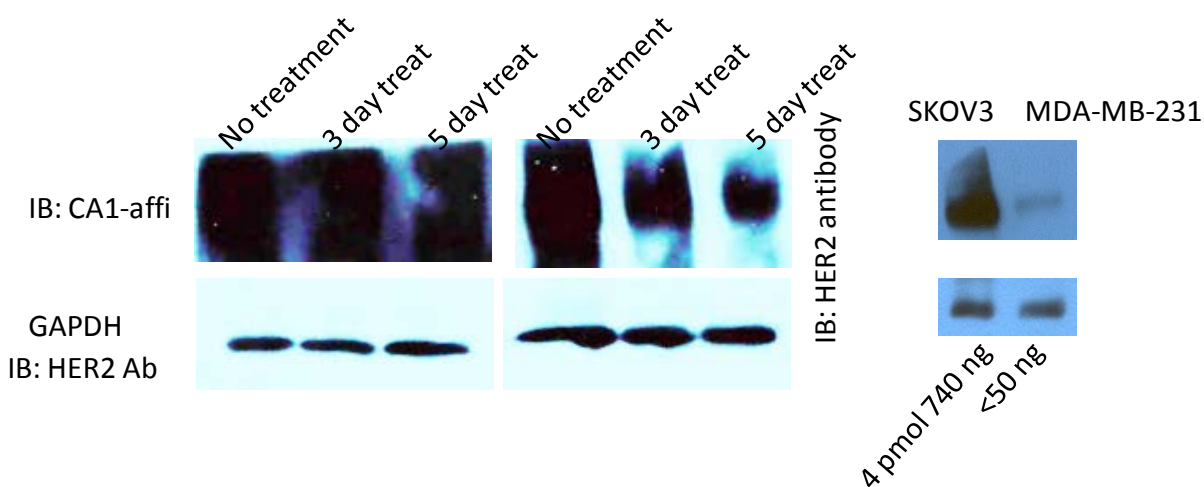


Figure 7.2 Western blotting results indicated that the total receptor number decreased about 35% after five days of treatments with Herceptin

### 7.2.2 Monitoring the receptor change after drug treatment using flow cytometry

In order to detect whether the expression level of HER2 is changed due to drug treatment, flowcytometry is also used to measure the receptor change. In each measurement  $2 \times 10^4$  cells of treated and non-treated samples were counted and the total fluorescent intensity was measured. The receptor was detected by HER2 antibody and ProCA1-affi342 respectively (Figure 7.3). Both detections show the receptor level change up to 10% percentage (Figure 7.4). However the ProCA1-affi342m detection sensitivity is much lower than antibody detection. This may due to an extra primary antibody need to be added to detect ProCA1-affi342m during sample preparation.

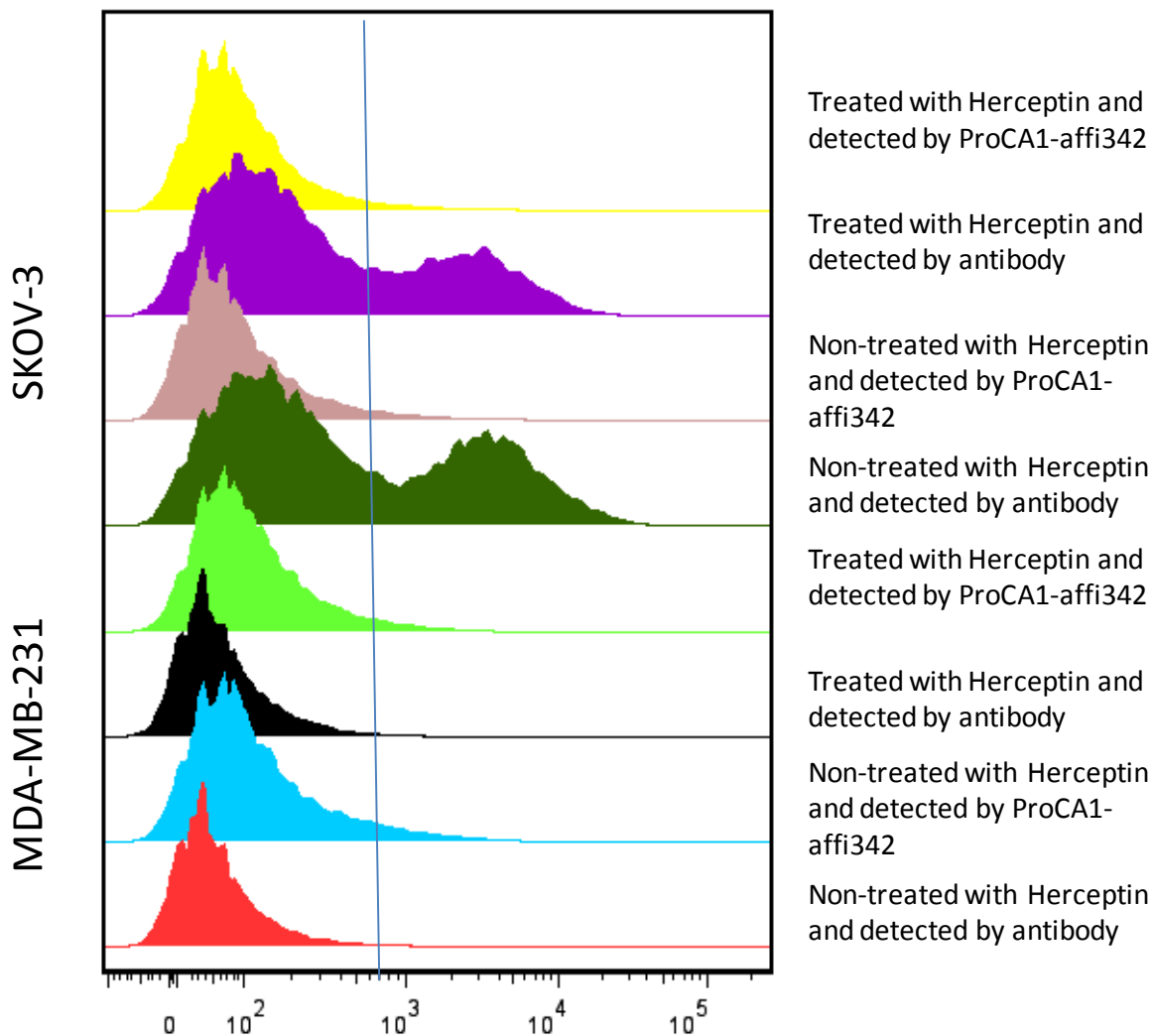


Figure 7.3 Drug treatment measured by flow cytometry

The cells were seeded in 10 cm dishes, and treated with Herceptin (5 nM) during the 5-day period. After 5 days, the cells were harvest and stained. Finally,  $2 \times 10^4$  cells were counted and the fluorescent intensity was measured by flow cytometry. The x-axis is fluorescent intensity. The y-axis is cell numbers been counted with staining.

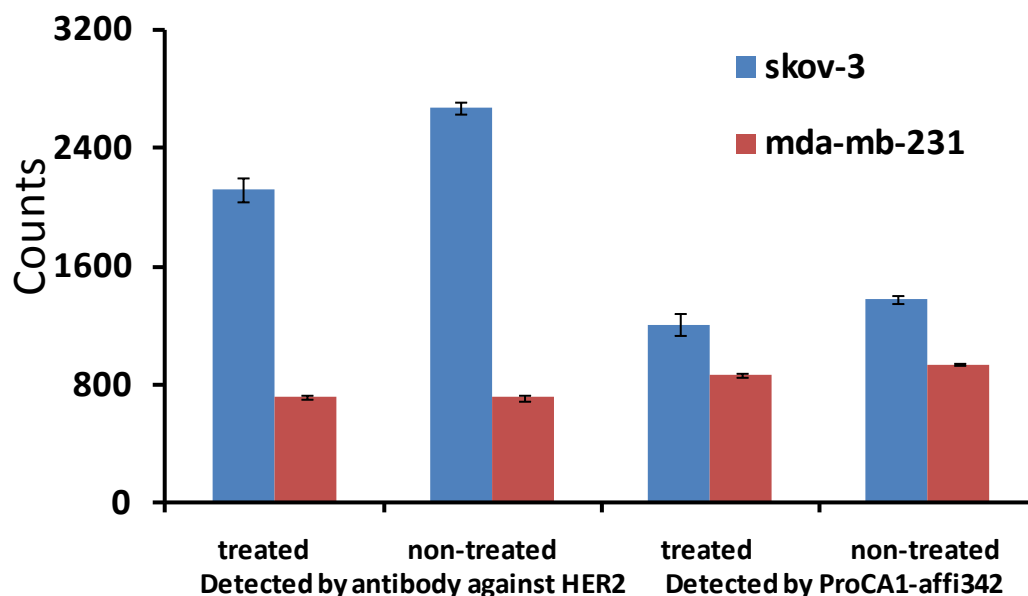


Figure 7.4 Flow cytometry demonstrated the receptor level change after being treated with Herceptin.

Both antibody and CA1-affibody can show the difference of cells after drug treatment. Due to the extra step by adding CA1 antibody, the sensitivity is lower of CA1-affibody than antibody.

### 7.2.3 ProCA1-affibody can monitor the total receptor change in cancer cells by MRI

Based on previous data, we confirmed that ProCA1-affi342m is able to monitor the receptor change in cell level by immune techniques. Then we further add Gd-ProCA1-affi342 to the drug treated cells and measured by MRI. Figure 7-5a shows that when cells are treated by various concentration of Herceptin, the receptor change will be different. We selected the highest treatment concentration 50  $\mu$ M of Herceptin to measure the effects on different time points (Figure7-5b). After 5 days treatment, the MRI intensity of cell samples is lower than non-treated samples and those with 3 days treatment. Since MRI is not a sensitive technique, and each scanning only counts 1 mm thickness of the sample, this makes the intensity change not

significant. When repeat this measurement in the future, the detection will be integral of up to 1 cm thickness of the samples.

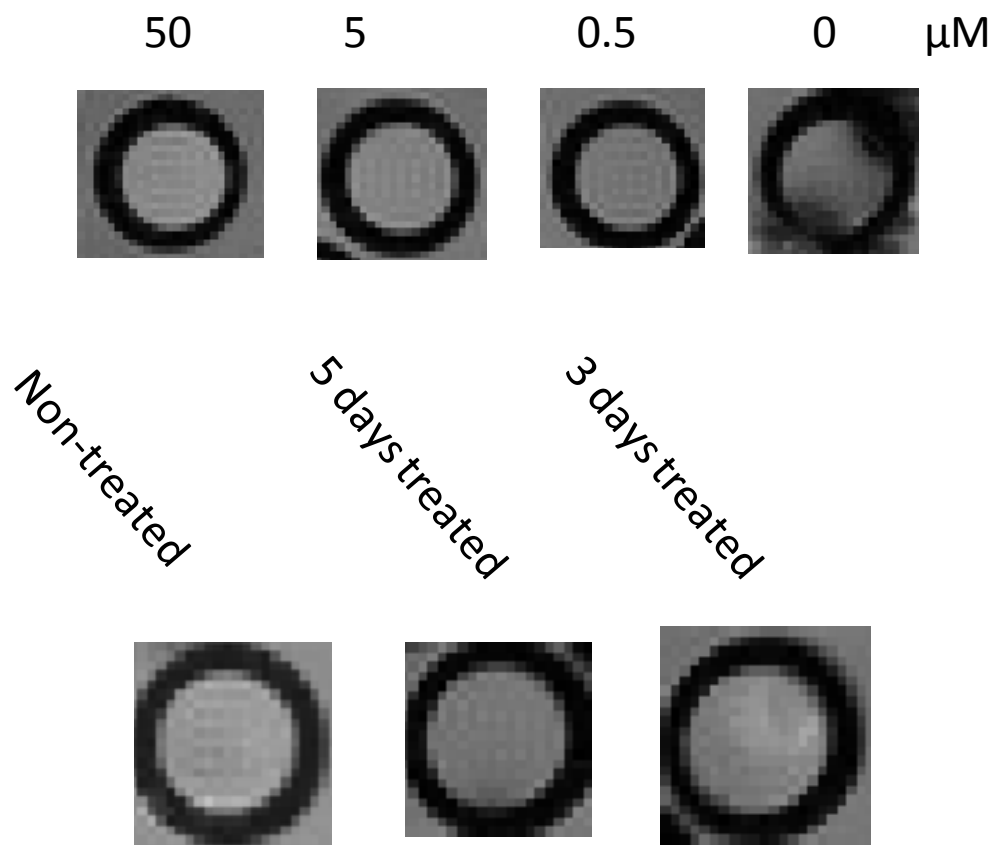


Figure 7.5 MR images of SKOV3 cells after various days of treatments by Herceptin

## **Chapter 8. MONITORING CHANGES IN BIOMARKERS OF DISTRIBUTIONS AND EXPRESSION LEVELS DURING BREAST CANCER PROGRESSION BY TARGETED PROTEIN BASED CONTRAST AGENTS**

### **8.1 Introduction**

Breast cancer is one of the diseases with highest occurrence in North America. The death rate is the second among different cancers [174]. There are several breast cancer types categorized based on its origination from ducts or lobules [175]. Table 8 lists different types of the breast cancers and their origination or properties. For example, Infiltrating Ductal Carcinoma (IDC) is the most common type of breast cancer representing 78% of all malignancies[176].

Among these cancer types with different morphologies (Figure 7-1), cancer originated from Ductal Carcinoma In-Situ (DCIS) is an invasive type of early breast cancer occurs inside of the ductal system[177]. The development of breast cancer is a multi-step process that initiates as premalignant atypical hyperplasia, transforms into pre-invasive DCIS, and progresses into invasive breast cancer[178-179]. With a proportion of 20—30% among all the breast cancers, DCIS turned to be a common type of breast cancer [180]. Currently, the clinical management of DCIS patients is still controversial, mainly because the natural development of DCIS is largely unknown [181]. Molecular basis on why and how often DCIS progresses to potentially lethal invasive breast cancer remains to be determined. Therefore, understanding the key molecular events in initiation and progression of DCIS should allow the identification of biomarkers for specific therapy to achieve the maximized efficacy of treatment as well as determining molecular targets for the development of new treatment approaches for DCIS.

Table 10 Table of different breast cancer types

<b>Breast Cancer Type</b>	<b>Characteristics</b>
Ductal Carcinoma in situ (DCIS)	The cancer cells are inside the ducts but have not spread through the walls of the ducts into surrounding breast.
Lobular Carcinoma in situ (LCIS)	It begins in the milk producing glands but does not grow through the wall of the lobules.
Infiltrating Ductal Carcinoma (IDC)	The cancer cell starts in a milk passage (duct) of the breast, breaks through the wall of the duct and grows into the fatty tissue of the breast.
Infiltrating Lobular Carcinoma (ILC)	ILC starts in the lobules as LCIS. It can spread to other parts of the body. About 10% of invasive breast cancers are ILC.
Triple-negative breast cancer	This type of breast cancer whose cells lack estrogen receptors and progesterone receptors, and do not have overexpression of HER2 on the cell membrane.
Medullary Carcinoma	This special type of infiltrating breast cancer has a rather well defined boundary between tumor tissue and normal tissue.
Metaplastic Carcinoma	This is a very rare type of invasive ductal cancer. They include cells that are normally not found in the breast.
Mucinous Carcinoma	This type of breast cancer is formed by mucus-producing cancer cells. The prognosis is better than other types of invasive breast cancers.
Tubular Carcinoma	They are called tubular because of the way the cancer cells are arranged when seen under microscope. It accounts about 2% of all the breast cancers.
Papillary Carcinoma	The cells of these cancers tend to be arranged in small, finger-like projections when viewed under the microscope.
Adenoid cystic Carcinoma	These cancers have both glandular and cylinder-like features when seen under the microscope.
Phyllodes tumor	This rare breast tumor develops in the stroma of the breast, which is a connective tissue.

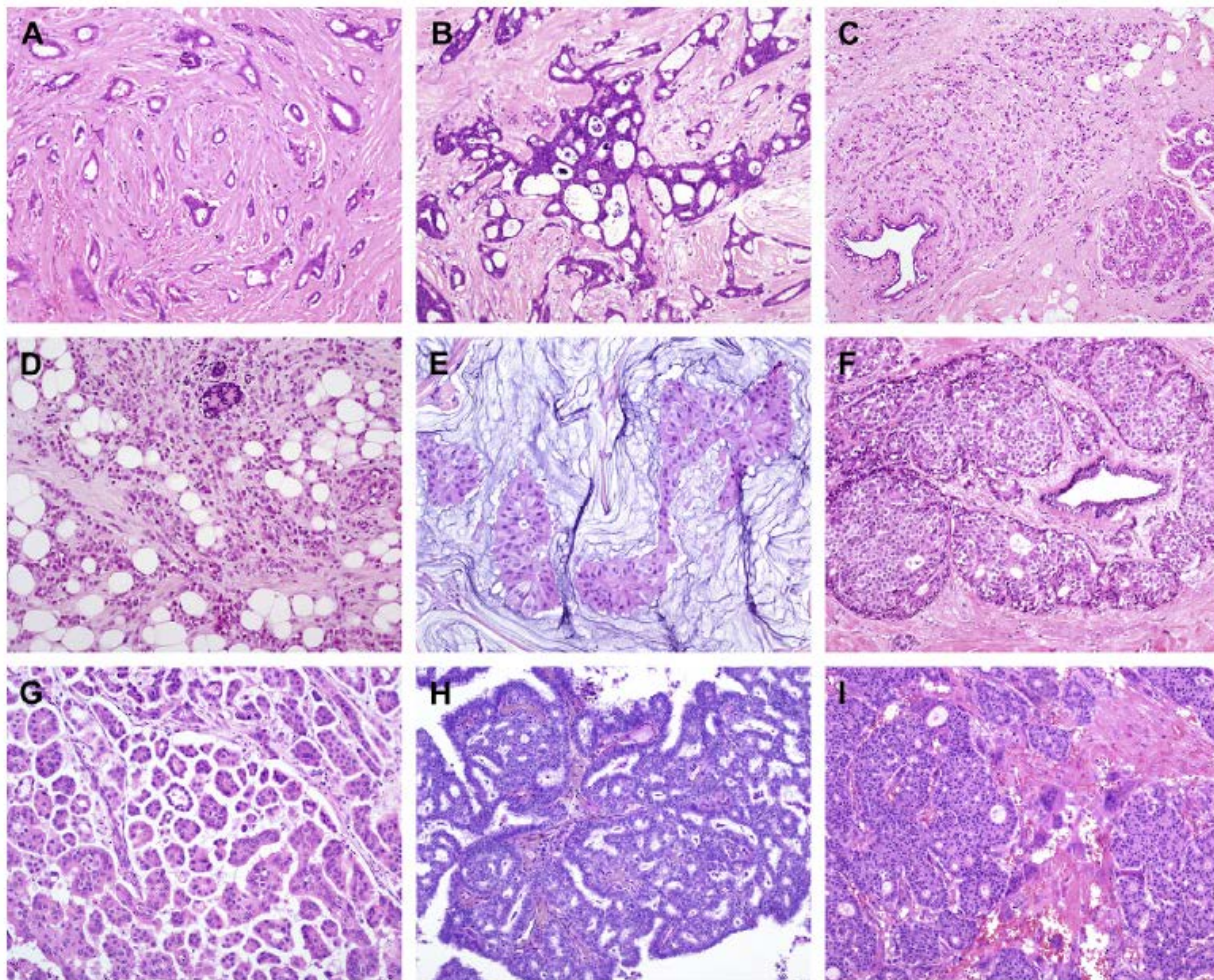


Figure 8.1 Histological special breast cancer types

(A) Tubular carcinoma, (B) cribriform carcinoma, (C) classic invasive lobular carcinoma, (D) pleomorphic invasive lobular carcinoma, (E) mucinous carcinoma, (F) neuroendocrine carcinoma, (G) micropapillary carcinoma, (H) papillary carcinoma, (I) low grade invasive ductal carcinoma with osteoclast-like giant cells.

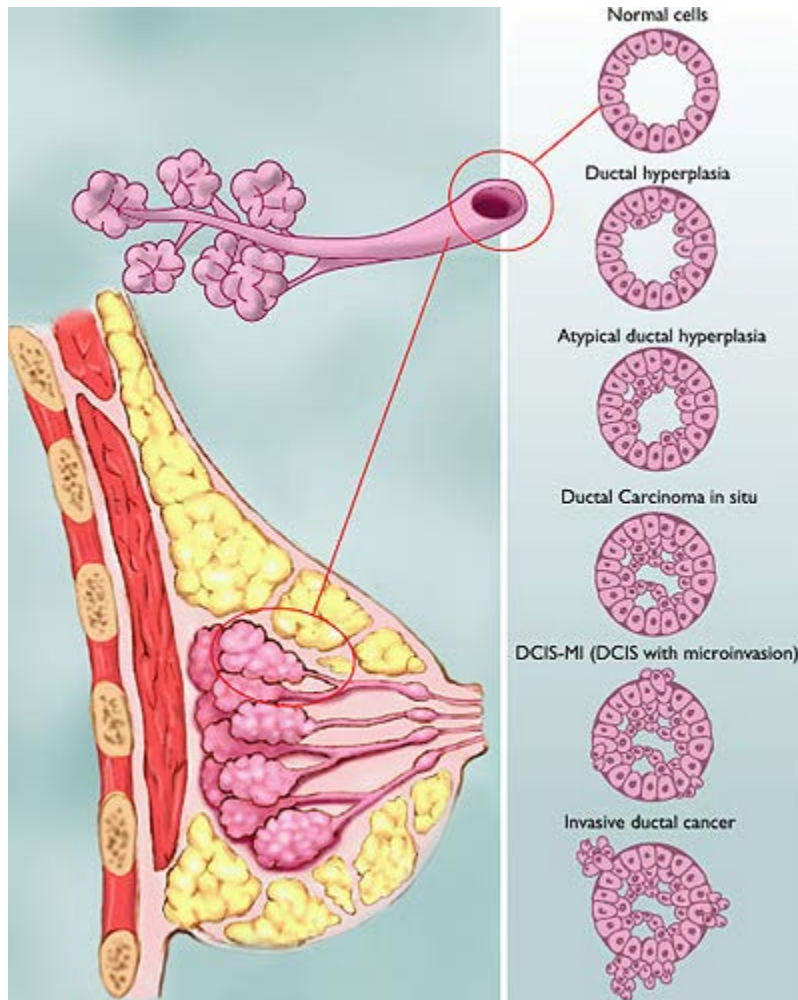


Figure 8.2 Progression of DCIS tumors

The progression stages of DCIS tumors show morphology changes as the DCIS tumor proceeds to the invasive tumors [176].



There are several biomarkers such as HER2, EGFR, estrogen (ER) and progesterone receptor (PR), which have been identified for the diagnostics of breast cancers (Figure 8.1). The breast carcinoma has been classified into subtypes based on the molecular classification [182]. For example, Infiltrating Lobular Carcinoma (ILC) is often positive for estrogen (ER) and progesterone receptor (PR) [183]. ER has overexpression in about 70% of breast cancers since the binding of estrogen to ER may cause proliferation of mammary cells [184]. PR also expressed in most of the breast cancer cells, however, for most ER negative breast cancers are often PR negative [185]. The biomarker of EGFR family has the advantages because they express on the cell membrane which benefits for the tumor targeting diagnosis and therapy.

The EGFR family also plays an important role in the breast cancers via the signaling pathway to regulate the cell progression, survival and differentiation [186]. About 70% percent of the DCIS tissues with high proliferation rate demonstrate a high expression level of EGFR or HER2 [187]. It has been shown that 14 to 91% of human breast carcinomas express a high level of the EGF receptors[186]. Most of the DCIS tissues identified is associated with a high proliferation rate, which is negative for estrogen receptor, and expresses high levels of EGFR or HER2/neu[187]. The importance of EGFR signaling in the growth of DCIS tissues is further supported by study results obtained from examination of the effects of an EGFR inhibitor, erlotinib, on human DCIS tissues xenografted in nude mice. Inhibition of EGFR induced apoptosis and decreased the growth of human DCIS tissue xenografts by 56% [188-189]. However, only 8% of non-basal-like breast cancers are EGFR positive [190].

Figure 8.2 shows that basal type human breast cancer cell line MCF-10 DCIS produces rapidly growing lesions in nude mice with predominant ductal carcinoma in situ (DCIS) characteristics of human DCIS during the first three weeks of tumor growth and gradually progressing to invasive tumor in 4 to 8 weeks. HER2/Neu is found in all DCIS lesions, whose expression is absent or very low in invasive tumor areas. In contrast, EGFR is not found in luminal tumor cells but only positive in the basal layer of the DCIS lesions. However, microinvasive lesions and invasive tumor areas express a very high level of EGFR, suggesting the role of EGFR signal in developing a basal type invasive breast cancer. To date, the role of EGFR family of proteins, including EGFR and HER2, in the progression of DCIS is still unclear.

Dr. Fred R. Miller at Wayne State University School of Medicine, Detroit, MI, developed the MCF10 series of cell lines that were originally derived from benign breast tissues from a woman with fibrocystic diseases [180, 191-194]. These cell lines exhibit distinct histopathological features of the progression from normal, to atypical hyperplasia, to DCIS and then to invasive breast cancer. MCF10A is a normal immortalized human mammary epithelial cell line with low levels of EGFR, ER, survivin and a wild type p53 gene. An H-ras-transformed derivative MCF10AT contains mostly premalignant cells. It has been shown that inoculation of MCF10AT cells into athymic mice produces sporadic DCIS and invasive cancers (25%) in about a year. A clonal cell line cultured from a MCF-10AT derived tumor xenograft, MCF10DCIS.com (or MCF-10 DCIS), produces rapidly growing lesions in about three weeks with predominant comedo DCIS characteristics, such as tightly packed tubular structures with central necrosis, distinct intact basement membrane surrounding each ductular structure containing luminal tumor cells with large and vesicular nucleoli, high mitotic figures and moderate foamy cytoplasm (Figure 7-4). In

this specific xenograft model, tumor progression has been observed by staining several biomarkers, like HER2, EGFR and ER with IHC. Based on these studies and our designed contrast agents targeting to biomarkers, we used the ProCA1-affi342 to image the xenograft tumor of MCF10-DCIS model at the early stage. We will also use ProCA1-affi342 and ProCA1-affi1907 to monitor the biomarker changes in different prognosis stages.

Dr. Lily Yang's lab has provide the orthotopic tumor model and her work on MCF10A cancer progression model has been described in Figure 8.3 and with other biomarkers like ER and PR been analyzed.

We previous have shown that HER2 targeted MRI contrast agents have been developed (discussed in Chapters 3.7). As discussed in Chapter 1.4 and developed by a Sweden group [195], affibody, which is a small protein with 58 amino acids, can target to EGFR or HER2 with a high affinity (nM in  $K_d$ ) and function as a ligand. In addition, affibody will not activate receptors like antibody [74]. At the same time affibody does not need post-translational modification, which makes it easy to express in *E. coli*.

In this study, we are going to first develop EGFR targeted MRI contrast agents based on the targeting capability of affibody 1970 to against EGFR. In addition, we will apply MRI based contrast agents ProCA1-affibody342 against HER2 and ProCA1-affibody1907 against EGFR to monitor the expression level of HER2 and EGFR respectively in various tumor stages of xenograft mouse model. Furthermore, we will monitor the receptor changes after treated with cancer drugs like Herceptin and Erlotinib by the designed MRI contrast agents.

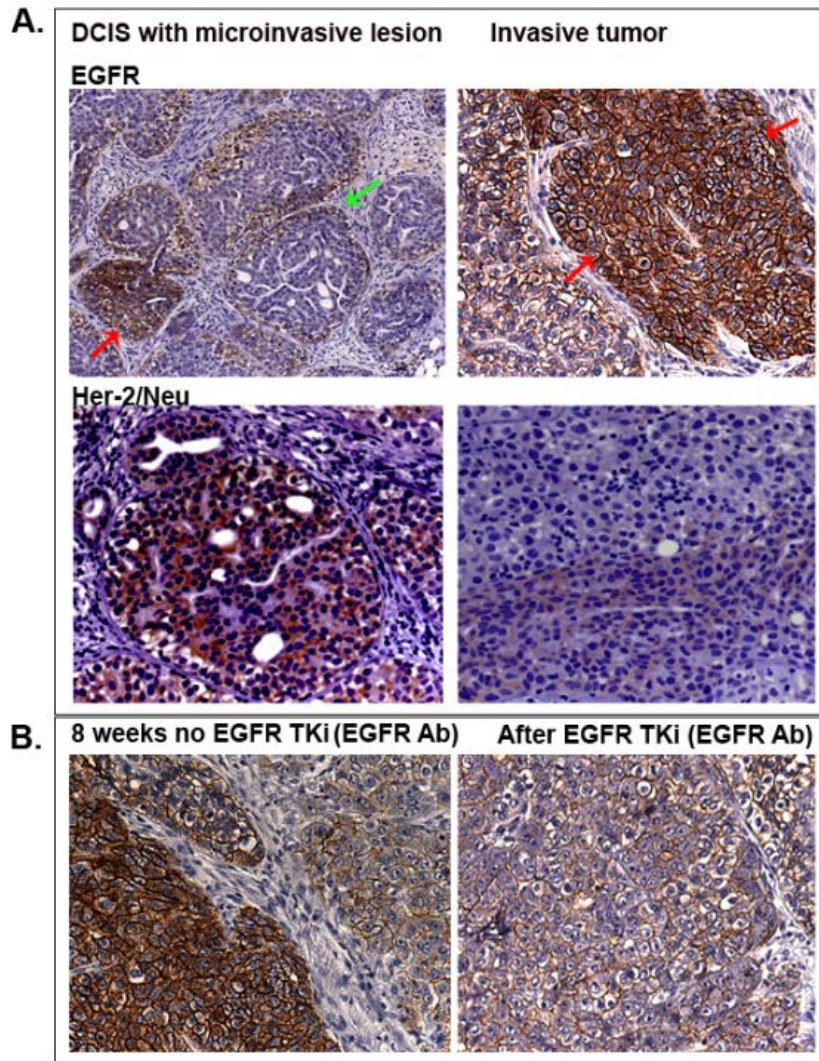


Figure 8.3 EGFR and HER expression levels in a human breast cancer xenograft derived from a basal type of breast cancer cell line (MCF-10DCIS)

The EGFR and HER2 expression level changes in early and late stages of MCF-10DCIS tumors. The expression level of EGFR increases as the tumor progresses to an invasive stage. And the distribution of EGFR extends. The HER2 expression decreased obviously. (Provided by Dr. Lily Yang)

## 8.2 Results and discussion

### 8.2.1 Biomarker changes during the prognosis

Based on the IHC results from Dr. Lily Yang's group, we already found that in the xenografted MCF10-DCIS model, the HER2 expressed in the whole tumor area within the basal layer of the DCIS lesions in the early pre-invasive stage. The EGFR was found mainly on the basal layers of the DCIS tumors at this stage. After 3-4 weeks, when the tumor turns into invasive tumors, the expression level of HER2 decrease dramatically; however, the EGFR expression increased in the whole invasive tumor tissue.

### 8.2.2 Generation of EGFR targeted contrast agent

The ProCA1-affi1907 was created by fusion of affibody  $Z_{EGFR1907}$  which can specifically target to EGFR [71]. The epitope locates in helix 1 and 2 with 13 amino acids (Figure 8.4). This three helix protein which consists of 58 amino acids were cloned to the C-terminal of ProCA1-CD2 with a GGSGG linker in between. In the fused protein ProCA1-affi1907, there is one Gd<sup>3+</sup> binding site in ProCA1-CD2 which can function as an MRI contrast agent [196]. The affibody  $Z_{EGFR1907}$  keeps the helix structure with the EGFR binding sites exposed.

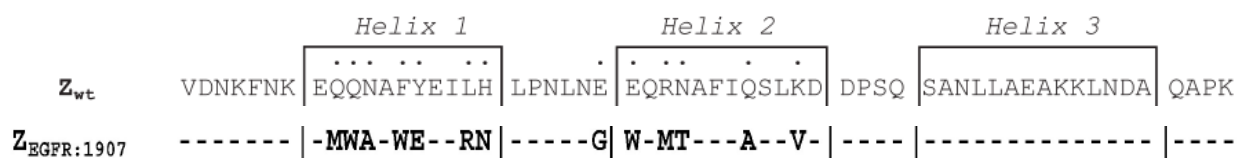


Figure 8.4 Sequence of ProCA1-affibody-EGFR

Same as the parental protein ProCA1-CD2, the constructed ProCA1-affi1907 was also expressed in *E.coli* and subsequently purified by GS-4B column for GST fusion protein. In order to apply this fusion protein in cells and animal experiments, PEGylation was also used to modify this protein, since PEGylation can increase the relaxivity and stability of the fusion protein. An optimized PEG size of 40 repeated PEG units was used for better tumor penetration and keeping the tumor binding capability.

We next examined whether ProCA1-affi1907 can specifically target to EGFR in cancer cells with high EGFR expression. Two cancer cell lines were used for immunostaining. One is breast cancer cell line MDA-MB-231, which overexpresses EGFR but HER2 negative. Another one is an ovarian cancer cell line SKOV-3, which overexpresses both EGFR and HER2. The parental protein ProCA1-CD2 was used as a negative control. Binding of the Gd-ProCA1-affi1907 to the selected cells was analyzed by immuno-fluorescence staining using the polyclonal antibody against PEGylated parental protein ProCA1 (PAbPGCA1) (Figure 4.13). A substantial staining intensity of ProCA1-affi1907 bound to MDA-MB-231 cells was observed and increased as incubation concentration increased. In contrast, the cells stained with ProCA1-CD2 demonstrated very weak binding. In SKOV-3 cells, it showed the same phenomena as MDA-MB-231 (Figure 8.5).

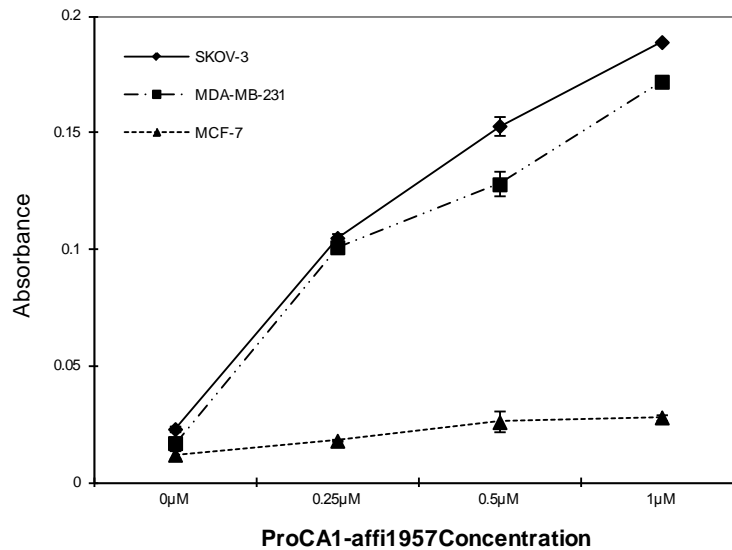


Figure 8.5 ELISA of cell binding with EGFR high expression

The ProCA1-affi1907 of different concentration was incubated with cancers with different expression level of EGFR. The breast cancer cell line MDA-MB-231 has highest expression level as indicated. SKOV-3 also shows high expression level of EGFR. MCF-7 is an EGFR negative cell line.

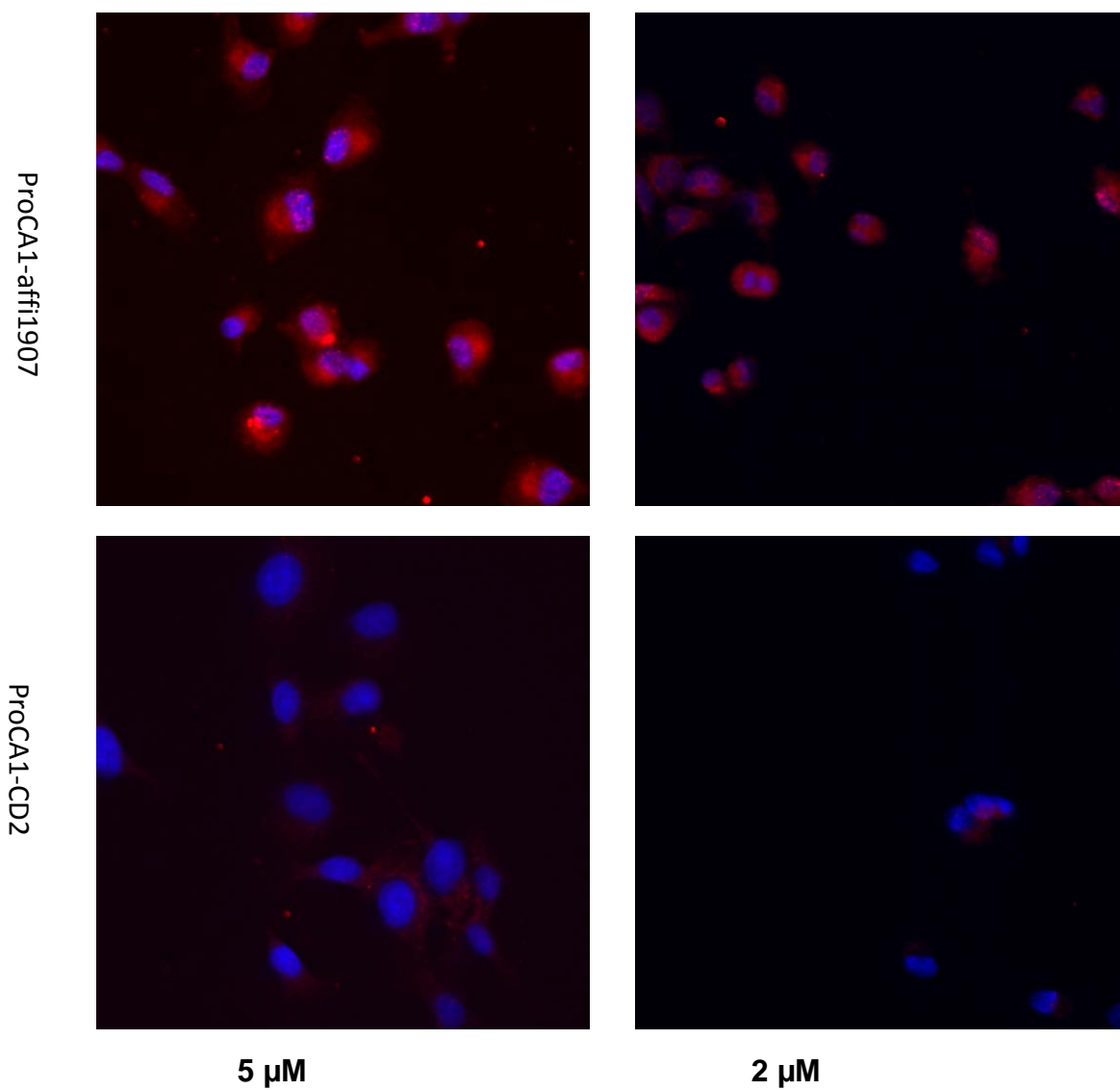


Figure 8.6 Immunostaining of cancer cells by ProCA1-affibody-EGFR

The EGFR positive cell line MDA-MB-231 was used for cell staining. ProCA1-CD2 was used as control.



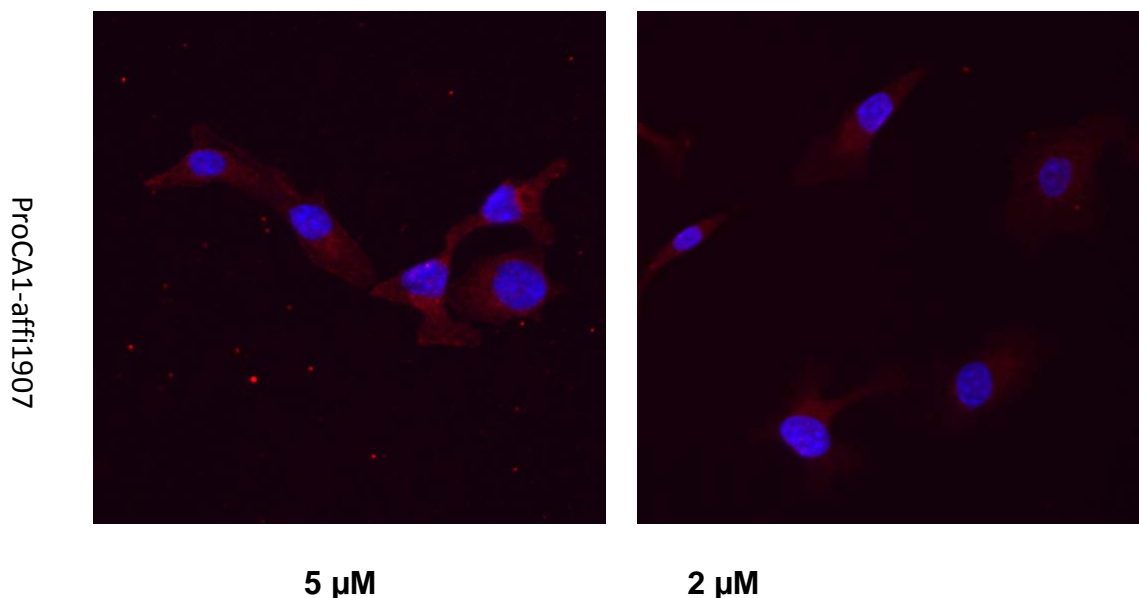


Figure 8.7 Immuno staining of ProCA1-affi1907 in SKOV-3 cancer cells  
SKOV-3 cells also have high expression of EGFR

### 8.2.3 MR imaging of orthotopic tumors

We then tested whether our designed contrast agent would result in MRI contrast enhancement in xenograft orthotopic models of MCF-10DCIS human cancer cell lines. The contrast agent  $Gd^{3+}$  ProCA1-affi342 at concentration of 3 mM (100 fold lower than clinically-approved contrast agent DTPA) was administered via the tail vein (80  $\mu$ l). Pre- and post-contrast MRI were collected at different time points using T1 and T2 weighted fast spin echo or T1 weighted gradient echo sequences. The mice were imaged using two pulse sequences: the T1 and T2 weighted fast spin echo sequence (TR=2 s, TE=0.022 or 0.066 s) and the T1 weighted gradient echo sequence (TR=0.088 s, TE=2 ms and P=0.009 s). The fields of view are 3 cm $\times$ 3 cm with matrix of 256  $\times$  256 and slice of 1 mm in thickness. Image J was used to quantitatively analyze the MRI images obtained. The regions of interest (ROI) were selected by circling the tumor sites. Then the signal intensities of the ROIs were calculated and compared. Six adjacent slides

were selected to measure signal changes which were averaged to obtain statistical significant results. At 3 hour time point, the tumor site exhibited significant contrast enhancement. Strong contrast enhancement was observed in the tumor 24 hours after injection. Such MRI contrast enhancement was decreased after 24 hrs post injection (Figure 7.4-6). In Figure 7.6, the tumor showed enhancement in edge area, however, the center of the tumor was still dark as pre-scan. These results demonstrated the heterogeneous structure of tumor.

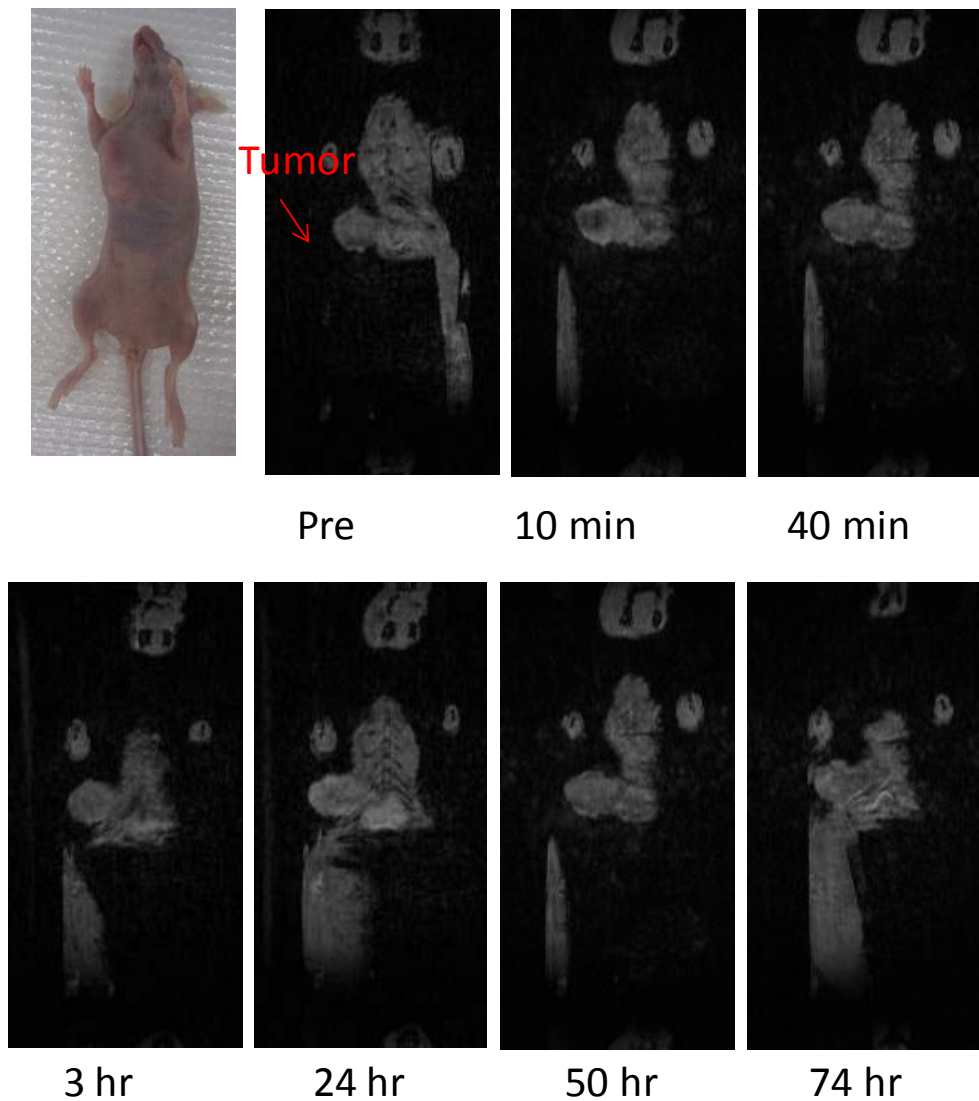


Figure 8.8 MRI of orthotopic model.  
Tissue or organ grafts may be transplanted to their normal situation in the animal.

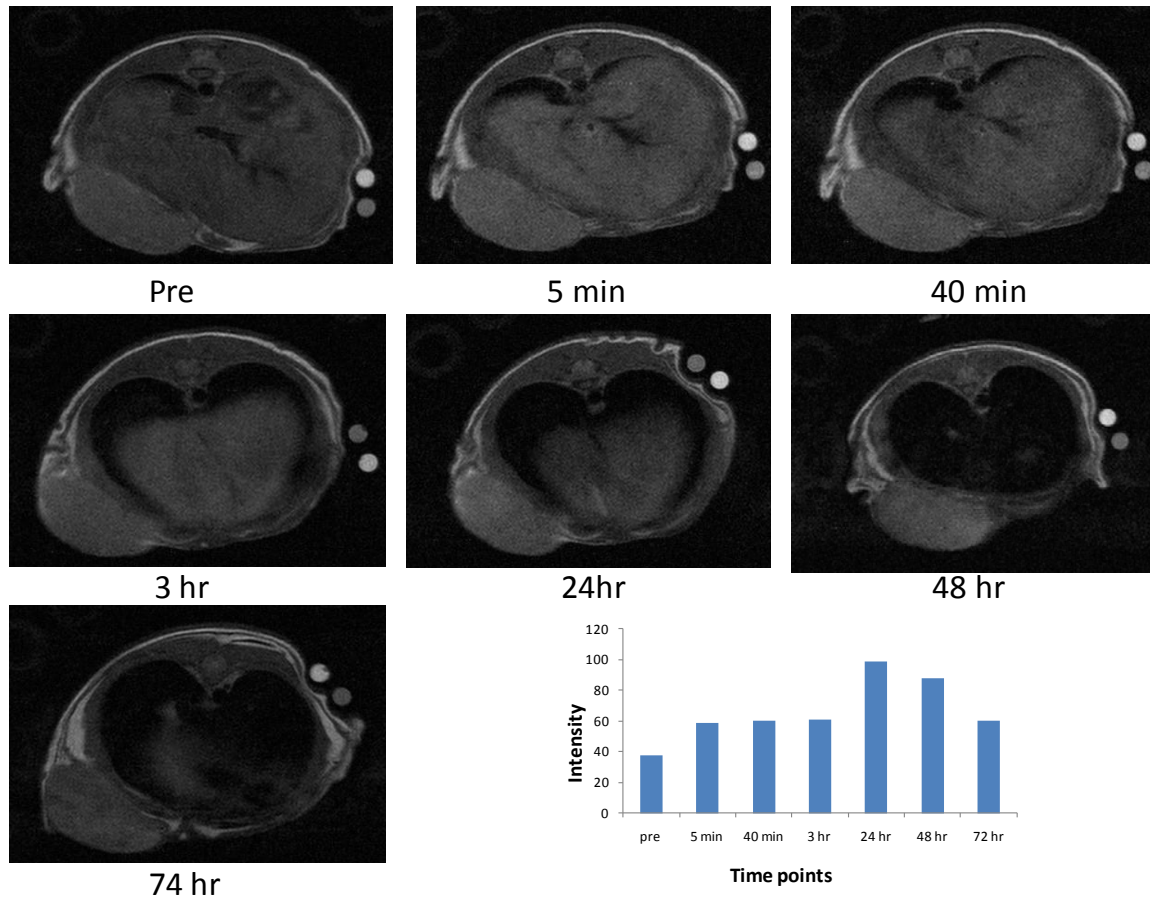


Figure 8.9 MRI of orthotopic tumor model with fast spin echo

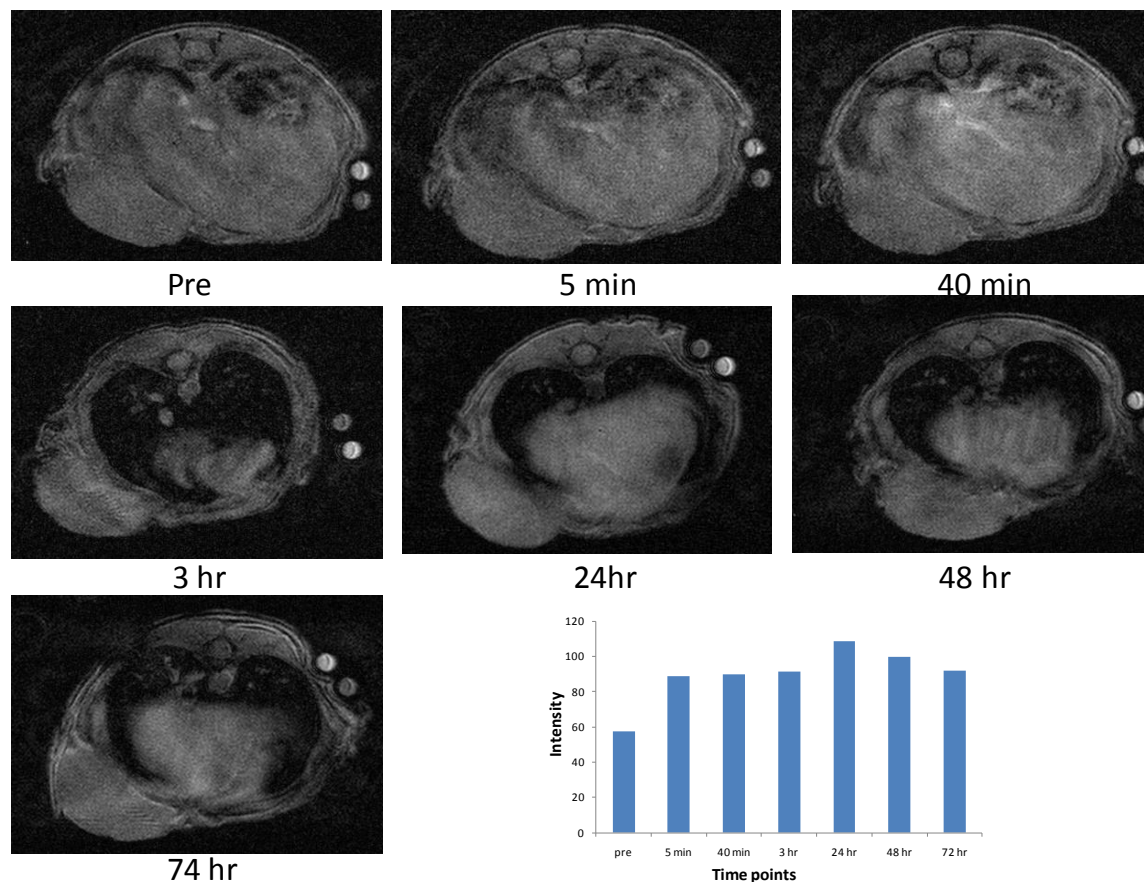


Figure 8.10 MRI of orthotopic tumor model with gradient echo

#### 8.2.4 MRI can monitor distribution of biomarkers

The biomarker may not only have expression level change during the progression and drug treatments, the morphology or the distribution of biomarkers may also change inside the tumor [13]. IHC can clearly demonstrate the distribution of biomarker in the tumor (Figure 8.11) by staining both the biomarker, like HER2 and nucleus. Since MRI is a technique with high resolution [197], we expect to use our designed MRI contrast agents to monitor the tumor structure (Figure 8-10). At the time point of 24 hr, when most contrast agents concentrated in the tumor area, the heterogeneous structure can be viewed (Figure 8.10). Figure 8-11 shows

the difference of MRI signal in the edge and core part of the tumor. This MRI results confirms the biomarkers like HER2 detected by ProCA1-affi342 inside the tumor area is heterogeneous. The MRI is able to image the structure of the tumor; however, the resolution is not as high as IHC to give the information of the distribution of HER2. The DCE-MRI (Dynamic Contrast Enhancement) is expected to give more information about the biomarker changes. [198]

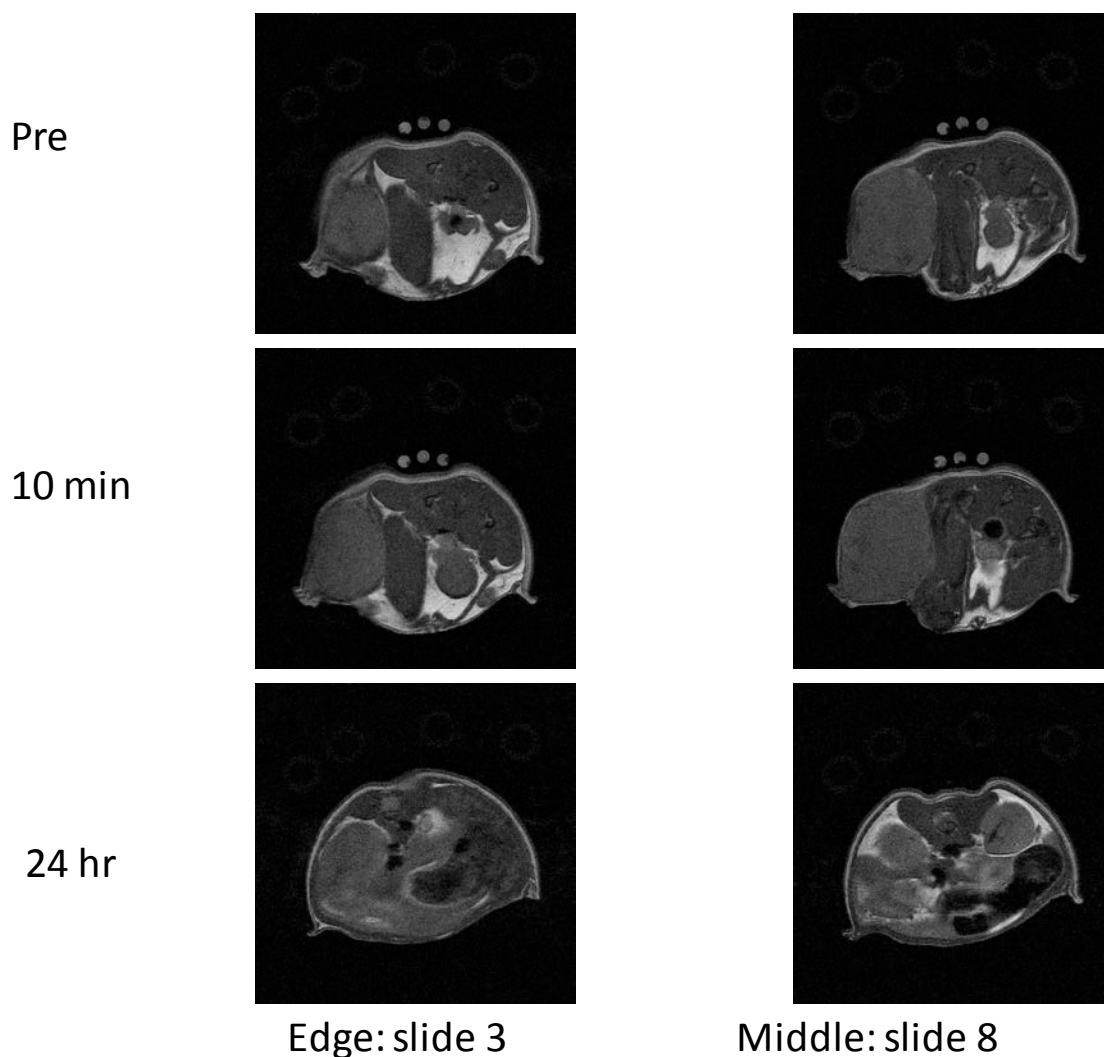


Figure 8.11 MR images can demonstrate the structure difference at the edge and core of the tumor

The tumor edge with lipids shows brightness after loaded with MRI contrast agents. The inner heterogeneous structure can also be viewed by MRI with high resolution.

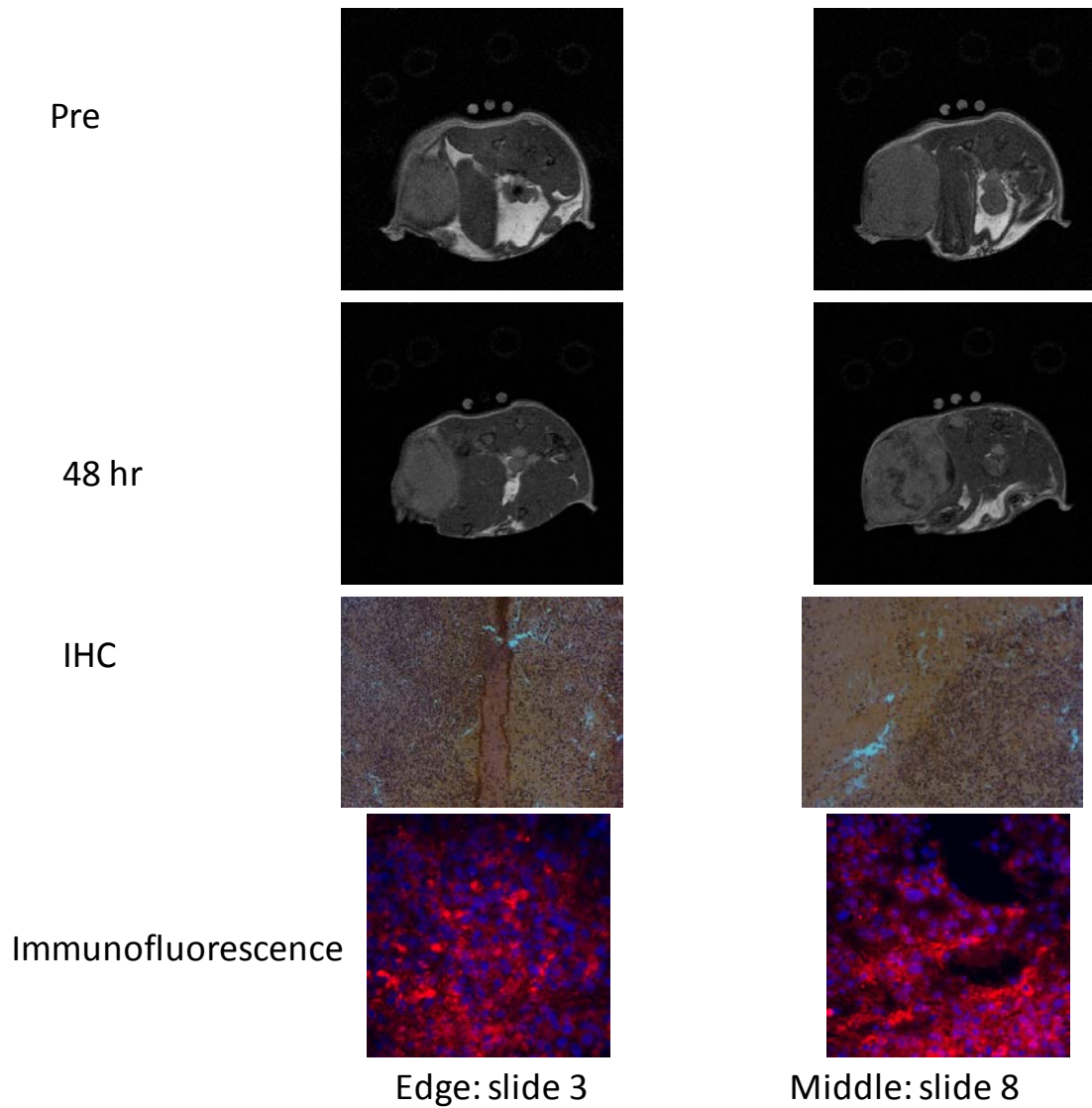


Figure 8.12 Tumor structure can be measured by MRI and IHC

Slide 3 shows the tumor structure of the edge area. Slide 8 shows the structure in the core area.

## Chapter 9. OTHER CONTRAST AGENTS WITH MULTIPLE METAL BINDING SITES

To further increase the contrast capability, protein-based MRI contrast agents with multiple  $Gd^{3+}$  binding sites have been engineered, expressed and characterized. New generation of protein-based contrasts, named ProCA2 and ProCA3, has two to four  $Gd^{3+}$  binding sites on single protein. Figure 9.3 shows that tail vein injection of 0.02 mmol/kg ProCA32 (~10 folds lower dosage (0.02 mmol/kg) than that of Gd-DTPA (0.2 mmol/kg) resulted in an enhancement of blood, liver and kidney 50 min post injection under MRI scanner. The blood circulation time is much longer than small molecular contrast agents, which indicates that ProCA32 could be potentially used as a blood pool contrast agent. The enhancement of tissue completely disappeared two days after injection, which indicates that our contrast agent could be completely secreted out after two days.

### 9.1 Designing HER2 targeted contrast agent by using mutated CaM as host protein (ProCA22-affi342)

After the first generation of protein contrast agent series with ProCA1-CD2 as host protein, we also linked tumor targeted peptide affibody  $Z_{HER2:342}$  to other designed contrast agents with multiple metal binding sites. Calmodulin with four metal binding sites has been designed and grafted to be  $Gd^{3+}$  binding protein. Affibody  $Z_{HER2:342}$  was grafted into the loop region of CaM and the fusion protein is named ProCA22-affi342. Initial data showed that this designed contrast agents is able to target to cancer cells with high expression of HER2.

## 9.2 Toxicity of protein based contrast agents

The acute toxicity of contrast agent on liver enzymes (ALT, ALP, AST, LDH), urea nitrogen, bilirubin, and total protein from CD1 mice 48 hours post-contrast agent injection were found to be negligible compared to a control subject (CD-1 mice). No acute toxicity was observed for mice (N > 10) after contrast agent injection, suggesting that our contrast agent is likely to maintain its metal complex stability and strong affinity for Gd<sup>3+</sup> *in vivo*.

The toxicity of the designed protein was analyzed with CD-1 mice. No acute toxicity was observed following tail vein injections of 4-fold greater dosages than that currently used in MRI, evaluated over a 2-day test period. Characterization of serum samples from the test mice receiving the agent detected no apparent damage to kidney, liver, or heart (Table 11).

Table 11 Acute Toxicity of ProCA1-affi342

	Sodium (mmol/L)	Potassium (mmol/L)	Calcium (mg/dL)	Creatinine (mg/dL)	ALT (U/L)	ALP (U/L)
<b>ProCA1-affi-m</b>	153.6±11.7	10.2±0.5	11.7±0.1	0.28±0.04	35±1	23±5
<b>Saline</b>	151.8±11.0	11.8±2.3	11.0±0.5	0.32±0.01	39±5	89±11



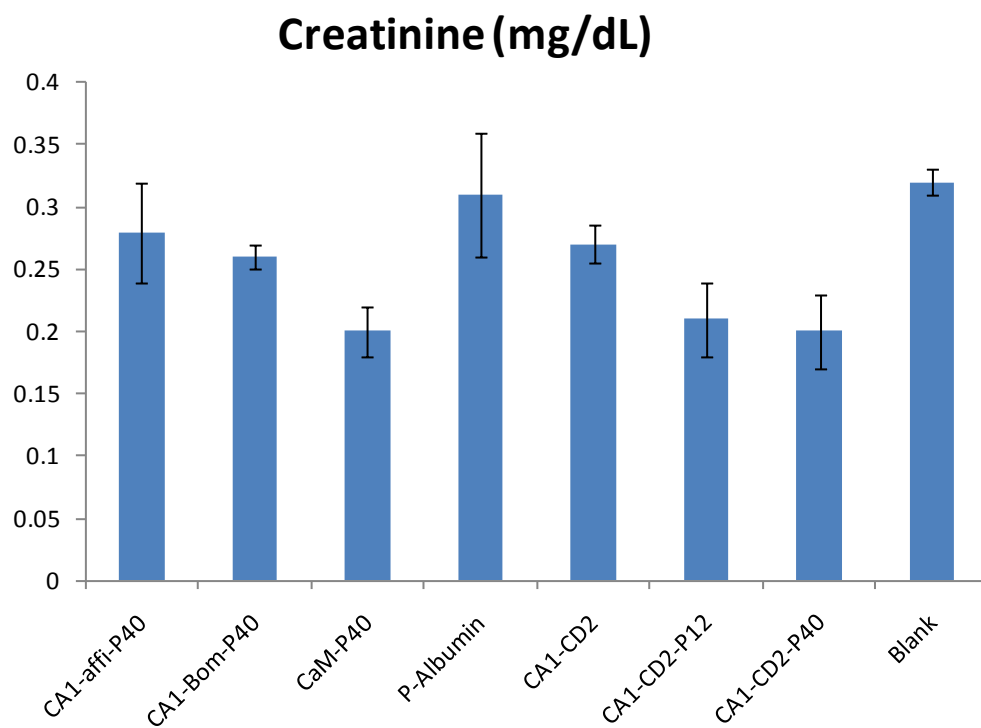


Figure 9.1 Measurement of creatinine concentration in mouse blood  
Creatine is a nitrogenous organic acid which provide energy mainly for muscle. No obvious change has been observed by measuring the concentration in mouse blood.

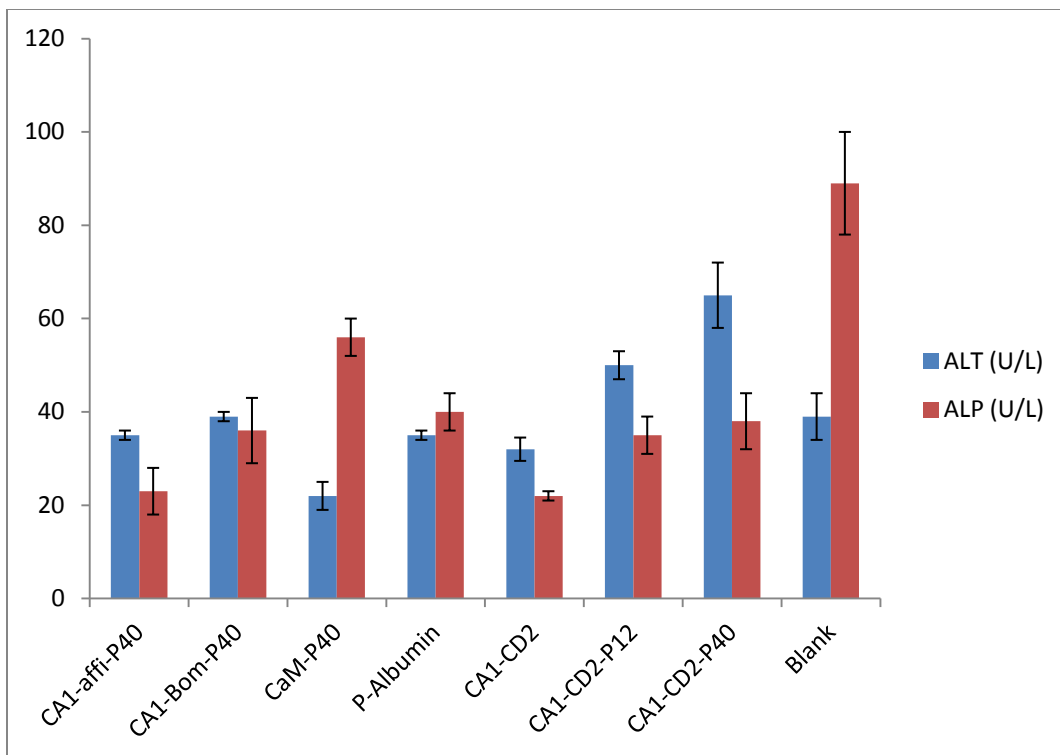


Figure 9.2 The enzyme in liver of ALT (alanine aminotransferase) and ALP(Alkaline Phosphatase) activity

Decreasing of ALP has been observed indicates that the protein based contrast agents accumulate mainly in liver.

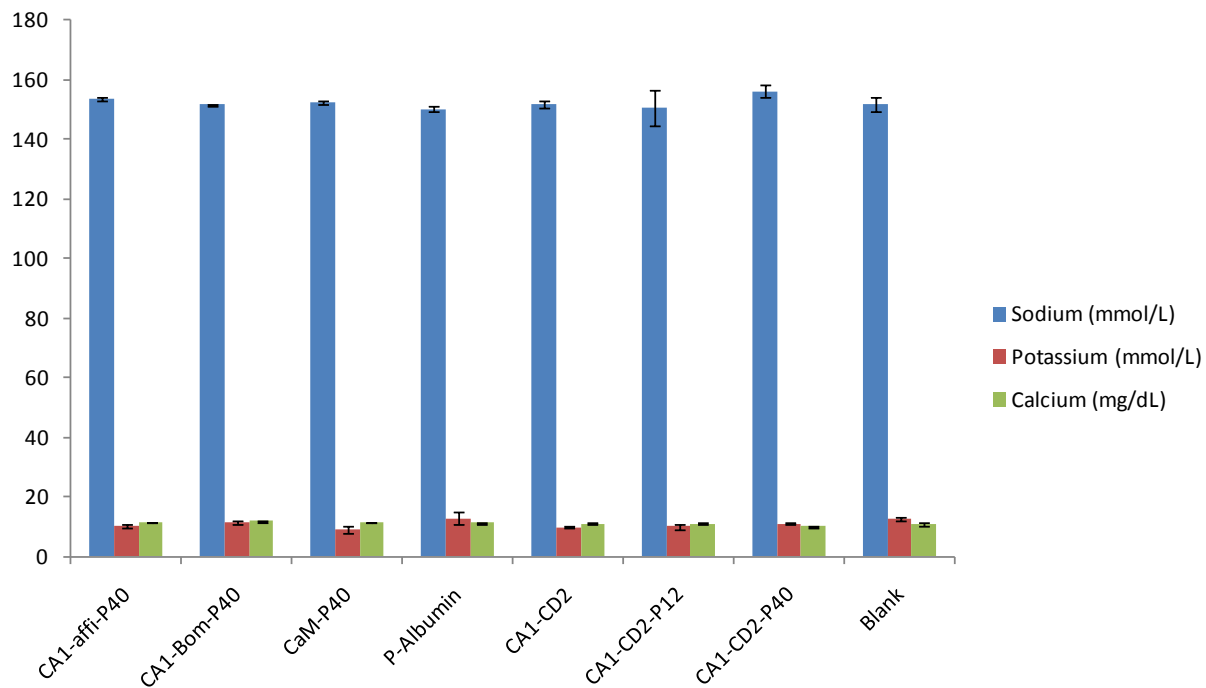


Figure 9.3 Metal concentration in blood has been measured

## Chapter 10. CONCLUSIONS AND MAJOR DISCOVERIES

Magnetic Resonance Imaging (MRI) is one of the primary oncological imaging modality capable of high resolution 3-dimensional imaging, exquisite soft tissue contrast with body depth without use of ionized radiation [164-166]. In addition, it enables the non-invasive and repetitive assessment of biological processes of the same living subject at different time points for monitoring treatment response and disease progression [78-79, 199-201]. Molecular imaging of cancer biomarkers using MRI potentially improves our understanding of the disease and drug activity during preclinical and clinical drug treatment [202-205]. However, lack of desired MRI contrast agents capable of enhancing the contrast between normal tissues and tumors with high relaxivity, tumor targeting, high intratumor distribution and no toxicity is one of the major barriers for the application of MRI to assess specific biomarkers for diagnosis and monitor drug effect.

Biomarkers such as the epidermal growth factor receptors EGFR and HER2/Neu are highly expressed in various diseases such as breast and ovarian cancers and play important roles in disease progression and survival. They are also major drug targets for targeted therapy. Since the clinical application of targeted therapy is largely limited because current methods for assessment of these cancer biomarkers involve invasive methods, such as biopsy and the effectiveness of the target therapy largely depends on the pre-selection of patients over-expressing these biomarkers. To date, one of five HER2/Neu clinical tests, including biopsy and immunostaining (IHC), provides incorrect results, leading to improper selection of appropriate patients for personalized treatment using biomarker targeted therapies [34, 64]. There is an urgent need

to develop non-invasive and accurate methods for diagnosis and selection of patients and to monitor biomarker levels/distribution and their changes upon treatment by targeted drugs.

In this dissertation, we developed novel protein based MRI contrast agents by fusion of affibody variants to the C-terminal of ProCA1-CD2. The results indicated that ProCA1-affi342 and ProCA1-affi1907 are able to target to HER2 and EGFR respectively. MRI and NIR imaging have been demonstrated to prove the capability of using the protein based contrast agents to monitor tumors types, tumor progression and drug treatments.

The targeted protein contrast agents were designed and generated by gene cloning. In vitro results showed that ProCA1-affi342 is well folded after GST purification. PEGylation of the ProCA1-affi342 not only increased the stability and decreased the immunogenicity, but also improved the metal binding and relaxivity. The metal binding affinity to Gd<sup>3+</sup> is up to 1.86 pM and the relaxivity with r1 and r2 of 21 and 30 mM<sup>-1</sup>s<sup>-1</sup> exhibited. In order to compensate the shortage of MRI with low sensitivity, a NIR dye Cy5.5 was successfully conjugated to the ProCA1-affi342 at the C-terminal. Spectra from UV-absorbance, MS and NMR confirmed the conjugation. All the *in vitro* measurements and results demonstrate that the ProCA1-affi342 is well designed as an MRI contrast agent, which will be able to generate dual signals of MRI and NIR *in vivo*. (Chapter 3)

After measuring the *in vitro* properties of ProCA1-affi342, the tumor binding capability is also evaluated in the cell assays. Several immune assays like western blotting, ELISA, immunofluorescent staining and flowcytometry have been used and detected by self generated antibody against ProCA1-CD2 (PAb-ProCA1-CD2). The results are consistent and show significant binding of ProCA1-affi342 to the HER2 overexpressed cancer cells. Besides monitoring the ProCA1-

affi342 by protein and protein interaction, the retention of ProCA1-affi342 in tumor cells was also measured by monitoring the  $Gd^{3+}$  signals with MRI and radioactive assay. The results showed that  $Gd^{3+}$  chelated in the ProCA1-affi342 can be retained in the tumor cells compared with the free  $Gd^{3+}$ . This *ex vivo* studying in the tumor cells provided good knowledge of ProCA1-affi342 for further studying in the tumor mouse. (Chapter 4)

In order to apply our contrast agents to tumor mice, the mouse model was carefully estimated and selected. Subcutaneous xenografted model was selected for the initial studying. Two tumor cell lines SKOV-3 and MDA-MB-231 with different HER2 expression level and moderate tumorigenicity were chosen. The MRI results clearly showed that the ProCA1-affi342 targeted to the HER2 positive SKOV-3 tumor specifically. The tumor got highest MRI intensity after 1 day injection with highest concentration of ProCA1-affi342 concentrated in this tumor site. Some primary organs like kidney and liver also got enhancements. MRI blocking results also supported this results that the ProCA1-affi342 accumulated in the positive tumor site specifically by the biomarker HER2 targeting. Further studying of IHC is consistent with the MRI results which show the ProCA1-affi342m accumulating in the positive tumor sites. The IHC results also show that ProCA1-affi342m has better tissue penetration and distribution than HER2 antibody. (Chapter 5)

Since the MRI enhancement has been observed in the positive tumor sites and some other primary organs like kidneys and liver, further quantitative results of on the distribution of ProCA1-affi342m are analyzed by NIR intensity, radioactive assay and ICP-OES. The NIR monitors the protein signal since the dye is covalently conjugated to the ProCA1-affi342. The radioactive assay and ICP-OES monitors the  $Gd^{3+}$  signals. By these two methods to monitor the

biodistribution, we can see that about 20% of ProCA1-affi342m accumulates in the positive site, however only less than 10% of  $Gd^{3+}$  stays in the tumor site after one day injection. We may conclude that since some disassociation of  $Gd^{3+}$  from ProCA1-affi342, the free  $Gd^{3+}$  will be secreted out of the body in short time. The pharmacokinetics of ProCA1-affi342m needs to be studied in the future. (Chapter 6)

After been proved that the ProCA1-affi342 has the capability to target to HER2 overexpressed tumors both *in vitro* and *in vivo*, further application of this contrast agent has started. First, we tried to use this contrast agent to monitor the effects of drug treatments. In Chapter 7, the receptor level changes have been detected by ProCA1-affi342 in cancer cells with both immunology techniques and MRI. Further studying of relaxivity changes related to the drug treatments in cells and the tumor changes in mouse model will be taken to better use ProCA1-affi342 with high relaxivity and tumor targeting capability. (Chapter 7) Second, we also try to use these protein contrast agents to monitor the tumor progression. A new type of contrast agent ProCA1-affi1907 has been generated to target to EGFR. Since in the specific tumor model MCD10-DCIS, both the biomarkers HER2 and EGFR will change during the progression, we may use our contrast agents to view the receptor level change and distribution change. Some initial work has been done with ProCA1-affi342m. The results showed that ProCA1-affi342m is able to bind to the orthotopic tumor with MCF10-DCIS in the early stage. We will continue this research by using both ProCA1-affi342m and ProCA1-affi1907 to monitor the tumor in early and late stage to see the biomarker changes. (Chapter 8)

In this dissertation, targeted protein based contrast agents have been generated and all the experimental conditions have been optimized, so that we first time successfully got the MRI

enhancement in the tumor model by tail vein injection of our contrast agents. This also paved the way for other contrast agents with multiple metal binding sites (Chapter 9). However, in order to apply our contrast agents clinically, there is still a long way in front; we are continuing this project by estimate the lowest dosage needed, the long term toxicity and other physiology researches. The capability to spatially and temporally visualize as well as quantify HER2 and EGFR would significantly improve our capability to follow the expression of these biomarkers during tumor progression and metastasis, monitor treatment efficacy, aid in drug selection for patients, and further apply and develop novel targeted therapy.



**PUBLICATIONS AND MANUSCRIPT IN REVISION**

**Jinjuan Qiao**, Shunyi Li, Jie Jiang, Lixia Wei, Robert Liang, Liya Wang, Hui Mao, Hua Yang, Hans Grossniklaus, Zhiren Liu and Jenny J. Yang. HER-2 Targeted Molecular MR Imaging Using a de novo Designed Protein Contrast Agent. PLOS ONE (2011). 6:e18103. DOI:10.1371/journal.pone.0018103 (PMID: 21455310)

Shunyi Li, Jie Jiang, Jin Zou, **Jinjuan Qiao**, Shenghui Xue, Lixia Wei, Robert Long, Liya Wang, Adriana Castiblanco, Natalie Maor, Jen Ngo, Hui Mao, Zhi-Ren Liu, and Jenny J. Yang. PEGylation of Protein-based MRI Contrast Agents Improves Relaxivities and Biocompatibilities. Journal of Inorganic Biochemistry. In Press

Shenghui Xue, **Jinjuan Qiao**, Jie Jiang, Kendra Hubbard, Lixia Wei, Shunyi Li, Zhi-Ren Liu and Jenny J. Yang. Design protein-based Gd<sup>3+</sup> MRI contrast agents with high dose efficiency and capability for molecular imaging of cancers. Submitted to Medicinal Research Reviews with revision.

**MANUSCRIPTS IN PREPARATION**

**Jingjuan Qiao**, Shenghui Xue, Jie Jiang, Fan Pu, Weiping Qian, Lily Yang, Zhi-Ren Liu and Jenny Yang. Monitoring tumor progression and biomarkers distribution by targeted MRI contrast agents. (In preparation)

**Jingjuan Qiao**, Shenghui Xue, Jie Jiang, Fan Pu, Weiping Qian, Lily Yang, Zhi-Ren Liu and Jenny Yang. Monitoring drug treatments of breast cancers by targeted MRI contrast agents. (In preparation)

## Appendix I

### **Establish mammalian expression and purification of HER2-ECD**

In this dissertation, we focused a lot on quantitative analysis of biomarkers with various techniques. In order to get quantitative results, pure biomarker proteins are needed to be a standard. Dr. Leahy in Johns Hopkins kindly provided stable cell line LEC1 with transfection of the HER2-ECD gene in pSGH vector [206]. This HER2-ECD is also His-tag fused. The LEC1 cell was first thawed and cultured in  $\alpha$ -MEM medium with 10% of FBS. After passaged to T250 flasks for 2 days, the medium was changed to DMEM/F12 medium with 1% FBS. This medium was changed every three days and collected to obtain the secreted HER2-ECD. The expression level was measured by western blotting (Figure A1). The HER2-ECD was purified from cell culture medium by His-tag column (Figure A3).

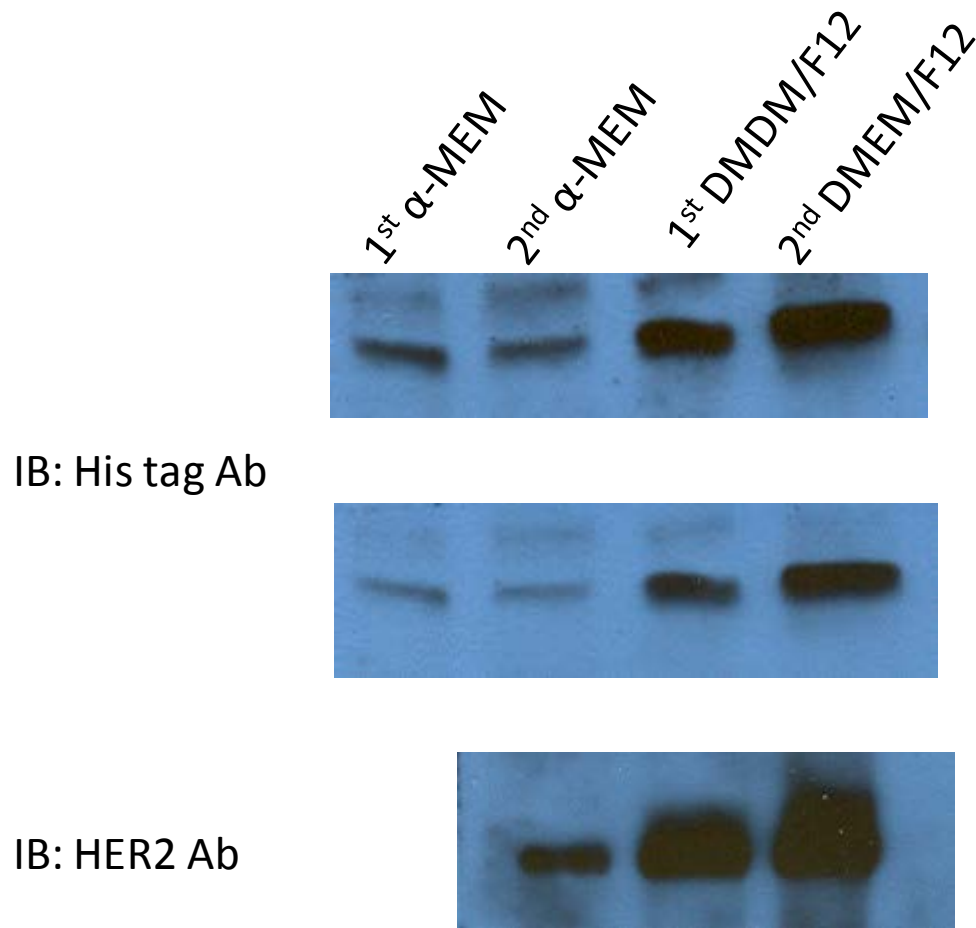


Figure A 1 Monitoring HER2-ECD expression by western blotting

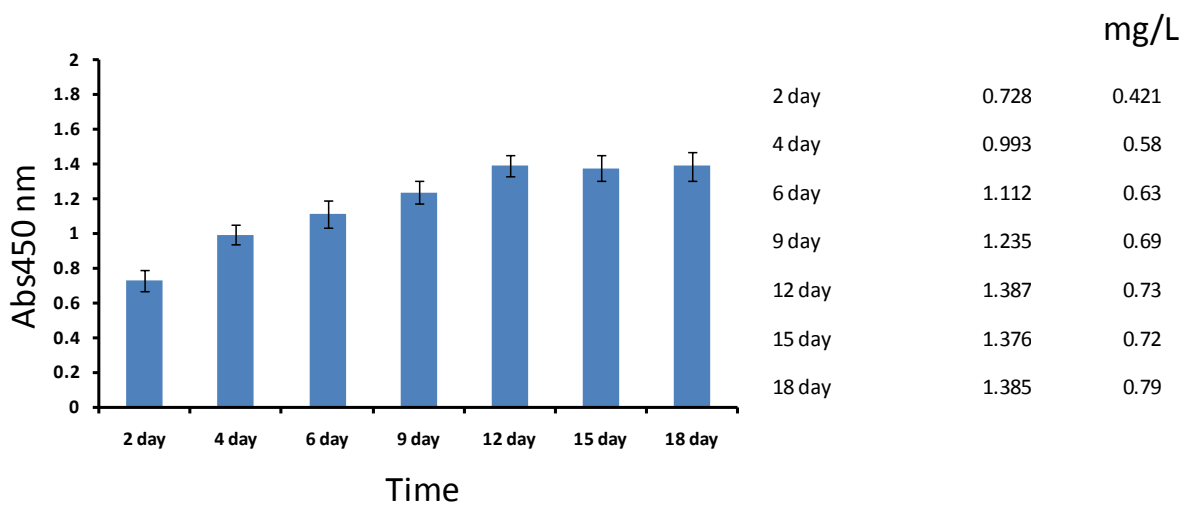


Figure A 2 Expression level of HER2-ECD was measured by ELISA

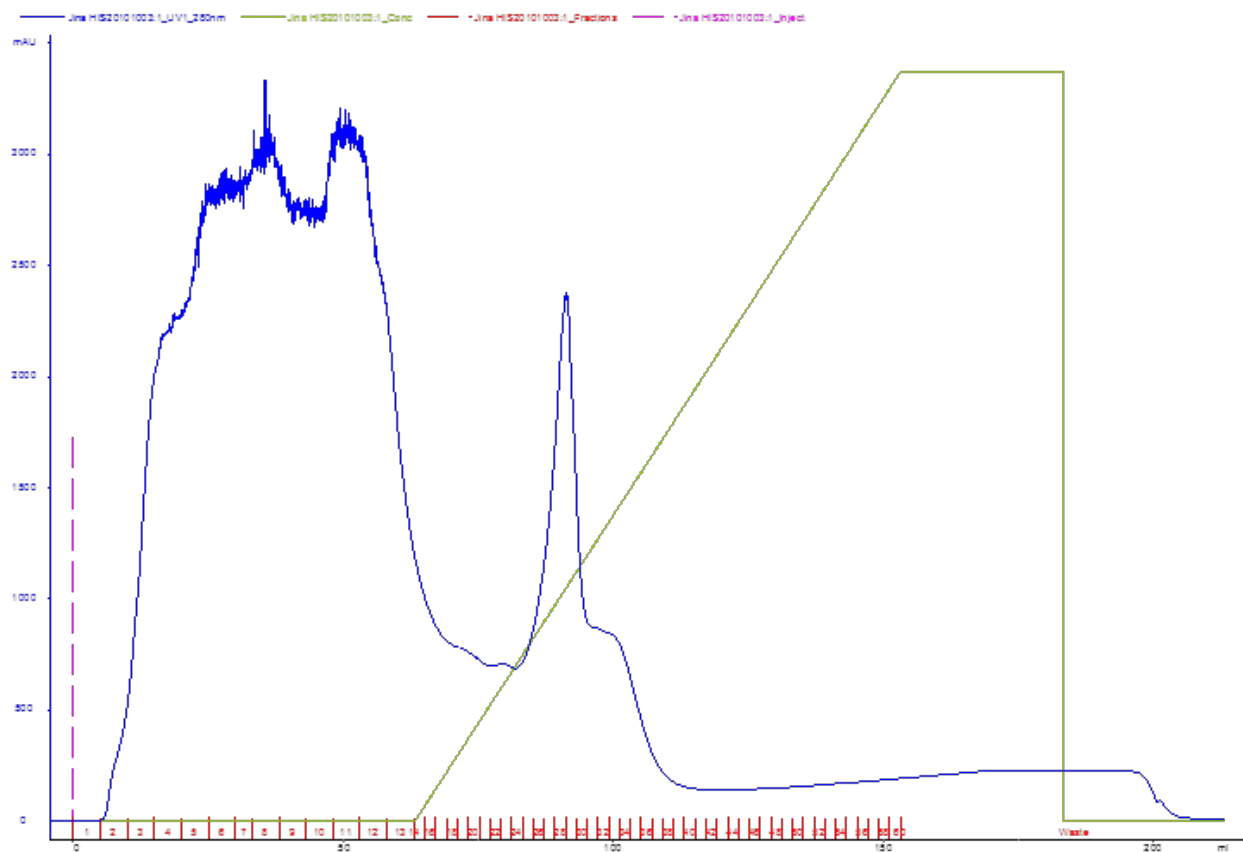


Figure A 3 Elution curve of HER2-ECD purification

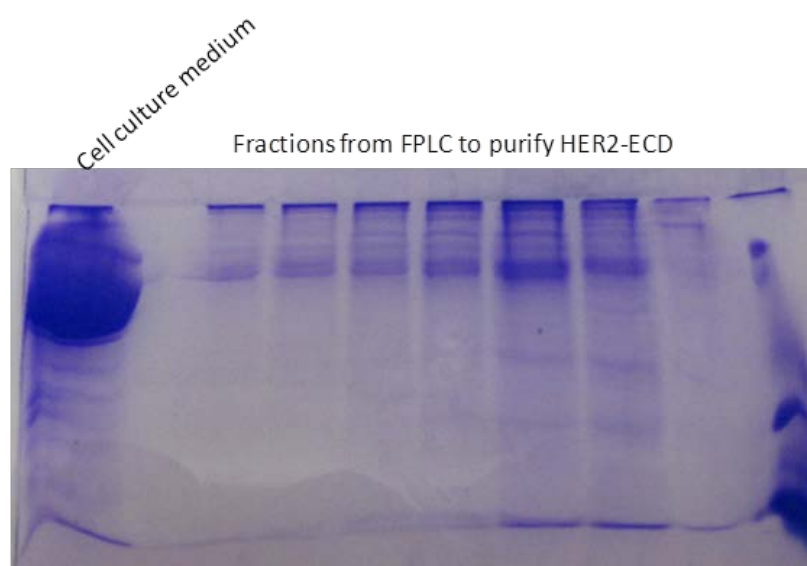


Figure A 4 Purity of HER2-ECD was detected by SDS-PAGE gel

## **Appendix II**

### **Vaccine and Monkey virus**

#### **Introduction**

Vaccinia virus is a member of the Poxviridae family, which is capable of causing severe systemic human disease [207]. Since the vaccinia virus contains some of the largest, most complex and most challenging viruses, it has been well characterized. It is a classic subject for viral studies. Other members of this family include variola virus, which is the cause of smallpox, monkeypox virus, cowpox virus and ectromelia virus. All these viruses are distinguished in morphology and cross-reactive antigenically. Therefore, any one of them confers some protection against other members of the family.

In this virus family, both the monkeypox and smallpox can cause infections on human. The monkeypox was observed when the smallpox had been eradicated [208]. Their signs and symptoms are very similar although the viruses are significantly different. In order to diagnose the monkeypox, several methods based on protein are used currently [209]. The significance of protein has provided ways to diagnose post viral infection and tool for epidemic analysis. Furthermore, the development of potential vaccine and new monoclonal antibodies are identified and characterized. But because of the similarity between monkeypox and smallpox, it is difficult to diagnose monkeypox or smallpox correctly by clinical presentation alone [210]. So we are going to find the selectivity of monoclonal antibodies against different virus. Our work will be based on the structural knowledge of viral fusion proteins.

A27L is one of the viral fusion proteins. The wide type protein sA27L is a vaccinia virus envelope protein encoded by the A27L gene. This protein contains 110 amino acids, which can be divided into four domains. The residues 1-20 form a signal peptide for protein processing; the second region including residues 21-32 is a lysine/arginine rich region, which is essential for binding to cell surface GAGs (glycosaminoglycans); the third region contains residues 43-84, which is coiled-coil structure involving self-assembly; and the last C-terminal sequence has interaction with another vaccinia virus protein A17L [210]. A29L is the orthologous gene of A27L gene, which is also called A27Lo.

As a virus protein, the A27L protein as well as the A27L gene is involved in the immune activities. The A27L gene with other virus genes in same family protects nonhuman primates against lethal monkeypox as a DNA vaccine. The other virus genes include L1R, A33R and B5R, in which the L1R is specific to IMV, A33R and B5R is specific to the EEV. The previous in vivo experiments demonstrated that the A27L or B5R alone couldn't protect significantly, while the combination of these genes made a high level of protection from challenge. Furthermore, the virus genes also have a combinational activity with the subdomains of the virus proteins. There are open reading frames of the virus proteins: A27Lo, A33Ro, B5Ro and L1Ro (o refers to ortholog). These subunits were expressed firstly by deleting the transmembrane region of the A27L, A33R, B5R and L1R genes respectively. Results showed that both the genes and protein products alone failed to generate high level antibodies. However, the DNA vaccine boosted by the subunit of its protein product induces high immune response [208].

Different antibodies may bind to different epitopes of antigens. The structure of the epitope contains lot information that benefits for preventing, diagnosing and curing diseases [211]. There are mainly two types of epitopes: linear and conformational epitopes. A linear epitope means the antibodies bind to antigen by recognizing its sequence of amino acids or primary structure [209]. Site directed mutation, western blotting, immunohisto- chemistry and ELISA can be applied to study the linear epitope. However, some of these techniques may not be suitable for conformational epitope research. For example, the protein samples boiled, treated with beta-mercaptoethanol are denatured; as a result, the samples may fail to keep their original three-dimensional conformation. Therefore, site mutation and western blotting cannot be applied strictly. In order study the conformational epitope, the three dimensional structure of the proteins should be studied. The best choice probably is to study the crystal structure of antibody-antigen structure [212]. The complex structure will show the accurate relationship of antibody and antigen when binding together. NMR is also a powerful technique to study protein structure, while large molecular weight of antibody (150KDa) hinders its application. However, it is possible to study the structure of CDR domain in antibody and small antigen by NMR. Then special software can be used for docking the structure between antibody and antigen [213].

The amino acids sequence of protein A29L is highly conserved. The sequences of A27L and A29L are as following [209]:



```

A27L MDGTLFFPGDDDLAIPATEFFSTKAAKKEEAKREAIVKADEDDNEETLKQRLTNLEKKITN
A29L MDGTLFFPGDDDLAIPATEFFSTKAAKNEEIKREAIVKAEGDDNEETLKQRLTNLEKKITN
M4   MDGTLFFPGDDDLAIPATEFFSTKAAKNEEIKREAIVKAEGDDNEETLKQRLTNLEKKITN
M2   MDGTLFFPGDDDLAIPATEFFSTKAAKKEEAKREAIVKADEDDNEETLKQRLTNLEKKITN

A27L VITTKFEEQIEKCKKRINDEVLFRLNHAETLRAAMISLAKKIDVQTGRRPYE
A29L IITTKFEEQIEKCKKHINDEVLFRLNHAETLRAAMISLAKKIDVQTGRRPYE
M4   VITTKFEEQIEKCKKRINDEVLFRLNHAETLRAAMISLAKKIDVQTGRRPYE
M2   IITTKFEEQIEKCKKHINDEVLFRLNHAETLRAAMISLAKKIDVQTGRRPYE

```

Figure A4 Sequences of monkey virus family proteins

The antibodies against monkeypox virus react with the orthologs of this virus. So the orthologous gene of A27L was cloned from the monkeypox virus [214]. Because of the high identity, only specific antibodies can identify A27L and A29L. The monoclonal antibody mAB 126-69-3-7 can recognize A29L with high specificity. The monoclonal antibody VVIV 4B4-2-1 only recognizes A27L. The mAB 126-69-3-7 is supposed to recognize the coil-coiled region of A29L. It is a conformational epitope. Therefore, we will use site mutation, SPR, Western Blot, CD, Mass Spectrum, NMR and other techniques to study the structure of A29L and the epitopes of the antibodies against A29L both in polymer and monomer.

## Materials and Methods

### Mini-scale expression

Competent cells BL21 were transformed with pET-A29L, pET-A27L-4M and pET-A27L-2M; and selected for growth on the Luria broth (LB) ampicillin plates overnight. The individual clone was used to inoculate in 200ml LB culture containing 100ug/ml ampicillin. The cells were grown overnight at 37°C to saturation. Then 50ml of the cells were used to inoculate into 1L LB medium with 100ug/ml ampicillin. The cells were grown at 37°C continuously. When the OD600

got 0.6, 1mM IPTG was added to induce the expression. Cells were harvest by centrifugation (7K, 20min). The precipitation was suspended by the lysate buffer (Tris) and sonicated completely. Then the emulsion was centrifuged (14K, 40min) and the supernatant was ready for purification.

### **Purification of A27L mutants and A29L**

The supernatant was harvest and filtered by the 0.45um membrane. Then the supernatant was applied to 2ml Ni<sup>2+</sup>-chelating affinity column. 20mM, 100mM and 250mM imidazole were added into the washing buffer (PBS) to elute the fusion protein. The fraction obtained from affinity purification was dialyzed by the buffer of 100mM Tris-HCl, pH7.4 and then loaded onto Superdex-G75 gel filtration and SP cation exchanging columns in consequence for further purification. The samples in each step were detected by SDS-PAGE with coomassie blue staining. After detecting, the parts of interest were collected and dialyzed by the 100mM Tris buffer again to store the protein.

### **Binding analysis by surface plasmon resonance**

The protein A29L was immobilized on the CM5 sensor chip directly. Then the antibody mAB 126-69-3-7 in different concentrations flows over the chip with A29L. Then the antibody will be immobilized on the chip by covalent bonds. Different concentration of virus proteins flowing through the chip with antibody give different signal changes based on their binding affinity and concentration.

### Site-directed mutagenesis

The A27L gene was cloned to pET-21 vector before. Four mutants called N27A T30A Y39A and G40A are made from A29L using site-directed mutagenesis. Four pairs of primers were used: N27A Forward 5-GCTAAAGCTCCAGAGACTAAACGC-3, Reverse 5-AGCCTTTGTAGAAA AAAATTCAGT-3; T30A Forward 5- CCAGAGGCTAAACGCGAAGCAATT-3, Reverse 5- CTTTTTAGCAGCCTTTGTAGAAAA-3; Y39A Forward 5- AAAGCCGCTGGAGACGACAATGAG-3, Reverse 5- AACAATTGCTTCGCGTTTAGTCT-3; G40A Forward 5- AAAGCCTATGCAGACGACAATGAG-3, Reverse 5-AACAATTGCTTCGCGTTTAGTCT-3. After phosphorylation, the primers were used in PCR to obtain mutated DNA. The anneal temperature is set to 60 °C. Then the whole PCR products were used in transformation in DH5a cell lines. Two single clones on the ampicillin plate are picked out and inoculated in 10ml LB medium. Plasmid DNA is extracted by mini preparation and sent to sequence. After getting the correct sequences, the plasmid DNA is transferred to BL21 competent cells and used to do expression.

### Results and Discussions

The SPR binding curves have been showed in figure 1. The protein A29L has specific binding with the antibody mAb 126-69-3-7. The binding affinity is much higher than A27L (Data not shown). The binding of the two mutants was tested to check the epitope of the antigen. The Mass Spectra have been tested on the virus proteins and their mutants. The results indicate that all of the virus protein exists in trimer. Figure 1 shows the PCR products of A27L mutants. The mutant M4 contains four amino acids being mutated: K27N A30T D39Y E40G; the mutant

M2 contains two amino acids being mutated: V61I R74H. The bands are solid and there is no other non-specific product. After extracting the DNA from agarose gel and mini preparation of plasmid DNA, the sequences are right after DNA sequencing.

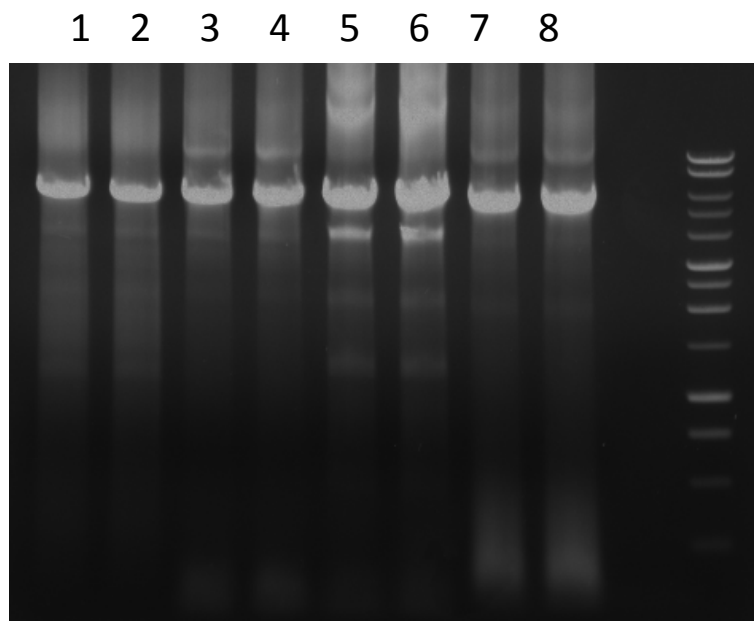


Figure A5. Mutation of A29L

1,2 N27A 3,4 T30A 5,6 Y39A 7,8 G40A

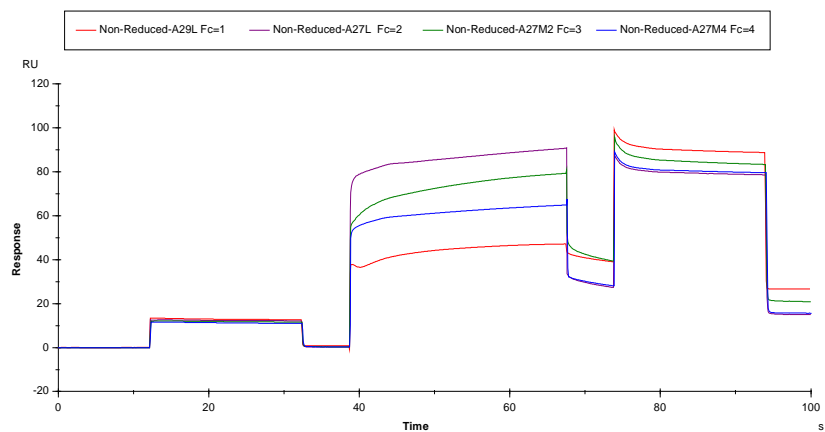


Figure A6. SPR spectra of A27L mutations to the antibody mAb 126-69-3-7

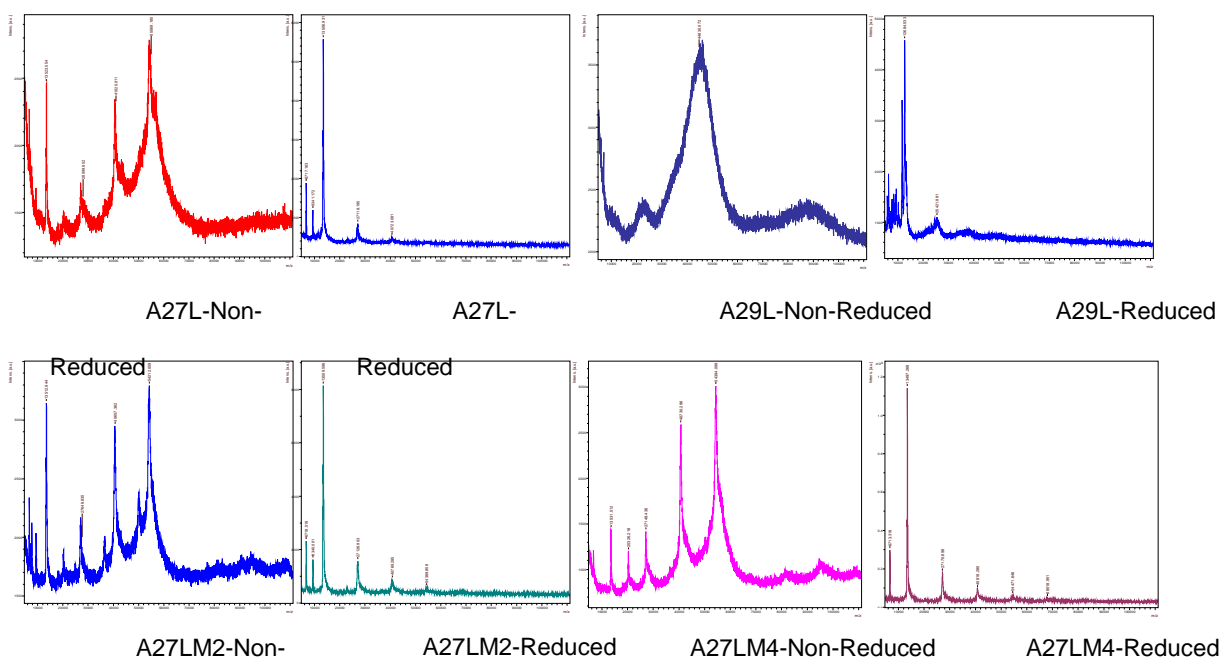


Figure A7 Mass spectra of virus proteins

All the SPR and MS data are provided by Dr. Yiming Ye in CDC

## Summary

Currently, the virus proteins A27L, A29L and the mutants M4, M2 have been expressed and purified. Some basic characters, like CD and SPR, also have been measured on these proteins. However, we are trying to find the epitope of mAb 126-69-3-7 and whether the epitope depends on the polymers. Based on the hypothesis, we use Biacore to measure the binding of mAb 126-69-3-7 with A27L, A29L, M4 and M2 both in polymer and monomer. The current results show that the mutant M4 has specific binding with the antibody, which means the epitope exists on the region of M4. Therefore, further mutation has been designed to study the exact epitope. Also fresh samples, which exist in monomer will be prepared to determine the function of trimer in supporting the epitope.

## REFERENCES

1. Arteaga, C., *Targeting HER1/EGFR: a molecular approach to cancer therapy*. Semin Oncol, 2003. **30**(3 Suppl 7): p. 3-14.
2. Diaz, R., et al., *Antitumor and antiangiogenic effect of the dual EGFR and HER-2 tyrosine kinase inhibitor lapatinib in a lung cancer model*. BMC Cancer, 2010. **10**: p. 188.
3. Baselga, J. and S.M. Swain, *Novel anticancer targets: revisiting ERBB2 and discovering ERBB3*. Nat Rev Cancer, 2009. **9**(7): p. 463-75.
4. Jemal, A., et al., *Cancer statistics, 2010*. CA Cancer J Clin, 2010. **60**(5): p. 277-300.
5. Myers, E., et al., *A positive role for PEA3 in HER2-mediated breast tumour progression*. Br J Cancer, 2006. **95**(10): p. 1404-9.
6. Nevalainen, M.T., et al., *Signal transducer and activator of transcription-5 activation and breast cancer prognosis*. J Clin Oncol, 2004. **22**(11): p. 2053-60.
7. Jemal, A., et al., *Cancer statistics, 2005*. CA Cancer J Clin, 2005. **55**(1): p. 10-30.
8. Colombo, M., et al., *HER2 targeting as a two-sided strategy for breast cancer diagnosis and treatment: Outlook and recent implications in nanomedical approaches*. Pharmacol Res, 2010. **62**(2): p. 150-65.
9. Wilken, J.A., K.T. Webster, and N.J. Maihle, *Trastuzumab Sensitizes Ovarian Cancer Cells to EGFR-targeted Therapeutics*. J Ovarian Res, 2010. **3**: p. 7.
10. Milanezi, F., S. Carvalho, and F.C. Schmitt, *EGFR/HER2 in breast cancer: a biological approach for molecular diagnosis and therapy*. Expert Rev Mol Diagn, 2008. **8**(4): p. 417-34.
11. Gambert, S.R., *Screening for prostate cancer*. Int Urol Nephrol, 2001. **33**(2): p. 249-57.
12. Li, L.Z., et al., *Quantitative magnetic resonance and optical imaging biomarkers of melanoma metastatic potential*. Proc Natl Acad Sci U S A, 2009. **106**(16): p. 6608-13.

13. Kerlikowske, K., et al., *Biomarker expression and risk of subsequent tumors after initial ductal carcinoma in situ diagnosis*. J Natl Cancer Inst, 2010. **102**(9): p. 627-37.
14. O'Connor, J.P., et al., *Quantitative imaging biomarkers in the clinical development of targeted therapeutics: current and future perspectives*. Lancet Oncol, 2008. **9**(8): p. 766-76.
15. Murukesh, N., C. Dive, and G.C. Jayson, *Biomarkers of angiogenesis and their role in the development of VEGF inhibitors*. Br J Cancer, 2010. **102**(1): p. 8-18.
16. Eisenberg, M.L., et al., *Prognostic implications of an undetectable ultrasensitive prostate-specific antigen level after radical prostatectomy*. Eur Urol, 2010. **57**(4): p. 622-9.
17. Lee, K.C., et al., *Prospective early response imaging biomarker for neoadjuvant breast cancer chemotherapy*. Clin Cancer Res, 2007. **13**(2 Pt 1): p. 443-50.
18. Aitken, S.J., et al., *Quantitative analysis of changes in ER, PR and HER2 expression in primary breast cancer and paired nodal metastases*. Ann Oncol, 2010. **21**(6): p. 1254-61.
19. Lee, C.M., et al., *Prostate cancer-targeted imaging using magnetofluorescent polymeric nanoparticles functionalized with bombesin*. Pharm Res, 2010. **27**(4): p. 712-21.
20. Sternlicht, M.D., *Key stages in mammary gland development: the cues that regulate ductal branching morphogenesis*. Breast Cancer Res, 2006. **8**(1): p. 201.
21. Tsiambas, E., et al., *HER2/neu expression and gene alterations in pancreatic ductal adenocarcinoma: a comparative immunohistochemistry and chromogenic in situ hybridization study based on tissue microarrays and computerized image analysis*. JOP, 2006. **7**(3): p. 283-94.
22. Li, X., et al., *Gastrin-releasing peptide promotes the growth of HepG2 cells via EGFR-independent ERK1/2 activation*. Oncol Rep, 2010. **24**(2): p. 441-8.
23. Ke, S., et al., *Near-infrared optical imaging of epidermal growth factor receptor in breast cancer xenografts*. Cancer Res, 2003. **63**(22): p. 7870-5.



24. Ryden, L., et al., *Epidermal growth factor receptor and vascular endothelial growth factor receptor 2 are specific biomarkers in triple-negative breast cancer. Results from a controlled randomized trial with long-term follow-up.* Breast Cancer Res Treat, 2010. **120**(2): p. 491-8.
25. Ozcelik, C., et al., *Conditional mutation of the ErbB2 (HER2) receptor in cardiomyocytes leads to dilated cardiomyopathy.* Proc Natl Acad Sci U S A, 2002. **99**(13): p. 8880-5.
26. Festuccia, C., et al., *Epidermal growth factor modulates prostate cancer cell invasiveness regulating urokinase-type plasminogen activator activity. EGF-receptor inhibition may prevent tumor cell dissemination.* Thromb Haemost, 2005. **93**(5): p. 964-75.
27. Farzadnia, M., et al., *Evaluation of HER2/neu oncoprotein in serum and tissue samples of women with breast cancer: correlation with clinicopathological parameters.* Breast, 2010. **19**(6): p. 489-92.
28. Ross, J.S., et al., *Breast cancer biomarkers and molecular medicine: part II.* Expert Rev Mol Diagn, 2004. **4**(2): p. 169-88.
29. Sternlicht, M.D., et al., *Mammary ductal morphogenesis requires paracrine activation of stromal EGFR via ADAM17-dependent shedding of epithelial amphiregulin.* Development, 2005. **132**(17): p. 3923-33.
30. Mitsudomi, T. and Y. Yatabe, *Epidermal growth factor receptor in relation to tumor development: EGFR gene and cancer.* FEBS J, 2010. **277**(2): p. 301-8.
31. Okamoto, I., *Epidermal growth factor receptor in relation to tumor development: EGFR-targeted anticancer therapy.* FEBS J, 2010. **277**(2): p. 309-15.
32. !!! INVALID CITATION !!!
33. Feinmesser, R.L., et al., *Ca<sup>2+</sup>/calmodulin-dependent kinase II phosphorylates the epidermal growth factor receptor on multiple sites in the cytoplasmic tail and serine 744 within the kinase domain to regulate signal generation.* J Biol Chem, 1999. **274**(23): p. 16168-73.

34. Allison, M., *The HER2 testing conundrum*. Nat Biotechnol, 2010. **28**(2): p. 117-9.
35. Dawood, S., et al., *Prognosis of women with metastatic breast cancer by HER2 status and trastuzumab treatment: an institutional-based review*. J Clin Oncol, 2010. **28**(1): p. 92-8.
36. Shankaran, H., et al., *Quantifying the effects of co-expressing EGFR and HER2 on HER activation and trafficking*. Biochem Biophys Res Commun, 2008. **371**(2): p. 220-4.
37. Cho, H.S., et al., *Structure of the extracellular region of HER2 alone and in complex with the Herceptin Fab*. Nature, 2003. **421**(6924): p. 756-60.
38. Burke, P., K. Schooler, and H.S. Wiley, *Regulation of epidermal growth factor receptor signaling by endocytosis and intracellular trafficking*. Mol Biol Cell, 2001. **12**(6): p. 1897-910.
39. Tolmachev, V., *Imaging of HER-2 overexpression in tumors for guiding therapy*. Curr Pharm Des, 2008. **14**(28): p. 2999-3019.
40. Zhao, X., et al., *Epidermal growth factor (EGF) induces apoptosis in a transfected cell line expressing EGF receptor on its membrane*. Cell Biol Int, 2006. **30**(8): p. 653-8.
41. Zhu, H., et al., *Oncogenic EGFR signaling cooperates with loss of tumor suppressor gene functions in gliomagenesis*. Proc Natl Acad Sci U S A, 2009. **106**(8): p. 2712-6.
42. Tokuda, Y., *Antibodies as molecular target-based therapy: trastuzumab*. Int J Clin Oncol, 2003. **8**(4): p. 224-9.
43. Rasul, K.I., et al., *Study of HER2/neu status in Qatari women with breast carcinoma*. Saudi Med J, 2003. **24**(8): p. 832-6.
44. Tang, X., et al., *EGFR tyrosine kinase domain mutations are detected in histologically normal respiratory epithelium in lung cancer patients*. Cancer Res, 2005. **65**(17): p. 7568-72.
45. Menard, S., et al., *HER2 overexpression in various tumor types, focussing on its relationship to the development of invasive breast cancer*. Ann Oncol, 2001. **12 Suppl 1**: p. S15-9.

46. Amin, D.N., et al., *Tumor endothelial cells express epidermal growth factor receptor (EGFR) but not ErbB3 and are responsive to EGF and to EGFR kinase inhibitors*. *Cancer Res*, 2006. **66**(4): p. 2173-80.
47. Cooke, T., et al., *HER2 as a prognostic and predictive marker for breast cancer*. *Ann Oncol*, 2001. **12 Suppl 1**: p. S23-8.
48. Tagliabue, E., et al., *The early relapse of premenopausal patients after surgery for node-positive breast carcinoma*. *Breast Cancer Res Treat*, 2001. **70**(2): p. 155-6.
49. Yonemura, Y., et al., *Evaluation of immunoreactivity for erbB-2 protein as a marker of poor short term prognosis in gastric cancer*. *Cancer Res*, 1991. **51**(3): p. 1034-8.
50. Hellstrom, I., et al., *Overexpression of HER-2 in ovarian carcinomas*. *Cancer Res*, 2001. **61**(6): p. 2420-3.
51. Buchler, P., et al., *Combination therapy for advanced pancreatic cancer using Herceptin plus chemotherapy*. *Int J Oncol*, 2005. **27**(4): p. 1125-30.
52. Yarden, Y., *Biology of HER2 and its importance in breast cancer*. *Oncology*, 2001. **61 Suppl 2**: p. 1-13.
53. Yamanaka, Y., et al., *Coexpression of epidermal growth factor receptor and ligands in human pancreatic cancer is associated with enhanced tumor aggressiveness*. *Anticancer Res*, 1993. **13**(3): p. 565-9.
54. Artemov, D., *Molecular magnetic resonance imaging with targeted contrast agents*. *J Cell Biochem*, 2003. **90**(3): p. 518-24.
55. Artemov, D., et al., *MR molecular imaging of the Her-2/neu receptor in breast cancer cells using targeted iron oxide nanoparticles*. *Magn Reson Med*, 2003. **49**(3): p. 403-8.
56. Artemov, D., et al., *Magnetic resonance molecular imaging of the HER-2/neu receptor*. *Cancer Res*, 2003. **63**(11): p. 2723-7.

57. Dancer, J., et al., *Coexpression of EGFR and HER-2 in pancreatic ductal adenocarcinoma: a comparative study using immunohistochemistry correlated with gene amplification by fluorescent in situ hybridization*. *Oncol Rep*, 2007. **18**(1): p. 151-5.
58. Bloomston, M., et al., *Epidermal growth factor receptor expression in pancreatic carcinoma using tissue microarray technique*. *Dig Surg*, 2006. **23**(1-2): p. 74-9.
59. Thybusch-Bernhardt, A., S. Beckmann, and H. Juhl, *Comparative analysis of the EGF-receptor family in pancreatic cancer: expression of HER-4 correlates with a favourable tumor stage*. *Int J Surg Investig*, 2001. **2**(5): p. 393-400.
60. Eck, M.J. and C.H. Yun, *Structural and mechanistic underpinnings of the differential drug sensitivity of EGFR mutations in non-small cell lung cancer*. *Biochim Biophys Acta*, 2010. **1804**(3): p. 559-66.
61. Leyland-Jones, B., et al., *Pharmacokinetics, safety, and efficacy of trastuzumab administered every three weeks in combination with paclitaxel*. *J Clin Oncol*, 2003. **21**(21): p. 3965-71.
62. Valabrega, G., et al., *HER2-positive breast cancer cells resistant to trastuzumab and lapatinib lose reliance upon HER2 and are sensitive to the multitargeted kinase inhibitor sorafenib*. *Breast Cancer Res Treat*, 2010.
63. Esteva, F.J., et al., *Molecular predictors of response to trastuzumab and lapatinib in breast cancer*. *Nat Rev Clin Oncol*, 2010. **7**(2): p. 98-107.
64. Morse, D.L. and R.J. Gillies, *Molecular imaging and targeted therapies*. *Biochem Pharmacol*, 2010. **80**(5): p. 731-738.
65. Baselga, J., et al., *Recombinant humanized anti-HER2 antibody (Herceptin) enhances the antitumor activity of paclitaxel and doxorubicin against HER2/neu overexpressing human breast cancer xenografts*. *Cancer Res*, 1998. **58**(13): p. 2825-31.

66. Akita, R.W. and M.X. Sliwkowski, *Preclinical studies with Erlotinib (Tarceva)*. *Semin Oncol*, 2003. **30**(3 Suppl 7): p. 15-24.
67. Knuefermann, C., et al., *HER2/PI-3K/Akt activation leads to a multidrug resistance in human breast adenocarcinoma cells*. *Oncogene*, 2003. **22**(21): p. 3205-12.
68. Tolaney, S., *Therapeutic Mechanisms of Antibody Conjugates*. *Monographs in Oncology*, 2007. **1**(1): p. 1-12.
69. Wallberg, H. and A. Orlova, *Slow internalization of anti-HER2 synthetic affibody monomer 111In-DOTA-ZHER2:342-pep2: implications for development of labeled tracers*. *Cancer Biother Radiopharm*, 2008. **23**(4): p. 435-42.
70. Gong, H., et al., *In vivo imaging of xenograft tumors using an epidermal growth factor receptor-specific affibody molecule labeled with a near-infrared fluorophore*. *Neoplasia*, 2010. **12**(2): p. 139-49.
71. Lyakhov, I., et al., *HER2- and EGFR-specific affiproboscopes: novel recombinant optical probes for cell imaging*. *Chembiochem*, 2010. **11**(3): p. 345-50.
72. Wikman, M., et al., *Selection and characterization of HER2/neu-binding affibody ligands*. *Protein Eng Des Sel*, 2004. **17**(5): p. 455-62.
73. Engfeldt, T., et al., *Imaging of HER2-expressing tumours using a synthetic Affibody molecule containing the 99mTc-chelating mercaptoacetyl-glycyl-glycyl-glycyl (MAG3) sequence*. *Eur J Nucl Med Mol Imaging*, 2007. **34**(5): p. 722-33.
74. Gostring, L., et al., *Quantification of internalization of EGFR-binding Affibody molecules: Methodological aspects*. *Int J Oncol*, 2010. **36**(4): p. 757-63.
75. Kramer-Marek, G., et al., *[18F]FBEM-Z(HER2:342)-Affibody molecule-a new molecular tracer for in vivo monitoring of HER2 expression by positron emission tomography*. *Eur J Nucl Med Mol Imaging*, 2008. **35**(5): p. 1008-18.

76. Cassidy, P.J. and G.K. Radda, *Molecular imaging perspectives*. J R Soc Interface, 2005. **2**(3): p. 133-44.
77. Adams, K.E., et al., *Comparison of visible and near-infrared wavelength-excitable fluorescent dyes for molecular imaging of cancer*. J Biomed Opt, 2007. **12**(2): p. 024017.
78. Partridge, S.C., et al., *Accuracy of MR imaging for revealing residual breast cancer in patients who have undergone neoadjuvant chemotherapy*. AJR Am J Roentgenol, 2002. **179**(5): p. 1193-9.
79. Kim, Y.R., et al., *Steady-state and dynamic contrast MR imaging of human prostate cancer xenograft tumors: a comparative study*. Technol Cancer Res Treat, 2002. **1**(6): p. 489-95.
80. Hayashi, T., C. Umeda, and N.D. Cook, *An fMRI study of the reverse perspective illusion*. Brain Res, 2007. **1163**: p. 72-8.
81. Wimmer, H., et al., *A dual-route perspective on poor reading in a regular orthography: an fMRI study*. Cortex, 2010. **46**(10): p. 1284-98.
82. Caravan, P., *Strategies for increasing the sensitivity of gadolinium based MRI contrast agents*. Chem Soc Rev, 2006. **35**(6): p. 512-23.
83. Bhattacharyya, S., et al., *Synthesis and evaluation of near-infrared (NIR) dye-herceptin conjugates as photoacoustic computed tomography (PCT) probes for HER2 expression in breast cancer*. Bioconjug Chem, 2008. **19**(6): p. 1186-93.
84. Kossodo, S., et al., *Dual In Vivo Quantification of Integrin-targeted and Protease-activated Agents in Cancer Using Fluorescence Molecular Tomography (FMT)*. Mol Imaging Biol, 2009.
85. Frangioni, J.V., *In vivo near-infrared fluorescence imaging*. Curr Opin Chem Biol, 2003. **7**(5): p. 626-34.
86. Kampmeier, F., et al., *Rapid optical imaging of EGF receptor expression with a single-chain antibody SNAP-tag fusion protein*. Eur J Nucl Med Mol Imaging, 2010. **37**(10): p. 1926-34.

87. Huang, P., et al., *Photosensitizer-conjugated magnetic nanoparticles for in vivo simultaneous magnetofluorescent imaging and targeting therapy*. Biomaterials, 2011.
88. Smith, A.M., X. Gao, and S. Nie, *Quantum dot nanocrystals for in vivo molecular and cellular imaging*. Photochem Photobiol, 2004. **80**(3): p. 377-85.
89. Ollinger, J.M., *Estimation algorithms for dynamic tracer studies using positron-emission tomography*. IEEE Trans Med Imaging, 1987. **6**(2): p. 115-25.
90. Sharma, V., G.D. Luker, and D. Piwnica-Worms, *Molecular imaging of gene expression and protein function in vivo with PET and SPECT*. J Magn Reson Imaging, 2002. **16**(4): p. 336-51.
91. Yang, D.J., E.E. Kim, and T. Inoue, *Targeted molecular imaging in oncology*. Ann Nucl Med, 2006. **20**(1): p. 1-11.
92. Winnard, P.T., Jr., et al., *Molecular imaging of metastatic potential*. J Nucl Med, 2008. **49 Suppl 2**: p. 96S-112S.
93. Swanson, S.D., et al., *Targeted gadolinium-loaded dendrimer nanoparticles for tumor-specific magnetic resonance contrast enhancement*. Int J Nanomedicine, 2008. **3**(2): p. 201-10.
94. Tweedle, M.F., *The ProHance story: the making of a novel MRI contrast agent*. Eur Radiol, 1997. **7 Suppl 5**: p. 225-30.
95. Zhou, G., et al., *Subcellular distribution of polyhydroxylated metallofullerene Gd@C82(OH)22 in different tissues of tumor-bearing mice*. J Nanosci Nanotechnol, 2010. **10**(12): p. 8597-602.
96. Ranganathan, R.S., et al., *Polymethylated DOTA ligands. 2. Synthesis of rigidified lanthanide chelates and studies on the effect of alkyl substitution on conformational mobility and relaxivity*. Inorg Chem, 2002. **41**(25): p. 6856-66.
97. Nonat, A., et al., *Gadolinium(III) complexes of 1,4,7-triazacyclononane based picolinate ligands: simultaneous optimization of water exchange kinetics and electronic relaxation*. Dalton Trans, 2009(38): p. 8033-46.

98. Villaraza, A.J., A. Bumb, and M.W. Brechbiel, *Macromolecules, dendrimers, and nanomaterials in magnetic resonance imaging: the interplay between size, function, and pharmacokinetics*. Chem Rev, 2010. **110**(5): p. 2921-59.
99. Major, J.L. and T.J. Meade, *Bioresponsive, cell-penetrating, and multimeric MR contrast agents*. Acc Chem Res, 2009. **42**(7): p. 893-903.
100. Gibby, W.A. and K.A. Gibby, *Comparison of Gd DTPA-BMA (Omniscan) versus Gd HP-DO3A (ProHance) retention in human bone tissue by inductively coupled plasma atomic emission spectroscopy*. Invest Radiol, 2004. **39**(3): p. 138-42.
101. Prince, M.R., et al., *Nephrogenic systemic fibrosis and its impact on abdominal imaging*. Radiographics, 2009. **29**(6): p. 1565-74.
102. Grobner, T., *Gadolinium--a specific trigger for the development of nephrogenic fibrosing dermopathy and nephrogenic systemic fibrosis?* Nephrol Dial Transplant, 2006.
103. Thomsen, H.S., S.K. Morcos, and P. Dawson, *Is there a causal relation between the administration of gadolinium based contrast media and the development of nephrogenic systemic fibrosis (NSF)?* Clin Radiol, 2006. **61**(11): p. 905-6.
104. Joffe, P., H.S. Thomsen, and M. Meusel, *Pharmacokinetics of gadodiamide injection in patients with severe renal insufficiency and patients undergoing hemodialysis or continuous ambulatory peritoneal dialysis*. Acad Radiol, 1998. **5**(7): p. 491-502.
105. Clarkson, R.B., *Blood-pool MRI contrast agents: Properties and characterization*. Contrast Agents I, 2002. **221**: p. 201-235.
106. Wedeking, P., et al., *Quantitative dependence of MR signal intensity on tissue concentration of Gd(HP-DO3A) in the nephrectomized rat*. Magn Reson Imaging, 1992. **10**(1): p. 97-108.
107. Funovics, M.A., et al., *MR imaging of the her2/neu and 9.2.27 tumor antigens using immunospecific contrast agents*. Magn Reson Imaging, 2004. **22**(6): p. 843-50.



108. Cacheris, W.P., S.C. Quay, and S.M. Rocklage, *The relationship between thermodynamics and the toxicity of gadolinium complexes*. Magn Reson Imaging, 1990. **8**(4): p. 467-81.
109. Kumar, K., et al., *Synthesis, Stability, and Crystal-Structure Studies of Some Ca<sup>2+</sup>, Cu<sup>2+</sup> and Zn<sup>2+</sup> Complexes of Macrocyclic Polyamino Carboxylates*. Inorganic Chemistry, 1995. **34**(26): p. 6472-6480.
110. Caravan, P., et al., *Gadolinium(III) Chelates as MRI Contrast Agents: Structure, Dynamics, and Applications*. Chem Rev, 1999. **99**(9): p. 2293-352.
111. Yang, J.J., et al., *Rational design of protein-based MRI contrast agents*. J Am Chem Soc, 2008. **130**(29): p. 9260-7.
112. Kiefer, F., et al., *The SWISS-MODEL Repository and associated resources*. Nucleic Acids Res, 2009. **37**(Database issue): p. D387-92.
113. Guex, N., M.C. Peitsch, and T. Schwede, *Automated comparative protein structure modeling with SWISS-MODEL and Swiss-PdbViewer: a historical perspective*. Electrophoresis, 2009. **30 Suppl 1**: p. S162-73.
114. Wahlberg, E., et al., *An affibody in complex with a target protein: structure and coupled folding*. Proc Natl Acad Sci U S A, 2003. **100**(6): p. 3185-90.
115. Landajo, A., et al., *Analysis of heavy metal distribution in superficial estuarine sediments (estuary of Bilbao, Basque Country) by open-focused microwave-assisted extraction and ICP-OES*. Chemosphere, 2004. **56**(11): p. 1033-41.
116. Davis, S.C., et al., *Comparing implementations of magnetic-resonance-guided fluorescence molecular tomography for diagnostic classification of brain tumors*. J Biomed Opt, 2010. **15**(5): p. 051602.
117. Biopal, *Gadoluminate an ultrasmall gadolinium oxide colloid for MRI and MRA imaging CPR/DEV/EVG*. 2010.

118. Bouchard, L.S., et al., *Picomolar sensitivity MRI and photoacoustic imaging of cobalt nanoparticles*. Proc Natl Acad Sci U S A, 2009. **106**(11): p. 4085-9.
119. Carbonaro, L.A., et al., *Breast MRI using a high-relaxivity contrast agent: an overview*. AJR Am J Roentgenol, 2011. **196**(4): p. 942-55.
120. Moon, H.G., et al., *Age and HER2 expression status affect MRI accuracy in predicting residual tumor extent after neo-adjuvant systemic treatment*. Ann Oncol, 2009. **20**(4): p. 636-41.
121. Judd, R.M. and R.J. Kim, *Imaging time after Gd-DTPA injection is critical in using delayed enhancement to determine infarct size accurately with magnetic resonance imaging*. Circulation, 2002. **106**(2): p. e6; author reply e6.
122. Aime, S., et al., *Targeting cells with MR imaging probes based on paramagnetic Gd(III) chelates*. Curr Pharm Biotechnol, 2004. **5**(6): p. 509-18.
123. Adzamli, K., et al., *NMRD assessment of Gd-DTPA-bis(methoxyethylamide), (Gd-DTPA-BMEA), a nonionic MRI agent*. Invest Radiol, 1999. **34**(6): p. 410-4.
124. Li, S., et al., *PEGylation of protein-based MRI contrast agents improves relaxivities and biocompatibilities*. Journal of Inorganic Biochemistry, 2011.
125. Corsi, F., et al., *HER2 Expression in Breast Cancer Cells Is Downregulated Upon Active Targeting by Antibody-Engineered Multifunctional Nanoparticles in Mice*. ACS Nano, 2011. **5**(8): p. 6383-93.
126. Orlova, A., et al., *Tumor imaging using a picomolar affinity HER2 binding affibody molecule*. Cancer Res, 2006. **66**(8): p. 4339-48.
127. Yang, D., et al., *Recombinant heregulin-Pseudomonas exotoxin fusion proteins: interactions with the heregulin receptors and antitumor activity in vivo*. Clin Cancer Res, 1998. **4**(4): p. 993-1004.
128. Park, J.G., et al., *Characteristics of cell lines established from human gastric carcinoma*. Cancer Res, 1990. **50**(9): p. 2773-80.

129. McKinney, M.M. and A. Parkinson, *A simple, non-chromatographic procedure to purify immunoglobulins from serum and ascites fluid*. J Immunol Methods, 1987. **96**(2): p. 271-8.
130. Weissleder, R. and M.J. Pittet, *Imaging in the era of molecular oncology*. Nature, 2008. **452**(7187): p. 580-9.
131. Waters, E.A. and S.A. Wickline, *Contrast agents for MRI*. Basic Res Cardiol, 2008. **103**(2): p. 114-21.
132. Sherry, A.D. and M. Woods, *Chemical exchange saturation transfer contrast agents for magnetic resonance imaging*. Annu Rev Biomed Eng, 2008. **10**: p. 391-411.
133. Nunn, A.D., K.E. Linder, and M.F. Tweedle, *Can receptors be imaged with MRI agents?* Q J Nucl Med, 1997. **41**(2): p. 155-62.
134. Artemov, D., Z.M. Bhujwalla, and J.W. Bulte, *Magnetic resonance imaging of cell surface receptors using targeted contrast agents*. Curr Pharm Biotechnol, 2004. **5**(6): p. 485-94.
135. Gillies, R.J., et al., *MRI of the tumor microenvironment*. J Magn Reson Imaging, 2002. **16**(4): p. 430-50.
136. Tweedle, M.F., *Peptide-targeted diagnostics and radiotherapeutics*. Acc Chem Res, 2009. **42**(7): p. 958-68.
137. Penichet, M.L., et al., *In vivo properties of three human HER2/neu-expressing murine cell lines in immunocompetent mice*. Laboratory animal science, 1999. **49**(2): p. 179-88.
138. Banerjee, S.R., et al., *Synthesis and evaluation of technetium-99m- and rhenium-labeled inhibitors of the prostate-specific membrane antigen (PSMA)*. J Med Chem, 2008. **51**(15): p. 4504-17.
139. Gown, A.M., *Current issues in ER and HER2 testing by IHC in breast cancer*. Mod Pathol, 2008. **21** Suppl 2: p. S8-S15.

140. Phillips, K.A., et al., *Clinical practice patterns and cost effectiveness of human epidermal growth receptor 2 testing strategies in breast cancer patients*. *Cancer*, 2009. **115**(22): p. 5166-74.
141. Allison, M., *The HER2 testing conundrum*. *Nat Biotechnol*. **28**(2): p. 117-9.
142. Yang, W., et al., *Design of a calcium-binding protein with desired structure in a cell adhesion molecule*. *J Am Chem Soc*, 2005. **127**(7): p. 2085-93.
143. Weinmann, H.J., et al., *Tissue-specific MR contrast agents*. *Eur J Radiol*, 2003. **46**(1): p. 33-44.
144. Crich, S.G., et al., *Magnetic resonance imaging visualization of targeted cells by the internalization of supramolecular adducts formed between avidin and biotinylated Gd<sup>3+</sup> chelates*. *Journal of Biological Inorganic Chemistry*, 2005. **10**(1): p. 78-86.
145. Sipkins, D.A., et al., *Detection of tumor angiogenesis in vivo by alphaVbeta3-targeted magnetic resonance imaging*. *Nat Med*, 1998. **4**(5): p. 623-6.
146. Aime, S., et al., *Tunable imaging of cells labeled with MRI-PARACEST agents*. *Angew Chem Int Ed Engl*, 2005. **44**(12): p. 1813-5.
147. Farokhzad, O.C., et al., *Nanoparticle-aptamer bioconjugates: a new approach for targeting prostate cancer cells*. *Cancer Res*, 2004. **64**(21): p. 7668-72.
148. Frullano, L., et al., *Towards targeted MRI: new MRI contrast agents for sialic acid detection*. *Chemistry*, 2004. **10**(20): p. 5205-17.
149. Morawski, A.M., et al., *Targeted nanoparticles for quantitative imaging of sparse molecular epitopes with MRI*. *Magn Reson Med*, 2004. **51**(3): p. 480-6.
150. Kobayashi, H., et al., *Micro-magnetic resonance lymphangiography in mice using a novel dendrimer-based magnetic resonance imaging contrast agent*. *Cancer Res*, 2003. **63**(2): p. 271-6.
151. Chen, T.J., et al., *Targeted Herceptin-dextran iron oxide nanoparticles for noninvasive imaging of HER2/neu receptors using MRI*. *J Biol Inorg Chem*, 2008.

152. Zhu, W., et al., *PAMAM dendrimer-based contrast agents for MR imaging of Her-2/neu receptors by a three-step pretargeting approach*. Magn Reson Med, 2008. **59**(4): p. 679-85.
153. Smith-Jones, P.M., et al., *Imaging the pharmacodynamics of HER2 degradation in response to Hsp90 inhibitors*. Nat Biotechnol, 2004. **22**(6): p. 701-6.
154. Buchler, P., et al., *Therapy for pancreatic cancer with a recombinant humanized anti-HER2 antibody (herceptin)*. J Gastrointest Surg, 2001. **5**(2): p. 139-46.
155. Le, U.M. and Z. Cui, *Biodistribution and tumor-accumulation of gadolinium (Gd) encapsulated in long-circulating liposomes in tumor-bearing mice for potential neutron capture therapy*. Int J Pharm, 2006. **320**(1-2): p. 96-103.
156. Deal, K.A., et al., *Evaluation of the stability and animal biodistribution of gadolinium (III) benzylamine-derivatized diethylenetriaminepentaacetic acid*. J Med Chem, 1996. **39**(16): p. 3096-3106.
157. Zhang, H., *Trisodium-[(2-(R)-[(4,4-diphenylcyclohexyl)phosphono-oxymethyl]-diethylene triaminepentaacetato)(aquo)gadolinium(III)]*. 2004.
158. Allard, M., et al., *Experimental study of DOTA-gadolinium. Pharmacokinetics and pharmacologic properties*. Invest Radiol, 1988. **23 Suppl 1**: p. S271-4.
159. Schuhmann-Giampieri, G., et al., *Preclinical evaluation of Gd-EOB-DTPA as a contrast agent in MR imaging of the hepatobiliary system*. Radiology, 1992. **183**(1): p. 59-64.
160. Fink-Retter, A., et al., *Differential spatial expression and activation pattern of EGFR and HER2 in human breast cancer*. Oncol Rep, 2007. **18**(2): p. 299-304.
161. Girardi, V., et al., *Fischer's score criteria correlating with histopathological prognostic factors in invasive breast cancer*. Radiol Med, 2010. **115**(3): p. 421-33.
162. Meade, T.J., A.K. Taylor, and S.R. Bull, *New magnetic resonance contrast agents as biochemical reporters*. Curr Opin Neurobiol, 2003. **13**(5): p. 597-602.

163. Cheng, L.L., et al., *Correlation of high-resolution magic angle spinning proton magnetic resonance spectroscopy with histopathology of intact human brain tumor specimens*. *Cancer Res*, 1998. **58**(9): p. 1825-32.
164. Hermann, P., et al., *Gadolinium(III) complexes as MRI contrast agents: ligand design and properties of the complexes*. *Dalton Trans*, 2008(23): p. 3027-47.
165. Bogdanov, A.A., M. Lewin, and R. Weissleder, *Approaches and agents for imaging the vascular system*. *Adv Drug Deliv Rev*, 1999. **37**(1-3): p. 279-293.
166. Zhao, M., et al., *Non-invasive detection of apoptosis using magnetic resonance imaging and a targeted contrast agent*. *Nat Med*, 2001. **7**(11): p. 1241-4.
167. Le, X.F., et al., *Specific blockade of VEGF and HER2 pathways results in greater growth inhibition of breast cancer xenografts that overexpress HER2*. *Cell Cycle*, 2008. **7**(23): p. 3747-58.
168. Jahanzeb, M., *Adjuvant trastuzumab therapy for HER2-positive breast cancer*. *Clin Breast Cancer*, 2008. **8**(4): p. 324-33.
169. Cerniglia, G.J., et al., *Epidermal growth factor receptor inhibition modulates the microenvironment by vascular normalization to improve chemotherapy and radiotherapy efficacy*. *PLoS One*, 2009. **4**(8): p. e6539.
170. Yu, H., et al., *Co-expression of EGFRvIII with ErbB-2 enhances tumorigenesis: EGFRvIII mediated constitutively activated and sustained signaling pathways, whereas EGF-induced a transient effect on EGFR-mediated signaling pathways*. *Cancer Biol Ther*, 2008. **7**(11).
171. Hendriks, B.S., H.S. Wiley, and D. Lauffenburger, *HER2-mediated effects on EGFR endosomal sorting: analysis of biophysical mechanisms*. *Biophys J*, 2003. **85**(4): p. 2732-45.
172. Allen, M.J. and T.J. Meade, *Synthesis and visualization of a membrane-permeable MRI contrast agent*. *J Biol Inorg Chem*, 2003. **8**(7): p. 746-50.

173. Steffen, A.C., et al., *Differences in radiosensitivity between three HER2 overexpressing cell lines*. Eur J Nucl Med Mol Imaging, 2008. **35**(6): p. 1179-91.
174. Shaughnessy, J., *Biological Therapy of Breast Cancer*. 2006.
175. Weigelt, B., F.C. Geyer, and J.S. Reis-Filho, *Histological types of breast cancer: how special are they?* Mol Oncol, 2010. **4**(3): p. 192-208.
176. Yu, K.D., et al., *Different distribution of breast cancer subtypes in breast ductal carcinoma in situ (DCIS), DCIS with microinvasion, and DCIS with invasion component*. Ann Surg Oncol, 2011. **18**(5): p. 1342-8.
177. Sung, K.E., et al., *Transition to invasion in breast cancer: a microfluidic in vitro model enables examination of spatial and temporal effects*. Integr Biol (Camb), 2011. **3**(4): p. 439-50.
178. Leonard, G.D. and S.M. Swain, *Ductal carcinoma in situ, complexities and challenges*. J Natl Cancer Inst, 2004. **96**(12): p. 906-20.
179. Chabner, E., S. Schnitt, and J. Harris, *Current Management of Patients with Ductal Carcinoma-in-Situ*. Oncologist, 1997. **2**(2): p. 76-82.
180. Miller, F.R., et al., *MCF10DCIS.com xenograft model of human comedo ductal carcinoma in situ*. J Natl Cancer Inst, 2000. **92**(14): p. 1185-6.
181. Marie, Y., et al., *EGFR tyrosine kinase domain mutations in human gliomas*. Neurology, 2005. **64**(8): p. 1444-5.
182. Subik, K., et al., *The Expression Patterns of ER, PR, HER2, CK5/6, EGFR, Ki-67 and AR by Immunohistochemical Analysis in Breast Cancer Cell Lines*. Breast Cancer (Auckl), 2010. **4**: p. 35-41.
183. Wasif, N., et al., *Invasive lobular vs. ductal breast cancer: a stage-matched comparison of outcomes*. Ann Surg Oncol, 2010. **17**(7): p. 1862-9.

184. Levin, E.R., *Integration of the extranuclear and nuclear actions of estrogen*. Mol Endocrinol, 2005. **19**(8): p. 1951-9.
185. Gelbfish, G.A., et al., *Relationship of estrogen and progesterone receptors to prognosis in breast cancer*. Ann Surg, 1988. **207**(1): p. 75-9.
186. Navolanic, P.M., L.S. Steelman, and J.A. McCubrey, *EGFR family signaling and its association with breast cancer development and resistance to chemotherapy (Review)*. Int J Oncol, 2003. **22**(2): p. 237-52.
187. Bobrow, L.G., et al., *Ductal carcinoma in situ: assessment of necrosis and nuclear morphology and their association with biological markers*. J Pathol, 1995. **176**(4): p. 333-41.
188. Chan, K.C., et al., *Blockade of growth factor receptors in ductal carcinoma in situ inhibits epithelial proliferation*. Br J Surg, 2001. **88**(3): p. 412-8.
189. Chan, K.C., et al., *Effect of epidermal growth factor receptor tyrosine kinase inhibition on epithelial proliferation in normal and premalignant breast*. Cancer Res, 2002. **62**(1): p. 122-8.
190. Salter, K.H., et al., *An integrated approach to the prediction of chemotherapeutic response in patients with breast cancer*. PLoS One, 2008. **3**(4): p. e1908.
191. Strickland, L.B., et al., *Progression of premalignant MCF10AT generates heterogeneous malignant variants with characteristic histologic types and immunohistochemical markers*. Breast Cancer Res Treat, 2000. **64**(3): p. 235-40.
192. Santner, S.J., et al., *Malignant MCF10CA1 cell lines derived from premalignant human breast epithelial MCF10AT cells*. Breast Cancer Res Treat, 2001. **65**(2): p. 101-10.
193. Dawson, P.J., et al., *MCF10AT: a model for the evolution of cancer from proliferative breast disease*. Am J Pathol, 1996. **148**(1): p. 313-9.



194. Wang, B., H.D. Soule, and F.R. Miller, *Transforming and oncogenic potential of activated c-Ha-ras in three immortalized human breast epithelial cell lines*. *Anticancer Res*, 1997. **17**(6D): p. 4387-94.
195. Friedman, M., et al., *Phage display selection of Affibody molecules with specific binding to the extracellular domain of the epidermal growth factor receptor*. *Protein Eng Des Sel*, 2007. **20**(4): p. 189-99.
196. Qiao, J., et al., *HER2 Targeted Molecular MR Imaging Using a De Novo Designed Protein Contrast Agent*. *PLoS One*, 2011. **6**(3): p. e18103.
197. Stemmler, H.J., et al., *Intrathecal trastuzumab (Herceptin) and methotrexate for meningeal carcinomatosis in HER2-overexpressing metastatic breast cancer: a case report*. *Anticancer Drugs*, 2008. **19**(8): p. 832-6.
198. Schuell, B., et al., *HER 2/neu protein expression in colorectal cancer*. *BMC Cancer*, 2006. **6**: p. 123.
199. Raghunand, N., et al., *Renal and systemic pH imaging by contrast-enhanced MRI*. *Magn Reson Med*, 2003. **49**(2): p. 249-57.
200. Wang, Z., M.Y. Su, and O. Nalcioglu, *Applications of dynamic contrast enhanced MRI in oncology: measurement of tumor oxygen tension*. *Technol Cancer Res Treat*, 2002. **1**(1): p. 29-38.
201. Mueller, G.C., et al., *Effectiveness of MR imaging in characterizing small hepatic lesions: routine versus expert interpretation*. *AJR Am J Roentgenol*, 2003. **180**(3): p. 673-80.
202. Winter, P.M., et al., *Molecular imaging of angiogenesis in nascent Vx-2 rabbit tumors using a novel alpha(nu)beta3-targeted nanoparticle and 1.5 tesla magnetic resonance imaging*. *Cancer Res*, 2003. **63**(18): p. 5838-43.
203. Tan, M., et al., *Peptide-targeted Nanoglobular Gd-DOTA monoamide conjugates for magnetic resonance cancer molecular imaging*. *Biomacromolecules*. **11**(3): p. 754-61.

204. Ye, F., et al., *A peptide targeted contrast agent specific to fibrin-fibronectin complexes for cancer molecular imaging with MRI*. *Bioconjug Chem*, 2008. **19**(12): p. 2300-3.
205. Wu, C.L., et al., *Metabolomic imaging for human prostate cancer detection*. *Sci Transl Med*, 2010. **2**(16): p. 16ra8.
206. Leahy, D.J., et al., *A mammalian expression vector for expression and purification of secreted proteins for structural studies*. *Protein Expr Purif*, 2000. **20**(3): p. 500-6.
207. Chung, C.S., et al., *A27L protein mediates vaccinia virus interaction with cell surface heparan sulfate*. *J Virol*, 1998. **72**(2): p. 1577-85.
208. Hooper, J.W., et al., *Smallpox DNA vaccine protects nonhuman primates against lethal monkeypox*. *J Virol*, 2004. **78**(9): p. 4433-43.
209. Vazquez, M.I., et al., *The vaccinia virus 14-kilodalton (A27L) fusion protein forms a triple coiled-coil structure and interacts with the 21-kilodalton (A17L) virus membrane protein through a C-terminal alpha-helix*. *J Virol*, 1998. **72**(12): p. 10126-37.
210. Vazquez, M.I. and M. Esteban, *Identification of functional domains in the 14-kilodalton envelope protein (A27L) of vaccinia virus*. *J Virol*, 1999. **73**(11): p. 9098-109.
211. Ho, Y., et al., *The oligomeric structure of vaccinia viral envelope protein A27L is essential for binding to heparin and heparan sulfates on cell surfaces: a structural and functional approach using site-specific mutagenesis*. *J Mol Biol*, 2005. **349**(5): p. 1060-71.
212. Lin, T.H., et al., *Structural analysis of the extracellular domain of vaccinia virus envelope protein, A27L, by NMR and CD spectroscopy*. *J Biol Chem*, 2002. **277**(23): p. 20949-59.
213. Hooper, J.W., D.M. Custer, and E. Thompson, *Four-gene-combination DNA vaccine protects mice against a lethal vaccinia virus challenge and elicits appropriate antibody responses in nonhuman primates*. *Virology*, 2003. **306**(1): p. 181-95.

214. Edghill-Smith, Y., et al., *Smallpox vaccine-induced antibodies are necessary and sufficient for protection against monkeypox virus*. Nat Med, 2005. **11**(7): p. 740-7.